



Technische Universität München
TUM School of Natural Sciences

**Tailor-made Sorbents to Enhance Sensitivity in
Stable Isotope Analysis of Aquatic Micropollutants**

**Comprehensive Investigations on the Selectivity of
Cyclodextrin Polymers**

David Christopher Glöckler

Vollständiger Abdruck der von der TUM School of Natural Sciences der
Technischen Universität München zur Erlangung des akademischen
Grades eines

Doktors der Naturwissenschaften (Dr. rer. nat.)

genehmigten Dissertation.

Vorsitz:

Prof. Dr. Michael Schuster

Prüfer*innen der Dissertation:

1. Prof. Dr. Martin Elsner

2. Prof. Dr. Nicole Strittmatter

3. Priv.-Doz. Dr. Thomas Hofstetter

Die Dissertation wurde am 21.07.2023 bei der Technischen Universität
München eingereicht und durch die TUM School of Natural Sciences
am 30.10.2023 angenommen.

Acknowledgements

Mit großer Freude und tief empfundener Dankbarkeit möchte ich an dieser Stelle meine Anerkennung für alle zum Ausdruck bringen, die mich die letzten Jahre auf meinem akademischen Weg begleitet und mit ihrem Rat und ihrer Unterstützung maßgeblich zum erfolgreichen Abschluss meiner Promotion beigetragen haben.

An erster Stelle gebührt ein großer Dank meinem Doktorvater Prof. Dr. Martin Elsner. Lieber Martin, ich danke Dir ganz herzlich für Dein Vertrauen, das ermöglichte, mich im spannenden Bereich der analytischen Chemie sowohl professionell als auch persönlich weiterzuentwickeln. Ich bin dankbar für all die Unterstützung, die Du mir in dieser Zeit gewährt hast – angefangen bei der Anschaffung neuer Laborgeräte, über wertvolles, kritisches Feedback zu meinen Forschungsergebnissen und die Möglichkeit, diese auf Konferenzen zu präsentieren, bis hin zu Ratschlägen für die persönliche Zukunft. Deine herzliche und empathische Art werde ich stets positiv in Erinnerung behalten!

I owe a very special debt of gratitude to my advisor, Dr. Rani Bakkour. Dear Rani, I was privileged to benefit from your deep knowledge and expertise in the field, which has been instrumental in shaping my research. Your guidance has been invaluable, providing me with clear direction and perspective throughout my PhD journey. Your unwavering support, encouragement and motivation during difficult times were a driving force that kept me focused and determined to overcome all obstacles. Thank you so much for being always available for discussion and feedback, showing empathy and understanding personal struggles and challenges, and always maintaining a positive and optimistic attitude!

Bei Prof. Dr. Nicole Strittmatter (TUM) und PD Dr. Thomas Hofstetter (ETH Zürich) bedanke ich mich herzlich für die Begutachtung meiner Dissertation. Prof. Dr. Dr. Philippe Schmitt-Kopplin und Dr. Mourad Harir ermöglichten mir dank der freundlichen Bereitstellung ihrer Laborinfrastruktur und Expertise FTICR-MS-Messungen, ohne die diese Arbeit in ihrer Form nicht möglich gewesen wäre. Vielen Dank für die erfolgreiche Kooperation sowie die sehr angenehme Atmosphäre mit stets ausgezeichnetem Kaffee bei meinen Besuchen am Helmholtz Zentrum München! Bei Prof. Dr. Christian Zwiener, Dr. Martina Werneburg und Dr. Maximilian Müller von der Eberhard Karls Universität Tübingen danke ich für die freundliche Unterstützung mit LC-MS/MS-Messungen.

Mein besonderer Dank geht auch an meine Mentorin Prof. Dr. Christine Stumpp (BOKU Wien). Ihre Empfehlung, meine wissenschaftliche Reise durch eine Doktorarbeit fortzusetzen, war für mich von unschätzbarem Wert. Danke, dass Du mich auf diesen Weg gebracht und im entscheidenden Moment ermutigt hast, durchzuhalten!

Ein ganz großer Dank gilt meinen Kolleginnen und Kollegen der Arbeitsgruppen *Targeted Environmental Analytics* und *Isotopes and Environmental Chemistry*, die mir während all der Höhen und Tiefen immer mit Rat und Tat zur Seite standen: Aoife Canavan, Armela Tafa, Christopher Wabnitz, Felix Anritter, Fengchao Sun, Gabriel Sigmund, Habib

Al-Ghoul, Leonhard Prechtel und Lihong Chai. Chris, zunächst möchte ich Dir für Deine Mitarbeit an meinem Promotionsprojekt als Masterstudent und die anschließende Zeit, die wir gemeinsam als Doktoranden verbracht haben, danken. Fengchao und Gabriel, die mich zu Beginn meiner Promotionszeit begleitet haben, danke ich besonders für die vielen wertvollen Gespräche mit oder ohne Wissenschaftsbezug. Aoife, Armela, Habib, Leo und Lihong, eure Verstärkung der Arbeitsgruppen hat mein Doktorandenleben im und außerhalb des Labors deutlich bunter und lebendiger gemacht – vielen lieben Dank! Felix, ich bin Dir sehr dankbar für Deine tatkräftige technische aber auch moralische Unterstützung im Labor, insbesondere mit dem GC-IRMS. Weiterhin bedanke ich mich bei allen ehemaligen Gruppenmitgliedern am Helmholtz Zentrum München für die freundliche Aufnahme und besonders bei Aileen Melsbach für die technische GC-IRMS Einführung. Mein Dank gilt auch den von mir betreuten Studierenden Anastasiya Khranchenkova, Hendrik Pfaadt, Johanna Reich, Korbinian Geißer, Lucas Hirschberger und Michael Becker, die mit ihrer Arbeit maßgeblich zu meinen Forschungsprojekten beigetragen haben. Es war mir eine Freude mit euch allen zusammenzuarbeiten! Allen CAMPOS Doktoranden und Kollegen, insbesondere Óscar Jiménez Fernández und Zhe Wang, danke ich für fachliche Diskussionen und schöne gemeinsame Zeiten bei Probennahmen, Science Meetings und PhD Retreats.

Bei allen aktuellen und ehemaligen Kolleginnen und Kollegen am Lehrstuhl für Analytische Chemie und Wasserchemie am alten Standort in Großhadern sowie am neuen in Garching danke ich ausdrücklich für die stets freundliche Arbeitsatmosphäre und den zahlreichen fachlichen und persönlichen Austausch bei gemeinsamen Kaffeepausen, Ausflügen oder Festen. Im Besonderen möchte ich mich bei Lisa Göpfert bedanken. Liebe Lisa, vielen Dank für die Unterstützung bei meinem Start am Lehrstuhl und all die späteren Korrekturen, sowie die gemeinsamen Spaziergänge während der Pandemie, die gemütlichen Kinoabende und die Einladungen auf das Land, die eine willkommenen Abwechslung zum Promotionsstress geboten haben. Außerdem bedanke ich mich herzlich bei Jessica Beyerl für das Training der MAF-Synthese, Katharina Zirngibl für die sehr angenehme gemeinsame Zeit im Labor in Großhadern und David Bauer, der meine Arbeit mit Raman-Messungen unterstützt hat. Susanne Mahler danke ich für all die Hilfe im Labor, den ein oder anderen Labor-Kaffee und die Versorgung mit Grundwasserproben. Des Weiteren wurde ich sehr freundlich von Christine Benning mit SEM-Messungen, Birgit Apel mit IC-Messungen und Joachim Langer mit TOC-Messungen unterstützt. Den Gruppenleitern am Lehrstuhl PD Dr. Michael Seidl, PD Dr. Natalia Ivleva und Prof. Dr. Christoph Haisch gebührt mein Dank für zahlreiche fachliche Diskussionen und die gute Zusammenarbeit im Zuge von Studentenpraktika. Vielen lieben Dank an Christine Beese, Cornelia Popp und Sonja Rottler für all die organisatorische Hilfe sowie an Roland Hoppe und Sebastian Wiesemann für die tolle und immer schnelle Hilfe in der Werkstatt.

Schließlich gilt mein besonderer Dank meinen Eltern. Ich danke euch von ganzem Herzen für eure bedingungslose Unterstützung, eure unendliche Geduld und eure vertrauensvolle Zuversicht, die mir stets eine unermüdliche Stütze und Motivation waren.

Abstract

The ubiquitous occurrence of organic micropollutants (MPs), such as pesticides and pharmaceuticals, in aquatic systems raises questions regarding their environmental behavior and fate. Compound-specific isotope analysis (CSIA), which measures changes in stable isotope ratios of individual compounds at natural abundance (e.g., $^{13}\text{C}/^{12}\text{C}$, $^2\text{H}/^1\text{H}$, $^{15}\text{N}/^{14}\text{N}$, $^{18}\text{O}/^{16}\text{O}$), offers unique means to detect, characterize, and quantify their degradation in environmental systems, especially when concentration-based data alone would not be conclusive. However, applying CSIA to MPs in field settings faces challenges of limited sensitivity and chromatographic resolution of gas and liquid chromatography coupled with isotope ratio mass spectrometry (GC- and LC-IRMS). Given the low contaminant concentrations in natural waters, extraction of large sample volumes (i.e., tens to hundreds of liters) becomes inevitable to enrich sufficient analyte mass for accurate isotope analysis. Although solid-phase extraction (SPE) methods are available for this task, conventional SPE sorbents typically lack the selectivity to exclusively extract the target analytes, resulting in concomitant enrichment of dissolved organic matter (DOM). In consequence, an unresolved complex mixture (UCM) of unknown isotopic composition interferes in GC- or LC-IRMS measurements and compromises the reliable isotope analysis of target compounds. Hence, the overarching goal of this dissertation was to extend the scope of CSIA to MPs at low concentrations by advancing sample preparation methodologies.

The major part of the thesis specifically aimed at (i) increasing the selectivity of SPE by employing cyclodextrin polymers (CDPs), which have shown promise as selective sorbents in water purification technologies, and (ii) gaining detailed knowledge on the control of sorbent selectivity toward both target analytes and interfering DOM. In the first research chapter, the efficacy of CDPs with different cavity sizes (α -, β -, γ -CDP) was systematically investigated for the selective extraction of a range of MPs in the presence of DOM. Applicability to carbon isotope analysis was assessed for selected pesticides, and the results were compared with commercially available sorbents. The presented CDP-based SPE method proved effective in obtaining environmental extracts that meet the stringent criteria of CSIA, notably by significantly reducing the UCM in GC-IRMS chromatograms after SPE with β -CDP. The sensitivity of carbon isotope analysis was enhanced by a factor of 7.5 compared to conventional SPE-CSIA. The new CDP-based SPE-CSIA method was successfully applied to surface water matrices without inducing isotopic fractionation. The superior selectivity was further confirmed by up to six-fold lower carbon-normalized $C_{\text{DOM}}/C_{\text{analyte}}$ ratios in β -CDP extracts as derived from dissolved organic carbon (DOC) and liquid chromatography-tandem mass spectrometry (LC-MS/MS) analysis. In addition, a weak competition between DOM and analyte on the three CDPs was proven by Gibbs free energies of adsorption obtained through column chromatography experiments.

The second research chapter employed nontargeted Fourier transform ion cyclotron resonance mass spectrometry (FTICR MS) analysis to comprehensively explore the selectivity of β -CDP at the molecular level. The ultrahigh-resolution MS data elucidated the molecular chemodiversity of DOM extracted from surface and groundwater, highlighting the reduced matrix complexity in β -CDP extracts compared to conventional sorbents. The selectivity of β -CDP was shown to be characterized by discrimination against highly oxygenated and unsaturated compounds, which are associated with classes of lignin-like, tannin-like, and carboxylic-rich alicyclic molecules (CRAMs). In contrast, conventional sorbents exhibited a more universal extraction behavior across a wide range of DOM compositions. The provided molecular-level insights can effectively be used as an *a priori* assessment for extraction procedures and cleanup strategies for environmental samples.

The third research chapter aimed to elucidate the molecular drivers underlying the observed selectivity of CDPs. The study employed a multifaceted approach: (i) synthesizing CDPs with different cavity sizes (α -, β -, γ -CDP), (ii) evaluating their extraction efficiencies for selected MPs in competition with different DOM size fractions (<1, 1-3, 3-10, >10 kDa) to test for size-selectivity, and (iii) performing FTICR MS analysis on CDP-extracted DOM compounds (<1 kDa) of different origin (surface water and Suwannee River Fulvic and Humic Acid) to probe for molecular properties governing their selective sorption. First, no evidence of size-selectivity was observed across the different CDP cavity sizes (i), or through the two independent approaches (ii) and (iii). Second, a dominant impact of sorbate oxygenation and polarity on extraction of DOM and MPs was found, with relatively oxygen-poor/nonpolar compounds exhibiting preferential retention on all three CDPs. Third, the results indicated the exclusion of anionic matrix, such as carboxylic acids, but revealed preferential sorption of cationic DOM. Consequently, the selectivity was attributed to a synergistic effect of nonpolar and additional electrostatic interactions with the negatively charged polymer cross-linker. The improved understanding of CDPs' sorption behavior can facilitate the refinement of sorbent design, enhancing both efficiency and selectivity for environmental and analytical applications.

The second part of the thesis addressed the challenging task of processing large sample volumes required for micropollutant CSIA. To tackle this issue, the fourth study evaluated the feasibility of graphene-modified polymer monoliths for high-throughput extraction of MPs from water. The aim was to harness the synergistic effects of the high porosity of monolithic adsorption filtration (MAF) polymers and the unique sorption properties of graphene, a carbon-based nanomaterial, to enable efficient SPE at high flow rates. The study successfully immobilized graphene oxide (GO) nanosheets onto the MAF surface, and the chemical reduction of GO enhanced its sorption affinity and capacity for selected pesticides by approximately half an order of magnitude. However, the low sorption kinetics and the insufficiently increased surface area resulted in a poor extraction performance of the modified polymer in a proof-of-concept SPE experiment. The presented findings provide a knowledge base for future method development and optimization.

Overall, the present work underscores the critical importance of meticulously selecting SPE sorbent materials, of conducting comprehensive sorbent selectivity assessment toward target analyte and matrix constituents, and of performing rigorous method evaluation and validation to ensure accurate and sensitive micropollutant CSIA. Specifically, β -CDP is presented as a favorable selective model sorbent for discriminating against environmental DOM in matrix-susceptible analytical applications. The developed CDP-based SPE-CSIA procedure, in combination with established sample cleanup techniques, offers new prospects for CSIA at environmentally relevant concentrations ranging from tens to hundreds of nanograms per liter. The extension of this method to a wide range of organic MPs for investigating their environmental behavior and fate holds significant promise for environmental protection, enabling a better understanding of pollutant sources and transformation pathways, thus facilitating the informed development of effective mitigation strategies to safeguard water resources and ecosystem health.

Zusammenfassung

Das allgegenwärtige Vorkommen von organischen Mikroschadstoffen wie Pestiziden und Arzneimitteln in aquatischen Systemen wirft Fragen zu ihrem Verhalten und Verbleib in der Umwelt auf. Die substanzspezifische Isotopenanalyse (engl. *compound-specific isotope analysis*, CSIA), die Veränderungen im Verhältnis stabiler Isotope einzelner Substanzen bei natürlicher Häufigkeit bestimmt (z. B. $^{13}\text{C}/^{12}\text{C}$, $^2\text{H}/^1\text{H}$, $^{15}\text{N}/^{14}\text{N}$, $^{18}\text{O}/^{16}\text{O}$), bietet einzigartige Möglichkeiten zum Nachweis, zur Charakterisierung und zur Quantifizierung des Schadstoffabbaus in Umweltsystemen, insbesondere wenn konzentrationsbasierte Daten allein nicht aussagekräftig sind. Anwendungen der CSIA für Mikroschadstoffe in Feldstudien sind jedoch limitiert aufgrund der begrenzten Empfindlichkeit und chromatographischen Auflösung der Gas- und Flüssigkeitschromatographie gekoppelt mit der Isotopenverhältnis-Massenspektrometrie (GC- bzw. LC-IRMS). Angesichts der geringen Schadstoffkonzentrationen in natürlichen Gewässern ist die Extraktion großer Probenmengen (bis zu Hunderten von Liter) unumgänglich, um eine ausreichende Analytmasse für eine genaue Isotopenanalyse anzureichern. Obwohl für diese Aufgabe Festphasenextraktionsverfahren (engl. *solid-phase extraction*, SPE) zur Verfügung stehen, fehlt den herkömmlichen SPE-Sorbenten in der Regel die Selektivität, um ausschließlich die Zielanalyten zu extrahieren, wodurch es zu einer gleichzeitigen Anreicherung von gelösten organischen Substanzen (engl. *dissolved organic matter*, DOM) kommt. Diese angereicherte Matrix unbekannter Isotopenzusammensetzung stört in der Folge die GC- oder LC-IRMS-Messungen und beeinträchtigt die zuverlässige Bestimmung der Isotopenverhältnisse der Zielanalyten. Daher war das übergeordnete Ziel dieser Dissertation, den Anwendungsbereich der CSIA auf niedrig konzentrierte organische Schadstoffe auszuweiten, indem die Methoden der Probenvorbereitung verbessert werden.

Der Hauptteil der Arbeit hatte zum Ziel, (i) die Selektivität der Festphasenextraktion durch den Einsatz von Cyclodextrinpolymeren (engl. *cyclodextrin polymers*, CDPs) zu erhöhen, die sich als vielversprechende selektive Sorbenten in der Wasseraufbereitungstechnik erwiesen haben, und (ii) detaillierte Kenntnisse über die Kontrolle der Sorbentenselektivität sowohl gegenüber der Zielanalyten als auch dem interferierenden DOM zu erlangen. Im ersten Forschungskapitel wurde die Effektivität von CDPs mit unterschiedlichen Kavitätsgrößen (α -, β -, γ -CDP) systematisch für die selektive Extraktion einer Reihe von Mikroschadstoffen in Gegenwart von DOM untersucht. Die Anwendbarkeit auf die Kohlenstoffisotopenanalyse wurde für ausgewählte Pestizide beurteilt, und die Ergebnisse wurden mit kommerziell erhältlichen Sorbenten verglichen. Die vorgestellte CDP-basierte SPE-Methode erwies sich als effektiv bei der Gewinnung von Umweltextrakten, die die strengen Kriterien der CSIA erfüllen, insbesondere durch eine signifikante Reduzierung von matrix-bedingtem Hintergrund in GC-IRMS-Chromatogrammen nach der Festphasenextraktion mit β -CDP. Die Empfindlichkeit der

Kohlenstoffisotopenanalyse wurde im Vergleich zu einem herkömmlichen SPE-CSIA-Verfahren um den Faktor 7,5 verbessert. Die neue CDP-basierte SPE-CSIA-Methode wurde erfolgreich auf Oberflächenwassermatrizes angewandt, ohne eine Isotopenfraktionierung zu verursachen. Die höhere Selektivität wurde außerdem durch bis zu sechsfach niedrigere Kohlenstoff-normierte DOM-zu-Analyt-Verhältnisse in β -CDP-Extrakten bestätigt, wie es aus der Analyse des gelösten organischen Kohlenstoffs (engl. *dissolved organic carbon*, DOC) und der Flüssigchromatographie-Tandem-Massenspektrometrie (LC-MS/MS) hervorging. Darüber hinaus wurde ein nur schwacher Einfluss von kompetitivem DOM auf die Sorption des Analyten auf den drei CDPs durch Gibbs Freie Adsorptionsenergien belegt, die durch Säulenchromatographie-Experimente bestimmt wurden.

Im zweiten Forschungskapitel wurde eine ungerichtete Analyse mittels Fourier-Transform Ionenzyklotronresonanz Massenspektrometrie (FTICR MS) durchgeführt, um die Selektivität von β -CDP auf molekularer Ebene umfassend zu untersuchen. Die ultrahochauflösenden MS-Daten gaben Aufschluss über die molekulare chemische Vielfalt von DOM, das aus Oberflächen- und Grundwasser extrahiert wurde, und verdeutlichten die geringere Matrixkomplexität in β -CDP-Extrakten im Vergleich zu herkömmlichen Sorbenten. Die Selektivität von β -CDP ist durch die Diskriminierung gegenüber stark sauerstoffhaltigen und ungesättigten DOM-Verbindungen gekennzeichnet, die den Klassen der Lignin-artigen, Tannin-artigen und Carboxyl-reichen alicyclischen Moleküle (engl. *carboxylic-rich alicyclic molecules*, CRAMs) zugeordnet werden konnten. Im Gegensatz dazu zeigten herkömmliche Sorbenten ein universelleres Extraktionsverhalten über einen weiten Bereich von DOM-Zusammensetzungen. Die gewonnenen Erkenntnisse auf molekularer Ebene können effektiv als Vorabbewertung für Extraktionsverfahren und Reinigungsstrategien für Umweltproben genutzt werden.

Das dritte Forschungskapitel verfolgte das Ziel, die Faktoren zu entschlüsseln, welche der beobachteten CDP-Selektivität zugrunde liegen. In der Studie wurde ein vielschichtiger Ansatz gewählt: (i) Synthese von CDPs mit verschiedenen Hohlraumgrößen (α -, β -, γ -CDP), (ii) Bewertung ihrer Extraktionseffizienz für ausgewählte Mikroschadstoffe in Konkurrenz zu verschiedenen DOM-Größenfraktionen (<1, 1-3, 3-10, >10 kDa), um eine Größenselektivität zu prüfen, und (iii) Durchführung von FTICR-MS-Analysen an CDP-extrahierten DOM-Verbindungen (<1 kDa) unterschiedlicher Herkunft (Oberflächenwasser und Suwannee River Fulvin- bzw. Huminsäuren), um die molekularen Eigenschaften zu untersuchen, die ihre selektive Sorption bestimmen. Erstens wurden keine Anzeichen für eine Größenselektivität der unterschiedlichen CDP-Kavitätsgrößen (i) oder mittels der beiden unabhängigen experimentellen Ansätze (ii) und (iii) beobachtet. Zweitens wurde eine dominante Auswirkung der Sorbat-Oxygenierung und Polarität auf die Extraktion von DOM und Zielanalyten festgestellt, wobei relativ sauerstoffarme/unpolare Verbindungen eine bevorzugte Retention auf allen drei CDPs aufwiesen. Drittens deuteten die Ergebnisse auf den Ausschluss anionischer Matrix, wie z. B. Carbonsäuren, hin, zeigten aber eine bevorzugte Sorption von kationischer DOM. Folglich wurde die Selektivität auf einen

Synergieeffekt unpolarer und zusätzlicher elektrostatischer Wechselwirkungen mit dem negativ geladenen Polymervernetzer zurückgeführt. Das vertiefte Verständnis des Sorptionsverhaltens von CDPs kann die Weiterentwicklung des Designs der Sorbenten erleichtern und so deren Effizienz und Selektivität für umwelttechnische und analytische Anwendungen steigern.

Der zweite Teil der Arbeit befasste sich mit der herausfordernden Handhabung großer Probenmengen, die für die CSIA von Spurenstoffen erforderlich sind. Um diese Problematik zu adressieren, wurde im vierten Forschungskapitel die Eignung von mit Graphen modifizierten Polymermonolithen für eine Hochdurchsatz-Extraktion von Mikro-schadstoffen aus Wasser untersucht. Ziel war es, die Synergieeffekte der hohen Porosität von monolithischen Adsorptionsfiltrationspolymeren (engl. *monolithic adsorption filtration*, MAF) und die einzigartigen Sorptionseigenschaften von Graphen, einem Nanomaterial auf Kohlenstoffbasis, zu nutzen, um eine effiziente SPE bei hohen Durchflussraten zu ermöglichen. In der Studie wurden Graphenoxid (GO)-Nanopartikel erfolgreich auf der MAF-Oberfläche immobilisiert, und die chemische Reduktion von GO verbesserte die Sorptionsaffinität und -kapazität für ausgewählte Pestizide um etwa eine halbe Größenordnung. Die geringe Sorptionskinetik und die unzureichend vergrößerte Oberfläche führten jedoch zu einer schwachen Extraktionsleistung des modifizierten Polymermonolithen in einem Proof-of-Concept SPE Experiment. Die vorgestellten Ergebnisse bilden eine Grundlage für künftige Methodenentwicklungen und -optimierungen.

Insgesamt unterstreicht die vorliegende Arbeit die große Bedeutung einer sorgfältigen Auswahl von SPE-Sorbenten, einer gründlichen Bewertung ihrer Selektivität gegenüber Zielanalyten und Matrix und einer sorgfältigen Methodenevaluierung und -validierung, um eine akkurate und sensitive Isotopenbestimmung für aquatische Mikroschadstoffe sicherzustellen. Insbesondere wird β -CDP als vorteilhaften, selektiven Modell-Sorbenten für die Abtrennung von Umwelt-DOM in matrix-anfälligen analytischen Anwendungen vorgestellt. Das entwickelte SPE-CSIA-Verfahren auf CDP-Basis bietet in Kombination mit etablierten Probenreinigungstechniken neue Perspektiven für die substanzspezifische Isotopenanalyse bei umweltrelevanten Konzentrationen im niedrigen Nanogramm pro Liter Bereich. Die Ausweitung dieser Methode auf weitere organische Spurenstoffe zur Untersuchung ihres Verhaltens und Verbleibs in der Umwelt bietet Chancen für den Umweltschutz, denn sie ermöglicht ein besseres Verständnis der Schadstoffquellen und der Transformationsprozesse und erleichtert so die fundierte Entwicklung wirksamer Maßnahmen zum Schutz der Wasserressourcen und der Gesundheit der Ökosysteme.

List of Publications

Parts of this doctoral thesis have been published in peer-reviewed scientific journals:

David Glöckler, Mourad Harir, Philippe Schmitt-Kopplin, Martin Elsner, Rani Bakkour. Selectivity of β -Cyclodextrin Polymer toward Aquatic Contaminants: Insights from Ultrahigh-Resolution Mass Spectrometry of Dissolved Organic Matter. *Analytical Chemistry* **2023**, *95* (42), 15505-15513. DOI: 10.1021/acs.analchem.3c01394

David Glöckler, Mourad Harir, Philippe Schmitt-Kopplin, Martin Elsner, Rani Bakkour. Discriminative Behavior of Cyclodextrin Polymers against Dissolved Organic Matter: Role of Cavity Size and Sorbate Properties. *Analytical Chemistry* **2023**, *95* (39), 14582–14591. DOI: 10.1021/acs.analchem.3c01881

David Glöckler, Christopher Wabnitz, Martin Elsner, Rani Bakkour. Avoiding Interferences in Advance: Cyclodextrin Polymers to Enhance Selectivity in Extraction of Organic Micropollutants for Carbon Isotope Analysis. *Analytical Chemistry* **2023**, *95* (20), 7839-7848. DOI: 10.1021/acs.analchem.2c05465

Co-author contributions beyond the scope of this doctoral thesis:

Jianrong Huang, Adrian Mellage, Julian Pavon Garcia, **David Glöckler**, Susanne Mahler, Martin Elsner, Natalia Jakus, Muammar Mansor, Hongchen Jiang, Andreas Kappler. Metabolic performance and fate of electrons during nitrate-reducing Fe(II) oxidation by the autotrophic enrichment culture KS grown at different initial Fe:N ratios. *Applied and Environmental Microbiology* **2023**, *89* (3), e00196-23. DOI: 10.1128/aem.00196-23

Natalia Jakus, Nia Blackwell, Karsten Osenbrück, Daniel Straub, James M. Byrne, Zhe Wang, **David Glöckler**, Martin Elsner, Tillmann Lueders, Peter Grathwohl, Sara Kleindienst, Andreas Kappler. Nitrate Removal by a Novel Lithoautotrophic Nitrate-Reducing, Iron(II)-Oxidizing Culture Enriched from a Pyrite-Rich Limestone Aquifer. *Applied and Environmental Microbiology* **2021**, *87* (16), e00460-21. DOI: 10.1128/AEM.00460-21

Torben Schädler, Anna-Cathrine Neumann-Cip, Karin Wieland, **David Glöckler**, Christoph Haisch, Thomas Brück, Dirk Weuster-Botz. High-Density Microalgae Cultivation in Open Thin-Layer Cascade Photobioreactors with Water Recycling. *Applied Sciences* **2020**, *10*, 3883. DOI: 10.3390/app10113883

Giuseppe Brunetti, Jiří Šimůnek, **David Glöckler**, Christine Stumpp. Handling model complexity with parsimony: Numerical analysis of the nitrogen turnover in a controlled aquifer model setup. *Journal of Hydrology* **2020**, *584*, 124681. DOI: 10.1016/j.jhydrol.2020.124681

Conference Contributions

Parts of this doctoral thesis have been presented on research conferences and science meetings (underlined name indicates presenting author):

David Glöckler, Christopher Wabnitz, Mourad Harir, Philippe Schmitt-Kopplin, Martin Elsner, Rani Bakkour. Universal vs. Selective Sorbents for Targeted Isotope Analysis of Aquatic Contaminants. *ANAKON Conference 2023*. April 11 – 14, 2023, Vienna, Austria. Poster presentation.

David Glöckler, Mourad Harir, Philippe Schmitt-Kopplin, Martin Elsner, Rani Bakkour. Selective Extraction by Cyclodextrin Polymers: New Perspectives for Compound-specific Isotope Analysis of Micropollutants. *Gordon Research Seminar & Conference on Environmental Sciences: Water*, June 18 – 24, 2022, Holderness, NH, USA. Poster presentation.

David Glöckler, Mourad Harir, Philippe Schmitt-Kopplin, Martin Elsner, Rani Bakkour. Universal vs. Selective Sorbents for Targeted Isotope Analysis of Aquatic Contaminants. *10th International Symposium on Isotopomers (ISI) and 12th Isotopes Conference*, May 29 – June 3, 2022, Zurich, Switzerland. Poster presentation.

David Glöckler, Christopher Wabnitz, Mourad Harir, Philippe Schmitt-Kopplin, Martin Elsner, Rani Bakkour. Cyclodextrin-Polymere als selektives Festphasenmaterial für die sensitive substanzspezifische Kohlenstoffisotopenanalytik von Mikroschadstoffen. *Jahrestagung der Wasserchemischen Gesellschaft*. May 23 – 25, 2022, Virtual Conference. Poster and oral short presentation.

David Glöckler, Christopher Wabnitz, Martin Elsner, Rani Bakkour. Selektive Extraktion von Pestiziden aus Oberflächenwasser mittels quervernetzten Cyclodextrin-Polymeren für die substanzspezifische Kohlenstoffisotopenanalytik. *Jahrestagung der Wasserchemischen Gesellschaft*. May 10 – 12, 2021, Virtual Conference. Oral presentation.

David Glöckler, Christopher Wabnitz, Rani Bakkour, Martin Elsner. Selective Extraction of Pesticides from Surface Water for Carbon Isotope Analysis using Crosslinked Cyclodextrin Polymers. *CAMPOS International Conference "Turnover of Diffuse Pollutants on the Catchment Scale"*. March 23 – 25, 2020, Virtual Poster Session.

David Glöckler, Rani Bakkour, Maximilian Müller, Martina Werneburg, Christian Zwiener, Martin Elsner. Occurrence of Organic Micropollutants in the Schönbrunnen Sub-catchment and its Implication for Higher Order Streams. *CAMPOS International Conference "Turnover of Diffuse Pollutants on the Catchment Scale"*. March 23 – 25, 2020, Virtual Poster Session.

David Glöckler, Martin Elsner. Cyclodextrin Polymers for the Selective Enrichment of Pesticides from Natural Water to Enable Sensitive Compound-specific Isotope Analysis. *3rd Science Meeting of the DFG Collaborative Research Center CAMPOS*. November 18, 2019, Tübingen, Germany. Oral presentation.

David Glöckler, Rani Bakkour, Christopher Wabnitz, Gabriel Sigmund, Michael Seidel, Martin Elsner. Graphene-modified Polymer Monoliths for High-Throughput Extraction of Micropollutants for Compound-specific Isotope Analysis. *Isotopes 2019 – The Cross-Disciplinary Conference on Stable Isotope Sciences*. July 7 – 12, 2019, Raitenhaslach, Germany. Poster presentation.

Christopher Wabnitz, Rani Bakkour, **David Glöckler**, Martin Elsner. Selective Extraction of Pesticides from Surface Water using Crosslinked Cyclodextrin Polymers. *Isotopes 2019 – The Cross-Disciplinary Conference on Stable Isotope Sciences*. July 7 – 12, 2019, Raitenhaslach, Germany. Poster presentation.

David Glöckler, Rani Bakkour, Christopher Wabnitz, Gabriel Sigmund, Michael Seidel, Martin Elsner. Graphen-modifizierte Polymermonolithe für die Extraktion von Mikroschadstoffen aus großen Probenvolumina für die substanzspezifische Isotopenanalytik. *Jahrestagung der Wasserchemischen Gesellschaft*. May 27 – 29, 2019, Erfurt, Germany. Poster presentation.

David Glöckler, Rani Bakkour, Christopher Wabnitz, Gabriel Sigmund, Michael Seidel, Martin Elsner. Graphene-Modified Polymer Monoliths for High-Throughput Extraction of Micropollutants for Compound-Specific Isotope Analysis. *ANAKON Conference 2019*. March 25 – 28, 2019, Münster, Germany. Poster presentation.

David Glöckler, Martin Elsner. Identifying the Turnover of Agricultural (Micro)pollutants in Sub-catchments using Compound-specific Isotope Analysis. *2nd Science Meeting of the DFG Collaborative Research Center CAMPOS*. February 12 – 13, 2019, Tübingen, Germany. Oral presentation.

David Glöckler, Rani Bakkour, Christopher Wabnitz, Gabriel Sigmund, Michael Seidel, Martin Elsner. Graphene-Modified Polymer Monoliths for High-Throughput Extraction of Micropollutants for Compound-Specific Isotope Analysis. *Jahrestagung der Arbeitsgemeinschaft Stabile Isotope e.V. (ASI)*. September 30 – October 3, 2018, Raitenhaslach, Germany. Poster presentation.

Table of Contents

ACKNOWLEDGEMENTS.....	III
ABSTRACT.....	V
ZUSAMMENFASSUNG	IX
LIST OF PUBLICATIONS.....	XIII
CONFERENCE CONTRIBUTIONS.....	XIV
1 GENERAL INTRODUCTION.....	1
1.1 POLLUTION OF AQUATIC SYSTEMS BY ORGANIC MICROPOLLUTANTS	2
1.2 ASSESSING THE ENVIRONMENTAL FATE OF ORGANIC POLLUTANTS USING COMPOUND-SPECIFIC ISOTOPE ANALYSIS (CSIA)	4
1.2.1 Principle of the CSIA Technique.....	4
1.2.2 Measurement of Compound-Specific Isotope Ratios.....	7
1.3 ANALYTICAL CHALLENGES ASSOCIATED WITH MICROPOLLUTANT CSIA	9
1.3.1 Target Analyte Enrichment from Large Sample Volumes	9
1.3.2 Matrix Effects Caused by Unresolved Complex Mixture.....	10
1.3.3 Laborious Handling of Large Sample Volumes.....	13
1.4 STRATEGIES TO TACKLE THE ANALYTICAL LIMITATIONS	15
1.4.1 Enhancing Selectivity in Solid-Phase Extraction Using Innovative Sorbent Materials	15
1.4.2 Sorbent Selectivity Assessment toward Dissolved Organic Matter (DOM).....	21
1.4.3 High-Throughput Extraction by Chemically Modified Polymer Monoliths	25
1.5 OBJECTIVES AND APPROACH OF THE THESIS.....	27
2 AVOIDING INTERFERENCES IN ADVANCE: CYCLODEXTRIN POLYMERS TO ENHANCE SELECTIVITY IN EXTRACTION OF ORGANIC MICROPOLLUTANTS FOR CARBON ISOTOPE ANALYSIS.....	29
ABSTRACT	30
2.1 INTRODUCTION.....	31
2.2 EXPERIMENTAL SECTION.....	33
2.2.1 Chemicals and Materials.....	33
2.2.2 Preparation and Characterization of Porous Cyclodextrin Polymers	33
2.2.3 Sampling and Pretreatment of Surface Water Samples.....	33
2.2.4 Sample Preparation Procedures Using Cyclodextrin-Based and Conventional Sorbents	34
2.2.5 Batch Equilibrium Sorption Studies	36
2.2.6 Column Sorption Studies	36
2.2.7 Chemical and Isotopic Analyses.....	39
2.3 RESULTS AND DISCUSSION	41
2.3.1 Carbon Isotope Analysis of Pesticides after Solid-Phase Extraction of Surface Water on β -Cyclodextrin Polymer and Oasis HLB Sorbent.....	41
2.3.2 Preferential Affinity of Cyclodextrin Polymers toward Target Analytes over Dissolved Organic Matter.....	44
2.3.3 Validation of Carbon Isotopic Integrity after Solid-Phase Extraction of Surface Water on β -Cyclodextrin Polymer.....	50
2.4 CONCLUSIONS	52

3	SELECTIVITY OF β-CYCLODEXTRIN POLYMER TOWARD AQUATIC CONTAMINANTS: INSIGHTS FROM ULTRAHIGH-RESOLUTION MASS SPECTROMETRY OF DISSOLVED ORGANIC MATTER.....	53
	ABSTRACT	54
3.1	INTRODUCTION.....	55
3.2	EXPERIMENTAL SECTION	57
3.2.1	<i>Chemicals, Materials, and Sorbents.....</i>	57
3.2.2	<i>Solid-Phase Extraction of Dissolved Organic Matter.....</i>	57
3.2.3	<i>FTICR Mass Spectrometry and Molecular Formula Assignment.....</i>	57
3.2.4	<i>Double Bond Equivalent and Aromaticity Index.....</i>	58
3.2.5	<i>Intensity-Weighted Average Values and Data Visualization.....</i>	59
3.2.6	<i>Intensity-Weighted Population Density and Statistical Analysis.....</i>	59
3.3	RESULTS AND DISCUSSION	61
3.3.1	<i>Characteristic Features in FTICR Mass Spectra of DOM Extracts.....</i>	61
3.3.2	<i>Chemodiversity of DOM Extracted by β-Cyclodextrin Polymer and Universal SPE Sorbents</i>	63
3.3.3	<i>High-Abundance and Unique Molecular DOM Signatures in SPE Extracts</i>	65
3.4	CONCLUSIONS AND ANALYTICAL IMPLICATIONS	67
4	DISCRIMINATIVE BEHAVIOR OF CYCLODEXTRIN POLYMERS AGAINST DISSOLVED ORGANIC MATTER: ROLE OF CAVITY SIZE AND SORBATE PROPERTIES	69
	ABSTRACT	70
4.1	INTRODUCTION.....	71
4.2	EXPERIMENTAL SECTION	73
4.2.1	<i>Chemicals, Materials, and Sorbents.....</i>	73
4.2.2	<i>Sample Preparation Procedures</i>	73
4.2.3	<i>Micropollutant Extraction in Presence of DOM of Different Molecular Sizes</i>	74
4.2.4	<i>Extraction of Dissolved Organic Matter for Molecular-Level Analysis.....</i>	75
4.2.5	<i>Chemical Analyses</i>	75
4.3	RESULTS AND DISCUSSION	77
4.3.1	<i>Low-Molecular-Weight DOM Does Not Adversely Affect MP Extraction at Environmentally Relevant Concentrations.....</i>	77
4.3.2	<i>TFN-Cross-Linked Cyclodextrin Polymers Strongly Discriminate Against Highly Oxygenated and Unsaturated Compounds</i>	79
4.3.3	<i>Degree of Oxygenation Determines the Sorption of CHO-Compounds on TFN-Cross-Linked Cyclodextrin Polymers</i>	81
4.3.4	<i>TFN-Cross-Linked Cyclodextrin Polymers Preferentially Extract Protonated Over Nonionic CHNO-Compounds.....</i>	83
4.4	CONCLUSIONS	85
5	GRAPHENE-MODIFIED POLYMER MONOLITHS FOR HIGH-THROUGHPUT EXTRACTION OF MICROPOLLUTANTS: A PROOF-OF-CONCEPT STUDY.....	87
5.1	INTRODUCTION.....	88
5.2	EXPERIMENTAL SECTION	90
5.2.1	<i>Chemicals and Materials.....</i>	90
5.2.2	<i>Chemical Reduction of Graphene Oxide</i>	90

5.2.3	<i>Preparation and Functionalization of Monolithic Adsorption Filters</i>	90
5.2.4	<i>Material Characterization</i>	93
5.2.5	<i>Sorption Experiments</i>	93
5.2.6	<i>Quantification by High-Performance Liquid Chromatography</i>	95
5.3	RESULTS AND DISCUSSION	96
5.3.1	<i>Effect of Chemical Reduction of Graphene Oxide on Sorption Affinity and Capacity toward Organic Micropollutants</i>	96
5.3.2	<i>Significance of Nonpolar Interactions for the Sorption Process</i>	97
5.3.3	<i>Sorption Kinetics of Reduced Graphene Oxide in Comparison to Commercial Oasis HLB</i>	99
5.3.4	<i>Proof-Of-Concept for Graphene-Modified MAFs in Micropollutant Extraction from Water</i>	100
5.4	CONCLUSIONS	102
6	GENERAL CONCLUSION AND OUTLOOK	103
6.1	EFFICACY AND LIMITATIONS OF CYCLODEXTRIN POLYMERS FOR SELECTIVE SAMPLE PREPARATION IN CSIA APPLICATIONS	104
6.2	IMPLICATIONS FOR LARGE-VOLUME EXTRACTION CONCEPTS	108
6.3	PERSPECTIVES FOR MICROPOLLUTANT CSIA IN FIELD STUDIES	108
	ABBREVIATIONS	111
	REFERENCES.....	115
	APPENDICES	139
S1	OCCURRENCE OF ORGANIC MICROPOLLUTANTS IN AQUATIC SYSTEMS: A CASE STUDY FROM SOUTHERN GERMANY	140
S1.1	<i>Scope of the Case Study</i>	140
S1.2	<i>Water Sampling</i>	140
S1.3	<i>Solid-Phase Extraction</i>	140
S1.4	<i>Liquid Chromatography – Tandem Mass Spectrometry</i>	141
S2	SUPPORTING INFORMATION TO CHAPTER 2	142
S2.1	<i>Chemicals</i>	142
S2.2	<i>Standard Solutions and Ultrapure Water</i>	143
S2.3	<i>Sorbents and Packing Materials</i>	143
S2.4	<i>Preparation and Characterization of Porous Cyclodextrin Polymers</i>	146
S2.5	<i>Sampling and Pretreatment of Surface Water Samples</i>	148
S2.6	<i>Sample Preparation Procedures Using Cyclodextrin-Based and Conventional Sorbents</i>	149
S2.7	<i>Sorption Parameter Determination by Batch Equilibrium Sorption Studies</i>	150
S2.8	<i>Column Sorption Experiments Using High-Performance Liquid Chromatography</i>	158
S2.9	<i>Compound Quantification Using LC-MS/MS and HPLC</i>	161
S2.10	<i>Compound-Specific Carbon Isotope Analysis</i>	163
S2.11	<i>Matrix-Dependent Limits of Accurate Carbon Isotope Analysis</i>	165
S2.12	<i>Recoveries of Target Analytes and Dissolved Organic Matter</i>	169
S2.13	<i>Effect of Concurrent Dissolved Organic Matter on Gibbs Free Energy of Adsorption</i>	171
S2.14	<i>Validation of Carbon Isotopic Integrity after Solid-Phase Extraction of Surface Water on β-Cyclodextrin Polymer</i>	172

S3	SUPPORTING INFORMATION TO CHAPTER 3	174
	S3.1 <i>Chemicals and Materials</i>	174
	S3.2 <i>Preparation and Characterization of β-Cyclodextrin Polymer</i>	174
	S3.3 <i>Water Sample Collection and Treatment</i>	176
	S3.4 <i>Solid-Phase Extraction of Dissolved Organic Matter</i>	178
	S3.5 <i>Determination of Dissolved Organic Matter</i>	179
	S3.6 <i>Compound Class Assignment in the Van Krevelen Diagram</i>	179
	S3.7 <i>Molecular-Level Characterization of SPE Permeates by FTICR MS</i>	180
	S3.8 <i>Molecular-Level Characterization of SPE Extracts by FTICR MS</i>	182
	S3.9 <i>Literature Data on Recovery of Nonionic Micropollutants after Solid-Phase Extraction Using β-CDP as Sorbent</i>	190
S4	SUPPORTING INFORMATION TO CHAPTER 4	192
	S4.1 <i>Chemicals and Materials</i>	192
	S4.2 <i>Standard Solutions and Ultrapure Water</i>	192
	S4.3 <i>Preparation and Characterization of β-Cyclodextrin Polymer</i>	195
	S4.4 <i>Sampling of Surface Water and Preparation of Dissolved Organic Matter Reference Standards</i>	198
	S4.5 <i>Sample Preparation Procedures</i>	199
	S4.6 <i>Chemical Analyses</i>	201
	S4.7 <i>Results</i>	204
S5	SUPPORTING INFORMATION TO CHAPTER 5	212
	S5.1 <i>Chemicals</i>	212
	S5.2 <i>MAF Functionalization</i>	214
	S5.3 <i>Results and Discussion</i>	214
S6	REPRINT PERMISSIONS	216
	S6.1 <i>Reprinted Figures in Chapter 1</i>	216
	S6.2 <i>Reprinted Publication in Chapter 2</i>	218
	S6.3 <i>Reprinted Publication in Chapter 3</i>	218
	S6.4 <i>Reprinted Publication in Chapter 4</i>	219

Chapter 1

General Introduction

1.1 Pollution of Aquatic Systems by Organic Micropollutants

Freshwater ecosystems, such as rivers, lakes, wetlands, and aquifers, play a pivotal role in support of the environment, society, and economy. The services they provide, including water supply, natural water purification, habitat provision for aquatic organisms, nutrient cycling, and climate regulation, are also of key importance to terrestrial ecosystems and as such, they essentially influence human well-being and health.^{1,2} Yet, freshwater systems are increasingly threatened by human activities and climate change³⁻⁵ so that problems related to water quality and quantity are among the major environmental issues of the present time.⁶ Nowadays, 69 % of global water withdrawal are used by agriculture,⁷ where over 2.6 million metric tons of pesticides are annually applied worldwide (in 2020)⁸ to increase crop yields by controlling pests, such as weeds, insects, fungi, or rodents. The industrial sector and municipalities account together for the remaining 31 % of global water withdrawal.⁷ They additionally produce large amounts of wastewater, thereby introducing tens of thousands of anthropogenic organic chemicals,^{9,10} for example, industrial additives and by-products, pharmaceuticals and hormones, or surfactants to environmental systems.¹¹⁻¹⁵

Once released to the environment, the fate of these organic pollutants is governed by their physicochemical properties (e.g., water solubility, polarity, volatility, charge state)¹⁶ and the surrounding environmental conditions, including topography,¹⁷ hydraulic properties^{17,18} and organic carbon content of the subsurface,¹⁹⁻²¹ pH and redox potential,²¹⁻²⁶ and *in situ* microbial communities.^{27,28} Depending on the interplay between these factors, the contaminant spread across environmental compartments may be either fostered or impaired through several processes, namely (i) transport to the atmosphere by volatilization,²⁹ or transport to surface and groundwater by run-off and leaching, respectively;³⁰⁻³³ (ii) sorption to soil or sediment;^{34,35} (iii) bioaccumulation in the food web,^{36,37} and/or (iv) (bio)chemical transformation (i.e., abiotic or biotic degradation).^{38,39}

With respect to water quality, polar organic compounds such as pesticides, pharmaceuticals, or personal care products are of particular concern because they are highly soluble in water and therefore hardly removed by sorption.⁴⁰ Furthermore, many of these mobile pollutants are inherently persistent (i.e., recalcitrant to degradation), which promotes their aqueous transport over large spatial and temporal scales. Consequently, the ubiquitous occurrence of these pollutants in aquatic systems has received increasing attention,^{13-15,41-49} especially since analytical developments, most notably the hyphenation of liquid chromatography to mass spectrometry (LC-MS) by electrospray ionization (ESI) in the 1990s, have fostered their detection.⁵⁰

Typically, polar organic contaminants occur in natural aquatic systems at concentrations in the pg L^{-1} to $\mu\text{g L}^{-1}$ range,^{42-44,51-53} and are therefore commonly referred to as organic micropollutants (MPs). However, even at trace levels they potentially cause adverse chronic effects to humans⁵⁴⁻⁵⁹ and aquatic organisms,⁶⁰⁻⁶⁵ which can even be enhanced by additive and synergistic effects when present as complex mixtures.⁶⁶⁻⁶⁹ Moreover, when degraded,

their transformation products can occur at higher concentrations³⁹ and may also be more persistent and toxic than the parent compounds,⁷⁰ rendering them highly relevant to environmental risk assessment.

The widespread risk potential posed by MPs and their transformation products is exemplified in Figure 1.1 for a small catchment (~1 km²) in southern Germany, in which surface (gray diamonds) and groundwater (gray circles) was screened for environmentally relevant contaminants in the course of this doctoral work (see S1). A total of 12 pesticides and 5 metabolites were detected throughout the study area, but only at low individual median concentrations ranging from 1 to 57 ng L⁻¹ (Figure 1.1a). However, the mixtures of MPs (i) amounted to up to 2.9 µg L⁻¹, thereby exceeding European drinking water quality limits,⁷¹ and (ii) their composition varied significantly in water bodies of spatial proximity (Figure 1.1b). Consequently, MP contamination potentially endangers the water quality of deeper aquifers used for drinking water production on the one hand (star symbol, Figure 1.1b), and exposes aquatic organisms to variable chemical stressors on the other.

Given the global importance of groundwater as a freshwater resource for drinking water and domestic use⁶ and the toxicity and persistence of organic contaminations, it is essential to understand the environmental behavior and fate of these pollutants. In this context, the assessment and quantification of natural degradation processes of organic contaminants is a prerequisite for the implementation of informed remediation strategies, in order to maintain aquatic systems in good chemical and ecological status.

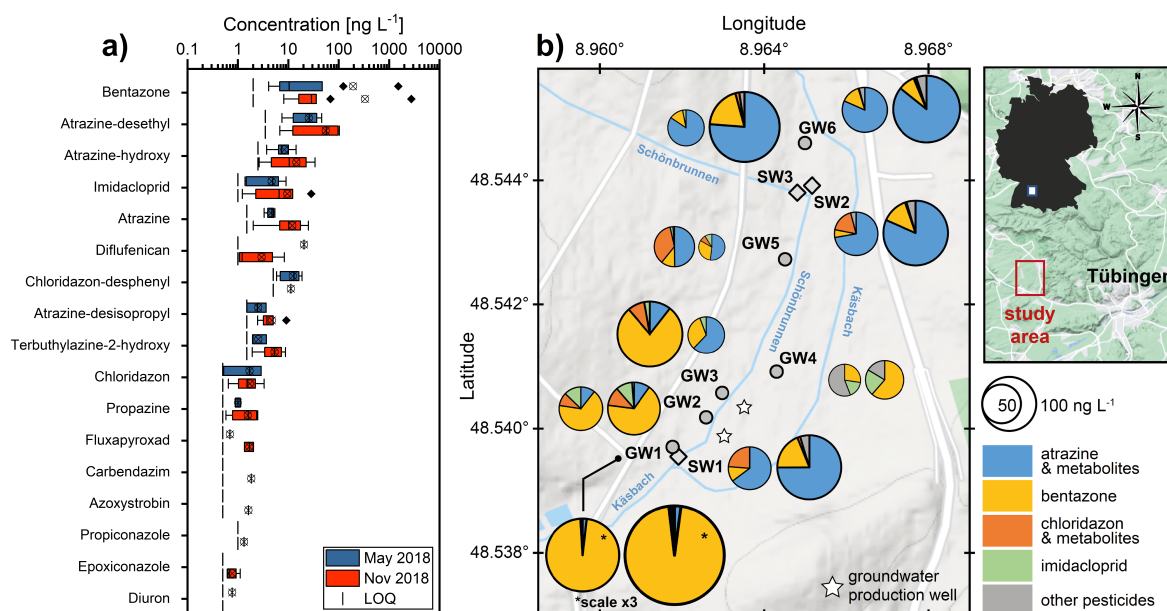


Figure 1.1. Occurrence of pesticides and metabolites in surface and groundwater of a catchment near Tübingen, Germany (for details see S1). (a) Concentration ranges in water samples taken in May (blue) and November 2018 (red). Vertical lines represent quantification limits, whereas crossed circles and black diamonds denote mean values and outliers, respectively. (b) Percentage distribution of pesticide and metabolite loads in groundwater (gray circles) and surface water (gray diamonds) samples in May (left pie chart) and November 2018 (right pie chart). Pie chart sizes represent summed concentrations and star symbols indicate the locations of groundwater production wells. Map data © 2023 GeoBasis-DE/BKG (©2009), Google.

1.2 Assessing the Environmental Fate of Organic Pollutants Using Compound-Specific Isotope Analysis (CSIA)

The assessment of natural (bio)degradation of organic pollutants in the environment is an intricate endeavor. On the one hand, degradation may occur in complex environmental settings over long timescales of years or even decades, which renders monitoring strategies challenging. On the other hand, traditional measurements of compound concentrations and compound-to-metabolite ratios are often not conclusive since (i) concurrent nonreactive processes, such as volatilization, dilution, or sorption, may also influence concentration dynamics, and (ii) mass balances are difficult to establish due to limitations in metabolite detection (e.g., fast degradation of the metabolite, lack of suitable analytical methods).⁷² In contrast, the stable isotope composition of elements, such as carbon, hydrogen, nitrogen, and oxygen, within organic MPs specifically changes due to reactions of the molecules.⁷³ The measurement of these changes in the reactant provides a type of information that is independent of both compound concentration and metabolite detection, and as such, can serve as a complementary line of evidence for *in situ* (bio)degradation.⁷⁴⁻⁷⁹

1.2.1 Principle of the CSIA Technique

Compound-specific stable isotope analysis (CSIA) enables the separation of organic compounds from complex mixtures and the subsequent determination of the stable isotope composition at natural abundance in the individual compounds (for the measuring principle, please refer to the next section).⁸⁰ The isotopic composition of an element E in an organic compound is given as the ratio of the heavier to the lighter isotope, $(^hE/^lE)_{comp}$ (e.g., $^{13}C/^{12}C$, $^2H/^1H$, $^{15}N/^14N$, $^{18}O/^16O$), and is typically expressed in the Delta notation, δ^hE (‰), relative to an international reference material, $(^hE/^lE)_{ref}$, according to equation 1.1:^{81,82}

$$\delta^hE_{comp} = \frac{(^hE/^lE)_{comp} - (^hE/^lE)_{ref}}{(^hE/^lE)_{ref}} = \frac{(^hE/^lE)_{comp}}{(^hE/^lE)_{ref}} - 1 \quad (1.1)$$

where negative δ^hE values indicate depletion, and positive values indicate enrichment of the heavier isotope in the compound relative to the reference material.

Similar to forensics,⁸³ doping control,⁸⁴ or food and beverage authentication,^{85,86} isotope ratios can serve in environmental applications as *isotopic fingerprints* to allocate and distinguish different contamination sources or the origin of otherwise identical substances.⁸⁷⁻⁹¹ Most notably, since these isotope ratios change during transformation reactions, they also offer unique means to detect and even quantify natural contaminant degradation,^{74,92-97} and thus they can also serve as *isotopic footprints* of degradation. This CSIA-based approach takes advantage of the so-called kinetic isotope effect (KIE) that is associated with many biotic and abiotic transformation reactions.⁷³ The KIE is defined as the ratio of the rate constants of the light (lk) to the heavy isotopologues (hk):

$$KIE = \frac{k_l}{k_h} \quad (1.2)$$

KIEs are caused by differences in activation energies of the light and heavy isotopologues which, in turn, depend on energy differences between the ground states of the isotopologues and their respective transition states during transformation.⁷³ Typically, light isotopologues have lower activation energies than heavy isotopologues, so their rate constants are greater (i.e., $KIE > 1$). Consequently, molecules with heavy isotopes in the reacting bond are transformed more slowly and become enriched in the remaining fraction of the contaminant as the reaction proceeds. This behavior is reflected in a shift in $\delta^h E$ to a more positive value and is referred to as *normal isotope fractionation*. Rarely, stiffer bonds are formed in the transition state resulting in a lower activation of the heavy isotopologues.⁷³ In this case of *inverse isotope fractionation*, the heavy isotopes become enriched in the transformation product (i.e., $KIE < 1$).

The extent of isotope fractionation is reflected in the bulk isotope enrichment factor, ε , which relates the changes in isotope ratios of a given compound to the extent of its transformation as described by the Rayleigh equation:⁹⁸

$$\frac{\partial^h E + 1}{\partial^h E_0 + 1} = f^\varepsilon \quad (1.3)$$

where $\delta^h E_0$ is the source isotope signature of the reactant at the beginning of the transformation ($t = 0$) and $\delta^h E$ is the average isotope ratio of the reactant at time t , when the transformation has progressed to a remaining fraction of the reactant f (i.e., c/c_0). Normal isotope effects are indicated by negative ε values, whereas positive ε values mean that heavy isotopologues are preferentially transformed (i.e., inverse fractionation). This trend of isotope fractionation is exemplarily illustrated in Figure 1.2a for the herbicide atrazine (blue) that is transformed in a closed system to hydroxyatrazine by *Arthrobacter aureescens* through biotic hydrolysis ($\varepsilon = -5.4$ ‰).⁹⁹ As the reaction proceeds, the carbon isotope value ($\delta^{13}C$) of atrazine demonstrates a progressively intensifying increase (blue line). Nevertheless, the isotopic signature of the instantaneously formed hydroxyatrazine (dotted line) consistently deviates by ε from that of atrazine. Once atrazine is completely transformed (i.e., $f = 0$), the accumulated hydroxyatrazine reaches the original carbon isotope value of atrazine ($\delta^{13}C_0$, horizontal black line).

Since KIEs resulting from bond cleavage during (bio)chemical transformations are often significantly larger than those induced by phase transfer processes, such as sorption or air-water partitioning,⁷⁸ the observed changes in isotope ratios of contaminants in environmental samples provide unique evidence of natural degradation. In fact, the extent of this degradation, B , can be estimated independently of data on concentration or transformation products using the inverse form of the Rayleigh equation:⁷⁴

$$B = 1 - f = \left(\frac{\delta^h E + 1}{\delta^h E_0 + 1} \right)^{\frac{1}{\epsilon}} \quad (1.4)$$

where $\delta^h E_0$ and $\delta^h E$ are the isotopic signatures of a given contaminant at the source and at a specific sampling location in the field, respectively, and f is the remaining contaminant fraction at the corresponding location.

The CSIA approach is most powerful when isotope compositions of at least two elements are determined in an individual contaminant (i.e., *dual element isotope analysis*). Plotting isotope values of one element versus another facilitates (i) a better contaminant source apportionment and (ii) the distinction of competing transformation reactions since changes in isotope ratios are often reaction-specific and chemical bonds with different elements give rise to distinct element-specific ϵ values.^{72,95,96} The latter case is exemplarily illustrated in Figure 1.2b for C and N isotope fractionation of atrazine associated with different reaction pathways. While atrazine transformation caused by photolysis (red pathway) induces inverse C and N isotope fractionation, oxidative transformation processes (green) preferentially enrich the heavy isotopologues of both elements, and hydrolysis (blue) yields normal C but inverse N fractionation.

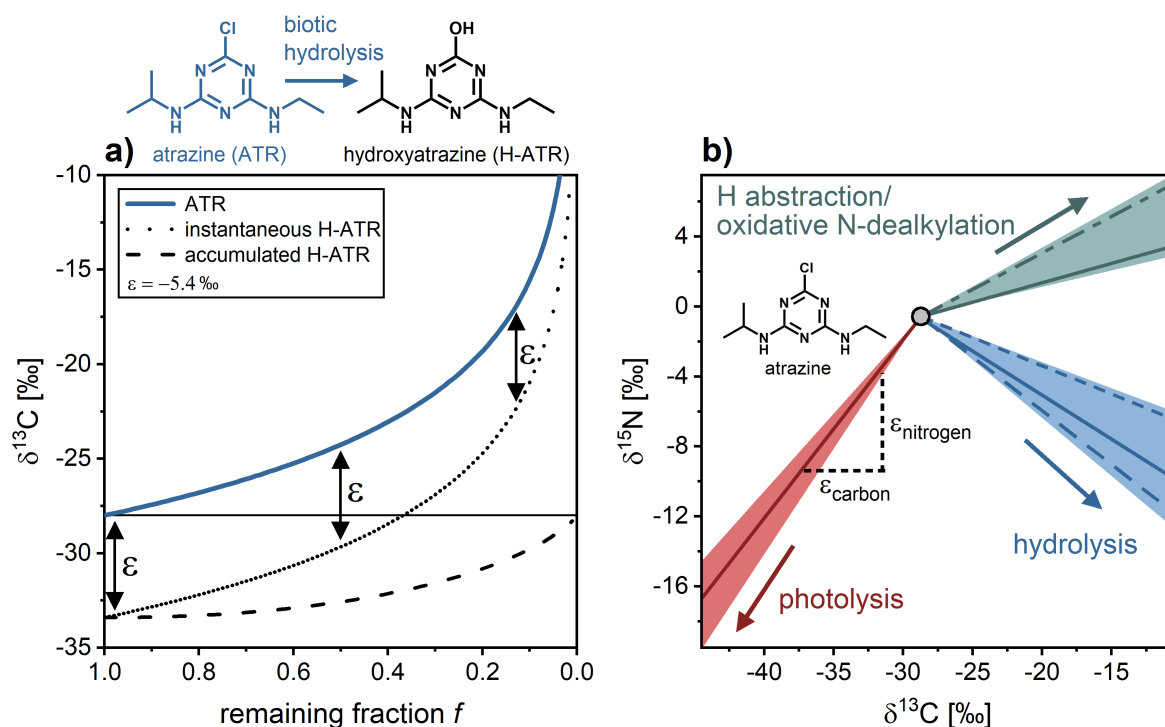


Figure 1.2. (a) Changes of carbon isotopic composition of atrazine ($\delta^{13}\text{C}_0 = -28$ ‰) and the instantaneous and accumulated product hydroxyatrazine as a function of the remaining atrazine fraction undergoing Rayleigh fractionation in a closed system through biotic hydrolysis (enrichment factor $\epsilon = -5.4$ ‰).⁹⁹ (b) Dual element isotope plot of $\delta^{13}\text{C}$ versus $\delta^{15}\text{N}$ for different atrazine transformation processes. The slopes of the regression lines ($\Delta\delta^{15}\text{N}/\Delta\delta^{13}\text{C}$) are approximately equal to $\epsilon_{\text{nitrogen}}/\epsilon_{\text{carbon}}$. Panel b is modified from Hofstetter et al.,¹⁰⁰ includes data from [99, 101, 102], and is reprinted with permission from Elsevier (see Chapter S6.1).

Moreover, when KIEs are masked by other rate-limiting steps involved in the reaction, the underlying transformation mechanisms are better characterized by dual element isotope analysis.⁸⁰ Since the potential masking influences the KIEs of all elements to the same extent,⁷⁶ the relative changes in isotope ratios, $\Delta\delta^h E_1/\Delta\delta^h E_2$ (i.e., the slope of the dual element plot, Λ , Figure 1.2b), remain the same and are approximately equal to the ratio of bulk isotope enrichment factors, $\varepsilon_{E_1}/\varepsilon_{E_2}$, according to equation 1.5:^{103,104}

$$\Lambda = \frac{\Delta\delta^h E_1}{\Delta\delta^h E_2} \approx \frac{\varepsilon_{E_1}}{\varepsilon_{E_2}} \quad (1.5)$$

1.2.2 Measurement of Compound-Specific Isotope Ratios

The analysis of variations in stable isotopic compositions has a long history in the geosciences, beginning with the discovery by Nier and Gulbransen in the mid-20th century that carbonates in limestone contain relatively more ^{13}C than organic carbon in plants.¹⁰⁵ Since then, the measurement of stable isotope ratios has become a standard analytical tool to investigate complex processes in various scientific disciplines, for instance (bio)geochemistry,^{106,107} paleoclimatology,¹⁰⁸ paleontology,¹⁰⁹ archeology,¹¹⁰ animal and plant ecology,^{111,112} and hydrogeology.¹¹³ To determine the isotope ratios of the light elements, namely carbon ($^{13}\text{C}/^{12}\text{C}$), hydrogen ($^2\text{H}/^1\text{H}$), nitrogen ($^{15}\text{N}/^{14}\text{N}$), and oxygen ($^{18}\text{O}/^{16}\text{O}$), molecules of interest are typically converted into a low molecular weight gas (i.e., CO_2 , H_2 , N_2 , CO , respectively) and then transferred into an isotope ratio mass spectrometer (IRMS). The functionality of these dedicated mass spectrometers has not changed significantly since they were developed by Alfred Nier and co-workers in the 1940s:^{114,115} the measurement gas molecules are (i) ionized by electron impact ionization; (ii) extracted and accelerated out of the ion source by an electrical potential; and (iii) guided through the mass analyzer, that is an uniform magnetic sector field in which the ions are deflected with a different radius depending on their mass-to-charge ratio.^{116,117} Lastly, (iv) an array of fixed Faraday collector cups simultaneously and continuously monitors the ion currents of the light and heavy isotopologues, thereby providing the high precision on the order of 10^{-2} to 10^{-4} % that is required for detecting isotopic variations at natural abundance.¹¹⁸

During the first decades, stable isotope analysis was solely performed on dual-inlet systems,⁸¹ which achieve highest precision at the expense of large sample amounts and labor-intensive offline sample preparation.¹¹⁹ In the 1970s, elemental analyzers were coupled to continuous-flow (CF-) IRMS systems in which the measurement gas molecules are carried to the ion source in a continuous helium stream after combustion of the bulk sample. The development of these online techniques minimized or overcame many limitations of offline preparation, such as the very low sensitivity (i.e., μg vs. mg sample amounts) or tedious offline gas separation.¹⁰⁶ Still, it was only possible to measure the isotopic composition of the bulk sample, whereas isotope ratios in the individual compounds

remained unresolved. The analytical breakthrough for CSIA was then achieved in 1978 when Matthew and Hayes¹²⁰ were the first to couple gas chromatography (GC) with CF-IRMS via a combustion interface that enabled a quantitative conversion of the analyte while maintaining chromatographic peak resolution (Figure 1.3a).¹²¹ With these modern GC-IRMS instruments, compound-specific $\delta^{13}\text{C}$ signatures could be measured relatively fast in even smaller sample sizes (i.e., ng quantities). The CSIA approach was subsequently extended in the 1990s to allow the measurement of compound-specific $\delta^{15}\text{N}$,^{122,123} $\delta^{18}\text{O}$,¹²⁴ and $\delta^2\text{H}$ values^{125,126} by introducing novel conversion interfaces for GC-IRMS. More recently, CSIA for non-GC-amenable (i.e., nonvolatile and/or thermally labile) compounds was enabled by coupling liquid chromatography with IRMS (LC-IRMS).¹²⁷ However, these systems are restricted to $\delta^{13}\text{C}$ determination and aqueous solvents since the analyte conversion is based on post-chromatographic wet chemical oxidation of the organic carbon to CO_2 using peroxydisulfate and concentrated phosphoric acid. The general measuring principle of CSIA by chromatography hyphenated with IRMS is illustrated in Figure 1.3b.

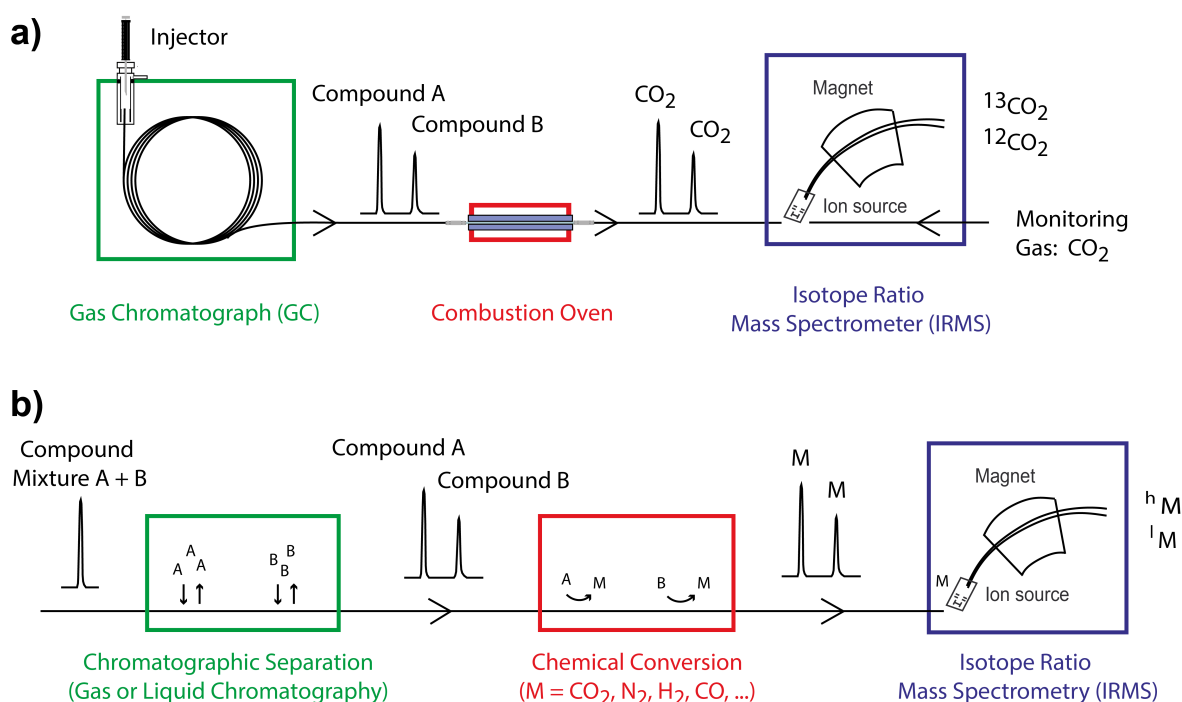


Figure 1.3. (a) Schematic set-up of a GC-IRMS system configured for carbon isotope analysis ($^{13}\text{C}/^{12}\text{C}$). (b) General principle of compound-specific isotope analysis (CSIA) based on chromatography hyphenated with continuous-flow isotope ratio mass spectrometry. Compound A and B are first baseline-separated by gas or liquid chromatography, then converted into small measurement gases (M) that consist of few isotopologues (^hM , ^lM), and finally transferred in a helium stream into the IRMS. The figure is modified from Elsner et al.⁸⁰ and reprinted with permission from Springer Nature (see Chapter S6.1).

1.3 Analytical Challenges Associated with Micropollutant CSIA

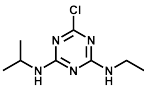
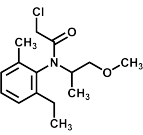
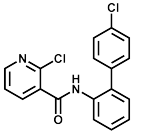
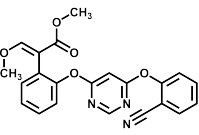
1.3.1 Target Analyte Enrichment from Large Sample Volumes

Nowadays, CSIA is a well-established analytical tool in environmental monitoring of legacy contaminants, for example chlorinated hydrocarbons, BTEX, or fuel oxygenates, which are typically present in the high $\mu\text{g L}^{-1}$ to mg L^{-1} concentration range at contaminated field sites (i.e., point sources).^{74,77,79,92} In contrast, environmental micropollutant CSIA investigations are mainly limited to either micro- and mesoscale experiments in the laboratory (e.g., aquifer models,¹²⁸⁻¹³² constructed wetlands^{133,134}, and soil micro-/mesocosms^{135,136}), or lysimeter¹³⁷ and point source contamination studies¹³⁸⁻¹⁴⁰ in the field. In contrast, applications in non-point source scenarios on the catchment scale are only emerging.^{97,141-143} The transfer of the CSIA approach to the field to study transformation processes of MPs under real-world conditions is challenged by the limited sensitivity of IRMS instruments (limit of quantification, LOQ, in mg L^{-1} range) in comparison to conventional molecular mass spectrometers (LOQ in ng L^{-1} range). This disparity arises due to the lower abundance of the heavy isotopes, necessitating larger sample volumes or higher analyte concentrations for accurate measurement. For instance, to achieve the high level of precision required for carbon or nitrogen isotope ratio determination, typically 0.8 nmol carbon or 3 nmol nitrogen need to be injected on-column into GC-IRMS systems.⁸⁰

Given the low occurrence of MPs in natural aquatic systems (Chapter 1.1), the masses required for IRMS measurements inevitably lead to extensive analyte preconcentration from large volumes of water. In addition, highly degraded samples (i.e., samples of lowest concentration) are of greatest interest since they reflect the largest changes in isotope ratios (Figure 1.2, Chapter 1.2). The latter is particularly important for relatively large molecules such as polar organic MPs, for which the KIEs become “diluted” by atoms that are not involved in the rate-limiting reaction.^{73,144} Table 1.1 provides an example calculation of the required volume of sample to analyze the herbicides atrazine and *S*-metolachlor, and the fungicides boscalid and azoxystrobin, which are the model compounds used for isotope analysis in Chapter 2. Assuming realistic aquatic MP concentrations in the range of 0.01 to $1 \mu\text{g L}^{-1}$ (Figure 1.1a), minimum SPE enrichment factors on the order of 10^4 to 10^6 must be achieved for the determination of $\delta^{13}\text{C}$ and on the order of 10^5 to 10^7 for $\delta^{15}\text{N}$ analysis. To accumulate enough analyte for multiple injections, these factors translate to large minimum extraction volumes of up to 45 and 1702 L for $\delta^{13}\text{C}$ and $\delta^{15}\text{N}$ analysis, respectively.

The preconcentration of polar target analytes from such large volumes of water entails further analytical challenges, namely (i) the substantial co-enrichment of organic matter by nonselective sorbent phases, which can lead to substantial interferences during GC-IRMS measurements, and (ii) the labor- and time-intensive sample handling of tens to hundreds of liters of water. These bottlenecks of micropollutant CSIA are addressed in detail in the following sections of this chapter.

Table 1.1. The minimum SPE enrichment factors and water extraction volumes required for compound-specific carbon ($\delta^{13}\text{C}$) and nitrogen ($\delta^{15}\text{N}$) isotope analysis by GC-IRMS of atrazine, *S*-metolachlor, boscalid, and azoxystrobin at typical environmental concentrations of 10 ng L^{-1} to $1 \text{ } \mu\text{g L}^{-1}$.

Analyte	Atrazine	<i>S</i> -metolachlor	Boscalid	Azoxystrobin	
Formula	$\text{C}_8\text{H}_{14}\text{ClN}_5$	$\text{C}_{15}\text{H}_{22}\text{ClNO}_2$	$\text{C}_{18}\text{H}_{12}\text{Cl}_2\text{N}_2\text{O}$	$\text{C}_{22}\text{H}_{17}\text{N}_3\text{O}_5$	
Structure					
Molar Mass (g mol^{-1})	215.7	283.8	343.2	403.4	
Environmental Concentration ($\mu\text{g L}^{-1}$)	0.01 to 1.0				
IRMS requirement*	$\delta^{13}\text{C}$	0.8 nmol C / 10 ng C			
	$\delta^{15}\text{N}$	3 nmol N / 42 ng N			
Minimum Enrichment Factor (-) [†]	$\delta^{13}\text{C}$	$(2.2 - 220) \times 10^4$	$(1.6 - 160) \times 10^4$	$(1.6 - 160) \times 10^4$	$(1.5 - 150) \times 10^4$
	$\delta^{15}\text{N}$	$(1.3 - 130) \times 10^5$	$(8.5 - 850) \times 10^5$	$(5.1 - 510) \times 10^5$	$(4.0 - 400) \times 10^5$
Minimum Extraction Volume (L) [‡]	$\delta^{13}\text{C}$	0.45 - 45	0.31 - 31	0.32 - 32	0.30 - 30
	$\delta^{15}\text{N}$	2.59 - 259	17.02 - 1702	10.29 - 1029	8.06 - 806

*according to Elsner et al.⁸⁰

[†]calculated based on an on-column GC-IRMS injection volume of $1 \text{ } \mu\text{L}$

[‡]calculated based on the corresponding minimum enrichment factor and a final sample volume of $20 \text{ } \mu\text{L}$ that allows for multiple sample injections

1.3.2 Matrix Effects Caused by Unresolved Complex Mixture

The prerequisite for accurate CSIA by chromatography-IRMS is high chromatographic resolution or, in other words, baseline-separated target analyte peaks.^{118,145} This arises from the inherently nonselective character of the technique due to the loss of structural information during the conversion of all analytes into the same chemical form before the transfer into the IRMS (e.g., CO_2 for $\delta^{13}\text{C}$, N_2 for $\delta^{15}\text{N}$ analysis). Hence, overlapping peaks can have a detrimental effect not only on the precision, but also on the trueness of isotopic data since the origin of the measurement gas can no longer be distinguished. This analytical drawback of high-precision IRMS is of particular concern for CSIA of analytes at low environmental concentrations and in the presence of complex matrices.^{80,146,147}

In natural aquatic systems, organic MPs invariably co-occur with dissolved organic matter (DOM), which is up to five orders of magnitude more abundant (i.e., low mg L^{-1} range) and represents thousands of heterogeneous and polydisperse compounds that are ultimately derived from decaying biota (for detailed discussion see Chapter 1.4.2.1). While this matrix can be cut off relatively easily during the enrichment of volatile organic contaminants by, for example, purge and trap,¹⁴⁸ the low volatility of polar organic MPs prevents the application of such selective and straightforward sample preparation techniques.

For the preconcentration of these contaminants from aqueous matrices, solid-phase extraction (SPE) has become the method of choice over the past decades.^{149,150} However, nonvolatile DOM constituents are substantially co-enriched during large-volume SPE, especially when common nonselective SPE sorbents are employed (see Chapter 1.4.1.1). In consequence, SPE extracts typically contain highly complex mixtures of target analytes and matrix constituents. The complete chromatographic resolution is often not achievable for these extracts and matrix components with unknown isotopic signatures co-elute with the targets as so-called *unresolved complex mixture* (UCM),^{116,151,152} as shown in Figure 1.4 for a GC-IRMS measurement. Besides, CSIA of highly polar (i.e., nonvolatile) or thermally labile analytes by LC-IRMS is even more prone to adverse matrix effects due to lower chromatographic resolution and sensitivity compared with GC-based techniques.¹⁴⁶

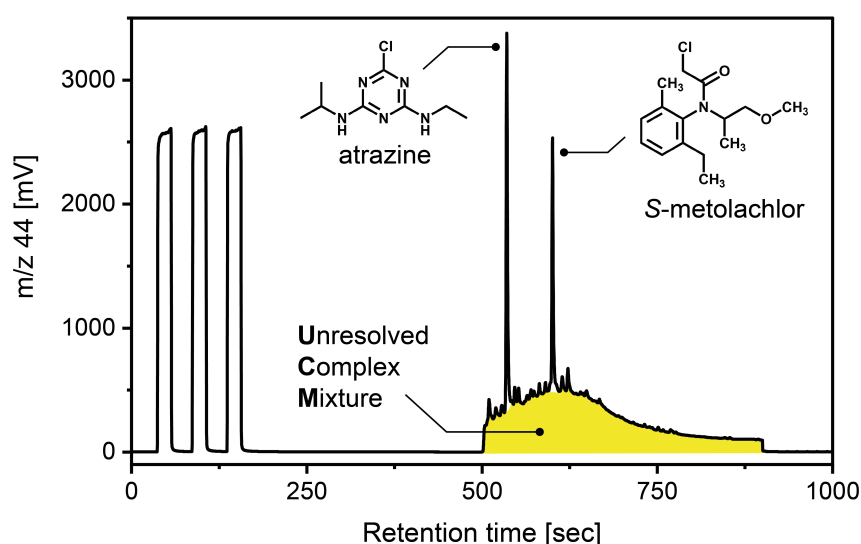


Figure 1.4. Gas chromatography – isotope ratio mass spectrometry (GC-IRMS) chromatogram of the main mass trace (m/z 44) for the $\delta^{13}\text{C}$ determination of atrazine and *S*-metolachlor post-spiked to a surface water matrix after solid-phase extraction (SPE) of 300 mL sample using the commercial Oasis HLB sorbent (Waters Corporation). The raised baseline, highlighted in yellow color, reflects unresolved complex mixture (UCM) as a result of co-enrichment of dissolved organic matter (DOM) from the water sample.

Bias in isotope analysis introduced by UCM can be corrected under two premises using the background correction algorithms that are provided by the companion software tool of the manufacturer.¹¹⁶ First, peak intensities of target analytes must be sufficiently larger than the raised matrix baseline. And second, differences in isotopic compositions between target analyte and UCM must be small. In fact, Bakkour found that reliable $\delta^{13}\text{C}$ determination by GC-IRMS for a typical freshwater matrix is limited to an approximate carbon-normalized DOM-to-analyte threshold concentration ratio ($C_{\text{DOM}}/C_{\text{analyte}}$) in the extract of $10 \text{ molC molC}^{-1}$.¹⁵³ In other words, if a sample extract contains more than ten times the amount of matrix- than analyte-borne organic carbon, the software will be unable to accurately subtract the chromatographic background. In consequence, the measured carbon isotope ratios would not reflect the compound-specific value, but a mixture of the isotopic signatures of both the target analyte and the interfering matrix.

The UCM can also pose analytical difficulties for nitrogen isotope analysis, even though the abundance of nitrogen in DOM is much lower than that of carbon (e.g., DOC/DON ratios typically range between 10 and 50 mgC mgN⁻¹ in surface waters).¹⁵⁴ For instance, large amounts of (co-)eluting interferences may exhaust the oxidation and reduction capacities of the reactors in the GC-IRMS interface, leading to incomplete conversion of the target analytes and consequently to inaccurate $\delta^{15}\text{N}$ determination.¹²² Furthermore, CO stemming from incomplete combustion of UCM can cause isobaric interferences at m/z 28 and 29 (i.e., CO⁺ fragment ions formed in the ion source), which can substantially affect the measured nitrogen isotope values.^{80,117}

Compromised carbon and nitrogen isotope analyses due to strong matrix effects have therefore been frequently reported in literature,^{97,141,155-157} and the combination of insufficient chromatographic resolution and low environmental pollutant concentration has been identified as a major bottleneck for CSIA applications in non-point source settings on the catchment scale.^{147,151,158} Hence, there is a strong demand for analytical developments to push limits of sensitive and accurate CSIA toward the environmentally relevant sub- $\mu\text{g L}^{-1}$ concentration range.^{146,157,159} To this end, two different avenues can be pursued: The first one is to increase sensitivity and peak resolution through instrumental advances, such as modified injection systems,¹⁶⁰ reduced peak broadening by narrow-bore capillaries,¹⁶¹ optimized reactor design,¹⁶² and comprehensive two-dimensional GC techniques.¹⁶³ The second is to avoid, or eliminate interfering matrix components by advanced sample preparation procedures, including sample extraction and cleanup.^{147,158} As Blessing et al. pointed out in a recent review on advances, pitfalls and perspectives for micropollutant CSIA, the analytical emphasis should be placed on optimized sample preparation in future research efforts.¹⁴⁶ Therefore, the context of this thesis focuses in the following on advances, shortcomings, and perspectives related to this aspect of analytical improvement for CSIA.

Recent method developments in sample preparation, including validated large-volume (LV) SPE protocols,¹⁶⁴ sample cleanup by preparative high-performance liquid chromatography (HPLC) combined with large-volume and cold-on-column injection,¹⁶⁵ and cleanup by molecularly imprinted SPE (MISPE),¹⁶⁶ enabled (i) analyte enrichment from large sample volumes (i.e., ≥ 10 L) without inducing isotope discrimination and (ii) accurate CSIA of MPs in environmental matrices down to approx. $0.5 \mu\text{g L}^{-1}$. However, even when LV SPE is implemented in combination with these selective cleanup procedures, matrix effects still hamper or even prohibit reliable isotope analysis in the sub- $\mu\text{g L}^{-1}$ concentration range, as illustrated in Figure 1.5. This is in particular true when the water sample contains high levels of dissolved organic carbon ($\text{DOC} > 2 \text{ mgC L}^{-1}$), as is the case for many natural surface waters (e.g., river systems, wetlands). Thus, additional optimization approaches of sample preparation workflows for target analytes in environmental matrices are direly needed. To fill this gap, a novel strategy complementary to sample cleanup is outlined in Chapter 1.4.1, which aims at increasing selectivity already in the analyte extraction step to avoid matrix co-enrichment in advance.

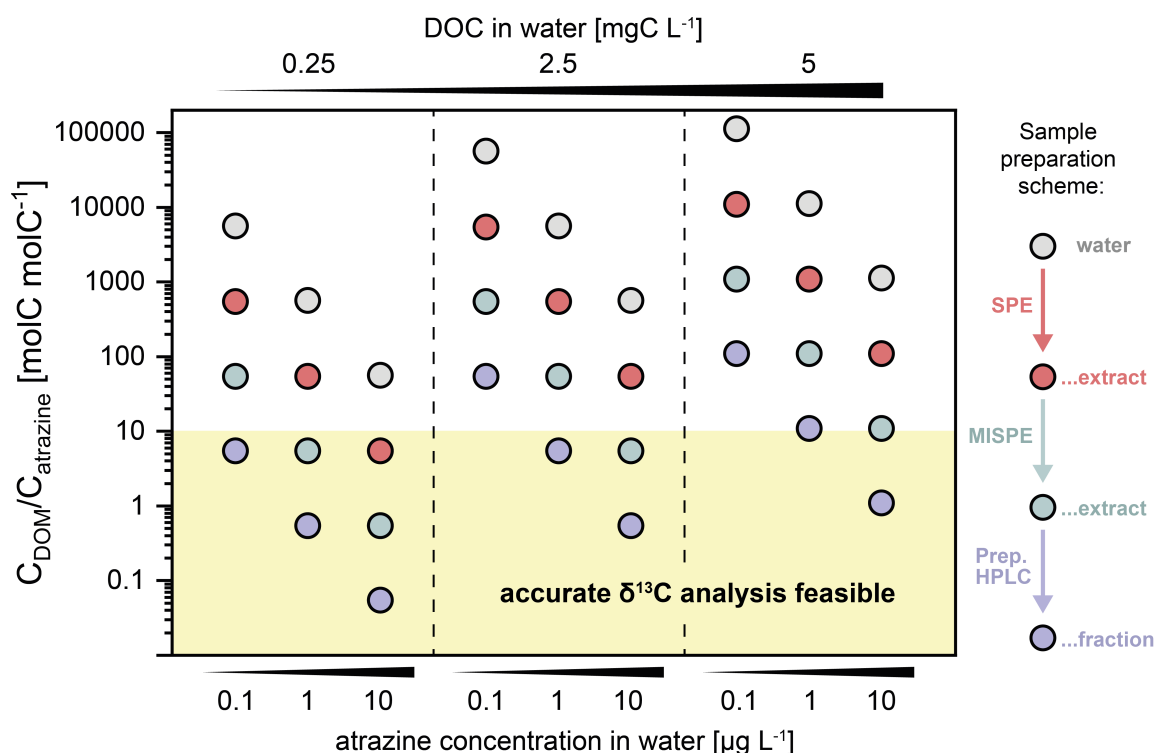


Figure 1.5. Carbon-normalized dissolved organic matter (DOM)-to-atrazine ratios, $C_{\text{DOM}}/C_{\text{atrazine}}$, in water samples and sample extracts after consecutive sample preparation by (i) solid-phase extraction (SPE) using the commercial Oasis HLB sorbent, followed by (ii) SPE with molecularly imprinted polymers (MISPE), and (iii) preparative high performance liquid chromatography (HPLC), depending on initial aqueous dissolved organic carbon (DOC) and atrazine concentration (top and bottom y-axis, respectively). Data points within the area highlighted in yellow (i.e., $C_{\text{DOM}}/C_{\text{atrazine}} \leq 10 \text{ molC molC}^{-1}$) represent sample extracts for which accurate $\delta^{13}\text{C}$ determination is feasible.¹⁵³

1.3.3 Laborious Handling of Large Sample Volumes

From a practical point of view, the laborious handling of tens to hundreds of liters of water is another key drawback for implementing micropollutant CSIA approaches into research and monitoring projects. First, the stringent analytical requirements for these large sample volumes entail technical, economic, and logistic difficulties which are associated with the active sampling in the field, the transport to the laboratory, as well as the sample preservation and storage. Second, and most notably, the subsequent analyte enrichment by LV SPE is highly labor-intensive and time-consuming. To better illustrate this practical issue, Table 1.2 summarizes technical parameters of three literature SPE methods (ref. 157,164,165) and the SPE protocol used for analyte preconcentration in Chapter 2 of this doctoral thesis. All these SPE methodologies were successfully validated for isotope integrity of the analyte atrazine during the enrichment process and used for preconcentration prior to CSIA. Given the required minimum extraction volumes for carbon (45 L) and nitrogen isotope analysis (259 L) of atrazine at an environmental concentration of 10 ng L^{-1} (Table 1.1), the SPE methods listed would involve between 4 and 12 ($\delta^{13}\text{C}$) and 22 and 65 ($\delta^{15}\text{N}$) parallel extractions in separate SPE cartridges/disks, respectively. The costs for consumables, solvents, and sorbent material (i.e., up to tens ($\delta^{13}\text{C}$) to hundreds ($\delta^{15}\text{N}$) of grams, Table 1.2) would consequently be significant even for a single sample.

Furthermore, the extraction procedures – if in the best case performed simultaneously – would last between 2 and 67 hours, since SPE is typically limited to relatively low flow rates in the mL min^{-1} range (Table 1.2). On top of this net SPE run time, there would be an additional need for extensive pre- and post-processing, including for instance sorbent packing, conditioning, washing, and elution, which would tie up considerable manpower in the laboratory. Micropollutant CSIA would therefore greatly benefit from advanced sample preparation methodologies based on high-throughput extraction concepts, which may even offer the potential to be implemented in automated onsite sampling devices. A strategy for transferring an efficient monolith-based LV extraction procedure for concentrating viruses and bacteria from water to a MP application is presented in Chapter 1.4.3.

Table 1.2. Solid-phase extraction (SPE) runtime and number of SPE cartridges/disks required (i.e., number of parallel extractions) for the extraction of atrazine at an environmental concentration of 10 ng L^{-1} to meet the stringent requirements of GC-IRMS. The parameters are given for three literature SPE methods and the protocol used in this thesis in Chapter 2, all of which were validated for isotope integrity during the enrichment of atrazine.

Reference	Schreglmann et al. (2013) ¹⁶⁵	Torrentó et al. (2019) ¹⁶⁴	Melsbach et al. (2020) ¹⁵⁷	Glöckler et al. (Chapter 2)*
SPE Sorbent	Bakerbond Speedisk H ₂ O-philic DVB	Phenomenex Septra ZT & Bakerbond SDB-1	Chromabond Easy	Oasis + Supel-Select HLB, LiChrolut EN, β -CDP
Sorbent Bed Weight (g)	n.a.	8 each	0.2	6
SPE Format	Disk (47 mm)	Cartridge (60 mL)	Cartridge (6 mL)	Cartridge (35 mL)
Volumetric Flow Rate (mL min^{-1})	100	5	1	20
Extraction volume per bed weight (L)	10	10	4	12
Required Extraction Volume [†] (L)	$\delta^{13}\text{C}$ $\delta^{15}\text{N}$		45 259	
Number of Parallel Extractions [‡]	$\delta^{13}\text{C}$ $\delta^{15}\text{N}$	5 26	5 26	12 65
Required Sorbent Mass [†] (g)	$\delta^{13}\text{C}$ $\delta^{15}\text{N}$	n.a. n.a.	40 each 208 each	2.4 13
Net Extraction Runtime [§] (h)		1.7	33.3	66.7

*up-scaled method for large-volume extraction based on linear flow velocities validated for carbon isotopic integrity

[†]volumes based on calculations for the enrichment of atrazine at a concentration of 10 ng L^{-1} as provided in Table 1.1

[‡]calculated based on required extraction volume and volume per bed weight

[§]assuming that all extractions are run in parallel at the same time

n.a. = not available

1.4 Strategies to Tackle the Analytical Limitations

1.4.1 Enhancing Selectivity in Solid-Phase Extraction Using Innovative Sorbent Materials

1.4.1.1 Lack of Selectivity in Conventional SPE Procedures

Owing to its versatility, ease of use, and relatively low cost, solid-phase extraction (SPE) has become the most widely used technique for analyte enrichment from liquid matrices.¹⁵⁰ In SPE, a liquid sample containing the target analytes is percolated through a solid phase, which is usually a sorbent packed in a polypropylene cartridge. The sorbent thereby retains the analytes by reversible dispersive (i.e., nonpolar), polar, and/or ionic intermolecular forces.¹⁶⁷ Inorganic and organic matrix components can then be partially washed off and, finally, the target analytes are recovered by elution with a suitable solvent (e.g., methanol or ethyl acetate). This separation process is based on the partitioning of the analytes between the solid and liquid phase, which is described by the equilibrium partitioning coefficient, K_d (L kg⁻¹), according to the Nernst's distribution law assuming a linear sorption at constant temperature and infinite dilution:

$$K_d = \frac{C_s}{C_l} \quad (T = \text{const.}) \quad (1.6)$$

where C_s (mg kg⁻¹) and C_l (mg L⁻¹) are the analyte concentrations in the solid and liquid phase, respectively. The analytes of interest are efficiently retained when their sorption affinity is significantly higher for the sorbent than for the liquid phase (i.e., $K_d \gg 1$).

Since the retention is governed by interactions between the functional groups of the target analytes and the sorbent, the choice of sorbent phase is key for an effective sample preparation workflow. To this end, a wide suite of reversed-phase SPE sorbents has been developed over the past few decades to provide high extraction efficiencies for a variety of different compounds, ranging from highly polar to moderately and nonpolar, and featuring acidic, basic, or neutral properties.¹⁴⁹ At this point, this work does not intend to provide an exhaustive list of commercially available sorbents (for this see for example ref. 149,168-170), but summarizes the most relevant developments and their major limitations for the application in micropollutant CSIA studies.

The first sorbents commercially introduced were silica-based and modified with functional groups, such as C₄, C₈, C₁₈, CH, NH₂, or phenyl. Later, they were followed by carbon-based sorbents, including activated carbon, graphitized carbon blacks, carbon nanotubes, and porous graphitic carbon. However, it was not until the development of high surface area polymeric sorbents with well-defined porosity that the limitations inherent to these early SPE sorbents could be overcome (e.g., low sorption capacities, pH limitations, irreversible sorption).¹⁶⁹ Conventional porous polymeric sorbents are mostly polystyrene divinylbenzene (PS-DVB) co-polymers with specific surface areas of up to 700 – 800 m² g⁻¹,

such as Amberlite XAD-4 manufactured by Rohm and Haas, PLRP-S and Bond Elut ENV by Agilent, or Strata SDB-L by Phenomenex. Their chemical structure and high surface area facilitate strong interactions with the target analytes through dispersive van der Waals and π - π interactions.¹⁶⁷ PS-DVB polymers have been further developed by hyper-cross-linking the monomers through a Friedel-Crafts reaction, which resulted in ultrahigh surface areas of up to $2000 \text{ m}^2 \text{ g}^{-1}$ and substantially increased retention capacities.¹⁷¹ Examples of commercial hypercross-linked sorbents are LiChrolut EN (Merck), Bakerbond SDB-1 (J.T. Baker), Chromabond HR-X (Macherey-Nagel), and Envi-Chrom P (Supelco).

The sorbent optimization continued with introducing polar moieties into the polymer network by copolymerization of DVB and a hydrophilic monomer, most notably *N*-vinylpyrrolidone and methacrylate.¹⁶⁷ The advantages of these so-called hydrophilic porous polymers are (i) the better water wettability of the resin that increases the contact between sorbent phase and analyte, and in turn the retention, and (ii) the promotion of additional polar interactions (i.e., dipole-dipole, hydrogen bonding) that especially improve the retention of polar analytes.¹⁶⁸ The most prominent polymeric sorbent is the hydrophilic lipophilic balanced (HLB) poly(vinylpyrrolidone-DVB) copolymer Oasis HLB (Waters Corporation). Owing to its high retention capacity and robustness, Oasis HLB has become the most widely used commercial sorbent in SPE of diverse compounds (e.g., pesticides, pharmaceuticals) from different sample matrices, including environmental waters, food, and biological fluids.¹⁷² Another way of manufacturing hydrophilic sorbents is to modify the surface of conventional PS-DVB polymers post-polymerization, for instance with acetyl, hydroxyl, benzoyl or pyrrolidone groups.¹⁶⁷ Chemically modified sorbents are commercially available, for example, under the brand names Supel-Select HLB (Supelco), Bond Elut PPL (Varian), and Strata-X/Sepra ZT (Phenomenex). All mentioned reversed-phase SPE sorbents were designed to suit various analytical fields by offering high capacity for uncharged compounds with a broad range of polarities. Consequently, they are also referred to as *low-specificity* or *nonselective* sorbents.¹⁷¹ The universal extraction character of commercial sorbents was complemented by mixed-mode phases that combine reversed-phase and ion-exchange functionalities for optimal retention of both neutral and ionizable compounds (e.g., Chromabond Easy or the Oasis mixed-mode suite: MCX, MAX, WCX, WAX).¹⁷³

As seen in Table 1.2, universal (i.e., nonselective) SPE sorbents given as examples in this chapter are frequently used for sample preparation in CSIA studies. However, their optimization toward a broad polarity range also fosters substantial coextraction of concurrent organic matrix. In quantitative terms, this can be illustrated by consulting the sorbents' system constants in polyparameter linear free energy relationships (pp-LFERs) for water as the sample solvent. pp-LFERs represent a robust approach to characterize the equilibrium partitioning of uncharged organic compounds in environmental and technical systems (e.g., SPE).¹⁷⁴ To this end, the most widely used pp-LFERs are the linear solvation energy relationships (LSERs) established by Abraham and co-workers,^{175,176} as presented in equation (1.7) for the partitioning between two condensed phases:

$$\log K_d = c + eE + sS + aA + bB + vV \quad (1.7)$$

where K_d is the free energy related equilibrium partitioning coefficient. The capital letters are solute descriptors, which are also referred to as Abraham or LSER descriptors: E , excess molar refraction; S , dipolarity/polarizability parameter; A , solute hydrogen bond acidity/donor; B , solute hydrogen bond basicity/acceptor; and V , McGowan molar volume. The small letters are the complementary solute-independent system constants, which are characteristic of the sorbent and liquid phase and which are determined experimentally by multi linear regression analysis.¹⁷⁶ The parameter c is a model constant which is not related to any specific interaction. The LSER equation consists of product terms of Abraham descriptor and corresponding system parameter, each of which represents the energetic contribution of a defined type of intermolecular interaction to the correlated K_d value. The eE term describes dispersive interactions (e.g., electron lone pair), sS describes interactions related to the surface polarity (e.g., dipole interactions), aA and bB represent hydrogen bonding interactions (i.e., aA : between H-bond donating solute and accepting sorbent, bB : vice versa), and vV represents energetic differences in cavity formation and dispersion interactions during the transfer of the analyte from the liquid to the solid phase.

Figure 1.6 depicts the system constants for the sorbents PLRP-S and Oasis HLB with water as the liquid phase, where only constants with a positive sign (red background) contribute to sorbent retention. For PLRP-S, which is deemed a nonselective PS-DVB sorbent,¹⁷⁷ retention is favored by the lower cohesion of the sorbent (v constant) and stronger electron lone pair interactions than water (e constant, mainly reflecting π - π interactions with the DVB monomer). However, the sorbent cannot compete with water for polar interactions in the form of dipole (negative s constant) and hydrogen bond interactions (negative a and b constants). This behavior is typical for all aqueous reversed-phase systems since the retention is inevitably dominated by the characteristic properties of water: (i) the strong cohesion that energetically promotes the analyte transfer to the sorbent phase, and (ii) the strong hydrogen-bond accepting capacity that reduces the retention of hydrogen-bond donating analytes.¹⁷¹ The further loss of selectivity of Oasis HLB is reflected by the increase of the a and b constants to less negative values (Figure 1.6), which means higher affinities of the optimized polymer design toward more polar compounds, including target analytes but also matrix components. The incorporation of the hydrophilic N-vinylpyrrolidone monomer into the polymer network explains the increased value of the hydrogen bond basicity for the solvated sorbent in contact with water (a constant).

The inherent lack of selectivity of commercial polymeric sorbents to exclusively extract the target analytes is thus recognized as a major drawback of MP analysis in surface water,¹⁷⁷ and resulting analytical interferences in chromatographic separation have been previously reported for different sorbents.^{178,179} It must be noted here that solutions exist for highly selective SPE applications, such as affinity chromatography-based phases (e.g., immuno-

affinity,¹⁸⁰ or molecular imprinting¹⁸¹). However, these selective SPE materials have to be tailor-made for every analyte of interest, which (i) requires expertise in for example the production of antibodies, (ii) entails high financial and time costs, and (iii) impedes straightforward and rapid method development. Therefore, increasing the selectivity in sample preparation by employing alternative sorbents that are not optimized for a wide polarity spectrum and thus exhibit high selectivity may offer a simple strategy to avoid substantial co-enrichment of matrix. Since sorbent chemistry is an active and dynamic research field in material sciences,¹⁷¹ matrix-susceptible analytical techniques, such as micropollutant CSIA, may therefore greatly benefit from novel and innovative sorbent technologies that have not (yet) crossed over to the commercial market.

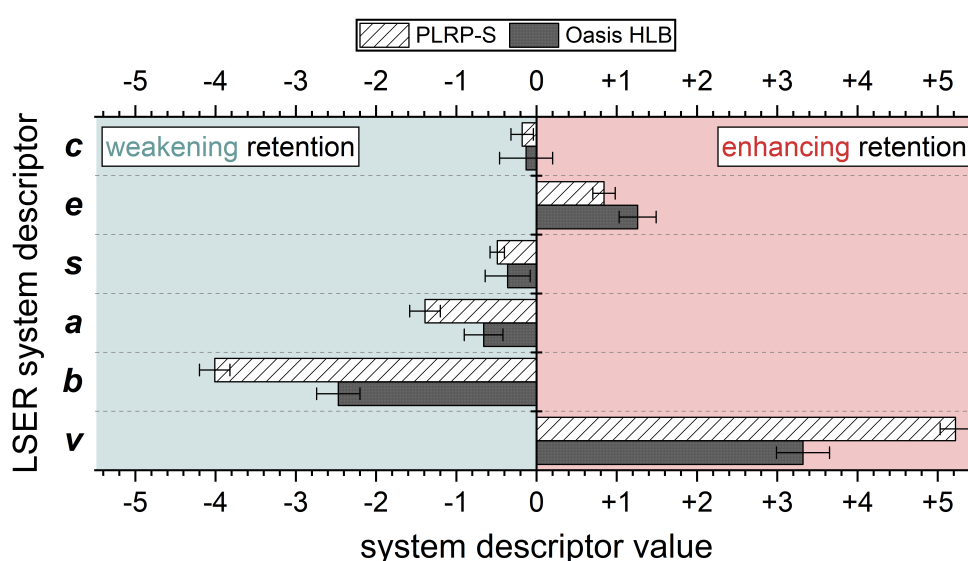


Figure 1.6. Linear solvation energy relationship (LSER) system constants for the polymeric SPE sorbents PLRP-S¹⁸² and Oasis HLB¹⁸³ for water as the sample solvent. Positive constants contribute to sorbent retention (red background), whereas negative constants indicate reduced retention (green background).

1.4.1.2 Porous Cyclodextrin Polymers as Selective Model Sorbent

Promising selective sorbent candidates are porous cyclodextrin-based polymers that recently emerged in the field of water purification technologies.¹⁸⁴ Discovered more than 130 years ago by Antoine Villiers, cyclodextrins (CDs) are macrocyclic oligosaccharides composed of several glucose units linked by α -1,4-glycosidic bonds, which can be economically and sustainably produced by the enzymatic degradation of starch.^{185,186} Owing to their toroidal, cone-shaped structure and apolar cavity (in relation to water), CDs can form inclusion complexes with thousands of organic compounds through host-guest interactions, which are mainly based on hydrophobic (i.e., favorable change in free energy during inclusion) and van der Waals forces.^{187,188} This characteristic encapsulation property and the advent of large-scale CD production in the 1980s stimulated a multitude of applications in various industrial sectors, including pharmaceuticals, food, biotechnology, agrochemistry, catalysis, or chromatography.¹⁸⁹ The long research and application history of CDs is comprehensively reviewed by Crini et al.^{185,190} Today, the so-called *native* CDs α -, β -, and γ -CD are

commercially available and are composed of six, seven, and eight glucose units, which translate into diameters of the interstitial cavity of 0.57, 0.78, and 0.95 nm, respectively.¹⁸⁶

To make use of CDs as efficient sorbent material, the water-soluble molecules must first be transferred into insoluble polymer networks.¹⁹¹ However, previous CD-based sorbents, especially those co-polymerized with epichlorohydrin, suffered from low surface areas and slow sorption kinetics so that they could not surpass the performance of traditional sorbents.¹⁹² By cross-linking β -CD with a perfluoroarene (i.e., tetrafluoroterephthalonitrile, TFN), Dichtel, Helbling, and co-workers succeeded in synthesizing the first high-surface-area CD polymer (TFN-CDP, $\sim 260 \text{ m}^2 \text{ g}^{-1}$)¹⁹³ as schematically illustrated in Figure 1.7. Its permanent mesoporous structure facilitates immediate access to the binding sites (i.e., superior sorption kinetics) and high sorption capacity so that TFN-CDP was demonstrated to outperform carbon-based¹⁹⁴ and polymeric sorbents (i.e., Oasis HLB)¹⁹⁵ in the removal of a variety of organic micropollutants from water (e.g., pesticides, pharmaceuticals, and lifestyle chemicals). Most notably, TFN-CDP offers a high selectivity for uncharged and cationic MPs over concurrent DOM as demonstrated by only limited inhibitory effects on micropollutant sorption onto CDPs in fresh- and wastewater.¹⁹⁴⁻¹⁹⁶ Although a low level of matrix co-enrichment has not yet been quantitatively proven, TFN-CDP holds promise as an ideal sorbent candidate for selective analyte extraction prior to sensitive CSIA.

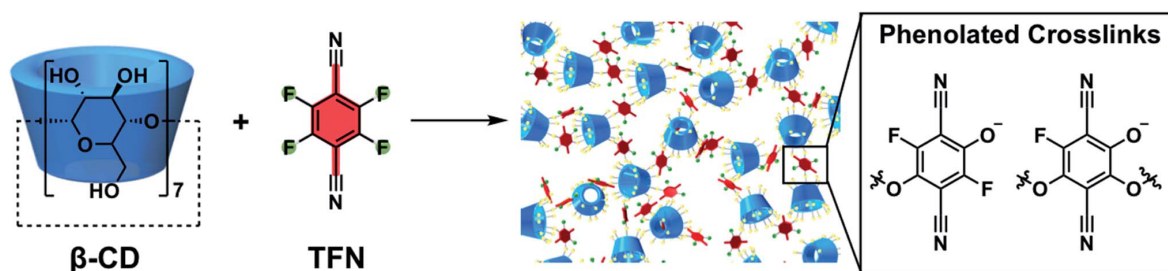


Figure 1.7. Scheme of cross-linking β -cyclodextrin (β -CD) with tetrafluoroterephthalonitrile (TFN) to yield TFN-CDP with phenolates in the cross-linkers as introduced by a side reaction of the polymerization. The figure was adapted from Klemes et al.¹⁹⁷ and is licensed under [CC BY 3.0](https://creativecommons.org/licenses/by/3.0/).

In order to further support selectivity optimization by sorbent design, a fundamental understanding of the sorption mechanisms is essential. However, although several attempts have been made to explain the observed selectivity of TFN-CDP, the underlying molecular drivers still remain elusive. Ling and co-workers concluded a size selectivity of the uniform CD cavities for compounds smaller than 0.6 kDa upon observing inhibited MP sorption in water samples rich in low-molecular weight DOM.¹⁹⁶ Yet, no size exclusion effect could be evidenced for selected MPs between 0.1 and 0.8 kDa applying quantitative structure-activity relationships (QSARs), so that the authors only postulated an upper size cut-off above 0.8 kDa.¹⁹⁸ In fact, the QSARs showed an opposite trend, namely a positive correlation between sorbate size and affinity to TFN-CDP. This was attributed to the fact that small molecules have access to the binding sites in the CD cavities, but interactions with them are limited due to their small size. Yet, this correlation can also be explained by the higher

amount of free energy required for water cavity formation for molecules of increasing size (cf. vV term in equation (1.7)), rendering their partitioning to the sorbent more favorable. On the other hand, it is known that the partitioning into the cavities of CD-based polymers is stronger for molecules of higher hydrophobicity,^{199,200} a compound-specific property that positively co-correlates with molecular size.

Furthermore, the importance of cross-linker interactions for the sorption process was highlighted by successfully tuning the sorbent selectivity toward different classes of organic contaminants (e.g., those of varying charge) through manipulation of the cross-linker chemistry. For example, the incorporation of protonated amines into the CDP-cross-linker increased the affinity for anionic compounds,²⁰¹⁻²⁰³ whereas negatively charged cross-linkers offer a high affinity for cationic compounds.^{194,197} The decisive role of electrostatic interactions for sorption on TFN-CDP was confirmed by QSARs, where descriptors representing interactions between negatively charged cross-linker moieties (i.e., phenolates introduced by a side reaction of polymerization, see Figure 1.7)¹⁹⁷ and cationic MPs were the most powerful sorption predictors.¹⁹⁸ It is therefore also conceivable that TFN-CDP strongly discriminates against negatively charged DOM constituents (e.g., carboxylic acids) through electrostatic repulsive forces. Moreover, Ching et al. identified the cross-linker hydrophobicity, in addition to its charge, as a crucial parameter for sorption to the polymer network.²⁰⁴

The notion of a synergistic interplay between inclusion complexes and complementary cross-linker interactions for TFN-CDP is consistent with previous literature on CD-based polymers, which stated that sorption depends on both the presence of CD moieties and the characteristics of the cross-linker (see Morin-Crini et al. 2018,²⁰⁰ and references therein). Still, important research questions remain open regarding the molecular drivers of TFN-CDP's selectivity for MPs over concurrent DOM. First, it has not yet conclusively elucidated whether size exclusion of large DOM compounds is the dominating factor, or whether other sorbent/sorbate properties, such as polarity (e.g., ability to form hydrogen bonds) or charge state, govern the selectivity. Second, the formation of host-guest inclusion complexes in TFN-CDP is generally challenged by recent atomistic molecular dynamics simulations for a closely related CDP (i.e., β -CD cross-linked with decafluorobiphenyl, DFB-CDP). In that study, analyte sorption was demonstrated to occur mainly onto the polymer network outside the CD cavities.²⁰⁵ To better understand the selective sorption behavior, which in turn can help optimize efficient sorbent design, determining the relative importance of the proposed sorption mechanisms is a prerequisite. To this end, further studies involving complex mixtures of target analytes and matrix compounds that are representative of a broad range of physicochemical properties (e.g., size, polarity, etc.) are required.

1.4.2 Sorbent Selectivity Assessment toward Dissolved Organic Matter (DOM)

1.4.2.1 Potential Control of DOM Composition on Sorbent Selectivity

As pointed out above, it is critical for accurate micropollutant CSIA to assess the SPE sorbent selectivity not only toward the target contaminant but also toward the most abundant interfering constituent of the natural water, namely DOM. However, when quantifying the coextracted DOM using bulk DOC analysis to obtain an *a priori* estimate of CSIA feasibility (i.e., $C_{\text{DOM}}/C_{\text{analyte}}$, as discussed in Chapter 1.3.2), it remains unclear which exact DOM fractions are retained or excluded by the sorbent. The detailed characterization of these fractions is, nonetheless, a crucial step to decipher their control on sorbent selectivity at the molecular level, thereby contributing to the further optimization of selective sample preparation workflows as outlined in this chapter.

DOM refers to the dissolved fraction of natural organic matter (NOM) in aquatic systems and is operationally defined as the organic molecules that pass through a membrane filter with a nominal pore size of 0.45 μm .²⁰⁶ It represents a complex mixture of thousands of organic compounds with extraordinary molecular diversity, formed as refractory decomposition products upon chemical and microbial degradation of dead matter (e.g., plants, animals, and microorganisms). The molecule sizes are highly variable, such that the molecular weight distribution of DOM in natural water can range from a few hundred to several thousand Daltons.²⁰⁷ As a source of energy, carbon, and other nutrients (e.g., nitrogen, phosphorous) for aquatic biota, DOM is an important component of freshwater ecosystems and involved in several biogeochemical processes, such as carbon cycling and microbial growth. Traditionally, DOM is classified into three major classes based on adsorption and ion exchange chromatography, namely *humic substances*, *hydrophilic acids*, and other *simple compounds* (e.g., small amino acids, carbohydrates, and hydrocarbons).²⁰⁸ Humic substances are the most prominent group of DOM compounds and are defined as the fraction that is isolated from water by sorption onto XAD resins.²⁰⁸ This group is further divided into sub-classes, where humic substances that precipitate in acidic solution (i.e., $\text{pH} = 1$) are referred to as *humic acids*, and those remaining dissolved are *fulvic acids*.²⁰⁹ However, this classification is operational and, thus, not necessarily based on compositional or structural differences of the molecules. Humic and fulvic acids, especially those provided by the *International Humic Substances Society* (e.g., Suwannee River, Pony Lake), are nonetheless routinely used as reference substances in DOM research.

More recently, the appreciation of the significant role of DOM in ecosystem functions together with analytical advances have stimulated the detailed DOM investigation at the molecular level.²¹⁰⁻²¹² These developments enabled the characterization and classification of DOM based on elemental composition and structural features of individual compounds resolved in the complex mixture. DOM compound classes are now assigned to their major biogeochemical precursor molecules and mainly encompass lipid-like, protein-like,

carbohydrate-like, lignin-like, tannin-like, and condensed aromatic compounds.²⁰⁷ Other common DOM structures worth mentioning are carboxylic-rich alicyclic molecules (CRAMs),²¹³ which are derived from linear terpenoids,^{212,214-216} and represent highly abundant constituents of freshwater DOM.²¹⁷⁻²²⁰ In general, DOM of all classes consist of (i) a carbonaceous structural framework, that is, an aromatic and/or aliphatic backbone,^{221,222} and (ii) a variety of functionalities, including neutral, acidic, and basic functional groups (Figure 1.8).^{207,208} As such, DOM is best described as an *organic matter continuum*, with compounds ranging from small to large, highly unsaturated to saturated, and nonpolar to highly polar.²⁰⁷ The retention of the individual DOM components during the SPE process strongly depends on possible interactions between their building blocks and the SPE sorbent. These mainly comprise nonpolar interactions with the aromatic and aliphatic DOM skeleton (i.e., van der Waals, π - π), polar interactions with polar neutral functionalities (i.e., hydrogen bonding, dipole-dipole), and electrostatic repulsive and attractive forces between localized charges on the sorbent surface and anionic or cationic DOM functional groups.

Hence, the examination of the sorption behavior of SPE sorbents from a matrix point of view, based on molecular information obtained from thousands of DOM compounds with widely varying physicochemical properties, bears great potential benefits for analytical advancements. First, insights into the chemodiversity of both retained and discriminated compounds can shed light upon molecular properties driving the sorbent selectivity (e.g., size, unsaturation, polarity), and may lead toward the development of even more selective polymer designs. Second, the identification of common molecular properties of retained DOM constituents can contribute to further optimizing the sample preparation procedure, since cleanup strategies could be specifically tailored for certain interfering compound classes. Third, molecular-level knowledge obtained from environmental samples can be transferred to other potential analytical fields, such as bio- or food analysis, to provide educated estimates of advantages and limitations of novel SPE materials (e.g., TFN-CDP) for different sample matrices.

In DOM research at the molecular level, an orthogonal analytical approach is often adopted, using complementary high-resolution techniques to compensate for limitations of one instrument with advantages of the other. Specifically, the combination of Fourier transform ion cyclotron resonance mass spectrometry (FTICR MS) and multi-dimensional (e.g., ^1H and ^{13}C) nuclear magnetic resonance (NMR) spectroscopy is most frequently applied to gain deep insights into the chemical composition and structure of complex DOM molecules.^{213,223,224} However, structural elucidation by NMR is limited to a small fraction of the total DOM pool and requires highly concentrated DOM isolates,²²⁵ which hampers the study of sorbent selectivity. Unlike NMR, FTICR MS offers detailed information on most individual compounds, and thus was primarily utilized in this work to establish a comprehensive and reliable understanding of DOM composition in sorbent extracts.

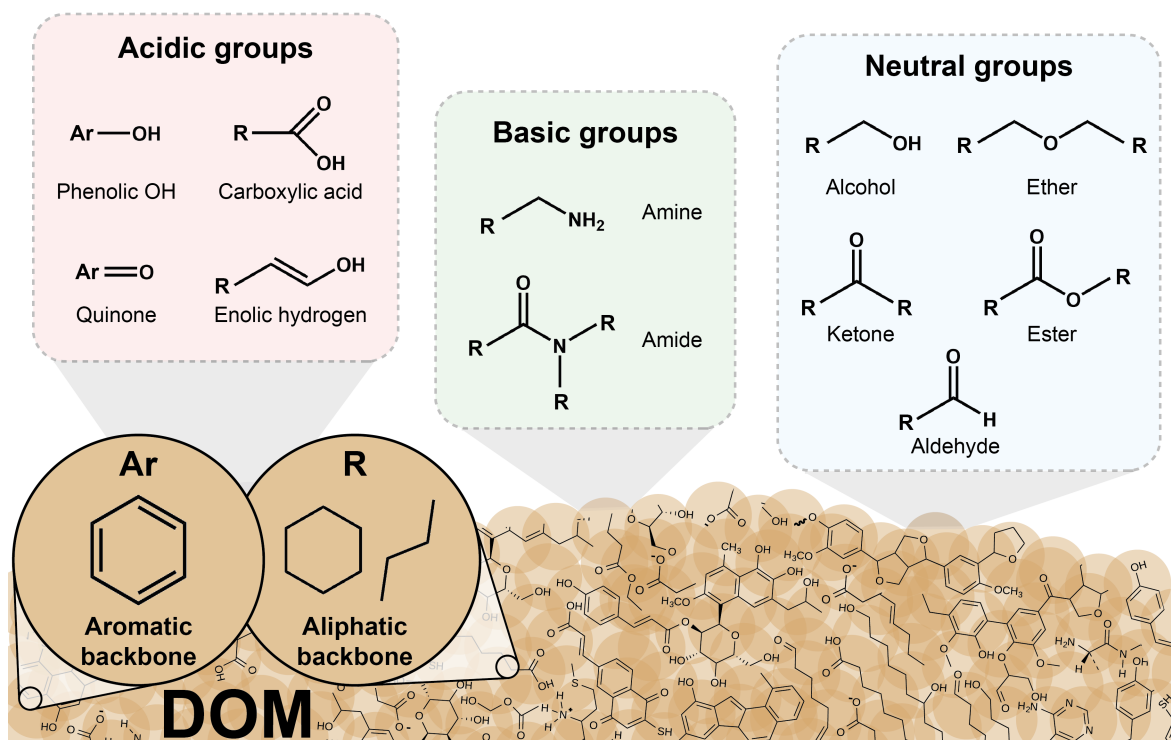


Figure 1.8. Graphical representation of the typical aromatic and aliphatic (e.g., alkyl or alicyclic groups) building blocks of the carbonaceous structural framework of dissolved organic matter (DOM) and important functionalities, including acidic, basic, and neutral functional groups.

1.4.2.2 Molecular DOM Characterization by Fourier Transform Ion Cyclotron Resonance Mass Spectrometry (FTICR MS)

FTICR MS is currently the technique of choice for state-of-the-art DOM research at the molecular level (e.g., ref. 210,211,226,227). In FTICR MS, the sample molecules are first ionized by electrospray ionization (ESI) and then transferred into an ion cyclotron cell, where they are trapped in a homogeneous magnetic field (usually 7 – 21 T) and circulate in spiral paths around the central axis of the cell at their characteristic cyclotron frequency, ω_c . The cyclotron frequency is determined by the magnitude of the magnetic field and inversely proportional to the mass-to-charge ratio m/z :

$$\omega_c = \frac{qB}{m} \quad (1.8)$$

where B is the magnetic field strength and q is the ion charge. The latter is calculated by multiplying the number of charges z by the charge of an electron, which means that m/q is directly related to m/z .

For detection, an electric field orthogonal to the magnetic field excites the ions, which increases the radius of their orbit but not their cyclotron frequency.²²⁸ Consequently, the ions oscillate closer to a pair of detector plates, where they can induce an image current on the electrodes. As the ions lose the orbit radius due to field inhomogeneities and collapse toward the central core of the cell, the image current trace is detected as a function of time and

recorded as the so-called *free induction decay* (FID). Software then performs a Fourier transformation on the FID to convert the signal from the time to the frequency domain and finally to the m/z domain by mass-calibration.²¹¹ Due to its highly accurate measurement of ion frequencies, FTICR MS possesses the advantage over other mass spectrometry techniques of an unparalleled ultrahigh mass resolving power (i.e., $R = 10^5 - 10^6$) and mass accuracy (i.e., parts-per-billion (ppb) level) across a wide mass range from a hundred to several thousand Daltons. These unique features allow for (i) sufficient resolution and distinction of peaks with close mass differences of a few millidaltons (e.g., O vs. CH₄, $\Delta m = 0.036$ Da) that are typical for complex chemical mixtures such as environmental DOM. Further (ii) they enable the confident assignment of elemental formulas (i.e., C_cH_hO_oN_nS_s, where c, h, o, n, and s are the numbers of the respective element) to thousands of individual compounds.

To reduce the complexity of FTICR MS data and to facilitate straightforward interpretation, several methods of data analysis have been developed. For example, visualization in the form of a *van Krevelen diagram* (i.e., the elemental H/C ratio of compounds plotted against the O/C or less common the N/C ratio) can be used as a molecular mapping technique to evaluate how DOM formulas overlap with those of general compound classes (e.g., lipid-like, lignin-like, tannin-like, etc., Figure S3.5).²²⁹ In addition, molecular properties of DOM compounds, including size, degree of oxygenation, or degree of unsaturation, can be examined using van Krevelen diagrams in combination with other data visualization such as *mass-edited H/C* and *O/C plots* (i.e., elemental ratios versus m/z values). Double bond equivalents (DBE) and the alternative *aromaticity index*, the latter also accounting for common C=O double bonds in DOM, are useful parameters to characterize the unsaturation and aromaticity of DOM molecules.^{230,231} Moreover, multivariate statistical approaches, such as principle component analysis (PCA) or hierarchical cluster analysis (HCA), are indispensable tools to reduce the large (normalized) datasets to a few factors, which allows for straightforward sample comparison.²³² FTICR MS is therefore ideally suited as a fingerprinting technique to (i) specifically pinpoint DOM compound classes that are preferentially retained and excluded by selective sorbent materials and (ii) to probe for characteristic molecular properties of DOM molecules that govern their selective sorption.

1.4.3 High-Throughput Extraction by Chemically Modified Polymer Monoliths

Porous monolithic materials are known as efficient sorbents in separation sciences (e.g., liquid and electrochromatography) and represent alternative stationary phases to particle packed SPE formats.^{233,234} For LV applications in CSIA workflows they appear particularly attractive, since their macroporous structure (i.e., pores in the μm range) enables analyte extraction at high flow rates (i.e., hundreds of milliliters to liters per minute) and moderate backpressures resulting in shorter sample processing times.²³⁵ The main types of monoliths are either silica-based (inorganic) or polymer-based (organic). Whereas silica-based monoliths are difficult to prepare, polymer-based monoliths offer excellent tuneability of the surface chemistry to target specific compound classes along with comparative ease of synthesis.²³⁶ They are readily produced by a single-step polymerization of a mixture of functional and cross-linking monomers, porogenic solvents that control the porosity, and a radical initiator.²³³ Common functional monomers are styrene and alkyl methacrylate, while dimethyl methacrylate and DVB are frequently used cross-linking monomers.²³⁵ The *in situ* synthesis is usually conducted in suitable molds or housings, which renders polymer-based monoliths highly versatile, as applications in a wide variety of formats are possible. In addition, the rigidity and portability of the monolithic discs facilitate the preconcentration of LV samples directly in the field using dedicated on-site extraction devices.

However, polymer-based monoliths typically lack a dual porosity, that is, they do not exhibit additional mesopores (i.e., 2 – 50 nm). As a consequence of the resulting low specific surface area in the low $\text{m}^2 \text{g}^{-1}$ range, polymeric monoliths are not efficient for SPE of small molecules, such as pesticides or pharmaceuticals,²³⁶ and show high affinities only for viruses and macromolecules (e.g., proteins, nucleic acids).²³⁷ A strategy for fast and efficient extraction of small molecules is to combine the high porosity of polymeric monoliths with the unique properties of nanomaterials by either embedding during polymerization or immobilization on the monolith surface post-polymerization. For instance, the incorporation of carbon-based nanomaterials, which exhibit an extremely high ratio of surface area to volume, can significantly increase the surface area of the monolith.²³⁸ As a result, sorption affinities and kinetics for small molecules are generally improved, while selectivity toward different analyte classes can be tailored through specific interactions provided by the functionalities of the chosen nanomaterial. Promising carbon-based nanoparticles are graphene sheets, which consist of two-dimensional, “honeycomb-like” layers of sp^2 -hybridized carbon atoms (Figure 1.9). The ultrahigh specific surface area of graphene (i.e., theoretically up to $2630 \text{ m}^2 \text{ g}^{-1}$) and its large delocalized π -electron system provide high sorption capacities for nonpolar aromatic ring structures (as ubiquitously present in organic MPs) due to strong van der Waals and π - π interactions.²³⁹ Graphene is considered highly nonpolar and is thus efficient in retaining nonpolar analytes with $\log K_{\text{ow}}$ values above 3.²⁴⁰ For more polar analytes, graphene oxide (GO) represents the more suitable sorbent material,

as its various functional groups (i.e., hydroxy, carboxy, epoxy, Figure 1.9) promote additional polar interactions.²⁴¹ Furthermore, the functionalities enhance the water wettability and facilitate the covalent coupling to the polymeric monolith. Graphene-modified monoliths have been successfully applied for the extraction of different contaminants from small volumes of water, for example, herbicides,²⁴² insecticides,²⁴³ benzotriazole,²⁴⁴ polychlorinated biphenyls and steroid hormones,²⁴⁵ and phenolic compounds.²⁴⁶ Moreover, it was shown that chemical reduction of the incorporated GO to reduced graphene oxide (rGO) yielded optimal sorption properties for reversed-phase SPE applications.²⁴⁷ rGO provides the best balance between affinity toward aromatic compounds through nonpolar π - π stacking, and residual polar functional groups (Figure 1.9) which impart a *hydrophilic lipophilic balanced* character to the sorbent material. Hence, monoliths modified with rGO are promising high-performance yet nonselective sorbent candidates for fast LV SPE applications in environmental analyses (e.g., micropollutant CSIA).

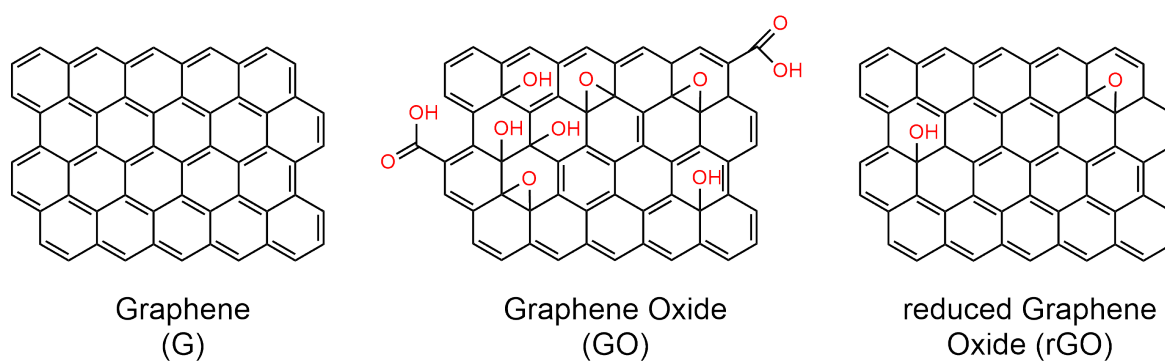


Figure 1.9. Structures of graphene (G), graphene oxide (GO), and reduced graphene oxide (rGO).

1.5 Objectives and Approach of the Thesis

CSIA is an indispensable tool for understanding the behavior of organic compounds in the environment, assessing their sources and degradation pathways, and identifying underlying transformation mechanisms (Chapter 1.2). However, as outlined in Chapter 1.3, analytical challenges associated with the limited sensitivity of the technique still hamper the transfer of the CSIA approach to low-occurring MPs in field applications. This work addresses these limitations by advancing sample preparation methodologies, with particular research emphasis on analyte extraction from environmental aquatic matrices, through implementing the strategies presented in Chapter 1.4: (i) Enhancing selectivity in SPE using innovative sorbent materials, (ii) assessing the sorbent selectivity toward organic matrix constituents at the molecular level by nontargeted FTICR MS analysis, and (iii) enabling high-throughput extraction using chemically modified polymer monoliths. The overarching goal of this dissertation is therefore to provide improved extraction methods, which in combination with established sample cleanup procedures can help push the lower limits of accurate CSIA toward the environmentally relevant sub- $\mu\text{g L}^{-1}$ concentration range.

To meet this goal, two different approaches were taken. The first approach addressed the analytical interferences caused by organic matter that is co-enriched during SPE using conventional universal sorbent phases. Here, the specific objectives were (i) to increase selectivity in the analyte extraction step by employing a cyclodextrin-based SPE sorbent to mitigate matrix co-enrichment in advance and (ii) to gain in-depth knowledge about the controls on sorbent selectivity that can contribute to further optimize selective sample preparation workflows. The second approach addressed the bottleneck of laborious large-volume sample preparation for micropollutant CSIA. It specifically aimed at developing a high-throughput extraction method that can be combined with selective cleanup strategies for effective CSIA applications. The following four research projects were designed and completed, with projects 1 to 3 pursuing the objectives of the first approach and project 4 following the second approach.

Chapter 2, entitled *Avoiding Interferences in Advance: Cyclodextrin Polymers to Enhance Selectivity in Extraction of Organic Micropollutants for Carbon Isotope Analysis*, presents the first application of novel cyclodextrin-based polymers as selective SPE sorbents in CSIA methodologies. Specifically, the synthesized polymers of different cavity size (i.e., α -, β -, γ -CDP) were (i) investigated for their selectivity toward a selection of pesticides in presence of interfering DOM based on recovery, partitioning, and Gibbs free energy of adsorption data, (ii) assessed for their applicability to carbon isotope analysis of the model compounds atrazine, *S*-metolachlor, boscalid, and azoxystrobin in natural water, and (iii) benchmarked against commonly used commercial, polymeric SPE sorbents (i.e., Oasis HLB, LiChrolut EN, and Supel-Select HLB). The study provides matrix-dependent limits of accurate carbon isotope analysis on GC-IRMS, as well as a comprehensive validation of carbon isotopic integrity for the cyclodextrin-based SPE-CSIA procedure.

In Chapter 3, entitled *Selectivity of β -Cyclodextrin Polymer toward Aquatic Contaminants: Insights from Ultrahigh-Resolution Mass Spectrometry of Dissolved Organic Matter*, the selective β -CDP-based SPE procedure presented in Chapter 2 was applied to pristine surface and groundwater samples. Subsequently, nontargeted Fourier transform ion cyclotron resonance mass spectrometry (FTICR MS) analysis was performed to elucidate the molecular chemodiversity of the extracted DOM in comparison to the universal SPE sorbents Oasis HLB, LiChrolut EN, and Supel-Select HLB. The ultrahigh-resolution MS data presented in this chapter offers detailed molecular-level information on thousands of matrix compounds retained and excluded by the sorbents, contributing to a better understanding of sorbent selectivity and thus to sample preparation optimization. In particular, the findings of this study are placed in a broader context to offer implications for matrix-susceptible methodologies to the general analytical chemist.

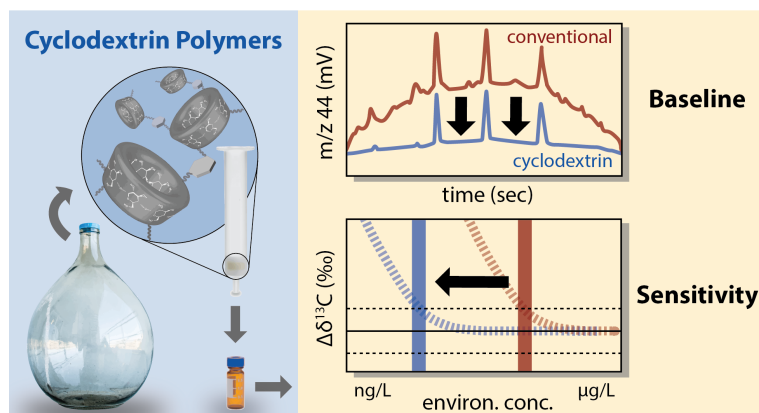
Chapter 4, entitled *Discriminative Behavior of Cyclodextrin Polymers against Dissolved Organic Matter: Role of Cavity Size and Sorbate Properties*, systematically investigated the underlying molecular drivers of α -, β -, and γ -CDP's selectivity, which was observed and described in Chapter 2 and 3, in order to contribute to future sorbent design and selectivity optimization. Specifically, the study examined the role of (i) a potential size-driven selectivity induced by the uniform CD cavities that has been previously suggested in literature and (ii) other sorbate properties that may govern their selective sorption on the CDPs (e.g., degree of oxygenation, unsaturation, and aromaticity). To this end, new insights into the sorption mechanisms were gained through independent experimental designs, including SPE experiments with a selection of MPs in competition with different DOM size fractions (i.e., <1, 1 – 3, 3 – 10, >10 kDa) and ultrahigh-resolution FTICR MS analysis of extracted DOM from different origin (i.e., pristine surface water, Suwannee River humic and fulvic acid), which is representative of a broad range of physicochemical properties.

Chapter 5, entitled *Graphene-Modified Polymer Monoliths for High-Throughput Extraction of Micropollutants: A Proof-Of-Concept Study*, exploited the synergistic effect of combining the high porosity of polymer-based monolithic stationary phases with the unique sorption properties of graphene, a carbon-based nanomaterial, for SPE of a suite of pesticides at high flow rates. The specific aim was to transfer the *Monolithic Adsorption Filtration (MAF)*, which had already been successfully established at the Chair of Analytical Chemistry and Water Chemistry at TUM for the extraction of viruses and bacteria, to a large-volume SPE application for small molecules such as organic MPs.

In Chapter 6, the main findings of this work are synthesized into a general conclusion, and areas are identified that require further investigation in future research.

Chapter 2

Avoiding Interferences in Advance: Cyclodextrin Polymers to Enhance Selectivity in Extraction of Organic Micropollutants for Carbon Isotope Analysis



Abstract

Compound-specific isotope analysis (CSIA) of organic water contaminants can provide important information about their sources and fate in the environment. Analyte enrichment from water remains nonetheless a critical yet inevitable step before measurement. Commercially available solid-phase extraction (SPE) sorbents are inherently nonselective leading to coextraction of concurrent dissolved organic matter (DOM) and in turn to analytical interferences, especially for low-occurring contaminants. Here, we (i) increased extraction selectivity by synthesizing cyclodextrin polymers (α -, β -, γ -CDP) as SPE sorbents, (ii) assessed their applicability to carbon isotope analysis for a selection of pesticides, and (iii) compared them with commonly used commercial sorbents. Extraction with β -CDP significantly reduced backgrounds in gas chromatography-isotope ratio mass spectrometry (GC-IRMS) and enhanced sensitivity by a factor of 7.5, which was further confirmed by lower carbon-normalized $C_{\text{DOM}}/C_{\text{analyte}}$ ratios in corresponding extracts as derived from dissolved organic carbon (DOC) and liquid chromatography-tandem mass spectrometry (LC-MS/MS) analysis. Gibbs free energies of adsorption demonstrated weak competition between DOM and analyte on the three CDPs. No isotopic fractionation ($\Delta\delta^{13}\text{C}$ within $\pm 0.3\text{‰}$) was observed for the investigated pesticides after using β -CDP as an SPE sorbent covering a range of concentrations ($5\text{--}500\ \mu\text{g L}^{-1}$), flow velocities ($5\text{--}40\ \text{cm min}^{-1}$), and sorbent regeneration (up to six times). The present study highlights the benefit of selecting innovative extraction sorbents to avoid interferences in advance. This strategy in combination with existing cleanup approaches offers new prospects for CSIA at field concentrations of tens to hundreds of nanograms per liter.

The results of this chapter were published in modified form in the peer-reviewed paper cited below.

Reprinted with permission* from:

David Glöckler, Christopher Wabnitz, Martin Elsner, Rani Bakkour. Avoiding Interferences in Advance: Cyclodextrin Polymers to Enhance Selectivity in Extraction of Organic Micropollutants for Carbon Isotope Analysis. *Analytical Chemistry* **2023**, 95 (20), 7839-7848. DOI: 10.1021/acs.analchem.2c05465

ACS Articles on Request author-directed link:

<https://pubs.acs.org/articlesonrequest/AOR-INFKP5IGVBZHWYDH838>

Copyright © 2023 American Chemical Society.

*For the reprint permission, refer to Chapter S6.2.

2.1 Introduction

Compound-specific isotope analysis (CSIA) has been established as a powerful analytical technique to evaluate the origin and fate of organic contaminants in environmental systems.^{73,100,116,144,158} While characteristic stable isotope ratios (e.g., $^{13}\text{C}/^{12}\text{C}$, $^2\text{H}/^1\text{H}$, $^{15}\text{N}/^{14}\text{N}$) in individual compounds can delineate different sources of otherwise identical chemicals,⁸⁷⁻⁹¹ the measurement of changes in such compound-specific isotope signatures can detect their (bio)degradation in field settings where concentration measurements alone would not be conclusive.⁹²⁻⁹⁷ When changes are measured for isotopes of different elements, the identification of characteristic isotope effects may even decipher underlying transformation mechanisms.^{72,76,248-251} Today, CSIA is well established for legacy contaminants (e.g., chlorinated hydrocarbons, BTEX, or fuel oxygenates) which are typically present in the high $\mu\text{g L}^{-1}$ to mg L^{-1} concentration range at contaminated sites.⁷⁷ In contrast, polar organic micropollutants, such as pesticides, pharmaceuticals, and personal care products, occur in much lower environmental concentrations rendering the transfer of the CSIA approach to field applications analytically challenging.^{80,146,147} Given that 1 to 10 nanomoles of carbon is the minimum for precise isotope analysis by gas or liquid chromatography coupled with isotope-ratio mass spectrometry (GC- or LC-IRMS),^{118,121} this implies that tens to hundreds of liters of water need to be extracted when micropollutant concentrations are in the nanogram per liter range.

A wide suite of solid-phase extraction (SPE) sorbents has been commercially introduced during the last decades, which are available for sample preconcentration.¹⁵⁰ In particular, the development of hyper-cross-linked and hydrophilic polymeric sorbents has overcome inherent limitations of traditional silica- or carbon-based sorbents, such as low sorption capacities, pH limitations, or irreversible sorption.¹⁶⁷ To suit a large variety of analytical applications, polystyrene-divinylbenzene (PS-DVB)-based polymers were designed to favor both hydrophobic and polar intermolecular interactions, thus capturing organic compounds with a broad range of polarities.¹⁶⁸ However, this broad-range substrate spectrum comes with a lack of selectivity²⁵² that inevitably promotes concomitant enrichment of dissolved organic matter (DOM) during sample preparation. In consequence, matrix constituents of unknown isotopic composition (hereafter referred to as unresolved complex mixture (UCM)) lead to analytical interferences and may compromise reliable isotope ratio measurements.^{145,151,152} Hence, there is a strong demand for improved and carefully validated sample preparation procedures to push quantification limits of sensitive and accurate CSIA toward environmentally relevant concentrations.^{146,157,159}

So far, the emphasis of sample preparation strategies for CSIA has been on cleanup approaches to eliminate co-enriched organic matrices from extracts using, for example, preparative high-performance liquid chromatography (HPLC)¹⁶⁵ or selective molecularly imprinted polymers (MIPs).¹⁶⁶ In contrast, this work has a fundamentally new focus. Our aim is to increase selectivity already in the analyte extraction step in order to mitigate co-

enrichment of DOM in advance. We hypothesize that sorbents, which are not optimized for a wide polarity spectrum, may possess the warranted selectivity by offering high affinities toward compounds of interest, while discriminating against polar organic matter. Recently, porous cyclodextrin polymers (CDPs) have gained growing attention as alternative sorbents for water purification technologies.^{184,193} Cyclodextrins are macrocyclic oligosaccharides composed of glucose units, which are linked by α -1,4-glycosidic bonds,¹⁸⁵ and their cavities are well known to form inclusion complexes with diverse organic compounds.¹⁸⁸ When the cyclodextrin composed of seven glucose units (β -CD) is cross-linked with rigid aromatic groups via nucleophilic aromatic substitution, the permanent mesoporous structure of this polymer derivate (β -CDP) entails a high surface area (i.e., $263 \text{ m}^2 \text{ g}^{-1}$) so that these materials offer the benefit of excellent sorption properties and regeneration capacity.¹⁹³ Comparative studies demonstrated that β -CDP outperformed carbon-based¹⁹⁴ and polymeric sorbents¹⁹⁵ in rapid removal of a variety of organic micropollutants from water, owing to a synergistic interplay of inclusion complexes and secondary cross-linker interactions.^{201,253} CDPs, therefore, hold promise as ideal sorbent candidates for analyte extraction before CSIA. In particular, concurrent DOM was shown to have only limited inhibitory effects on micropollutant sorption onto CDPs,^{194,196} implying a low level of matrix co-enrichment. Yet, a quantitative assessment of DOM coextraction by CDPs and its impact on accurate isotope ratio determination has never been explored.

The objectives of this work were therefore (i) to assess the applicability of β -CDP for carbon isotope analysis of micropollutants in natural water and define matrix-dependent limits of accurate isotope analysis on GC-IRMS; (ii) to quantitatively assess selectivity of CDPs of varying cavity size (i.e., α -, β -, γ -CDP) for a selection of pesticides; (iii) to accomplish this through determining the relative recoveries of target analytes and DOM in SPE, measuring partition coefficients of target analytes in batch experiments, and exploring competition between target analyte and DOM in column experiments; and lastly (iv) to validate carbon isotopic integrity after CDP-based enrichment in regard to analyte concentrations, flow rates, and reusability potential. The performance of CDPs was benchmarked against Oasis HLB, LiChrolut EN, and Supel-Select HLB as three commercial, polymeric SPE sorbents.

2.2 Experimental Section

2.2.1 Chemicals and Materials

A detailed description of chemicals and materials is provided in the Supporting Information including CAS number, purity, grade, and supplier (S2.1); standard solutions and ultrapure water (S2.2); sorbents and packing materials (S2.3); and physicochemical properties of the selected target analytes (Table S2.2).

2.2.2 Preparation and Characterization of Porous Cyclodextrin Polymers

Porous cyclodextrin polymers were synthesized based on the nucleophilic aromatic substitution of cyclodextrin hydroxyl groups by tetrafluoroterephthalonitrile (TFN). The improved procedure reported by Alsbaiee et al.¹⁹³ was utilized for the synthesis of β -CDP and adapted for the synthesis of α - and γ -CDP. To this end, a flame-dried 500 mL round-bottom flask was charged with the respective amounts of reagents (Table S2.5) at a molar ratio of 1.0:2.9:12.8 of cyclodextrin:cross-linker:potassium carbonate, respectively. After adding 160 mL of an anhydrous tetrahydrofuran/dimethylformamide mixture (9:1, v/v) the flask was connected to a reflux condenser and the system was flushed with nitrogen for 10 min. Subsequently, the nitrogen inlet was removed and the reflux condenser was closed with a septum. The mixture was placed in an oil bath (85 °C) and stirred for 48 h. Thereafter, the suspension was slowly cooled to room temperature while the solids could settle at the bottom of the flask. The supernatant was decanted and the residual potassium carbonate was removed by washing with 1 M hydrochloric acid until CO₂ evolution stopped. The remaining suspension was filtered and sequentially washed with 250 mL of ultrapure water, 200 mL of tetrahydrofuran, 200 mL of dichloromethane, and 200 mL of methanol. The polymers were finally dried under vacuum for 48 h and, subsequently, sedimented in methanol to obtain particle sizes larger than 40 μ m. Scanning electron microscopy imaging (S2.4.2) and Fourier transform infrared spectroscopy (S2.4.3) confirmed successful synthesis of the polymers.

2.2.3 Sampling and Pretreatment of Surface Water Samples

Surface water samples were taken in the creek Wiesäckerbach, Garching, Germany (latitude 48.121905, longitude 11.511416) using glass bottles, which were pre-washed with methanol and ultrapure water. Samples were immediately passed through pre-rinsed 0.45 μ m nylon membrane filters (47 mm, GVS, USA). In accordance with dissolved organic carbon (DOC) stability tests (Figure S2.3), further experiments were performed within 5 days of sample storage at 4 °C in the dark. DOC concentrations of water samples ranged between 2.3 and 3.5 mg L⁻¹. Other physicochemical parameters of the surface water are given in Table S2.6.

2.2.4 Sample Preparation Procedures Using Cyclodextrin-Based and Conventional Sorbents

Sample preparation in this work consisted of SPE of pristine or analyte-spiked surface water samples using CDPs and commercial SPE sorbents, and different pre- and post-treatment steps. Throughout all SPE experiments, self-packed polypropylene SPE cartridges (1, 3, and 6 mL, Supelco) were used with sorbent bed weights ranging from 20 to 500 mg and a constant ratio between sorbent bed weight and sample volume at 0.5 mg mL^{-1} . Before extraction, water samples were adjusted to either pH 3 or pH 7 using 1 M HCl or 1 M NaOH. Unless specified otherwise, SPE was performed using a 12-port vacuum SPE manifold at a volumetric flow rate of $\leq 1.0 \text{ mL min}^{-1}$ corresponding to linear flow velocities of $\leq 4.1 \text{ cm min}^{-1}$ (1 mL cartridge), $\leq 1.6 \text{ cm min}^{-1}$ (3 mL) and $\leq 0.8 \text{ cm min}^{-1}$ (6 mL). Upon elution with methanol, extracts were further processed to suit the analytical requirements of subsequent chemical and isotopic analyses. Detailed information on the experimental design is given in the following sections. All SPE experiments were conducted in triplicates and associated uncertainties were propagated according to the Gaussian error propagation law.

2.2.4.1 Impact of Organic Matrix on GC-IRMS Determination of $\delta^{13}\text{C}$

To explore the impact of co-enriched organic matrix on carbon isotope analysis of pesticides using GC-IRMS and to investigate the role of selective SPE, we compared identical SPE-CSIA procedures utilizing either β -CDP or Oasis HLB. To this end, 1 L pristine water samples (2.3 mgC L^{-1} , pH 7) were extracted using 500 mg of sorbent in 6 mL cartridges, which were conditioned with 10 mL of methanol and 20 mL of ultrapure water. Once the samples were loaded, cartridges were dried under vacuum overnight and subsequently eluted with 6 mL of methanol. Eluates were evaporated to dryness ($65 \text{ }^\circ\text{C}$, N_2 , TurboVap LV, Biotage, Sweden) and then reconstituted in 0.5 mL of methanol. A series of different organic matrix amounts were obtained by transferring different volumes of the eluate (i.e., 10 to 150 μL , equivalent to 20 to 300 mL of extracted water) to separate vials. After evaporation, the dry residues were reconstituted in 30 μL of methanolic in-house standard, containing the GC-amenable analytes atrazine, *S*-metolachlor, boscalid, and azoxystrobin of known isotopic composition and at concentrations of 0.21, 0.11, 0.09, and 0.08 mmol L^{-1} , respectively (i.e., equivalent to 5 nmol C injected into the GC column). Finally, carbon isotope ratios were measured by GC-IRMS.

2.2.4.2 Micropollutant and DOM Extraction

We compared the extraction efficiencies of CDPs and commercial sorbents for 11 target analytes at environmentally relevant concentrations of $1 \text{ } \mu\text{g L}^{-1}$ (for spiking refer to S2.6.1) and DOM, the latter being quantified by dissolved organic carbon (DOC) analysis. The influence of the pH on the sorption behavior was studied by performing SPE experiments at both acidic (pH 3) and neutral (pH 7) conditions. Initial analyte and DOC concentrations

were determined immediately before experiments. Before sample loading, SPE cartridges were conditioned with 1 mL of methanol followed by 500 mL of ultrapure water. In pre-experiments, this procedure was shown to reduce organic carbon bleeding from sorbent material to a constant low level (Figure S2.4). Twenty mL of water sample was then loaded onto 10 mg of sorbent. Filtrates were collected and subjected to DOC analysis. After loading, sorbents were dried under vacuum and subsequently eluted with 0.5 mL of methanol. Similarly, we prepared procedural blanks by loading every sorbent with ultrapure water. Finally, analytes and DOC were quantified in eluates.

Recoveries of analyte i (R_i) and DOC (R_{DOC}) were calculated according to equation (2.1) and (2.2), respectively:

$$R_i [\%] = \frac{\left(\frac{C_{i,eluate}}{EF}\right)}{C_{i,initial}} \times 100 \quad (2.1)$$

$$R_{DOC} [\%] = \frac{m_{C,eluate}}{m_{C,initial}} \times 100 \quad (2.2)$$

where $C_{i,analyte}$ and $C_{i,initial}$ ($\mu\text{g L}^{-1}$) are the measured concentrations in the eluate and the original sample, respectively, and EF is the enrichment factor of SPE. $m_{C,eluate}$ and $m_{C,initial}$ (μg) are the carbon masses determined in the eluate (corrected for carbon bleed from sorbent material) and in the original water sample, respectively. DOC mass balances were calculated on the basis of measured DOC concentrations in filtrates and eluates, which were corrected for organic carbon bleed stemming from sorbent material, according to equation (2.3):

$$m_{C,initial} = (m_{C,filtrate\ sample} - m_{C,filtrate\ blank}) + (m_{C,eluate\ sample} - m_{C,eluate\ blank}) \quad (2.3)$$

where $m_{C,initial}$, $m_{C,filtrate\ sample}$ and $m_{C,eluate\ sample}$ are the determined carbon masses in the original water sample, as well as in the filtrate and eluate, respectively. $m_{C,filtrate\ blank}$ and $m_{C,eluate\ blank}$ are the quantified carbon bleed values in the ultrapure water directly collected before sample loading and in the eluates of procedural blanks, respectively. Based on recoveries of analytes and DOC, we calculated carbon-normalized ratios of DOM and analyte concentrations in the extracts, $C_{DOM}/C_{analyte}$, given in molC molC^{-1} .

2.2.4.3 Validation of the SPE-CSIA Procedure Using β -CDP

Potential carbon isotope discrimination of atrazine, *S*-metolachlor, boscalid, and azoxystrobin induced by the extraction using β -CDP was examined for varying concentrations (i.e., 5–500 $\mu\text{g L}^{-1}$) and linear flow velocities (i.e., 4.9–39.3 cm min^{-1}). In addition, regeneration of β -CDP was validated by repetitively loading the same SPE cartridges with spiked surface water, followed by elution and subsequent sorbent washing with 2 x 2.5 mL of methanol. SPE of spiked surface water (3.5 mgC L^{-1}) was performed at

pH 7 as mentioned above, except for experiments with varying flow velocities. Here, an automated SPE system (SmartPrep Extractor, Horizon Technology) allowed the exact and constant adjustment of volumetric flow rates (i.e., 0.5–4.0 mL min⁻¹). Detailed experimental parameters are summarized in Table S2.7. Fifty µL aliquots of eluates were taken for concentration determination by HPLC analysis after dilution with ultrapure water (10 times). The remaining volume was carefully evaporated at room temperature under a gentle stream of N₂ to obtain analyte concentrations in the linear range of GC-IRMS analysis.

2.2.5 Batch Equilibrium Sorption Studies

Sorption parameters were determined for the 11 model compounds on CDPs and commercial sorbents by means of the batch equilibrium method following OECD²⁵⁴ and US EPA guidelines²⁵⁵ as described in detail in the Supporting Information (S2.7). The amount of analyte sorbed per mass of sorbent at equilibrium (q) was calculated via mass balance and sorption isotherms were fitted to the Freundlich and Langmuir sorption model according to equation (2.4) and (2.5), respectively:

$$q = K_F \times C_{aq}^{1/n} \quad (2.4)$$

$$q = \frac{q_{max} \times K_L \times C_{aq}}{1 + K_L \times C_{aq}} \quad (2.5)$$

where q (mg g⁻¹) is the amount of analyte sorbed per mass of sorbent at equilibrium, C_{aq} (mg L⁻¹) is the aqueous equilibrium concentration of the compound, K_F [(mg/g)/(mg/L)^{1/n}] and K_L (L mg⁻¹) are the Freundlich and Langmuir sorption coefficients, respectively, $1/n$ (-) is the degree of isotherm nonlinearity and q_{max} (mg g⁻¹) is the maximum sorption capacity. Isotherm fitting was performed using the software OriginPro 2020 and uncertainties were propagated according to the Gaussian error propagation law.

2.2.6 Column Sorption Studies

We studied the influence of background DOM on the sorption of 2,6-dichlorobenzamide (BAM) to the different sorbent materials by adopting an HPLC-based flow-through approach.²⁵⁶⁻²⁵⁸ To this end, the column packing procedure was adapted from literature protocols²⁵⁸⁻²⁶⁰ as described in Chapter S2.8.1. Characteristics of all packed columns are listed in Table S2.10. The retention of BAM on the columns, filled with silicon carbide (SiC)-supported sorbent material, was then studied in HPLC experiments under stimulated competition between DOM and analyte as explained in Chapter 2.2.6.1. Finally, the affinity of BAM to the different sorbents under variable DOM background concentrations was quantified by determining the Gibbs free energy of adsorption, ΔG^0 , from the adsorption partition coefficients (K_d) which were derived from retention times on the different sorbent columns (Chapter 2.2.6.2).

2.2.6.1 Experimental HPLC-Based Approach

Retention of 2,6-dichlorobenzamide (BAM) on the sorbent columns was studied on a Nexera XR HPLC system (Shimadzu, Japan) equipped with a diode array detector (SPD-M20A, Shimadzu, Japan). Thiourea was used as conservative tracer to determine the system hold-up time. We used an optimized mobile phase consisting of ultrapure water and ethanol (9:1, v/v, pH 7, 10 mM CaCl₂) for elution. The influence of background DOM on analyte sorption was studied by adding different amounts of Aldrich humic acid (AHA) to the mobile phase (i.e., 0.0 to 5.0 mgC L⁻¹). After changing the eluent, columns were equilibrated for at least 3 h until both backpressure and detector signal were stable. Thereafter, triplicate 5 µL injections of BAM standards (10 mg L⁻¹, 1 % MeOH) and blanks (1 % MeOH) were performed at a flow rate of 0.1 mL min⁻¹. The temperature of the column oven was set to 25 ± 1 °C and the breakthrough curves were detected at λ = 200 nm. Chromatograms were corrected for interfering co-solvent peaks (1 % MeOH) by subtracting the signal of blanks that were measured together with samples in a bracketing sequence. Mean retention times (t_R) were then determined by the half mass approach,²⁵⁹ that is, the time point at which the breakthrough curve is divided into two equal parts, to account for peak asymmetry caused by tailing.

2.2.6.2 Determination of Partition Coefficient and Gibbs Free Energy of Adsorption

Equilibrium partition coefficients of BAM influenced by the co-solvent EtOH present in the mobile phase, $K_{d w, EtOH}$ (L kg⁻¹), were derived from measured net retention times on the different columns according to equation (2.6), as described elsewhere.²⁵⁸

$$K_{d w, EtOH} = (t_{R, net} - t_{R, net}^{SiC}) \times \frac{Q}{m_s} \quad (2.6)$$

where $t_{R, net}$ (min) is the measured retention time corrected for the hold-up time, $t_{R, net}^{SiC}$ (min) is the corresponding corrected retention time on the reference column filled with 100 % SiC (for determination refer to next paragraph), Q (L min⁻¹) is the flow rate, and m_s (kg) is the mass of the sorbent in the column.

Even though SiC is considered to be quasi-inert, potential sorption of BAM was examined on a reference column, which was filled with 100 % SiC (Table S2.10, column #7). As previously reported,²⁵⁸ analyte sorption on the SiC support in the sorbent columns, $t_{R, net}^{SiC}$ (min), can be derived by extrapolation to the actual amount of SiC present in the sorbent column according to equation (2.7):

$$t_{R, net}^{SiC} = (t_R^{SiC} - t_0^{SiC}) \times \varepsilon \quad (2.7)$$

where t_R^{SiC} (min) is the measured retention time of the analyte in the reference column, t_0^{SiC} (min) is the hold-up time, and ε (-) is the mass ratio of SiC in the sorbent vs. reference column.

Partition coefficients between the sorbent and pure water, $K_{d w}$ (L kg^{-1}), are affected by the co-solvent according to equation (2.8):¹⁶

$$K_{d w} = K_{d w, \text{EtOH}} \times \frac{\gamma_{w, \text{EtOH}}}{\gamma_w} \quad (2.8)$$

where $\gamma_{w, \text{EtOH}}$ and γ_w are the activity coefficients of 2,6-dichlorobenzamide in water/EtOH mixtures and pure water, respectively. Corrected activity coefficients were therefore estimated by applying poly-parameter linear free energy relationships (pp-LFERs) that describe the co-solvent effect of EtOH on activity coefficients of organic solutes according to equation (2.9):¹⁶

$$\log \left(\frac{\gamma_{i w}}{\gamma_{i w, \text{EtOH}}} \right) = v_{w, \text{EtOH}} V_i + e_{w, \text{EtOH}} E_i + s_{w, \text{EtOH}} S_i + a_{w, \text{EtOH}} A_i + b_{w, \text{EtOH}} B_i + c \quad (2.9)$$

where $\gamma_{i w}$ and $\gamma_{i w, \text{EtOH}}$ are the activity coefficients of compound i (i.e., BAM) in water and in the water/EtOH mixture, respectively. Capital letters represent compound-specific descriptors (so-called Abraham parameters) which are relevant for the partitioning process: the McGowan characteristic volume (V_i) given in $\text{cm}^3 \text{mol}^{-1} 100^{-1}$, the excess molar refractivity (E_i) given in $\text{cm}^3 \text{mol}^{-1} 10^{-1}$, the dipolarity/polarizability parameter (S_i), the H-donor property (A_i), and the H-acceptor property (B_i). Small letters represent the complementary, solute-independent descriptors of the water/EtOH system. Abraham parameters for BAM, obtained from the UFZ-LSER database,²⁶¹ and descriptors for the water/EtOH system, derived by Abraham and Acree,²⁶² are summarized in Table S2.11 and Table S2.12.

We calculated standard Gibbs free energies of adsorption, ΔG^0 (kJ mol^{-1}), according to equation (2.11), after converting partition coefficients to dimensionless parameters (equation (2.10))²⁶³, K_d^0 (-), to comply with provisions of the IUPAC.²⁶⁴

$$K_d^0 = K_{d w} \times M_{\text{sorbate}} \times 55.5 \text{ mol L}^{-1} / 10^3 \quad (2.10)$$

$$\Delta G^0 = -RT \times \ln (K_d^0) \quad (2.11)$$

where M_{sorbate} (g mol^{-1}) is the molecular weight of BAM, 55.5 mol L^{-1} is the molar concentration of water, R is the gas constant ($8.314 \text{ J K}^{-1} \text{ mol}^{-1}$), and T is the absolute temperature (298.15 K). As a measure of the change in energy between the phase transfer of BAM in the absence and presence of AHA in the eluent, we derived $\Delta \Delta G^0$ values as a function of DOC, $\Delta \Delta G^0$ f(DOC) [$(\text{kJ mol}^{-1})/(\text{mgC L}^{-1})$], by a linear regression of the determined ΔG^0 values.

2.2.7 Chemical and Isotopic Analyses

2.2.7.1 Compound Quantification Using LC-MS/MS and HPLC

Analyte concentrations in SPE eluates were quantified by ultrahigh-performance liquid chromatography (UHPLC, PLATINblue, Knauer, Germany) coupled to tandem mass spectrometry (MS/MS, AB Sciex Triple Quad 6500, Sciex). Concentrations of atrazine, *S*-metolachlor, boscalid, and azoxystrobin in extracts obtained from the SPE validation experiments were measured by an HPLC system (Nexera XR, Shimadzu, Japan) equipped with a diode array detector (SPD-M20A, Shimadzu, Japan). Details on both methods are given in the Supporting Information (S2.9).

2.2.7.2 Compound-Specific Carbon Isotope Analysis

Carbon isotope ratio measurements of atrazine, *S*-metolachlor, boscalid and azoxystrobin were performed on a GC-IRMS system consisting of a TRACE GC Ultra gas chromatograph which was coupled to a Finnigan MAT 253 isotope ratio mass spectrometer via a Finnigan GC Combustion III interface (all Thermo Fisher Scientific, Germany). Liquid samples of 3 μL were injected by a GC PAL autosampler (CTC, Switzerland) into a split/splitless injector equipped with a splitless liner (5 mm inner diameter x 105 mm length, Thermo Fisher Scientific, Germany) at a temperature of 250 $^{\circ}\text{C}$. The injector was operated for 1 min in splitless mode with a surge pressure of 250 kPa followed by split mode with a split flow of 20 mL min^{-1} . Separation of analytes was accomplished at a constant helium flow rate of 1.4 mL min^{-1} (corresponding to 34.5 cm s^{-1} linear flow velocity) with an Agilent J&W DB-5MS UI column (30 m length x 0.25 mm inner diameter x 1.0 μm film thickness), which was protected by a 1 m deactivated fused silica guard column (0.25 mm inner diameter, Agilent, USA). The temperature program of the GC oven started at 120 $^{\circ}\text{C}$ (1 min hold time), followed by temperature ramps of 22 $^{\circ}\text{C min}^{-1}$ to 250 $^{\circ}\text{C}$ and 40 $^{\circ}\text{C min}^{-1}$ to 325 $^{\circ}\text{C}$ (hold time 11 min). Upon elution from the column, target analytes were combusted at a temperature of 1050 $^{\circ}\text{C}$ in a customized oxidation reactor, which was re-oxidized after every measurement for 20 min with O_2 . The reactor consisted of an alumina tube (320 mm length, 0.5 mm ID, 1.5 mm OD, Friatec, Germany) enclosing two nickel wires (0.1 mm diameter, 99.99 % purity, Alfa Aesar, Germany) and one platinum wire (0.1 mm diameter, 99.99 % purity, Goodfellow, GB). Interfering nitrogen oxides were reduced at 650 $^{\circ}\text{C}$ using an identically constructed reactor, which contained three copper wires (0.1 mm diameter, 99.9999 % purity, Alfa Aesar, Germany). Peak detection was automatically performed by the software Isodat (Thermo Fisher Scientific, Germany) using the individual background algorithm for baseline correction. The isotope ratios were calibrated against a laboratory monitoring gas (CO_2), which in turn was calibrated against the international reference standards USGS 61, 62, 63, and 67. Method quantification limits were determined according to the moving mean procedure reported by Jochmann et al.²⁶⁵ (Figure S2.11) and are reported in Table S2.14.

To comply with the principle of identical sample treatment,¹¹⁹ triplicates of samples were bracketed within the measurement sequence with at least four in-house standards. Carbon isotope ratios are reported as arithmetic means of at least triplicate measurements with one standard deviation ($\pm\sigma$) in the form of isotopic signatures ($\delta^{13}\text{C}$) in per mil (‰) relative to the international reference material Vienna PeeDee Belemnite (VPDB):

$$\delta^{13}\text{C} = \frac{(^{13}\text{C}/^{12}\text{C})_{\text{sample}} - (^{13}\text{C}/^{12}\text{C})_{\text{reference}}}{(^{13}\text{C}/^{12}\text{C})_{\text{reference}}} \quad (2.12)$$

Shifts of isotopic signatures are reported as the deviation, $\Delta\delta^{13}\text{C}$ (‰), between the measured isotope ratios in the processed sample ($\delta^{13}\text{C}_{\text{sample}}$) and a solution of the same isotopic in-house standard ($\delta^{13}\text{C}_{\text{standard}}$) according to equation (2.13):

$$\Delta\delta^{13}\text{C} = \delta^{13}\text{C}_{\text{sample}} - \delta^{13}\text{C}_{\text{standard}} \quad (2.13)$$

Uncertainties associated with measurements were propagated according to the Gaussian error propagation law and are reported as 95 % confidence intervals. In addition, carbon isotope ratios influenced by interfering UCM, $\delta^{13}\text{C}_{\text{calc}}$, were predicted using isotope mass balances as described in the Supporting Information (S2.10.2).

2.2.7.3 Organic Carbon Measurements

DOC concentrations were determined as nonpurgeable organic carbon using a total organic carbon analyzer (TOC-L, Shimadzu, Japan) equipped with a combustion catalytic oxidation reactor (680 °C) and a nondispersive infrared (NDIR) detector. The instrument was calibrated immediately before sample analysis by measuring standard solutions of potassium hydrogen phthalate. Quality control measurements of blanks, constantly run alongside with samples, ensured background DOC values below the detection limit of the instrument (i.e., 0.05 mg L⁻¹). DOC concentrations in methanolic extracts were measured after complete evaporation of the organic solvent (65 °C, N₂, TurboVap LV, Biotage, Sweden), followed by reconstitution of the dry residues in ultrapure water by ultrasonication for 15 min and vortex mixing for 1 min.

2.3 Results and Discussion

2.3.1 Carbon Isotope Analysis of Pesticides after Solid-Phase Extraction of Surface Water on β -Cyclodextrin Polymer and Oasis HLB Sorbent

2.3.1.1 Selectivity Assessment through Unresolved Complex Mixture

We assessed the applicability of β -CDP for the selective analyte extraction from surface water for CSIA. Figure 2.1 compares GC-IRMS chromatograms of carbon isotopic measurements of a surface water sample (containing 2.3 mgC L^{-1}) extracted under identical conditions with either Oasis HLB (panel a) or β -CDP (panel b) and compared with a pure analyte standard mixture of identical concentration (panel c). The chromatograms correspond to eluates that had been enriched by a factor of 5000 and to which target compounds were spiked postextraction with the four target analytes in concentrations equivalent to $9.0 \text{ } \mu\text{g L}^{-1}$ (atrazine), $6.3 \text{ } \mu\text{g L}^{-1}$ (*S*-metolachlor), $6.4 \text{ } \mu\text{g L}^{-1}$ (boscalid), and $6.1 \text{ } \mu\text{g L}^{-1}$ (azoxystrobin) in the pristine water sample.

Superior selectivity of β -CDP over Oasis HLB is qualitatively evident through a comparison of the two baselines of the measured chromatograms. A prominent hump-shaped baseline in Figure 2.1a (i.e., retention time 500–700 s) reflects significant unresolved complex mixture (UCM) originating from co-enrichment of concurrent DOM from the water sample by the conventional SPE sorbent. In contrast, water extraction using the selective β -CDP sorbent reveals noticeably less UCM as shown in Figure 2.1b. In fact, the maximum elevation of the hump-shaped baseline at 595 s was quantitatively reduced from a maximum of $218 \pm 17 \text{ mV}$ (Figure 2.1a, Oasis HLB) to $67 \pm 1 \text{ mV}$ (Figure 2.1b, β -CDP). While β -CDP reduced intensities of UCM over the whole chromatogram, the reduction magnitude varied as a function of retention times. UCM was reduced by factors of 3.0 ± 0.1 , 3.3 ± 0.3 , 1.6 ± 0.1 , and 1.6 ± 0.1 at the retention times of the target analytes atrazine (540 s), *S*-metolachlor (604 s), boscalid (947 s), and azoxystrobin (1127 s), respectively.

The detrimental effect of observed differences in SPE selectivity on accurate CSIA is demonstrated through the carbon isotopic shift ($\Delta\delta^{13}\text{C}$) of boscalid. Indeed, SPE employing β -CDP yielded a $\Delta\delta^{13}\text{C}$ value of $0.4 \pm 0.3 \text{ ‰}$ within the typical instrumental uncertainty of GC-IRMS measurements (i.e., $\pm 0.5 \text{ ‰}$),²⁶⁶ whereas UCM present in the Oasis HLB eluate adversely affected both trueness and precision of isotope analysis ($\Delta\delta^{13}\text{C} = 1.4 \pm 0.5 \text{ ‰}$). These results show that despite the relatively small differences in background interferences between the two sorbents for boscalid (i.e., factor 1.6 ± 0.1), this can have a considerable impact on the interpretability of isotopic data highlighting the importance of careful selection of extraction sorbents. Nonetheless, carbon isotopic integrity of atrazine, *S*-metolachlor, and azoxystrobin was not influenced by UCM. This warrants a closer insight into the dependency of accurate isotope analysis as a function of interfering matrix as presented in the next section.

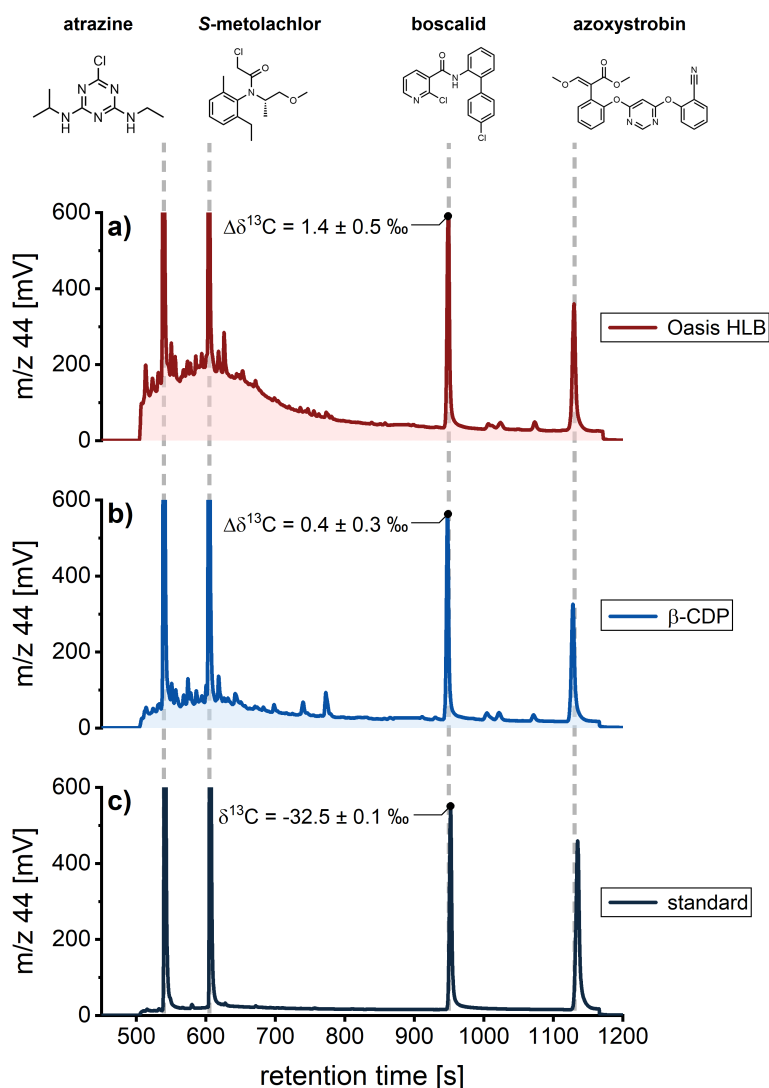


Figure 2.1. Comparison of GC-IRMS chromatograms of the main mass trace (m/z 44) for carbon isotope ratio determination of an identical surface water sample (2.3 mg L^{-1} DOC) extracted with either (a) Oasis HLB or (b) β -CDP and postspiked with the target analytes atrazine, *S*-metolachlor, boscalid, and azoxystrobin. The chromatogram of a pure standard mixture is displayed in panel (c).

2.3.1.2 Matrix-Dependent Limits of Accurate Carbon Isotope Analysis

We further investigated the impact of sorbent selectivity on accurate carbon isotope analysis as a function of increasing volume of extracted sample containing riverine DOM employing either Oasis HLB or β -CDP as sorbents. Figure 2.2 depicts deviations of the carbon isotopic signature from its original value for the four previously shown analytes, $\Delta\delta^{13}\text{C}$ (Figure 2.2, left axis), as well as GC-IRMS baseline values (Figure 2.2, right axis) for extracts that contained constant analyte concentrations (i.e., equivalent to $1.67 \text{ mmolC L}^{-1}$ or 20.0 mgC L^{-1}) but different amounts of extracted DOM, which are together expressed as carbon-normalized ratios of $C_{\text{DOM}}/C_{\text{analyte}}$ (Figure 2.2, top axis) and corresponding to different volumes of extracted water (Figure 2.2, bottom axis). The full set of data is provided in Table S2.15.

It comes as no surprise that interfering baseline values steadily increased with larger extraction volumes for all compounds (Figure 2.2, gray diamonds) with lower baseline

responses measured for the more selective β -CDP compared with Oasis HLB (Table S2.16). Despite this, isotope ratios were accurately determined in all samples within 0.5 ‰ precision, except for boscalid, and regardless of the sorbent type or matrix amount (Figure 2.2, colored circles). We hypothesize that the absence of isotopic deviation for atrazine, *S*-metolachlor, and azoxystrobin as a function of increasing DOM amount is caused by the accidental match of their original isotopic signature (i.e., $\delta^{13}\text{C} = -27.0 \pm 0.1 \text{ ‰}$, $-28.8 \pm 0.0 \text{ ‰}$, and $-27.8 \pm 0.1 \text{ ‰}$, respectively) with the average isotopic composition of DOM (i.e., $\delta^{13}\text{C} \approx -27 \pm 1 \text{ ‰}$).²⁶⁷ In contrast, the boscalid original value ($\delta^{13}\text{C} = -32.5 \pm 0.1 \text{ ‰}$) is $5.5 \pm 1.0 \text{ ‰}$ lighter than that of DOM which can conceivably explain the strong impact of interfering DOM on this compound. Indeed, a theoretical isotope mass balance – based on the above isotopic signatures and the relative contributions of DOM and target analytes derived from peak areas of converted CO_2 – confirms our hypothesis as discrepancies between observed and calculated values were insignificant for all four analytes (i.e., $\Delta\delta^{13}\text{C}_{\text{obs}} - \Delta\delta^{13}\text{C}_{\text{calc}}$ ranging from -0.5 ± 0.4 to $0.7 \pm 0.6 \text{ ‰}$, Table S2.17). This implies that validation by an identical treatment of sample and standard will not work if the standard does not sufficiently deviate from the isotope value of the background interferences. For further discussions, we consider only boscalid.

We derived a matrix-dependent limit for Oasis HLB and β -CDP as sorbents, for which accurate CSIA of boscalid was possible. For both sorbents, the limits corresponded to consistent $C_{\text{DOM}}/C_{\text{analyte}}$ ratios in the extracts of 7.4 and 9.2 molC molC⁻¹, respectively (Figure 2.2, green vertical bars). This consistent ratio is indeed a plausible result for a matrix-dependent limit because it is expected to be a function of signal-to-noise ratio of the GC-IRMS and independent of how the sample was prepared. Moreover, these results agree well with the work of Bakkour,¹⁵³ who observed compromised isotope analysis of atrazine in presence of DOM beyond $C_{\text{DOM}}/C_{\text{analyte}}$ ratios in SPE extracts of 10 molC molC⁻¹. Furthermore, the SPE-CSIA procedure using β -CDP acquired accurate $\delta^{13}\text{C}$ values up to a sample volume of 150 mL compared with only 20 mL for the procedure using Oasis HLB. Our conclusion that it was the interfering matrix – and not other artifacts – which led to inaccurate $\delta^{13}\text{C}$ values beyond the found limits, indicated by the green bars in Figure 2.2, is supported by the following additional considerations: (i) Samples were spiked with target analytes after SPE, and thus, isotope fractionation induced by incomplete recovery of the analytes was excluded. (ii) Spiked concentrations were in the linear range of the GC-IRMS method (Figure S2.11). (iii) Quality control measures on the GC-IRMS system served to identify and eliminate active spots caused by sorption of nonvolatile matrix constituents onto the GC system; further, quantification of carry-overs of matrix between runs did not significantly influence $\delta^{13}\text{C}$ values of bracketing standards (Figure S2.12). (iv) Comparison of nine background correction algorithms offered by the Isodat software gave identical results (Figure S2.13 and Table S2.18). These results show that limits of accurate CSIA of boscalid are enhanced by a factor up to 7.5 toward lower environmental concentrations when using β -CDP as an SPE sorbent.

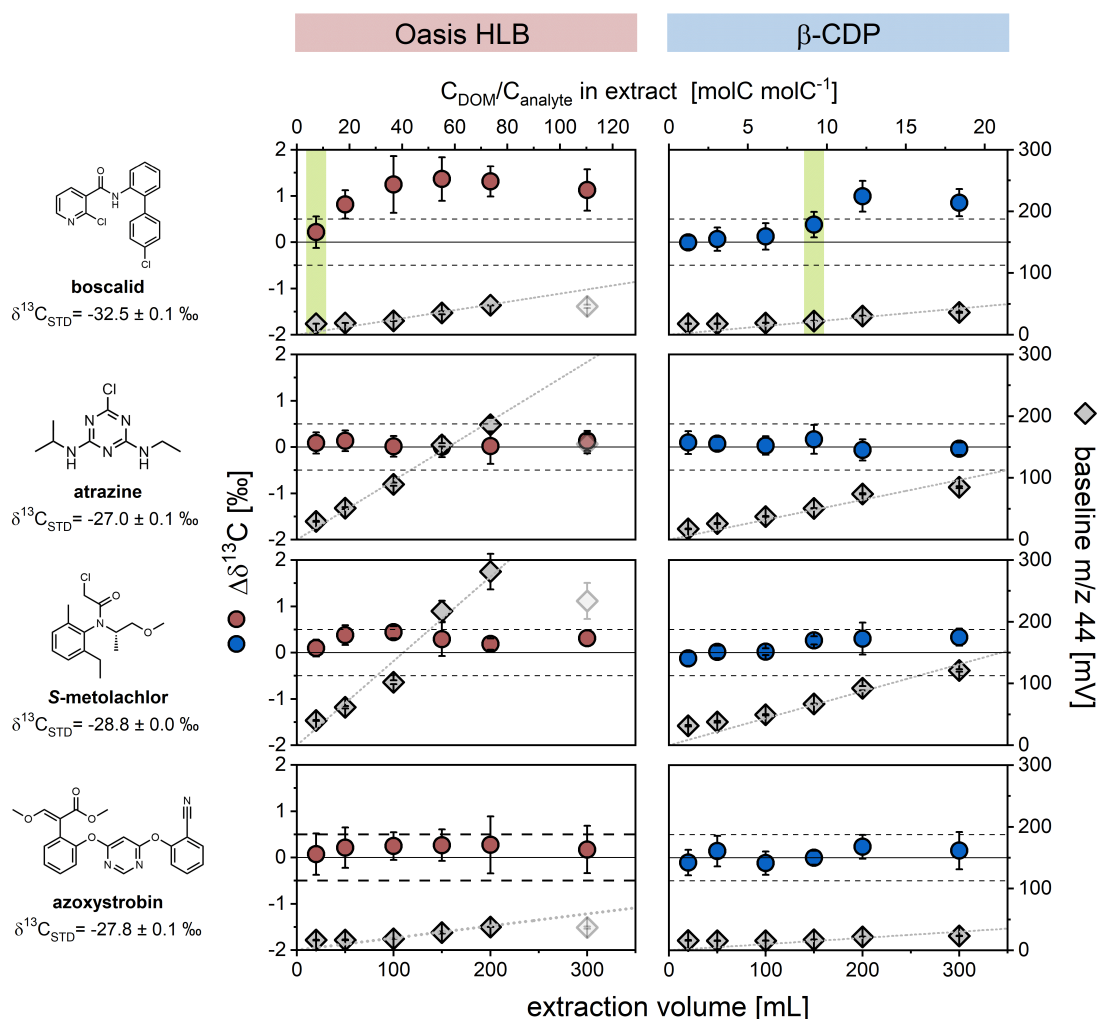


Figure 2.2. Deviations of carbon isotopic signatures ($\Delta\delta^{13}\text{C}$) of atrazine, *S*-metolachlor, boscalid, and azoxystrobin from original values ($\delta^{13}\text{C}_{\text{STD}}$) and associated GC-IRMS baseline values at m/z 44 vs extraction volume on Oasis HLB (red) and β -CDP (blue) and corresponding carbon-normalized ratios of C_{DOM} and C_{analyte} in the extract. Horizontal dashed lines represent the typical uncertainty for $\delta^{13}\text{C}$ measurements on GC-IRMS (± 0.5 ‰) and vertical green bars indicate matrix-dependent limits. Error bars of $\Delta\delta^{13}\text{C}$ values reflect 95 % confidence intervals and uncertainties of baseline values are given as one standard deviation ($\pm\sigma$) of triplicate measurements. Outliers are presented as transparent symbols.

2.3.2 Preferential Affinity of Cyclodextrin Polymers toward Target Analytes over Dissolved Organic Matter

2.3.2.1 Recoveries of Target Analytes and DOM

Extraction performance of target analytes and DOM – as quantified by LC-MS/MS and DOC analysis, respectively – was examined on β -CDP and compared with the conventional sorbents Oasis HLB, LiChrolut EN, and Supel-Select HLB. To this end, a spiked surface water sample containing 2.7 mgC L^{-1} and 11 target analytes at environmentally relevant concentrations of $1 \text{ } \mu\text{g L}^{-1}$ was extracted at pH 3 and 7. Recoveries of DOC and target analytes as well as resultant carbon-normalized ratios of C_{DOM} to C_{analyte} in the SPE extracts are depicted in Figure 2.3 and summarized in the Supporting Information (S2.12).

Evidence for a significantly lower degree of DOM co-enrichment by β -CDP compared with commercial sorbents is illustrated in Figure 2.3a. At neutral pH, 4.0 ± 0.2 , 6.2 ± 1.8 ,

and 9.6 ± 1.2 % of DOC were recovered by Supel-Select HLB, LiChrolut EN, and Oasis HLB, respectively, whereas β -CDP yielded only 1.6 ± 0.1 %. These results agree with our observation of reduced background interferences in the GC-IRMS chromatograms (Figure 2.1) and the resultant lower limits of CSIA when target analytes were extracted by β -CDP instead of the commercial sorbent (Figure 2.2). All sorbents coextracted considerably less DOC at pH 7 (1.6 ± 0.1 to 9.6 ± 1.2 %) compared to pH 3 (29.5 ± 0.5 to 47.0 ± 0.5 %, Figure 2.3a). These results are backed up by complete mass balances when DOC in eluates and filtrates is summed up (96 ± 3 to 102 ± 0 % at pH 3 and 99 ± 1 to 101 ± 1 % at pH 7, Table S2.22). A likely explanation for the greater recovery at pH 3 is that approx. 90 % of DOC in natural waters occurs in the form of carboxylic acids which are deprotonated at neutral pH²⁰⁸ and thus are not as strongly retained by the polymers. Hence, matrix-susceptible analytes can substantially benefit from SPE performed at circumneutral conditions, as previously reported for HPLC-DAD detection of pesticides after SPE using polymeric sorbents such as SDB-1¹⁷⁹ and LiChrolut EN.¹⁷⁸

In contrast to DOM recovery, analyte extraction was enhanced when SPE was performed at neutral pH as reflected by higher mean analyte recoveries of Oasis HLB (97 vs. 87 %), LiChrolut EN (90 vs. 79 %), Supel-Select HLB (84 vs. 73 %), and β -CDP (88 vs. 80 %) (Figure 2.3b). By increasing the pH, extraction performance especially increased for atrazine and terbuthylazine which are partially protonated under acidic conditions (Table S2.2). The nonspecific affinity of Oasis HLB and LiChrolut EN toward the different analytes is reflected in the narrower distribution of recoveries for the investigated compounds (smaller range of box and whisker plots in Figure 2.3b) as opposed to compound-specific affinity for β -CDP and Supel-Select HLB. Particularly, the smallest and most polar analytes BAM and metamitron (McGowan volume: 1.2 and 1.5 $\text{cm}^3 \text{mol}^{-1} 100^{-1}$, $\log K_{\text{ow}} < 1$) could not be well retained on Supel-Select HLB (29 ± 3 and 57 ± 5 % at pH 7, respectively) or β -CDP (31 ± 3 and 67 ± 2 %). For all other compounds, recoveries of β -CDP were comparable to the best-performing conventional materials. This observation is consistent with a previous study that benchmarked β -CDP against Oasis HLB and reported equal or superior extraction performance of β -CDP for up to 189 organic micropollutants.¹⁹⁵

Altogether, combining recoveries for target analytes and DOM (Figure 2.3c) reveal that extraction by β -CDP at neutral pH is the most selective as indicated by lowest carbon-normalized $C_{\text{DOM}}/C_{\text{analyte}}$ ratios among all sorbents (62 ± 2 to $324 \pm 29 \text{ molC molC}^{-1}$). Considering only moderately polar compounds ($\log K_{\text{ow}} > 1$), β -CDP even outperformed conventional sorbents by factors of 5.3 ± 0.2 to 6.1 ± 0.1 (Oasis HLB), 3.6 ± 0.2 to 5.2 ± 0.2 (LiChrolut EN), and 2.3 ± 0.2 to 2.9 ± 0.3 (Supel-Select HLB).

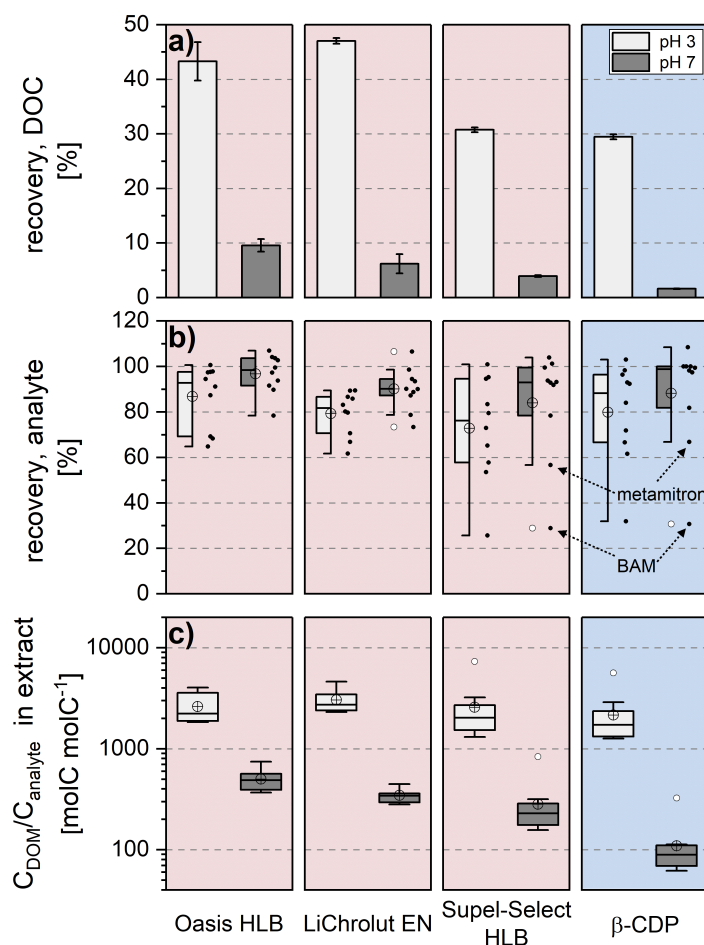


Figure 2.3. Recoveries of (a) dissolved organic carbon (DOC) and (b) target analytes after solid-phase extraction of spiked surface water at either pH 3 or pH 7 using conventional (i.e., Oasis HLB, LiChrolut EN, Supel-Select HLB) or custom-synthesized β -CDP. Panel (c) represents resultant carbon-normalized ratios of C_{DOM} to C_{analyte} in the SPE extracts. Data sets in panels (b, c) are illustrated as box and whisker plots, where boxes indicate median, 25th, and 75th percentile and whiskers extend up to 1.5 times the interquartile distance. Black dots denote average recoveries for individual compounds. Crossed and white circles denote mean values and outliers, respectively.

2.3.2.2 Effect of Smaller CDP Cavity on Partition Coefficients and Recoveries

To gain a compound-specific understanding of the observed different affinities of β -CDP toward the investigated compounds, we synthesized α -CDP which features a smaller cavity size of 0.57 nm, compared with 0.78 nm for β -CDP. This strategy follows a suggestion by Ling and co-workers^{194,198} who hypothesize an increase of the α -CDP affinity toward compounds of smaller sizes (i.e., McGowan volume $< 1.7 \text{ cm}^3 \text{ mol}^{-1} 100^{-1}$; BAM, metamitron, and atrazine in our study) if the selectivity is merely size-driven. Contrary to the hypothesis, α -CDP exhibited lower recoveries for BAM, metamitron, and atrazine than β -CDP (20 ± 1 vs. 31 ± 3 %, 55 ± 0 vs. 67 ± 2 % and 66 ± 3 vs. 100 ± 0 %) and a slightly higher variation of analyte recoveries in comparison to β -CDP (19 to 113 vs. 28 to 111 %, respectively). Batch sorption studies further confirmed these results, showing no statistically significant enhancement in measured affinity for α -CDP toward metamitron ($K_{\text{d}, \alpha\text{-CDP}} = (11.1 \pm 0.7) \times 10^3 \text{ L kg}^{-1}$ vs. $K_{\text{d}, \beta\text{-CDP}} = (9.3 \pm 1.1) \times 10^3 \text{ L kg}^{-1}$, $p = 0.07$) and atrazine ($K_{\text{d}, \alpha\text{-CDP}} = (7.9 \pm 1.3) \times 10^3 \text{ L kg}^{-1}$ vs. $K_{\text{d}, \beta\text{-CDP}} = (7.3 \pm 1.0) \times 10^3 \text{ L kg}^{-1}$, $p = 0.58$), and

even a reduced sorption for BAM ($K_{d, \alpha\text{-CDP}} = (1.9 \pm 0.4) \times 10^3 \text{ L kg}^{-1}$ vs. $K_{d, \beta\text{-CDP}} = (3.7 \pm 0.5) \times 10^3 \text{ L kg}^{-1}$, $p = 0.01$) (Table S2.9). Besides, the sorbent affinity (K_d) positively correlated with the molecular size of the sorbate (McGowan volume), with the most polar analytes ($\log K_{ow} < 1.3$) showing lowest affinities (Figure 2.4a) and recoveries (Figure 2.4b). Ling et al.¹⁹⁸ reported for β -CDP a similar positive correlation between K_d and van der Waals volume and suggested a weaker interaction between small analytes and the sorption sites within the CD cavities. However, this correlation is also evident for Oasis HLB and Supel-Select HLB sorbents (Figure 2.4a), for which no size-exclusion mechanism in the size range of the model analytes is known. In fact, it is conceivable that the size-dependent free-energy differences in water cavity formation for the transfer of sorbates from the water to the sorbent phase give rise to such correlation on all sorbents.^{175,268} These results suggest that size-selective host-guest interactions with the CD moieties are not the dominant drivers of selectivity, but that possibly also interactions with the cross-linker play a role,^{201,202,253} which are governed by other molecular properties of the sorbate, such as the polarity. Further research on the nature of dominant binding mechanisms behind the observed selectivity is nonetheless warranted with a larger data set of compounds.

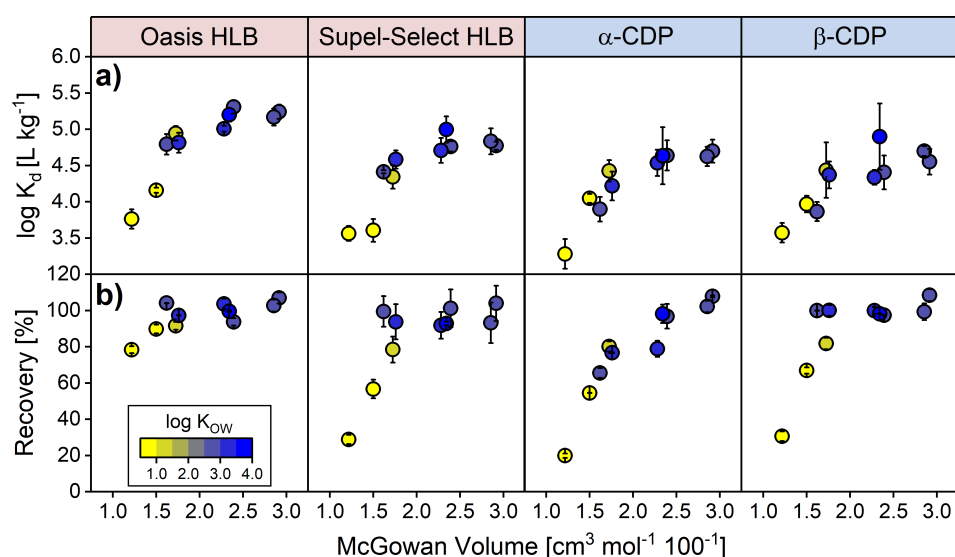


Figure 2.4. (a) Partition coefficients obtained from batch sorption experiments ($\log K_d$) and (b) recoveries obtained from SPE experiments (pH 7) for the investigated target analytes versus the McGowan volume. The $\log K_{ow}$ value, representing a proxy for the polarity of the analytes, is indicated as color-code.

2.3.2.3 Effect of Concurrent DOM on Gibbs Free Energy of Adsorption

When DOM is coextracted along with analytes, it does not only lead to interferences in subsequent analysis but may potentially also change the affinity of analytes to the sorbent phase, as expressed by changes in the Gibbs free energy of adsorption. To investigate this effect in a systematic manner, we selected 2,6-dichlorobenzamide (BAM) as an analyte with the lowest sorption affinity, and determined its Gibbs free energy of adsorption, ΔG^0 , from adsorption partition coefficients (K_d , Table S2.23) that were derived from retention times in columns filled with different sorbent materials. Competition between analyte and DOM on

the respective sorbent materials (Oasis HLB, Supel-Select HLB, and LiChrolut EN, as well as α -, β -, and γ -CDP, the latter featuring the biggest cavity size of 0.95 nm) was stimulated by modifying the concentration of Aldrich humic acid (AHA) in the mobile phase between 0 and 5 mgC L⁻¹. BAM served as a convenient model compound because (i) it allowed identical experimental conditions for all sorbents (e.g., composition of mobile phase, temperature), (ii) its low sorption affinity gave reason to expect that effects of surface competition with DOM would be immediately observable, and (iii) interactions between BAM and AHA were negligible ($K_{OCW} = 6 \text{ L kg}^{-1}$, >99.99 % of BAM in the free form at all AHA concentrations, see S2.8.3), implying that observations could be pinpointed to processes at the sorbent phase.

Negative Gibbs free energies of adsorption were measured for BAM sorption on all sorbents (Table 2.1), which reflect the spontaneous nature of the sorption process, whereas their magnitudes (ΔG^0 from -15.22 ± 0.04 to $-21.74 \pm 0.01 \text{ kJ mol}^{-1}$) are in a typical range of physisorption as expected for predominant van der Waals forces.²⁶⁹ With increasing AHA concentrations in the mobile phase, competition with organic matrix suppressed interactions of BAM with all sorbents as indicated by the slightly but steadily less negative ΔG^0 values (Table 2.1). As a measure of the change in energy upon sorption of BAM in the absence and in the presence of DOM, we derived $\Delta\Delta G^0$ values (Table 2.1) as a function of AHA concentration by well-fitted linear regressions (R^2 range from 0.83 to 0.97, Figure S2.14). Although the derived $\Delta\Delta G^0$ values are small for all investigated sorbents, the differences are still statistically significant and differ by a factor of ten ranging from 0.024 ± 0.002 for β -CDP to $0.217 \pm 0.023 \text{ kJ mol}^{-1}/\text{mgC L}^{-1}$ for Oasis HLB.

Table 2.1. Changes in Gibbs Free Energy (ΔG^0) Involved in the Sorption Process of 2,6-Dichlorobenzamide (BAM) onto Conventional (i.e., Oasis HLB, LiChrolut EN, Supel-Select HLB) and Cyclodextrin-Based Sorbents (i.e., α -, β -, γ -CDP) at $25 \pm 1 \text{ }^\circ\text{C}$.*

sorbent	ΔG^0 [kJ mol ⁻¹]					$\Delta\Delta G^0 \text{ f(DOC)}^\ddagger$ [kJ mol ⁻¹ /mgC L ⁻¹]
	Aldrich humic acid concentration in eluent [mgC L ⁻¹]					
	0.00	1.25	2.50	3.75	5.00	
Oasis HLB	-18.35 ± 0.03	-17.82 ± 0.02	-17.77 ± 0.13	-17.46 ± 0.12	n.a. [§]	0.217 ± 0.023
Supel-Select HLB	-16.69 ± 0.05	-16.30 ± 0.03	-16.19 ± 0.05	-16.15 ± 0.03	-15.95 ± 0.05	0.109 ± 0.011
α -CDP	-15.22 ± 0.04	-15.00 ± 0.05	-15.01 ± 0.05	-14.93 ± 0.05	-14.75 ± 0.06	0.083 ± 0.013
LiChrolut EN	-21.74 ± 0.01	-21.69 ± 0.02	n.a. [§]	-21.64 ± 0.02	-21.55 ± 0.03	0.034 ± 0.006
γ -CDP	-18.94 ± 0.02	-18.84 ± 0.01	n.a. [§]	-18.81 ± 0.03	-18.76 ± 0.03	0.032 ± 0.008
β -CDP	-17.10 ± 0.02	-17.05 ± 0.02	-17.03 ± 0.03	-17.00 ± 0.05	-16.98 ± 0.03	0.024 ± 0.002

*Values were obtained by column chromatography experiments under the influence of varying concentrations of concurrent Aldrich humic acid. [§]n.a. = not available. [‡]Changes of ΔG^0 as a function of concurrent DOC ($\Delta\Delta G^0 \text{ f(DOC)}$) were derived by linear regression; propagated uncertainties of ΔG^0 reflect one standard deviation ($\pm\sigma$) of experimental triplicates and the standard error of the regression slope was used as uncertainty for $\Delta\Delta G^0 \text{ f(DOC)}$.

The lowest $\Delta\Delta G^0$ value of β -CDP suggests a weak competition effect of DOM on β -CDP, which confirms a previously reported small influence of DOM on the interaction between sorbate and cyclodextrin-based sorbent.¹⁹⁴ Moreover, sorbents that showed less retained DOC in our SPE experiments, also experienced thermodynamically less influence by competing DOM in column experiments. In fact, a correlation was found between $\Delta\Delta G^0$ for BAM and the sorbed organic carbon (Figure 2.5). This relationship however did not hold true for LiChrolut EN, which can be caused by its large surface area (i.e., 1200 m² g⁻¹). These results demonstrate that the observed reduced extraction of DOM was not an operational artifact of SPE experiments, and they elucidate a thermodynamic driver for weaker competition on β -CDP compared with commercial sorbents.

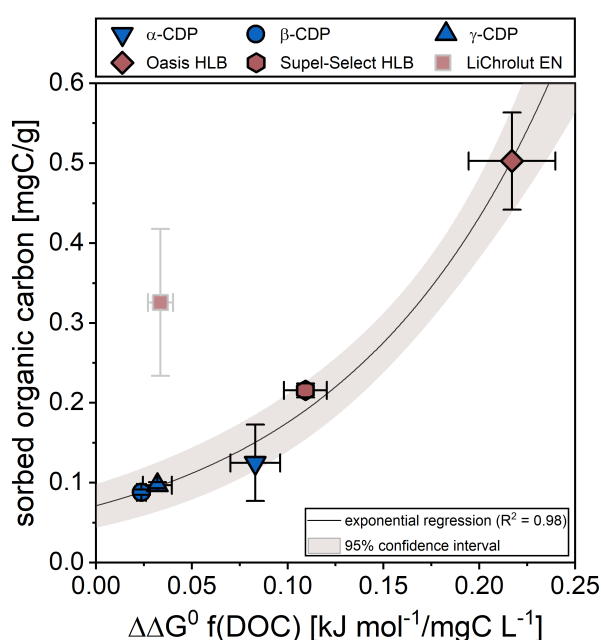


Figure 2.5. $\Delta\Delta G^0$ values as a function of concurrent DOC derived by column chromatography studies for 2,6-dichlorobenzamide (BAM) versus amount of organic carbon sorbed per mass unit sorbent obtained from SPE experiments. A well fitted ($R^2 = 0.98$) exponential correlation of the data of α -, β -, and γ -CDP as well as Oasis HLB and Supel-Select HLB is represented by the black line encompassed by the 95 % confidence interval. The data point of LiChrolut EN is considered an outlier and therefore displayed transparently.

2.3.3 Validation of Carbon Isotopic Integrity after Solid-Phase Extraction of Surface Water on β -Cyclodextrin Polymer

We validated the measured $^{13}\text{C}/^{12}\text{C}$ integrity, as well as recoveries, of boscalid, atrazine, *S*-metolachlor, and azoxystrobin on GC-IRMS after SPE on β -CDP for surface waters containing 3.5 mgC L^{-1} DOC and different analyte concentrations. Furthermore, a validation of different loading flow rates of water samples on SPE is warranted when SPE must be upscaled for large-volume extractions using larger SPE cartridges or disks at higher flow rates. Lastly, recycling of SPE materials may be required if sorbents are not yet launched on the market and synthesis in the laboratory is a limiting factor.

Surface water samples spiked with analytes at concentrations ranging from 5 to $500 \text{ }\mu\text{g L}^{-1}$ were successfully extracted with β -CDP as reflected by recoveries between 99 ± 2 and $103 \pm 0 \%$ for boscalid, 93 ± 0 and $99 \pm 3 \%$ for atrazine, 100 ± 5 and $105 \pm 1 \%$ for *S*-metolachlor, as well as 90 ± 1 and $101 \pm 2 \%$ for azoxystrobin (Figure 2.6, first column; Table S2.24). Measurement of accurate carbon isotope ratios across the entire concentration range (i.e., $\Delta\delta^{13}\text{C}$ between -0.1 ± 0.3 and $0.2 \pm 0.4 \text{ ‰}$) verified that β -CDP can be used to enrich selected target analytes without inducing an isotope fractionation. Moreover, increased flow rates did not induce a significant analyte breakthrough (86 ± 2 to $103 \pm 3 \%$ recovery) and thus carbon isotope ratios of all analytes could be accurately measured with $\Delta\delta^{13}\text{C}$ values between -0.2 ± 0.2 and $0.2 \pm 0.1 \text{ ‰}$ (Figure 2.6, second column). Note that the chosen velocity range in our experiment was applied to custom-made SPE cartridges and would correspond to the following volumetric flow rates in conventional SPE formats: 1.2 to 9.7 mL min^{-1} (1 mL cartridge), 3.1 to 24.4 mL min^{-1} (3 mL), 6.1 to 49.0 mL min^{-1} (6 mL), and 85.2 to $681.8 \text{ mL min}^{-1}$ (47 mm disk) (Table S2.25). Lastly, owing to the high regeneration capacity of β -CDP,^{193,196} no isotopic fractionation was observed for the target analytes upon repetitive loading, elution, and regeneration of the materials (Figure 2.6, third column). Indeed, quantitative recoveries (96 ± 3 to $103 \pm 4 \%$) and deviations of isotopic signatures within typical uncertainty (-0.1 ± 0.1 and $0.2 \pm 0.2 \text{ ‰}$) rendered a six-fold recycling of β -CDP for *S*-metolachlor and boscalid possible. In contrast, recoveries of atrazine and azoxystrobin (97 ± 3 and $98 \pm 1 \%$ with fresh sorbent material) declined after regeneration to lowest values of 86 ± 2 and $72 \pm 3 \%$, respectively. However, this slight decline in recoveries did not cause significant carbon isotopic shifts ($\Delta\delta^{13}\text{C}$ between -0.3 ± 0.2 and $0.1 \pm 0.2 \text{ ‰}$).

This validated procedure suggests that β -CDP is a promising sorbent for CSIA of aquatic organic micropollutants offering a high dynamic range of analyte concentrations and operational SPE conditions. Variable analyte recoveries after regenerating β -CDP, nonetheless, stress that the entire sample preparation procedure must be scrutinized for potential isotopic fractionation of each target analyte.

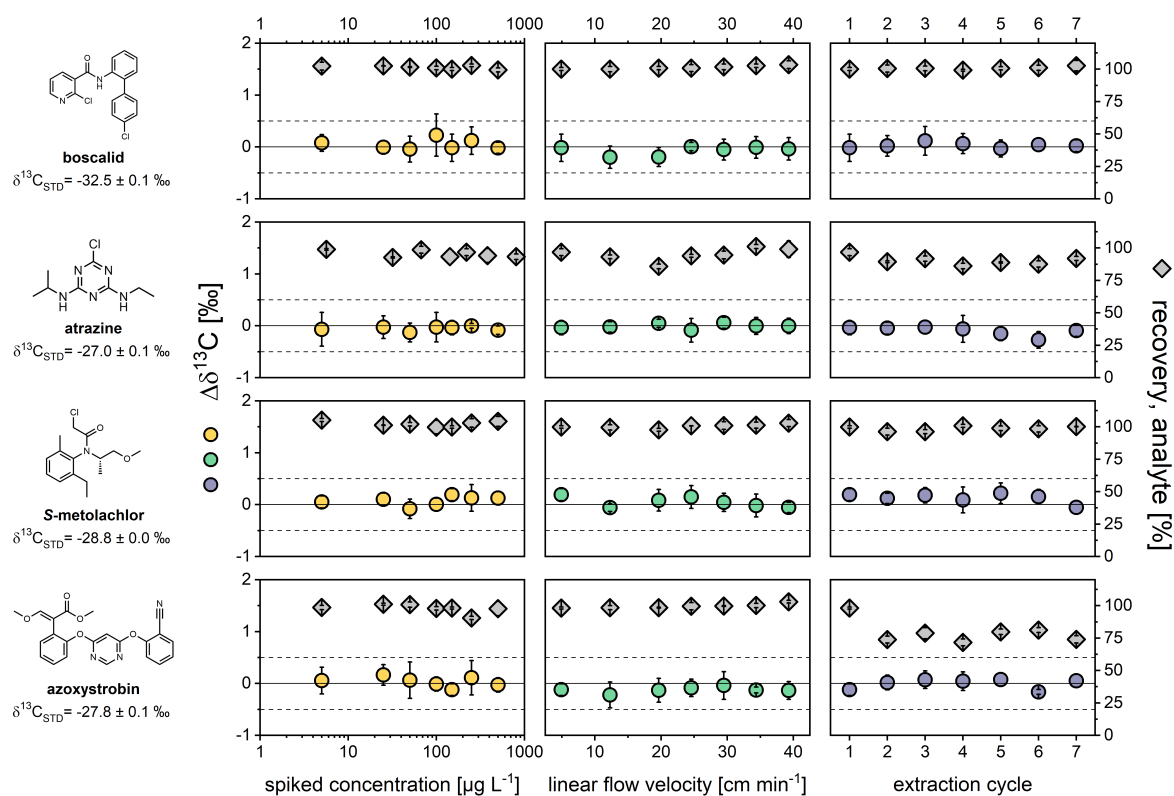


Figure 2.6. Validation of carbon isotope integrity after SPE using β -CDP. Deviations of carbon isotopic signatures from original values ($\Delta\delta^{13}\text{C}$) and corresponding recoveries of boscalid, atrazine, *S*-metolachlor, and azoxystrobin vs prespiked analyte concentration, linear flow velocity, or extraction cycle after sorbent regeneration. Horizontal dashed lines represent the typical uncertainty of GC-IRMS for $\delta^{13}\text{C}$ determination ($\pm 0.5 \text{ ‰}$). Propagated uncertainties of $\Delta\delta^{13}\text{C}$ are represented as 95 % confidence intervals and error bars of recovery data reflect one standard deviation ($\pm\sigma$) of triplicate experiments.

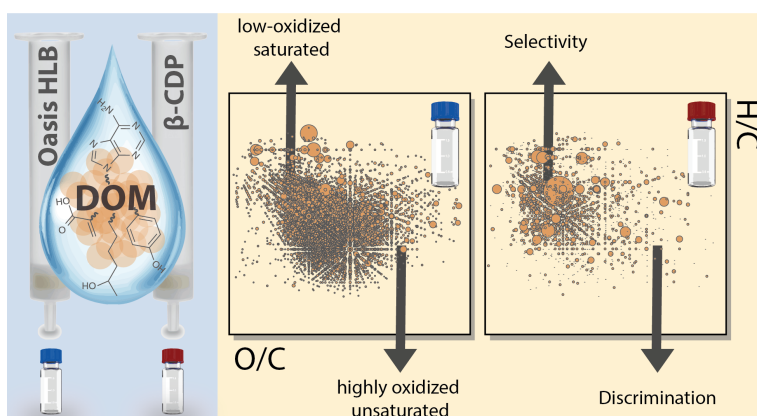
2.4 Conclusions

The present study highlights that CSIA methodologies substantially benefit from sample preparation procedures involving analyte enrichment of natural water samples using innovative, cyclodextrin-based sorbents. We demonstrated an up to six times higher selectivity of β -CDP for target analytes over concurrent DOM in comparison to conventional SPE sorbents. Co-enrichment of interfering matrix constituents was successfully reduced in β -CDP extracts as reflected in significant elimination of unresolved complex mixture (UCM) in GC-IRMS chromatograms. Hence, limits of accurate CSIA could be improved to 7.5 times lower environmental contaminant concentrations when compared with an identical SPE-CSIA procedure using the benchmark sorbent Oasis HLB. We observed for both SPE-CSIA procedures similar matrix-dependent limits above which accuracy of $\delta^{13}\text{C}$ determination was significantly impaired, namely, approx. 10 times more matrix- than analyte-born carbon in the extract. A systematic investigation is warranted to conclusively assess whether such a $C_{\text{DOM}}/C_{\text{analyte}}$ threshold ratio of around 10 molC molC⁻¹ is universally applicable for SPE-CSIA procedures involving different matrices.

Our findings further indicate that sorbent selectivity of CDPs is not dominated by their cavity size but might be governed by the polarity of their building blocks. Polymers optimized to capture a wide range of compound polarities, including highly polar matrix, are therefore not necessarily the first choice for targeted CSIA studies. Advantageous discrimination against polar DOM fractions by CDPs may however be associated with limited extraction performance for highly polar target analytes. The presented selective SPE using β -CDP combined with an advanced cleanup strategy (involving for instance preparative HPLC¹⁶⁵ and MIPs¹⁶⁶) opens up new prospects for micropollutant CSIA at field concentrations of tens to hundreds of nanograms per liter. Future research on the sorption behavior of a wider suite of analytes and DOM from different water matrices on CDPs will help (i) to shed more light on the predominant binding mechanism and thus (ii) to specifically tune sorbent selectivity for analytes of interest, and (iii) to further optimize the cleanup of remaining matrix.

Chapter 3

Selectivity of β -Cyclodextrin Polymer toward Aquatic Contaminants: Insights from Ultrahigh-Resolution Mass Spectrometry of Dissolved Organic Matter



Abstract

Selectivity in solid-phase extraction (SPE) materials has become increasingly important for analyte enrichment in sensitive analytical workflows to alleviate detrimental matrix effects. Molecular-level investigation on matrix constituents, which are preferentially extracted or excluded, can provide the analytical chemist with valuable information to learn about their control on sorbent selectivity. In this work, we employ nontargeted Fourier transform ion cyclotron resonance mass spectrometry (FTICR MS) to elucidate the molecular chemodiversity of freshwater-derived dissolved organic matter (DOM) extracted by the selective model sorbent β -cyclodextrin polymer (β -CDP) in comparison to conventional, universal SPE sorbents (i.e., Oasis HLB, Supel-Select HLB, and LiChrolut EN). Statistical analysis of MS data corroborated the highly selective nature of β -CDP by revealing the extracted DOM spectra that are most dissimilar to original compositions. We found that its selectivity was characterized by pronounced discrimination against highly oxygenated and unsaturated DOM compounds, which were associated with the classes of lignin-like, tannin-like, and carboxylic-rich alicyclic molecules. In contrast, conventional sorbents excluded less highly oxygenated compounds and showed a more universal extraction behavior for a wide range of DOM compositional space. We lay these findings in a larger context that aids the analyst in obtaining an *a priori* estimate of sorbent selectivity toward any target analyte of interest serving thereby an optimization of sample preparation. This study highlights the great value of nontargeted ultrahigh-resolution MS for better understanding of targeted analytics and provides new insights into the selective sorption behavior of novel sorbents.

The results of this chapter were published in modified form in the peer-reviewed paper cited below.

Reprinted with permission* from:

David Glöckler, Mourad Harir, Philippe Schmitt-Kopplin, Martin Elsner, Rani Bakkour. Selectivity of β -Cyclodextrin Polymer toward Aquatic Contaminants: Insights from Ultrahigh-Resolution Mass Spectrometry of Dissolved Organic Matter. *Analytical Chemistry* **2023**, 95 (42), 15505–15513. DOI: 10.1021/acs.analchem.3c01394

ACS Articles on Request author-directed link:

<https://pubs.acs.org/articlesonrequest/AOR-92DRND342BGJCRXZHWGQ>

Copyright © 2023 American Chemical Society.

*For the reprint permission, refer to Chapter S6.3.

3.1 Introduction

Complex matrices in environmental,²⁷⁰⁻²⁷² biological,²⁷³⁻²⁷⁶ or food samples,^{277,278} pose a major challenge to targeted analytical approaches based on liquid or gas chromatographic separation hyphenated to mass spectrometry (MS). Co-eluting endogenous interferences often lead to matrix effects, such as altered ionization efficiency,^{279,280} enhanced chromatographic response,^{277,281} and/or elevated baseline noise,¹⁵¹ which detrimentally affect method validation parameters (e.g., accuracy, reproducibility, linearity, or detection and quantification limits) and may ultimately compromise reliable target analysis. Selective sorbent materials become, therefore, increasingly important for analyte enrichment in sensitive analytical workflows including (ultra)trace residue analysis,²⁷⁷ or ultrasensitive bioanalytical assays.²⁸² For this purpose, solid-phase extraction (SPE) has become the method of choice for aqueous matrices.¹⁵⁰ Yet, the lack of selectivity inherent to commonly used, universal reversed-phase SPE sorbents²⁵² (e.g., poly(styrene-divinylbenzene) polymers) still challenges matrix-susceptible analytical techniques. Innovative sorbent chemistries featuring selectivity for target analytes over an interfering matrix are thus warranted to develop tailor-made analytical procedures for current and future challenges in various fields of quantitative analysis.

Recently, tunable sorbents such as porous cyclodextrin-based polymers have emerged in the area of water remediation,¹⁸⁴ which can potentially be designed toward different classes of organic contaminants by manipulating the cross-linker chemistry.^{201,202,253,283,284} The polymer obtained from cross-linking β -cyclodextrin with tetrafluoroterephthalonitrile (β -CDP)¹⁹³ showed excellent extraction performance for various micropollutants, including pesticides, pharmaceuticals, and lifestyle chemicals, with only limited interferences from dissolved organic matter (DOM) in freshwater.^{194,195} To date, the selectivity of β -CDP has been described based on its lower sorption affinity for organic matrix constituents when compared with conventional sorbents. For example, Ling and co-workers observed less sorption inhibition for target analytes in the presence of fresh- or wastewater-derived DOM when β -CDP was used as sorbent instead of activated carbon.^{194,196} In addition, our previous study showed that β -CDP coextracted considerably less DOM than universal, polymeric SPE sorbents as unveiled by a sum parameter quantification of dissolved organic carbon (DOC) in extracts.²⁸⁵ The preferential exclusion of DOM constituents from its binding sites renders β -CDP an ideal selective model sorbent that is attractive for many targeted analytical applications. For example, significant enhancement of sensitivity by a factor of 7.5 was found by lowering backgrounds in gas chromatography-isotope ratio MS after using β CDP as an SPE sorbent compared with conventional Oasis HLB.²⁸⁵ Yet, it is unknown which specific fractions of the chemically diverse DOM are retained/excluded by the sorbent. Their detailed characterization can, in fact, help in understanding the sorbent selectivity on the molecular level and therefore contribute to further optimization of selective sample preparation workflows.

Fourier transform ion cyclotron resonance (FTICR) MS is the state-of-the-art technique for molecular characterization of heterogeneous and polydisperse chemical mixtures, such as freshwater DOM (e.g., refs 210,211,226,227). During the past decade, environmental DOM research has been successfully applying nontargeted FTICR MS analysis for assessing SPE sorbents in their ability to nonselectively extract the most from the DOM pool and obtain, thus, concentrated extracts that are as representative of the original composition as possible.²⁸⁶⁻²⁹² For instance, it was demonstrated that a proprietary functionalized styrene-divinylbenzene polymer was best suited for the most complete and representative DOM extraction,^{287,292} whereas hydrophilic lipophilic balanced (HLB) polymeric sorbents were shown to be particularly efficient in retaining a broad range of oxidized compounds.^{289,291} Here, we take an opposite approach and use FTICR MS as a fingerprinting technique to specifically pinpoint preferentially retained and excluded DOM fractions under extraction conditions optimized for targeted analytics and hence to evaluate their control on sorbent selectivity.

The overall goal of this work was, therefore, to elucidate the molecular chemodiversity of DOM extracted by β -CDP and commonly used universal sorbents (i.e., Oasis HLB, Supel-Select HLB, and LiChrolut EN) from natural water matrices (i.e., surface and groundwater) and to deduce implications for the general analytical chemist. To meet this goal, we (i) explore characteristic features and trends among FTICR mass spectra of the original and sorbent DOM as exemplified on the nominal mass scale and across the entire assigned molecular formula pool; (ii) evaluate qualitatively the different DOM chemodiversities by visualization in van Krevelen diagrams; (iii) compare them quantitatively by categorization into molecular compound classes; and (iv) identify high-abundance and unique molecular signatures in the different sorbent extracts.

3.2 Experimental Section

3.2.1 Chemicals, Materials, and Sorbents

Detailed information on chemicals and materials is given in the Supporting Information (SI, S3.1) including CAS number, purity, grade, and supplier. Preparation of β -CDP followed the procedure reported by Alsbaiee et al.,¹⁹³ as detailed in the SI (S3.2.1). Confirmation of successful synthesis of the polymer was obtained through characterization with scanning electron microscope imaging (S3.2.2) and Fourier transform infrared spectroscopy (S3.2.3).

3.2.2 Solid-Phase Extraction of Dissolved Organic Matter

DOM was isolated from 50 mL surface water (SW) and groundwater (GW) samples at pH 7 by means of SPE using synthesized β -CDP and the conventional SPE sorbents Oasis HLB, LiChrolut EN, and Supel-Select HLB (for water collection and treatment, refer to S3.3). To this end, we used self-packed SPE cartridges (1 mL, polypropylene, Supelco, USA) with 25 mg sorbent bed weights, in accordance with guidelines of Dittmar et al.²⁹³ for DOM extraction that are based on both sample volume and DOC concentration (Table S3.3). All experiments were performed utilizing a 12-port vacuum SPE manifold (Visiprep, Supelco, USA) at a volumetric flow rate of $\leq 1.0 \text{ mL min}^{-1}$, corresponding to a linear flow velocity of $\leq 4.1 \text{ cm min}^{-1}$.

Prior to sample loading, SPE cartridges were conditioned with 1 mL of methanol followed by at least 650 mL of ultrapure water (pH 7), which reduced leaching of sorbent material into sample permeates (Figure S3.4). Subsequently, samples at neutral pH were percolated through the cartridges and permeates were collected for a second extraction step. Once cartridges were loaded with sample, sorbents were washed with 1 mL of ultrapure water (pH 7), dried under vacuum for 24 h, and finally eluted with 1 mL of methanol. Similarly, we prepared procedural blanks by loading every sorbent with ultrapure water to account for contaminations introduced by the sorbent material. To characterize molecular DOM compositions of both the original water samples and SPE permeates, we extracted these samples using the functionalized styrene-divinylbenzene sorbent Bond Elut PPL (Agilent, CA, USA), as proposed by Li and co-workers²⁹² (see S3.4.2). DOM characterized after PPL-based SPE of pristine water samples is hereafter referred to as the *original DOM*. Upon elution, 100 μL of aliquots of all extracts was separated for DOC analysis, which is described in the Supporting Information (S3.5). The remaining methanolic samples were stored at $-20 \text{ }^\circ\text{C}$ until FTICR MS analysis.

3.2.3 FTICR Mass Spectrometry and Molecular Formula Assignment

Nontarget analysis of the extracted DOM after SPE was performed by high-field FTICR MS. The mass spectra were acquired using a 12 T Bruker Solarix mass spectrometer hyphenated to an Apollo II electrospray ionization (ESI) source (Bruker Daltonics, Bremen, Germany).

The ionization source was operated in negative mode [ESI(-)] to allow for the detection of a large diversity in molecular compositions including highly oxygenated compounds.²⁹⁴ In order to decrease ionization suppression and adduct formation and to prevent overloading of the ICR cell, all methanolic extracts were diluted to an optimal, pre-tested concentration of 5 $\mu\text{gC mL}^{-1}$ prior to injection. The flow rate was held constant at 2 $\mu\text{L min}^{-1}$ with a nebulizer gas pressure of 138 kPa, a drying gas pressure of 103 kPa, and a source heater temperature of 200 °C. The autosampler was programmed to wash with 600 μL of 80:20 MeOH:water to prevent carryover. Mass spectra were acquired with a time domain of 4 megawords within a mass range of m/z 174.4 to 1400, and 400 scans were accumulated for each mass spectrum. All spectra were first externally calibrated based on clusters of arginine and then internally calibrated using DOM reference mass lists, reaching accuracy values lower than 100 ppb. Postprocessing of the spectra was executed using the software Compass DataAnalysis 4.1 (Bruker Daltonics, Bremen, Germany).

Sorbent-specific peaks caused by polymer leaching were first identified by the FTICR MS analysis of sorbent blanks and then removed from the peak lists of the corresponding sample extracts. The molecular formulas were assigned based on a restricted list of selected small molecular units with defined mass differences, corresponding to common chemical functional groups (i.e., CH_2 , H_2 , O , CO_2 , S , SO_3 , and NH) and transformations (NetCalc approach).²⁹⁵ Molecular formula assignments correspond to a multiple Kendrick analogue mass defect analysis and generate all homologous series according to the chosen transformations simultaneously. To account for ionization artifacts, data sets of permeate samples were filtered for assigned formulas that were also found in the original DOM compositions, as both were extracted under identical conditions using the Bond Elut PPL sorbent. The final molecular formula assignments of all samples were grouped into molecular series containing CHO, CHNO, and CHOS molecular compositions.

3.2.4 Double Bond Equivalent and Aromaticity Index

Chemical indices including double bond equivalent (DBE), carbon-normalized DBE (DBE/C), and the modified aromaticity index (AI_{mod}) were derived according to equation (3.1) and (3.2), as described by Koch and Dittmar:^{230,231}

$$\text{DBE} = 1 + \frac{1}{2}(2C - H + N) \quad (3.1)$$

$$\text{AI}_{\text{mod}} = \frac{1 + C - \frac{1}{2}O - S - \frac{1}{2}(H + N)}{C - \frac{1}{2}O - N - S} \quad (3.2)$$

where C, H, N, O, and S are the numbers of carbon, hydrogen, nitrogen, oxygen, and sulfur atoms, respectively, in the molecular structure. We applied the AI_{mod} parameter to examine the degree of unsaturation of compounds due to a high number of carboxylic acids present

in freshwater DOM,^{208,213,219} where AI_{mod} values ≥ 0.5 indicate the aromatic character of molecules.

3.2.5 Intensity-Weighted Average Values and Data Visualization

Intensity-weighted averages (X_{wa}) of bulk parameters (X_i), such as elemental ratios or chemical indices, were calculated based on peak intensities (Int) of each assigned formula (i) according to equation (3.3):

$$X_{\text{wa}} = \frac{\sum_{i=1}^n X_i \times Int_i}{\sum_{i=1}^n Int_i} \quad (3.3)$$

To reduce the complexity of the FTICR MS spectra, we visualized the data sets in the form of van Krevelen diagrams,²²⁹ which depict the elemental H/C ratio of each assigned molecular formula as a function of its O/C ratio. The assignment of compound classes in the van Krevelen diagram based on characteristic H/C and O/C ratios of major biogeochemical precursor materials, such as lipid-, lignin-, or tannin-like molecules, was derived from several previous studies,^{213-216,294,296-299} as depicted in the SI (Figure S3.5). Van Krevelen diagrams were complemented by plots projecting H/C or O/C elemental ratios versus m/z values (hereafter referred to as *mass-edited H/C* or *O/C diagrams*) to explore the mass distribution of the extracted compounds. Symbol sizes in both van Krevelen and mass-edited diagrams reflect relative peak intensities (RI), which were calculated based on the sum of the total peak intensity according to equation (3.4):

$$RI = \frac{Int_i}{\sum_{i=1}^n Int_i} \times 1000 \quad (3.4)$$

3.2.6 Intensity-Weighted Population Density and Statistical Analysis

For a more robust, quantitative comparison of molecular compositions in different SPE extracts, intensity-weighted population densities were calculated for six distinctly delimited molecular classes, which were predefined according to atomic ratios (i.e., H/C and O/C) and modified aromaticity indices, as described by Kellerman et al.²⁹⁷ These molecular classes included *saturated* ($H/C \geq 1.5$, $O/C < 0.3$, $N = 0$), *N-containing aliphatic* ($H/C \geq 1.5$, $N \geq 1$), *aliphatic and alicyclic* ($H/C \geq 1.5$, $O/C \geq 0.3$, $N = 0$), *low-oxidized unsaturated* ($H/C < 1.5$, $O/C \leq 0.5$, $AI_{\text{mod}} < 0.5$), *highly oxidized unsaturated* ($H/C < 1.5$, $O/C > 0.5$, $AI_{\text{mod}} < 0.5$), and *aromatic and condensed* ($AI_{\text{mod}} \geq 0.5$) compounds. The intensity-weighted population density was determined for each molecular class based on the sum of relative intensities according to equation (3.5):³⁰⁰

$$D_k = \frac{\sum_{i=1}^{N_k} Int_i}{\sum_{j=1}^N Int_j} \quad (3.5)$$

where D_k is the intensity-weighted population density of molecular class k , $\sum Int_i$ is the sum of relative intensities for mass peaks in each class, and $\sum Int_j$ is the sum of relative intensities for all mass peaks.

Hierarchical cluster analysis (HCA) was performed using the software Hierarchical Clustering Explorer 3.0 (University of Maryland, USA) where clustering of the normalized data sets was achieved by applying the average linkage method (UPGMA) and distance metrics based on Pearson correlation coefficients. Principal component analysis (PCA) was performed with SIMCA-P 9.0 software (Umetrics AB, Sweden).

3.3 Results and Discussion

We explored the extraction selectivity of β -CDP and three conventional polymeric SPE sorbents (i.e., Oasis HLB, LiChrolut EN, and Supel-Select HLB) by high-field FTICR MS analysis of DOM in both SPE permeates (Table S3.4) and extracts (Table S3.5). To this end, SW and GW samples were extracted at neutral pH, at which a high degree of sorbent selectivity (i.e., low level of DOC coextraction) was previously demonstrated.²⁸⁵ Owing to the high mass accuracy obtained by ultrahigh-resolution MS, we assigned a total of 16,769 individual mass peaks to their corresponding unique elemental composition in the C, H, O, N, and S chemical space. Since DOM extraction efficiencies are typically low at neutral pH for the tested sorbents (i.e., < 10 %),²⁸⁵ the majority of DOM constituents were not retained and molecular signatures in SPE permeates largely resembled original DOM compositions (Figure S3.6). We therefore focus our further discussion on molecular DOM compositions obtained from FTICR MS analysis of only sorbent extracts.

3.3.1 Characteristic Features in FTICR Mass Spectra of DOM Extracts

The negative ESI FTICR mass spectra of the original SW and GW DOM revealed skewed near Gaussian-type mass peak distributions with maximum intensities around m/z 400, typical of freshwater-derived DOM (Figure S3.7).^{216,286,294} Extraction selectivity of the investigated sorbents becomes evident upon inspection of the mass spectra of their corresponding extracts, as shown in Figure 3.1. Compared with the original SW DOM spectrum, the sorbent spectra showed less intense bulk DOM signatures and several scattered mass peaks with relatively higher intensities, especially in the β -CDP extract (panel a1). GW sorbent extracts followed the same trend; DOM signatures were however better developed (panel b1). Multivariate statistical analyses involving the complete, normalized FTICR MS data sets demonstrated distinct differences between original DOM and sorbent extracts, as samples were separated in HCA dendrograms (panels a2 and b2) and PCA score plots (Figure S3.8). Both HCA and PCA unveiled a high degree of similarity between DOM extracted with Oasis HLB and LiChrolut EN, while Supel-Select HLB extracts were either more similar to β -CDP (in case of SW) or the other conventional sorbents (in case of GW). Confirming its selective behavior, β -CDP extracts comprised the most dissimilar DOM compared with the original compositions, as particularly reflected in most distanced clustering of β -CDP samples in PCA score plots.

Characteristic molecular-level differences among the sorbent extracts are revealed by relative peak intensities at the nominal mass scale as exemplified for CHO-assigned formulas at m/z 471 (Figure 3.1, panel a3 and b3). The nine mass peaks in both original DOM spectra were assigned to two formula series (i.e., $C_{22}H_{15}O_{12}^-$ to $C_{26}H_{31}O_8^-$ indicated in green, $C_{19}H_{19}O_{14}^-$ to $C_{22}H_{31}O_{11}^-$ indicated in black, panels a4 and b4), which are characterized by mass spacings attributed to the nominal substitution of O with CH_4 (i.e., 36.4 mDa),³⁰¹ and thus decline in degree of both oxygenation (O/C) and unsaturation (H/C,

DBE, DBE/C, and AI_{mod}) with increasing m/z (Table S3.6). Compared with original spectra, all sorbents discriminated against relatively oxygen-rich and unsaturated (i.e., hydrogen-deficient) compounds as reflected in a gradual decrease of relative intensities for compounds with higher O/C and lower H/C ratios, as well as higher DBE, DBE/C, and AI_{mod} indices. In fact, this trend has also been observed for the entire assigned formula pool, as shown by intensity-weighted averages of elemental ratios and chemical indices (Table S3.5). While the average H/C and O/C values of the original DOM (i.e., SW, 1.18 and 0.48, and GW, 1.11 and 0.49, respectively) agreed with the reported values for freshwater DOM,^{287,291,302} we observed distinct shifts to higher, more saturated H/C values of 1.32 (SW) and 1.25 (GW) for Oasis HLB, followed by a gradual increase to maxima of 1.48 and 1.39, respectively, in the order LiChrolut EN < Supel-Select HLB < β -CDP (Figure S3.9). Correspondingly, chemical indices representing relative unsaturation (i.e., DBE, DBE/C, and AI_{mod}) declined in the same order. The average O/C values decreased from 0.42 to 0.32 (SW) and from 0.38 to 0.29 (GW) in the order LiChrolut EN > Oasis HLB > Supel-Select HLB > β -CDP. Thus, β -CDP extracted on average the most hydrogen-saturated (highest %H and H/C) and oxygen-deficient (lowest %O and O/C) DOM pool, indicative of the most pronounced selectivity among the tested sorbents.

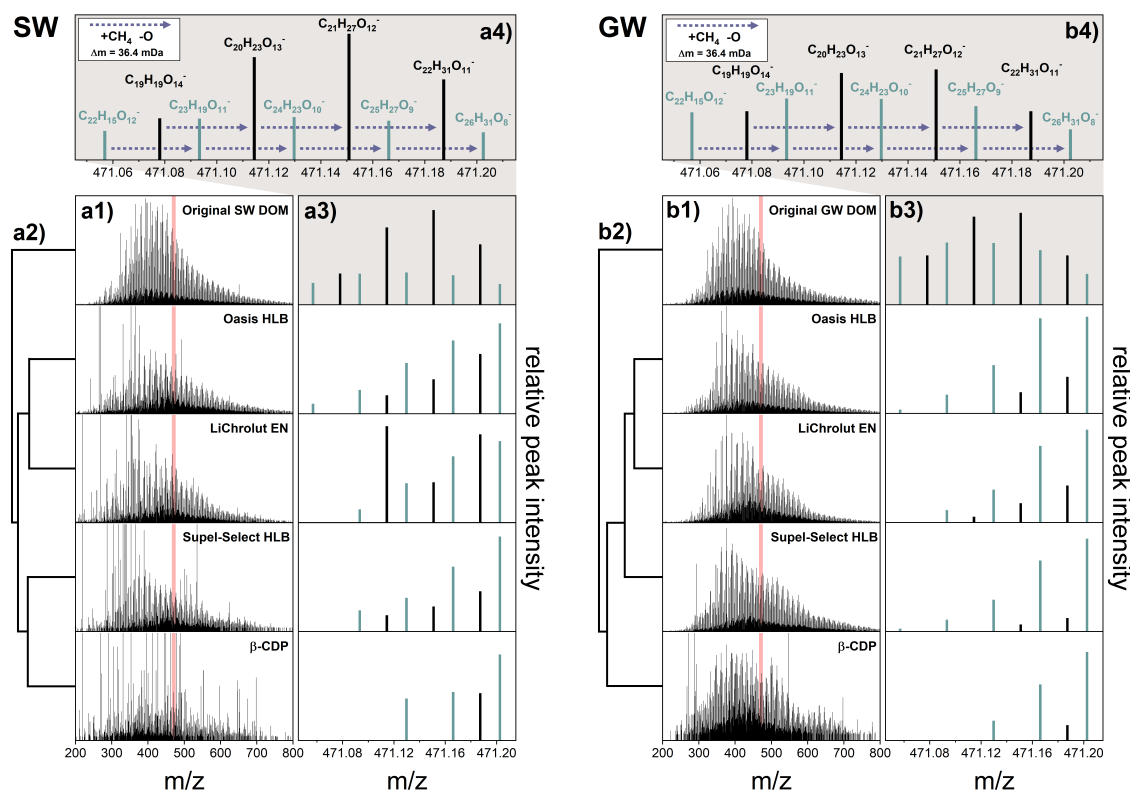


Figure 3.1. Negative ESI 12 T FTICR mass spectra of the original SW and GW DOM and the respective extracts of the conventional SPE sorbents (i.e., Oasis HLB, LiChrolut EN, and Supel-Select HLB) and β -cyclodextrin polymer (β -CDP). Panels a1 and b1 display the spectra from m/z 200 to 800. Corresponding dendrograms of an HCA of all m/z ions based on normalized peak intensities and Pearson similarity indices are shown in panels a2 and b2. The 170 mDa mass scale-expanded segments at nominal m/z 471 are presented in panels a3 and b3, with magnifications of the original SW and GW composition provided in panels a4 and b4. Two series of assigned CHO formulas are indicated in black and green, which are both characterized by the recurring CH_4 vs O mass spacing ($\Delta m = 36.4$ mDa, purple arrows).

3.3.2 Chemodiversity of DOM Extracted by β -Cyclodextrin Polymer and Universal SPE Sorbents

The further elucidation of DOM chemodiversity in sorbent extracts was facilitated by projecting the chemical compositions of all mass peaks assigned to CHO, CHNO, and CHOS molecular series onto van Krevelen (Figure 3.2a) and mass-edited H/C diagrams (Figure S3.11). Rich chemodiversity was found in the original SW and GW DOM as revealed by the high numbers of assigned formulas (i.e., 7549 for SW, 6126 for GW) occupying a wide range in the CHO compositional space (H/C, 0.5 – 2.0; O/C, 0.04 – 0.9; m/z , 160 - 940; for further characterization, see S3.8.2). This confirms the suitability of the investigated sample matrices to comprehensively assess the extraction performance of selective and universal sorbent materials. As expected for freshwater DOM, the majority of assigned formulas in both samples covered regions in the van Krevelen diagrams commonly ascribed to the major biogeochemical precursors of lignin-like,^{214,215,298,299} tannin-like,^{216,296} and refractory carboxylic-rich alicyclic molecules (CRAMs).²¹³ CRAMs represent the highly diverse transformation products of ultimately terpenoid origin,²¹² which are prominent constituents in terrestrially derived DOM.²¹⁷⁻²²⁰

SPE at neutral pH using β -CDP and universal sorbents resulted in discriminative DOM pools as reflected in (i) predominantly lower numbers of assigned formulas ranging from 2031/7549 (27 %) to 3469/6126 (57 %) for β -CDP, and from 5571/7549 (74 %) to 6173/6126 (101 %) for Oasis HLB in SW and GW, respectively, and (ii) shifts in chemodiversity that manifested in different coverage of the van Krevelen plots compared with original compositions. As an overarching trend, we observed less densely populated areas in van Krevelen diagrams assigned to highly oxygenated (O/C > 0.5) and unsaturated compounds (H/C < 1.5) of all molecular members (Figure 3.2a). Correspondingly, we identified a wide array of unsaturated, oxygen-rich compounds present in the original samples (i.e., 2961 in SW and 2148 in GW) that were not detected in any sorbent extract (Figure S3.13). Tendentially lower DBE yet higher DBE-O values of CHO-assigned compounds in sorbent extracts suggest molecules rich in carboxylic moieties as principal constituents of this missing compound group (Figure S3.14),²⁸⁶ in line with the observed trends toward higher average H/C and lower O/C in sorbent extracts.²¹⁰ These results are conceivable since carboxylic acids belong to the most prominent functionalities in DOM²⁰⁸ where their high degree of deprotonation at neutral pH³⁰³ renders them highly soluble in water and thus reduces their nonionic interactions with the sorbent phase. On the one hand, this is consistent with recent studies investigating the impact of sample acidification on molecular SPE-DOM compositions.³⁰⁴⁻³⁰⁶ On the other hand, it emphasizes from a target analysis point of view the importance of pH optimization, which can lead to cleaner samples alleviating the need for multistep cleanup prior to analysis, provided that extraction pH is uncritical for the retention of target analyte(s).

Furthermore, the van Krevelen diagrams were quantitatively evaluated based on intensity-weighted population densities for six distinct molecular classes (Figure 3.2b). In contrast to the original compositions, all sorbent extracts were dominated by low-oxidized unsaturated (Figure 3.2b, light green), presumably lignin-like compounds mostly without carboxylic functionalities,³⁰⁷ which accounted for 40 to 80 % of total extracted DOM. The contribution of highly oxidized unsaturated compounds (dark green) decreased from originally 40 to 8 – 21 % (SW) and 3 – 10 % (GW), respectively, reflecting the loss of carboxylated species, such as hydrolyzable tannins and CRAMs.^{307,308} The lower abundance of aromatic and condensed compounds in sorbent extracts, reflected in both intensity-weighted (2 – 4 %, Figure 3.2b, black) and total percentage (4.1 – 9.9 %, Table S3.5), implies an additional loss of possibly condensed tannins and aromatic carboxylic acids. Altogether, β -CDP selectively extracted the most restricted compositional space (i.e., ≥ 90 % of total coverage in the low-oxidized unsaturated and saturated/aliphatic regions, Figure 3.2b, light green to red) while discriminating strongest against highly O-functionalized unsaturated and aromatic DOM constituents. In contrast, universal sorbents showed less discrimination with most selective sorbents following the order Supel-Select HLB > LiChrolut EN > Oasis HLB, in accordance with shifts in bulk average H/C and O/C values, and HCA similarity.

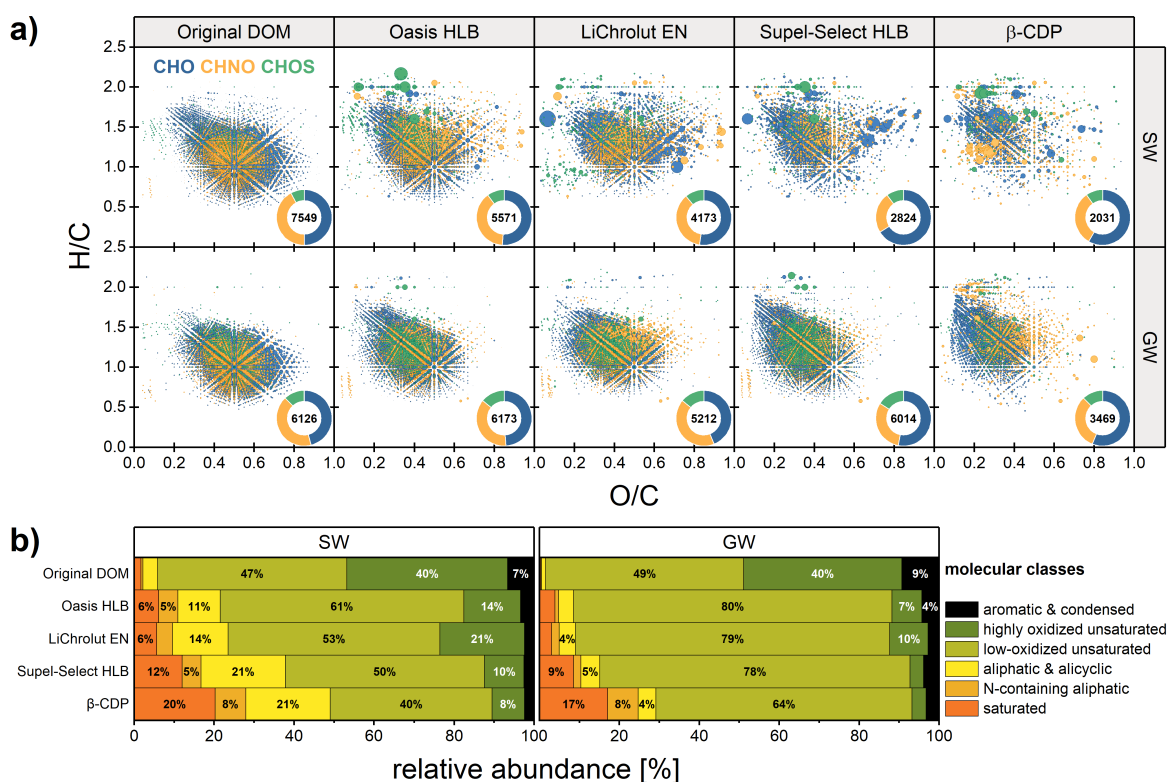


Figure 3.2. (a) Molecular composition of the original SW and GW DOM and DOM in conventional (i.e., Oasis HLB, LiChrolut EN, and Supel-Select HLB) and β -CDP sorbent extracts projected onto van Krevelen diagrams. Symbols are color-coded according to the CHO (blue), CHNO (orange), and CHOS (green) molecular series, and symbol sizes reflect relative signal intensities of each mass peak. The insert pie charts indicate the relative proportions of molecular series, with total number of assigned formulas provided. (b) Molecular class distributions on the basis of intensity-weighted population densities obtained by partitioning of van Krevelen diagrams into molecular classes based on elemental ratios and modified aromaticity indices.

3.3.3 High-Abundance and Unique Molecular DOM Signatures in SPE Extracts

Specific extraction preferences of the sorbents are unveiled by the most abundant mass peaks found in the corresponding extract. These are presented in mass-edited O/C diagrams (Figure 3.3) for spectra of highest similarity as identified through HCA (cf. Figure 3.1). The horizontal dotted lines in Figure 3.3 indicate the O/C ratio above which 95 % of peak intensities were present in the respective cluster. The progressive decline of these lines from O/C of 0.45 in the original DOM (Figure 3.3, left panels) to 0.28 in sorbent cluster 1 (middle panels) and to 0.11 – 0.17 in sorbent clusters 2 (right panels) demonstrates the discrimination against ionized and highly polar DOM species under neutral extraction conditions. Nonetheless, conventional sorbents specifically showed a preference for compounds within an O/C window from 0.28 to 0.45, where most compounds (94 %) were found especially in GW extracts (cluster 1; Figure 3.3b). In SW extracts of cluster 1 (Figure 3.3a, middle panel), several abundant compounds were additionally found at O/C > 0.45 and primarily comprised saturated CHNO compounds (Figure S3.15a). In contrast, β -CDP (cluster 2) exhibited extraction preference for even more oxygen-deficient compounds as reflected in (i) a majority of abundant compounds with O/C < 0.28 as opposed to cluster 1 and (ii) the lowest 95 % dividing lines. Additional abundant compounds of higher oxygenation (O/C > 0.28) in cluster 2 mainly comprised low-molecular-weight ($m/z < 550$) molecules of relative aliphatic character (H/C \sim 1.5, Figure S3.15). We note that Supel-Select HLB exhibited extraction preferences either more similar to β -CDP (SW) or to the other conventional sorbents (GW), implying that sorbent selectivity can also be impacted by the nature of the matrix itself, in line with previous studies.^{289,309}

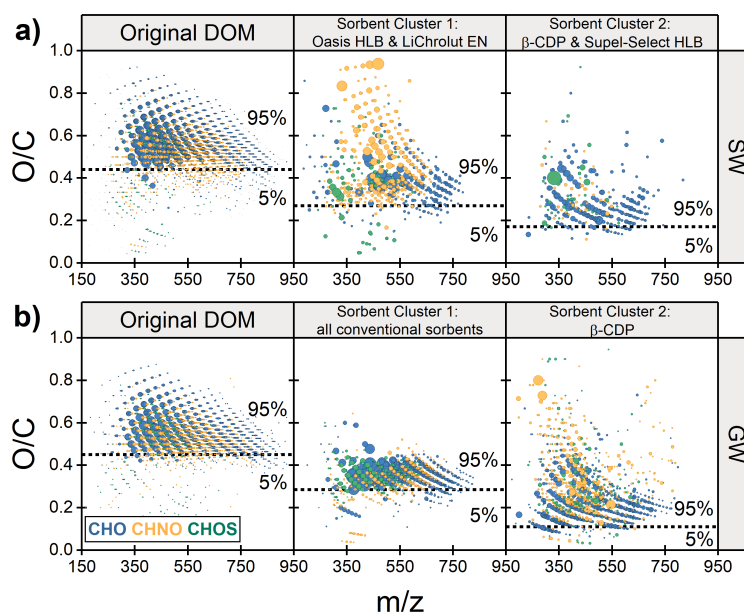


Figure 3.3. Mass-edited O/C diagrams of highly abundant molecular compositions in (a) SW and (b) GW samples of highest similarity identified by HCA (cf. Figure 3.1). Symbols are color-coded according to CHO (blue), CHNO (orange), and CHOS (green) molecular series, and symbol sizes reflect relative signal intensities of each mass peak. The dotted lines indicate O/C ratios above which 95 % of peak intensities were present.

Scarce unique molecular signatures of 678 and 817 assigned formulas for the SW and GW sample, respectively, further underpin the selective sorption behavior of β -CDP. As displayed in Figure 3.4, these features were primarily relatively saturated and oxygen-deficient ($H/C > 1$, $O/C < 0.5$) and cluster in the region of lipid-like and O-deficient lignin-like compounds in the van Krevelen diagram. In addition, mass-edited H/C ratios reveal that mostly compounds of molecular weight below approximately 600 Da were uniquely retained by β -CDP. In contrast, the multitude of approximately 5700 molecular compositions exclusively detected in conventional sorbent extracts of both water types (i) covered the entire mass range and (ii) span across a wide range of compositional space (see also Figure S3.16), namely, from highly saturated ($H/C = 2$) to aromatic compounds ($H/C < 1$ and $AI_{\text{mod}} \geq 0.5$) with low to extremely high degrees of oxidation ($O/C = 0.02 - 0.95$), including lignin- and tannin-like compounds, as well as CRAMs. This markedly universal extraction behavior agrees with the reported capability of HLB sorbents^{289,291} and the hyper-cross-linked LiChrolut EN^{178,310} to also efficiently retain highly oxygenated compounds. Additional extraction preferences toward certain compound classes, such as saturated and unsaturated sulfolipids,²²³ carbohydrate-like molecules,²⁹⁸ as well as oxygen-deficient black sulfur²²⁴ and nitrogen,³¹¹ even extended the molecular diversity of DOM extracted by conventional sorbents (cf. label A to G in Figure 3.4).

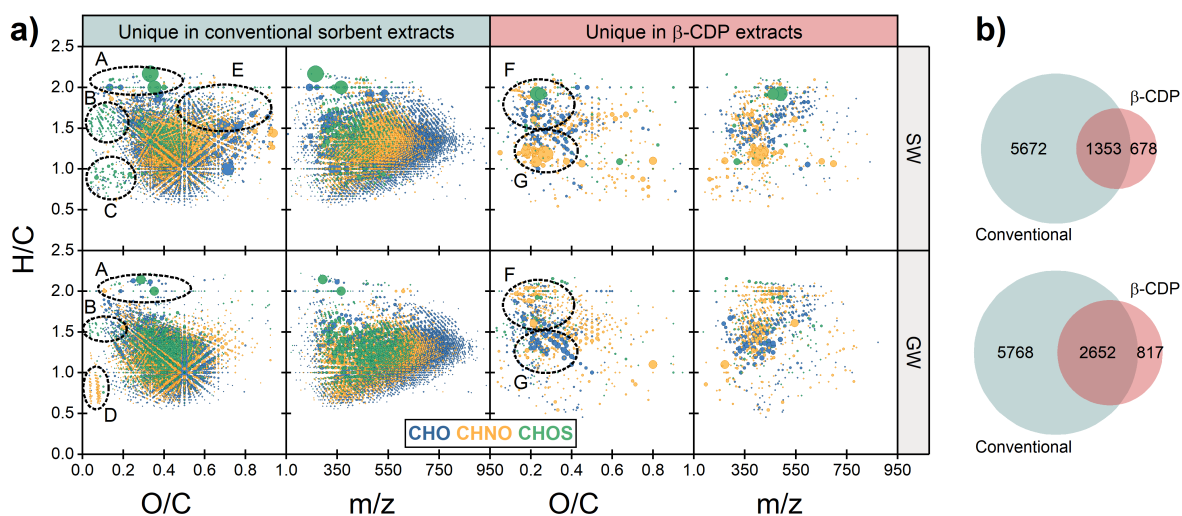


Figure 3.4. (a) Van Krevelen and mass-edited H/C diagrams of unique molecular signatures present in either conventional sorbent or β -CDP extracts. Symbols are color-coded according to CHO (blue), CHNO (orange), and CHOS (green) molecular series, and symbol sizes reflect the relative signal intensities of each mass peak. Assignment of selected compound classes: saturated (A) and unsaturated (B) sulfolipids, oxygen-deficient black sulfur (C) and nitrogen (D), carbohydrate-like (E), lipid-like (F), and oxygen-deficient lignin-like compounds (G). (b) Venn diagrams indicating counts of shared and unique molecular compositions.

3.4 Conclusions and Analytical Implications

The current work offers a molecular-level insight into the selective character of the model sorbent β -CDP, which was previously only indirectly observed as resilience to sorption inhibition of target analytes caused by fouling from DOM^{194,196} or directly measured as reduced matrix coextraction by bulk DOC analysis.²⁸⁵ The small numbers of retained DOM compounds on β -CDP, as revealed by FTICR MS and compared with those of the investigated universal sorbents, have in fact important analytical implications. For instance, when target analytes are equally well captured by a selective and universal sorbent, as it is the case for β -CDP with a multitude of micropollutants when compared with Oasis HLB,¹⁹⁵ it is more sensible to choose the selective sorbent to obtain cleaner sample extracts and subsequently less interferences during target analysis. In fact, the comparison between FTICR MS data and DOC measurements, which were obtained for the extraction of the same water sample under identical conditions,²⁸⁵ revealed an excellent correlation between the number of assigned molecular formulas and recovered DOC in sorbent extracts ($r^2 = 0.988$, Figure 3.5a). The straightforward and simple measurement of the DOC sum parameter can thus serve as a reliable proxy for the sorbent selectivity during analytical method development.

Compared with the universal sorbents, β -CDP was found to discriminate most strongly against some of the most ubiquitous terrigenous DOM constituents: oxygenated and unsaturated compounds. Since these are the typical main components in freshwater-derived organic matrices, these findings can effectively be used as an *a priori* assessment for extraction procedures as well as cleanup strategies for environmental samples. In fact, we show in Figure 3.5 an example of using the chemical space extracted by β -CDP to roughly predict the sorbent selectivity toward molecular compositions of potential target compounds. Indeed, the approach reveals that β -CDP is particularly efficient (i.e., reported recoveries $\geq 75\%$) in retaining nonionic compounds that mainly appear in the van Krevelen diagram in the region of $O/C < 0.5$ (Figure 3.5b), which largely overlaps with the compositional space of DOM that is preferentially extracted by the sorbent. The overlap also suggests that variability in the original compositional space of DOM will impact the selectivity magnitude of β -CDP. From an analytical perspective, it is a drawback when similar compounds are coextracted that cause matrix effects, such as (phospho)lipids or proteins in biological and food matrices,^{280,312} or in algae-derived environmental DOM,³⁰⁹ which are particularly known to suppress ionization efficiencies in LC-MS. This underscores the necessity for (i) a critical method validation for each individual sample matrix and (ii) careful tailoring of sample preparation protocols to the particular needs of the analytical approach.

This study highlights the outstanding suitability of a nontargeted ultrahigh-resolution MS approach for sorbent selectivity assessment on the molecular level and certifies β -CDP as an advantageous sorbent for selective SPE to discriminate against environmental DOM in matrix-susceptible analytical applications. Further research on the exact binding

mechanisms that govern the selectivity of β -CDP could contribute to designing even more efficient and selective CD-based sorbent materials.

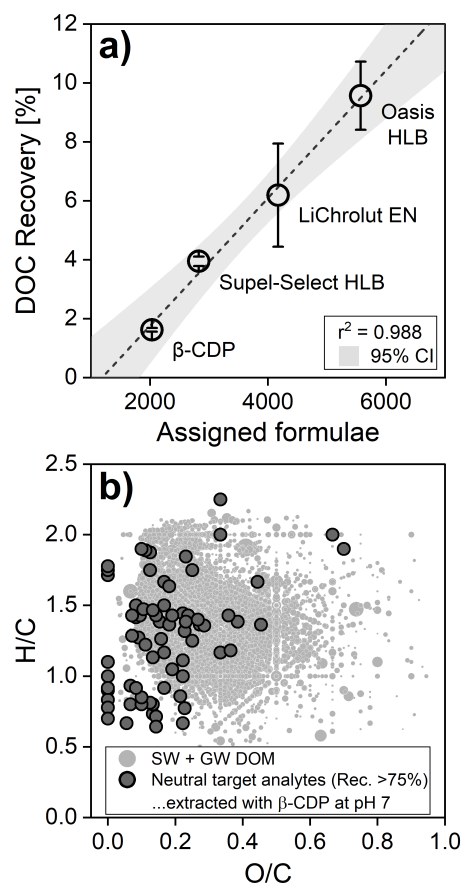
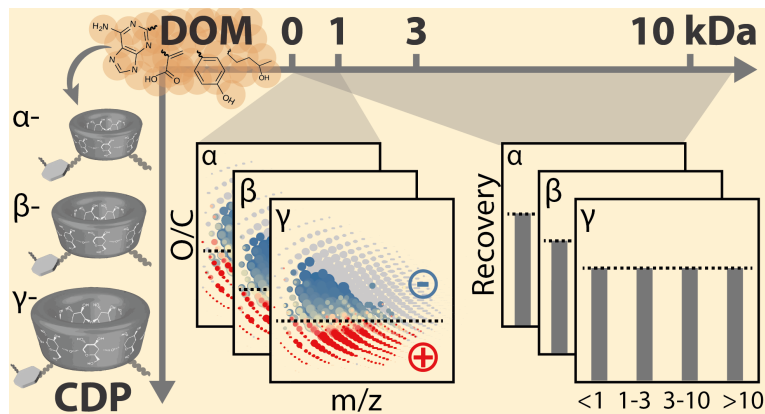


Figure 3.5. (a) Recovery of DOC after SPE of SW sample versus the number of assigned molecular formulas derived from FTICR MS analysis. DOC data was obtained from ref. 285, where the same SW sample was extracted under identical experimental conditions. (b) Van Krevelen diagram of SW and GW DOM (light gray circles) superimposed by the molecular composition of nonionic target analytes with recoveries >75 %, both extracted using β -CDP at pH 7. The figure is original and has been produced using data from this study, DOC recovery data from Glöckler et al., 2023 (ref. 285), and target analyte recoveries data from Glöckler et al., 2023 (ref. 285), Li et al., 2018 (ref. 195), and Ling et al., 2017 (ref. 194).

Chapter 4

Discriminative Behavior of Cyclodextrin Polymers against Dissolved Organic Matter: Role of Cavity Size and Sorbate Properties



Abstract

Cyclodextrin polymers (CDPs) are promising next-generation adsorbents in water purification technologies. The selectivity of the polymer derivate cross-linked with tetrafluoroterephthalonitrile (TFN-CDP) for nonionic and cationic micropollutants (MPs) over dissolved organic matter (DOM) renders the adsorbent also attractive for many analytical applications. The molecular drivers of the observed selectivity are, nonetheless, not yet fully understood. To provide new insights into the sorption mechanism, we (i) synthesized TFN-CDPs with different cavity sizes (α -, β -, γ -CDP); (ii) assessed their extraction efficiencies for selected nonionic MPs in competition with different DOM size fractions (<1, 1-3, 3-10, >10 kDa) to test for size-selectivity; and (iii) performed nontargeted, ultrahigh-resolution Fourier transform ion cyclotron resonance mass spectrometry (FTICR MS) analysis on CDP-extracted DOM compounds (<1 kDa) to probe for molecular sorbate properties governing their selective sorption. First, no evidence of size-selectivity was obtained through neither the different CD cavity sizes (i) or the two independent approaches (ii) and (iii). Second, we found a dominant impact of sorbate oxygenation and polarity on extraction of DOM and MPs, respectively, with relatively oxygen-poor/nonpolar molecules favorably retained on all α -, β -, and γ -CDP. Third, our data indicates exclusion of an anionic matrix, such as carboxylic acids, but preferential sorption of cationic nitrogen-bearing DOM, pointing at repulsive and attractive forces with the negatively charged cross-linker as a likely reason. Therefore, we ascribe TFN-CDP's selectivity to nonpolar and electrostatic interactions between MPs/DOM and the polymer building blocks. These molecular insights can further aid in the optimization of efficient and selective sorbent design for environmental and analytical applications.

The results of this chapter were published in modified form in the peer-reviewed paper cited below.

Reprinted with permission* from:

David Glöckler, Mourad Harir, Philippe Schmitt-Kopplin, Martin Elsner, Rani Bakkour. Discriminative Behavior of Cyclodextrin Polymers against Dissolved Organic Matter: Role of Cavity Size and Sorbate Properties. *Analytical Chemistry* **2023**, 95 (39), 14582–14591.

DOI: 10.1021/acs.analchem.3c01881

ACS Articles on Request author-directed link:

<https://pubs.acs.org/articlesonrequest/AOR-6QHDGYZFIJNEZDWWX69W>

Copyright © 2023 American Chemical Society.

*For the reprint permission, refer to Chapter S6.4.

4.1 Introduction

The ubiquitous contamination of natural water by organic micropollutants (MPs), such as pesticides, pharmaceuticals, and industrial chemicals, is recognized as a major global environmental issue, potentially threatening aquatic ecosystems and human health.^{3,313} As water scarcity increases, there is a growing need for monitoring and remediation strategies to identify and remove pollutant substances from both wastewater and freshwater. Cyclodextrin-based polymers (CDPs) have raised interest as cost-effective, regenerable next-generation adsorbents for environmental and analytical applications, including adsorption-based water treatment,^{199,314,315} and solid-phase extraction (SPE) prior to chemical analysis.^{191,316-319} Cyclodextrins (CDs) are a group of cyclic oligosaccharides composed of several glucose units linked by α -1,4-glycosidic bonds, which can be sustainably produced by the enzymatic degradation of starch.^{185,186} Their toroidal, cone-shaped structure and apolar interstitial cavity enable the formation of inclusion complexes with thousands of organic compounds through host-guest interactions, which are mainly based on hydrophobic (i.e., favorable change in free energy during inclusion) and van der Waals forces.^{187,188} This characteristic encapsulation property has led to numerous applications of CDs in diverse industrial sectors, such as pharmaceuticals, food, biotechnology, agrochemistry, catalysis, and chromatography.^{185,189}

To benefit from their unique binding properties in purification or separation processes, it is necessary to immobilize the soluble native CDs in a water-insoluble network through polymerization reactions.^{191,192} By introducing a perfluoroarene cross-linker (i.e., tetrafluoroterephthalonitrile, TFN) into the polymer network, Alsbaiee and co-workers recently synthesized the first high-surface-area polymer derivate (TFN-CDP, Figure 4.1),¹⁹³ whose mesoporous structure facilitated immediate access to the binding sites and a high sorption capacity. TFN-CDP rapidly removed a multitude of MPs from water, outperforming traditional carbon-based¹⁹⁴ and polymeric sorbents.¹⁹⁵ Most notably, TFN-CDP offers a high selectivity for MPs over concurrent dissolved organic matter (DOM) which renders it less susceptible to fouling in water purification systems¹⁹⁶ and can reduce analytical interferences caused by coextracted organic matrix when employed as an SPE sorbent.²⁸⁵ Although several attempts have been made to explain the observed selectivity of TFN-CDP, the underlying molecular drivers have not yet been fully elucidated. A sound understanding of the sorption process is nonetheless critical for further development of efficient and selective polymer designs.

One proposed mechanism that may be responsible for the selectivity is size exclusion of molecules larger than 0.6 kDa by the uniform CD cavities, as suggested by Ling and co-workers.¹⁹⁶ This conclusion was derived indirectly on the basis of inhibited sorption of MPs in water samples rich in low-molecular weight (MW) DOM. Yet, no size exclusion was observed in a subsequent quantitative structure-activity relationship (QSAR) study for selected MPs between 0.1 and 0.8 kDa and an upper size boundary was postulated for

molecules above that range.¹⁹⁸ On the contrary, a positive correlation between sorbate size and affinity to TFN-CDP was found, which was explained by the fact that small molecules have access to the binding sites in the CD cavities, but interactions with them would be limited due to their small size. However, this correlation can also be ascribed to the higher amount of free energy required for water cavity formation for larger and thus less polar molecules, rendering their partitioning to the sorbent phase more favorable.^{175,268} In fact, we observed a similar correlation but also for conventional reversed-phase sorbents that are not supposed to be driven by size-selectivity.²⁸⁵ We rather found indication of the importance of polarity for the sorption of nonionic sorbates by revealing the lowest affinities and recoveries for most polar analytes on TFN-CDP²⁸⁵ and a shift in chemodiversity of extracted matrix constituents toward oxygen-poor, saturated (i.e., nonpolar) compounds.³²⁰ This is conceivable since less polar molecules are known to show higher affinity for the apolar CD cavity^{14,26} as well as hydrophobic cross-linkers.²⁰⁴ Furthermore, cross-linker interactions^{205,253,284,321,322} were suggested to control CDP sorption through van der Waals, hydrogen bond, electron donor-acceptor and/or electrostatic forces.²⁰⁰ For instance, protonated amines in the CDP-cross-linker can increase the affinity for anionic MPs,²⁰¹⁻²⁰³ whereas negatively charged cross-linkers offer a high affinity for cationic MPs.^{194,197} Electrostatic interactions were confirmed by QSAR studies for TFN-CDP, where descriptors representing interactions between negatively charged cross-linker moieties (i.e., phenolates introduced by a side reaction of polymerization,¹⁹⁷ Figure 4.1) and cationic MPs were the most powerful sorption predictors.¹⁹⁸ It is therefore likely that selectivity of TFN-CDP may be induced by discrimination against anionic DOM (e.g., carboxylic acids) through electrostatic repulsion. To disentangle the relative importance of size exclusion, nonpolar sorption, and electrostatic interactions for selectivity, it is beneficial to conduct a combined, systematic investigation of the sorption behavior of target analytes and DOM on TFN-CDP, which includes both the entire DOM size spectrum (i.e., < 1 kDa to 0.45 μm) and different sizes of the CD cavities.

Therefore, the objectives of this study were (i) to test for a size-selective sorption mechanism by assessing extraction efficiencies and possible sorption inhibition for MPs at environmentally relevant concentrations in competition with different DOM MW fractions (i.e., <1, 1-3, 3-10, >10 kDa) on TFN-CDPs featuring different cavity sizes (i.e., α -, β -, γ -CDP) and (ii) to identify physicochemical sorbate properties that determine the sorption process (e.g., degree of oxygenation, unsaturation, aromaticity, charge, or molecular size) based on robust molecular-level information obtained from thousands of chemically diverse compounds. To meet the latter objective and to scrutinize the molecular size range in which size-exclusion was previously hypothesized (i.e., 0.2 – 1 kDa), we applied nontargeted, ultrahigh-resolution Fourier transform ion cyclotron resonance (FTICR) mass spectrometry analysis on heterogeneous and polydisperse DOM compounds, which were extracted by α -, β -, and γ -CDP from natural surface water (SW) and Suwannee River fulvic and humic acid (SRFA, SRHA) reference standards.

4.2 Experimental Section

4.2.1 Chemicals, Materials, and Sorbents

A detailed description of chemicals and materials is provided in the Supporting Information (SI) including CAS number, purity, grade, and supplier (S4.1), as well as standard solutions and ultrapure water (S4.2). Physicochemical properties of the selected MPs, namely 2,6-dichlorobenzamide (BAM), metamitron (MTM), thiacloprid (TIA), azoxystrobin (AZO), dimethomorph (DIM), atrazine (ATR), boscalid (BOS), *S*-metolachlor (SME), methiocarb (MET), terbuthylazine (TER), and propiconazole (PRO) are given in Table S4.2. The synthesis protocol reported by Alsbaiee et al.¹⁹³ was followed to prepare β -CDP and adapted for the synthesis of α - and γ -CDP, as depicted in Figure 4.1 and detailed in the SI (S4.3.1). Confirmation of the successful synthesis of the polymers was obtained through characterization with scanning electron microscopy (S4.3.2) and Fourier-transform infrared spectroscopy (S4.3.3). The polymer material was sedimented in methanol to obtain particle sizes larger than 40 μm .

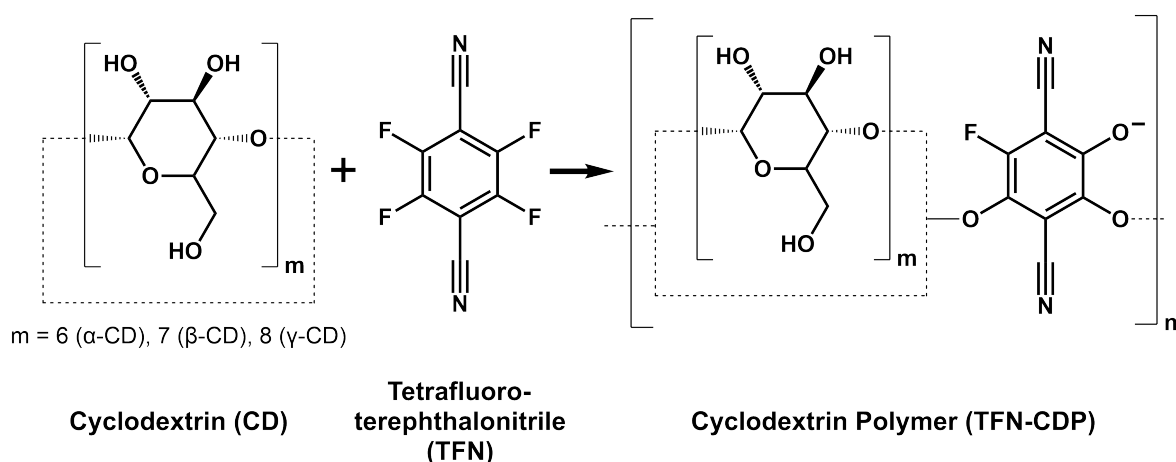


Figure 4.1. Synthesis scheme for the cross-linking of α -, β -, or γ -CD with TFN to form mesoporous CD polymers (TFN-CDPs).

4.2.2 Sample Preparation Procedures

Sample preparation in this work consisted of SPE of SW samples and aqueous SRFA and SRHA reference standards with different pre- and post-treatments. For water sampling and standard preparation, we refer to the SI (S4.4). We utilized self-packed polypropylene SPE cartridges (1 and 3 mL, Supelco, USA) with sorbent bed weights ranging from 10 to 50 mg. Extraction was performed using a 12-port vacuum SPE manifold (Visiprep, Supelco, USA) at a volumetric flow rate of $\leq 1.0 \text{ mL min}^{-1}$, corresponding to linear flow velocities of $\leq 4.1 \text{ cm min}^{-1}$ (1 mL cartridge) and $\leq 1.6 \text{ cm min}^{-1}$ (3 mL). Detailed information about the experimental design is given in the following sections.

4.2.3 Micropollutant Extraction in Presence of DOM of Different Molecular Sizes

First, DOM in the SW sample was fractionated according to MW by ultrafiltration following a previously reported procedure,³²³ as described in the SI (S4.5.1). The concentrated MW fractions, namely <1, 1 – 3, 3 – 10, and >10 kDa, were then diluted with ultrapure water to obtain sufficient volumes for SPE experiments with typical dissolved organic carbon (DOC) concentrations of SW in the range of 2.1 to 5.3 mgC L⁻¹. After adjustment to pH 7, the fractions were spiked with a selection of 11 nonionic MPs (Table S4.2) at concentrations between 0.45 and 1.15 µg L⁻¹, which maintained consistent, environmentally relevant DOC-to-analyte ratios of 4611 ± 43 (µgC L⁻¹)/(µg analyte L⁻¹) in all samples (Table S4.6). To remove the organic solvent, which would have compromised subsequent DOC analysis, the analyte standard mixture was transferred to clean glass bottles, followed by complete evaporation under a gentle stream of N₂ and reconstitution in the water samples by using a magnetic stirring system. Initial DOC and analyte concentrations were determined immediately before SPE experiments.

The samples (20 mL) were extracted in triplicate using 10 mg of either α-, β-, or γ-CDP as sorbents. Prior to sample loading, SPE cartridges were conditioned with 1 mL of methanol and 650 mL of ultrapure water (pH 7) to remove the remaining small CDP particles (Figure S4.4). Once the samples were percolated through the cartridges, sorbents were washed with 1 mL of ultrapure water (pH 7), dried under vacuum, and finally eluted with 500 µL of methanol, where exact elution volumes were gravimetrically determined. Procedural blanks were prepared in the same way by loading the sorbents with ultrapure water. While 100 µL aliquots of extracts were separated for MP quantification using LC-MS/MS, the remaining sample volumes were used for DOC analysis.

Recoveries of analyte *i* (R_i) and DOC (R_{DOC}) were calculated according to equation (4.1) and (4.2), respectively:

$$R_i = \frac{\left(\frac{C_{i,eluate}}{EF}\right)}{C_{i,initial}} \times 100 \% \quad (4.1)$$

$$R_{DOC} = \frac{m_{C,eluate}}{m_{C,initial}} \times 100 \% \quad (4.2)$$

where $C_{i,analyte}$ and $C_{i,initial}$ (µg L⁻¹) are the measured concentrations in the eluate and original sample, respectively, and EF is the enrichment factor of SPE. $m_{C,eluate}$ and $m_{C,initial}$ (µg) are the carbon masses determined in the eluate (corrected for carbon bleed from the sorbent material) and in the original water sample, respectively.

4.2.4 Extraction of Dissolved Organic Matter for Molecular-Level Analysis

SW samples and SRHA/SRFA reference standards (50 mL) were extracted at pH 7 using α -, β -, and γ -CDP, as described above. Following the guidelines of Dittmar et al.,²⁹³ we chose sorbent bed weights according to sample volume and DOC concentration, namely 25 and 50 mg for the SW samples and DOM reference standards, respectively (Table S4.7). Once cartridges were loaded, washed, and dried, samples were eluted with 1 mL of methanol. To identify sorbent-specific mass peaks caused by polymer leaching, we correspondingly prepared procedural blanks by loading every sorbent with ultrapure water.

To characterize the molecular DOM compositions of both the original SW sample and DOM reference standards, we additionally extracted the samples using the functionalized styrene-divinylbenzene sorbent Bond Elut PPL (Agilent, CA, USA), which provides a representative spectrum of the pristine DOM pool.^{287,289,293} FTICR mass spectra obtained by analyzing PPL-based SPE extracts thus well represent the original water sample and are hereafter referred to as the original sample. We followed the protocol of Li and co-workers,²⁹² where SPE was performed as described above with minor modifications. First, samples and ultrapure water for equilibration and washing were adjusted to pH 2 using 1M HCl, and second, cartridges were equilibrated with only 1 mL of ultrapure water (pH 2). To confirm both reproducible DOM isolation and FTICR MS analysis, we extracted the SRFA standard with β -CDP in triplicate. One hundred μ L aliquots of the extracts were used for DOC determination, whereas the remaining methanolic samples were stored at -20 °C until FTICR MS analysis.

4.2.5 Chemical Analyses

4.2.5.1 Micropollutant Quantification by Liquid Chromatography – Tandem Mass Spectrometry

Quantification of MPs was performed using an ultrahigh-performance liquid chromatography system (PLATINblue, Knauer, Germany) coupled to tandem mass spectrometry (AB Sciex Triple-Quad 6500, Sciex, USA) using electrospray ionization (ESI) in positive mode. Detailed information on the method is provided in the SI (S4.6.1).

4.2.5.2 Analysis of Dissolved Organic Carbon

DOC concentrations were determined as nonpurgeable organic carbon (NPOC) using a total organic carbon analyzer (TOC-L, Shimadzu, Japan) equipped with a combustion catalytic oxidation reactor (680 °C) and a nondispersive infrared (NDIR) detector. The instrument was calibrated immediately prior to sample analysis by measuring standard solutions of potassium hydrogen phthalate. Quality control measurements of blanks, constantly run alongside samples, ensured background DOC values below the detection limit of the instrument (i.e., 0.05 mg L⁻¹). DOC concentrations in methanolic extracts were measured

after complete evaporation of the organic solvent under a gentle stream of nitrogen at 65 °C using an automated solvent evaporation system (TurboVap LV, Biotage, Sweden), followed by reconstitution of the dry residues in ultrapure water by ultrasonication for 15 min and vortex mixing for 1 min.

4.2.5.3 Molecular-Level Analysis by Ultrahigh-Resolution Mass Spectrometry

Ultrahigh-resolution FTICR mass spectra were acquired in negative ionization mode using a Solarix mass spectrometer equipped with a 12 T superconducting magnet and coupled to an Apollo II electrospray ionization (ESI) source (Bruker Daltonics, Bremen, Germany), as described in the SI (S4.6.2). Sorbent-specific peaks caused by polymer leaching were first identified by FTICR MS analysis of sorbent blanks and then removed from the peak lists of the corresponding sample extracts. Formulas of remaining peaks were assigned with an in-house written software tool (NetCalc)²⁹⁵ based on a restricted list of selected small molecular units with defined mass differences, corresponding to common chemical functional groups (i.e., CH₂, H₂, O, CO₂, S, SO₃, and NH) and transformations. Molecular formula assignments corresponded to a multiple Kendrick analogue mass defect analysis and generated all homologous series according to the chosen transformations simultaneously. Final molecular formula assignments were grouped into molecular series containing the CHO, CHNO, and CHOS compositions.

Details and equations on intensity weighted average values, relative peak intensities, and chemical indices used to study the degree of unsaturation and aromaticity of compounds (i.e., double bond equivalent, DBE; carbon-normalized DBE, DBE/C; modified aromaticity index, AI_{mod}) are given in the SI (S4.6.2). The difference in relative intensity of peaks between sorbent extract and original sample, ΔRI (%), was derived using equation (4.3):²⁸⁹

$$\Delta RI = \frac{RI_{sorbent\ extract} - RI_{original}}{RI_{original}} \times 100 \% \quad (4.3)$$

Hierarchical cluster analysis (HCA) was performed using the software Hierarchical Cluster Explorer 3.0 (University of Maryland, USA) where clustering of the normalized data sets (relative peak intensities) was achieved by applying the average linkage method (UPGMA) and distance metrics based on Pearson correlation coefficients.

4.3 Results and Discussion

As a preface to the discussion of sorption mechanisms of TFN-CDPs, we note that the term *polarity* is used in this work exclusively with respect to nonionic molecules and specifically describes (i) the ability to undergo hydrogen bond interactions with a counterpart molecule capable of hydrogen accepting and/or donating, such as water, and (ii) sorbates that have less favorable changes in free energy upon inclusion into the CD cavity, typically described as “apolar”, in relation to changes of free energy when interacting with water. As for ionized substances, we base the discussion on *electrostatic attractive* and *repulsive interactions* between localized charges of opposite and same signs, respectively.

4.3.1 Low-Molecular-Weight DOM Does Not Adversely Affect MP Extraction at Environmentally Relevant Concentrations

We examined a potentially size-driven selectivity of TFN-CDP by testing for the hypothesis that (i) low-MW (LMW) DOM (< 1 kDa) competes with target analytes for binding sites in the CD cavities, leading to lower analyte recoveries and (ii) that high-MW (HMW) DOM is excluded.¹⁹⁶ To this end, the recoveries of 11 nonionic MPs in presence of DOM of different MWs (i.e., < 1, 1 – 3, 3 – 10, > 10 kDa, Figure S4.5) were assessed at environmentally relevant concentrations (analytes: 0.5 to 1.2 $\mu\text{g L}^{-1}$, DOC: 2.1 to 5.3 mgC L^{-1} , constant $C_{\text{DOC}}/C_{\text{analyte}}$) after SPE using tailor-synthesized α -, β -, and γ -CDP, which feature cavity sizes of 0.57, 0.78, and 0.95 nm, respectively.¹⁸⁵ In addition, we determined the recoveries for the specific DOM size fractions by quantifying the DOC in the SPE extracts. Figure 4.2a depicts the statistical results of a one-way analysis of variance (ANOVA) evaluating the differences among the mean recoveries that were obtained in the presence of the different DOM size fractions (Table S4.9). The green color scale indicates probabilities (p-values) above the significance level ($\alpha = 0.05$) denoting mean recoveries to be equal among all samples, and thus, (i) MP sorption was not inhibited by competition with DOM (target analytes in Figure 4.2a) or (ii) equal amounts of DOC were recovered for all DOM size fractions (last column in Figure 4.2a). In contrast, the red color signifies statistically significant differences between the group mean values (i.e., $p > 0.05$).

From a target analyte perspective, the preponderance of the color green in Figure 4.2a clearly demonstrates that the size distribution of concurrent DOM has no significant effect on the vast majority of MP recoveries on any TFN-CDPs, regardless of their cavity size. This is depicted exemplarily in Figure 4.2b where propiconazole was extracted equally well by β -CDP in presence of all DOM size fractions (mean recovery: $102 \pm 6\%$, $p = 0.66$). This finding is in agreement with our previous study that revealed no significant competition between DOM and analytes on the three TFN-CDPs in HPLC column studies as demonstrated by Gibbs free energies of adsorption.²⁸⁵ Significant differences were only detected for the extraction of azoxystrobin on β -CDP and dimethomorph on α -CDP (red symbols, Figure 4.2a). A closer look at the specific fractions of DOM associated with a

reduced recovery identified DOM < 1 kDa for azoxystrobin but fraction 3-10 kDa for dimethomorph (Tukey-Kramer posthoc test, Figure 4.2c). These discrepancies neither revealed a consistent trend, nor were they found in more than one sorbent extract at a time, and we, hence, could not provide a possible explanation. Yet, the general trend of our data suggests no evidence for sorption inhibition caused by LMW DOM (< 1 kDa) under environmentally relevant conditions [hypothesis (i)].

Testing hypothesis (ii) returned results similar to MP extraction, where the ANOVA revealed no sorption preference for the smaller DOM size fractions on any of the investigated CDPs as indicated by equal mean DOC recoveries (Figure 4.2a, last column, $p > 0.05$). Interestingly, DOM larger than 10 kDa, corresponding to hydrodynamic diameters of $> 3 \text{ nm}$,^{208,324} was recovered just as well as the smaller fractions, although theoretically it is not expected to access the sorption sites in the mesopore space at all (i.e., $1.8 - 3.5 \text{ nm}$)¹⁹³. Moreover, α -CDP featuring the smallest cavity size of 0.57 nm recovered as much DOC as γ -CDP with the greatest cavity of 0.95 nm ($\sim 4 \%$, Figure 4.2d). In comparison, the polymer derivate with the intermediate cavity size (β -CDP) discriminated strongest against concurrent DOM of all sizes ($\sim 2 \%$ recovery, $p < 0.001$), in line with our previous study.²⁸⁵

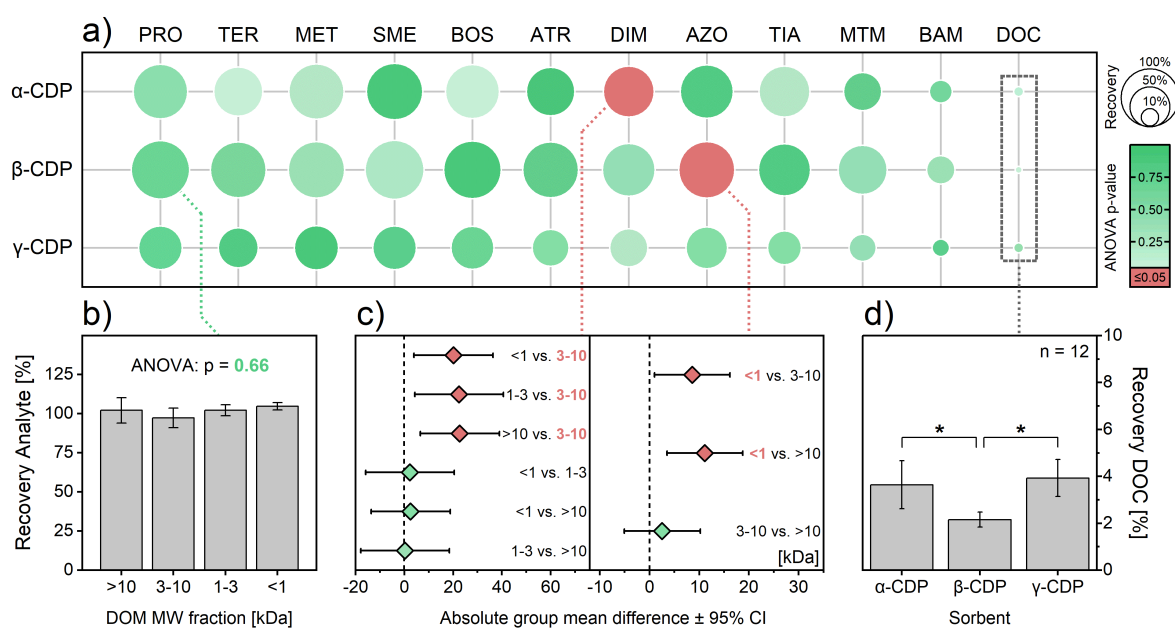


Figure 4.2. (a) Mean recoveries (symbol size) and ANOVA probability (p) values of 11 MPs (three-letter acronyms) and DOC extracted with α -, β -, or γ -CDP in the presence of different DOM MW fractions (i.e., <1, 1-3, 3-10, >10 kDa) as exemplarily shown in panel (b) for propiconazole on β -CDP. The green color scale indicates p-values above the significance level ($\alpha = 0.05$) denoting that mean recoveries are equal among all samples, whereas the red color signifies statistically significant differences (i.e., $p < 0.05$). (c) Tukey-Kramer posthoc test of differences in mean recoveries between pairs of MW fractions for dimethomorph on α -CDP (left) and azoxystrobin on β -CDP (right). Horizontal bars represent 95 % confidence intervals, where no overlap with 0-value means a significant difference of the corresponding mean values (red). (d) Mean DOC recoveries including all MW fractions after extraction with α -, β -, or γ -CDP. Asterisks signify significant differences ($p < 0.05$).

Altogether, these results suggest that size-selective host-guest interactions with the CD moieties are not the dominant driver of the selectivity of TFN-CDPs. This finding (i) agrees with Linden et al., who showed that CD inclusion complexes with structurally complex chemicals (comparable to the MPs and DOM in this study) can be sterically hindered,³²⁵ and thus, (ii) points to significant sorption outside the cavities that is driven by other sorbate properties than size. In fact, the recoveries for the 11 MPs selected in this work, in combination with a larger literature data set (i.e., 88 MPs, Table S4.10), imply that sorbate polarity is the important parameter for the sorption of nonionic molecules to TFN-CDPs (Figure 4.3). This is indicated for β -CDP by a sharp decline of recoveries for highly polar analytes as proxied by $\log K_{OW}$ values below approximately 0.7 (Figure 4.3a). In contrast, no trend in recoveries was observed when compared to the molecular size of the target analytes (McGowan volume: 0.9 – 3.0 $\text{cm}^3 \text{mol}^{-1} 100^{-1}$, corresponding to a MW of 0.12 – 0.50 kDa, Figure 4.3b). However, since a size cutoff around 0.6 kDa was previously claimed for TFN-CDP,¹⁹⁶ our findings motivate a closer insight into the sorption behavior of the chemically complex DOM system in the size region below 1 kDa.

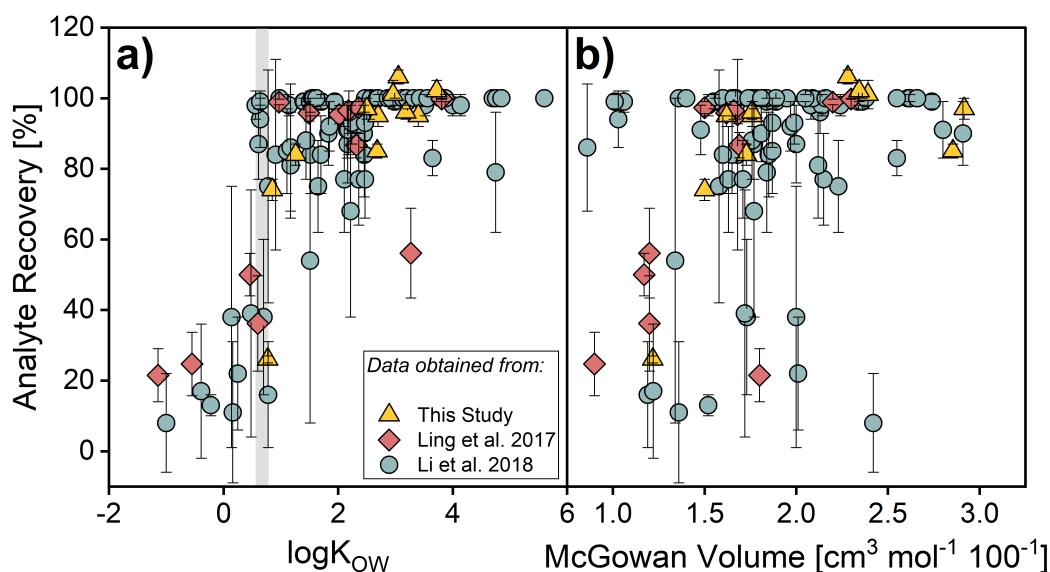


Figure 4.3. Recoveries of 99 nonionic target analytes after SPE using β -CDP versus $\log K_{OW}$ as proxy for polarity (a) and McGowan volume as indicator for size (b). The vertical gray line in panel a indicates the $\log K_{OW}$ of approximately 0.7 under which analyte recoveries sharply declined. The data was obtained from experiments in this study (triangles, 11 analytes) and from literature (diamonds and circles, 88 analytes).^{194,195}

4.3.2 TFN-Cross-Linked Cyclodextrin Polymers Strongly Discriminate Against Highly Oxygenated and Unsaturated Compounds

To probe for sorbate properties that govern the selective TFN-CDP sorption (e.g., degree of oxygenation and unsaturation or molecular size), we characterized the chemical composition of the chemically complex DOM extracted by α -, β -, and γ -CDP from (i) natural SW and (ii) SRFA and SRHA reference standards on a molecular level. We subsequently compared them to their original chemical signature, as extracted by PPL-based SPE, which is best suited for representing the original composition of DOM.^{287,289,292} To this end, highly-

resolved negative ESI FTICR mass spectra enabled the assignment of a total of 11,611 individual mass peaks to their corresponding unique elemental composition and the distinction into CHO, CHNO and CHOS molecular series (Figure S4.6a, Table S4.11). Mass spectra of SRFA DOM extracted in triplicate with β -CDP showed the highest degree of similarity (Figure S4.6b), proving reproducibility of both the extraction procedure and ESI ionization. This nontargeted ultrahigh-resolution MS approach provided insights into key molecular characteristics for thousands of pristine and selectively extracted DOM compounds in the m/z window between 0.2 and 1 kDa (Table S4.11).

Van Krevelen diagrams reveal for all extracted samples a distinct shift from original, average O/C and H/C ratios of 0.5 and 1.0 – 1.1, respectively (green symbol, Figure 4.4a) to less oxygen-rich (Δ O/C: -0.1 to -0.2) and more hydrogen-rich (Δ H/C: +0.1 to +0.3) signatures in TFN-CDP extracts (blue symbols). This trend was found to increase in the order β -CDP < α -CDP < γ -CDP. Corresponding to higher H/C values, average DBE/C ratios, which are a measure for the double bond density in molecules, significantly decreased in CDP-extracts (Δ DBE/C: -0.1 to -0.2, Figure 4.4b). Both shifts in H/C and DBE/C suggest a sorption preference of TFN-CDPs for compounds with higher saturation. We further observed a marginal shift from the initial ~500 Da to 15 – 40 Da lower average m/z values in CDP extracts (Figure 4.4b), with the exception of SRFA and SRHA extracted by γ -CDP that showed a higher shift by 60 – 70 Da. This mass fractionation is indeed indicative of a slightly higher affinity of TFN-CDPs for compounds of lower MW. However, the mass fractionation also followed the order β -CDP < α -CDP < γ -CDP and did not correlate with CD cavity size. Moreover, corresponding to shifts in average O/C ratios, DOM in CDP extracts of all samples showed strong discrimination against molecules with multiple oxygen atoms (Figure 4.4c). While 94 % of the original DOM contained between 4 and 20 oxygen atoms, TFN-CDPs preferentially extracted (> 90 %) molecular compositions containing merely 4 to 12 oxygen atoms.

Consequently, the fractionation pattern of average bulk FTICR MS parameters suggests that the degree of oxygenation and unsaturation play an important role in the sorption process of TFN-CDPs, in line with previously reported shifts in chemodiversity of DOM extracted with β -CDP from other water matrices.³²⁰ In fact, the observed correlation between oxygenation and unsaturation implies that TFN-CDPs particularly discriminated against DOM rich in oxygen-containing, unsaturated carbonyl functional groups, such as carboxylic acids, aldehydes, esters, or ketones.^{210,286} Yet, the question arises as to whether the degree of oxygenation or unsaturation is the governing sorbate property for selectivity. Therefore, a more in-depth analysis of changes in the molecular DOM composition after selective SPE is presented in the following sections. There, the discussion focuses on the most relevant molecular series, CHO and CHNO, which together represent ≥ 93 % of all extracted DOM compounds (Table S4.11).

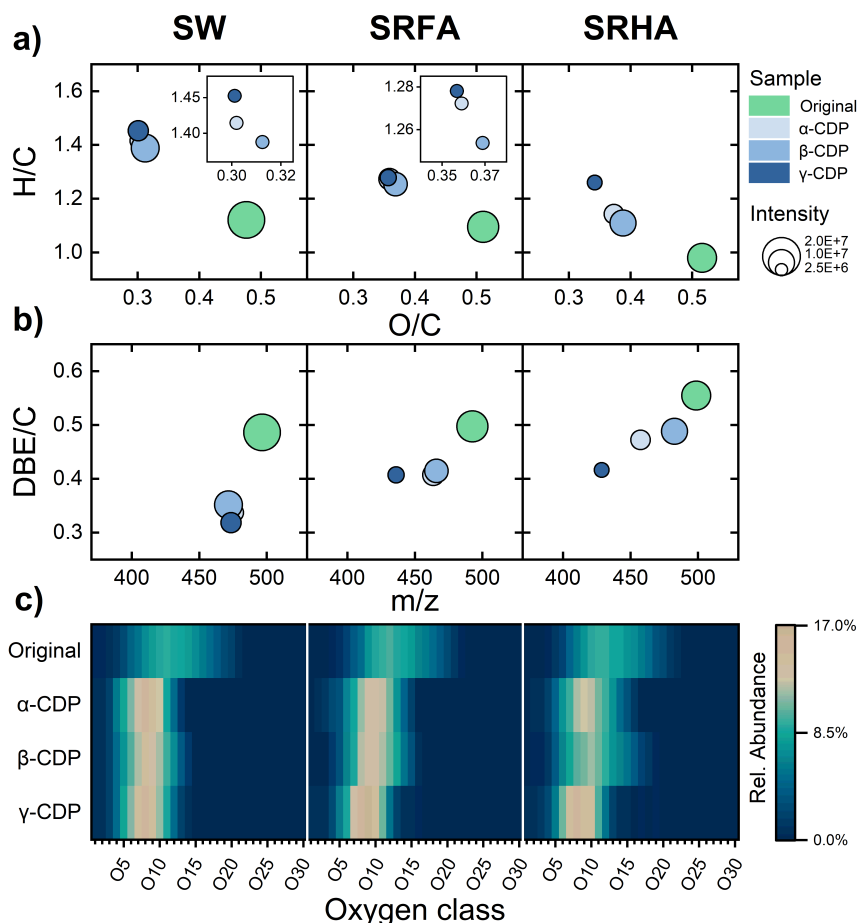


Figure 4.4. (a) Average elemental H/C versus O/C ratios (Van Krevelen diagrams) and (b) average double bond equivalent per carbon (DBE/C) versus m/z values for samples of the original SW and SRFA and SRHA samples, respectively (green symbols) and the respective α -, β -, and γ -CDP extracts (blue symbols). (c) Distribution of pristine and CDP-extracted DOM among the oxygen classes, that is, the number of oxygen atoms present in the molecular formula. Values were obtained from negative ESI FTICR mass spectra.

4.3.3 Degree of Oxygenation Determines the Sorption of CHO-Compounds on TFN-Cross-Linked Cyclodextrin Polymers

To pinpoint the underlying molecular drivers of selectivity, we visualized the differences in relative intensities of CHO-annotated formulas between TFN-CDP extracts and original DOM compositions.²⁸⁹ Figure 4.5 depicts the percental shifts in relative intensities (Δ RI) in O/C ratios either as a function of mass (left panels) or H/C ratio (right panels). Whereas blue and red colors indicate relative depletion and enhancement of the molecular structures in TFN-CDP extracts, respectively, gray symbols represent original DOM constituents that were not detected in the extracts.

A consistent O/C ratio of ~ 0.4 (horizontal dashed lines, Figure 4.5) was found to be separating the features that were depleted (blue and gray symbols) from those enhanced (red) regardless of CD cavity size (i.e., α -, β -, or γ -CDP) or sample type (i.e., SW, SRFA, or SRHA). This O/C ratio appears to follow two patterns: (i) constant across the entire range of molecular size (Figure 4.5, left panels) and the degree of unsaturation (right panels) for SW samples, whereas (ii) deviations from the constant ratio of ~ 0.4 were exhibited for SRFA and SRHA samples within certain ranges.

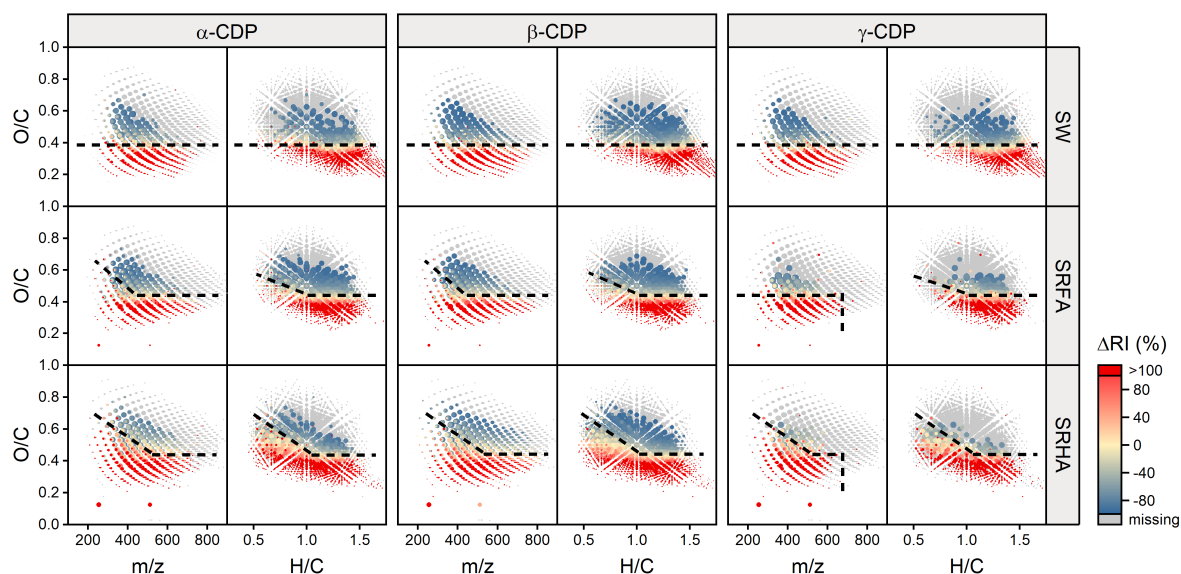


Figure 4.5. O/C versus m/z and H/C diagrams of CHO-annotated molecular DOM compositions in α -, β -, or γ -CDP extracts of SW and SRFA and SRHA samples. Differences in relative intensities (Δ RI) were calculated relative to the original sample composition and dashed lines denote approximate boundaries between relative enhancement (red) and depletion (blue, gray) of compounds in CDP extracts. Symbol sizes reflect the relative signal intensities of mass peaks in the original mass spectra.

To reduce the complexity of discussion, we elaborate first on pattern (i), where the constant O/C ratio means sorption dependency on DOM oxygenation. This is conceivable when considering the building block chemistries of the three polymers. On the one hand, the partitioning into the apolar CD cavities is (i) energetically less favorable for polar nonionic DOM molecules, which are rich in O-containing functionalities (e.g., ketones, aldehydes, and phenolic or alcoholic hydroxyls),²⁰⁸ than for less polar (i.e., less oxygenated) compounds^{187,200} or (ii) may be sterically hindered depending on the position of the functional groups.³²⁵ In addition, weak hydrogen bond acceptor (i.e., fluorine and nitrile moieties)³²⁶⁻³²⁸ and donor (i.e., electron-deficient aromatic ring) capacities of the cross-linker (Figure 4.1) are unlikely to compete with strong hydrogen bond interactions between oxygen-containing sorbate functionalities and water molecules. On the other hand, oxygen-rich anionic DOM molecules abundant in carboxylic moieties, which are the most prominent functional groups in environmental DOM,²⁰⁸ are highly water-soluble and additionally electrostatically repelled by the negatively charged cross-linker. Indeed, higher DBE yet lower DBE-O values of compounds missing in CDP extracts compared with the original composition indicate that C=O double bonds significantly contributed to their high degree of unsaturation (Figure S4.7).^{210,286} Consequently, the shift toward higher average saturation observed in Figure 4.4 is identified as a codependency on sorbate oxygenation based on the negative charge of oxygen-rich ionizable DOM and the ability of polar nonionic DOM to form hydrogen bonds with water.

Furthermore, upon comparison of DOM compounds with equal O/C ratios in the area of relative depletion (blue and gray symbols), it becomes apparent that primarily compounds of higher mass were missing, while smaller compounds were heavily depleted yet still

detected in TFN-CDP extracts. We attribute this to the typical skewed, near Gaussian-type mass peak distributions of freshwater-derived DOM with maximum intensities in the lower mass range (symbol size in Figure 4.5, Figure S4.6a).²⁹⁴ In other words, when oxygenated compounds were depleted by selective extraction, the larger, less easily ionizable compounds in the ion source with already low signal intensities fell below the detection limit first. We therefore ascribe the mass fractionation indicated by shifting average m/z values (Figure 4.4) not to a size-exclusion mechanism of the sorbent but to this ionization artifact.

The conclusions stated also apply for pattern (ii) seen for SRFA and SRHA samples; however, the following deviations from the consistent O/C ratio were noticed. First, several unsaturated LMW compounds (< 500 Da) with O/C ratios between 0.4 and 0.6 (tilted dashed lines, Figure 4.5) showed relative enhancement, especially in SRHA samples. And second, γ -CDP extracts revealed an apparent size cutoff around 650 Da (vertical dashed lines, Figure 4.5). These discrepancies could be erroneously interpreted as an impact of molecular sorbate size, either in preference for smaller masses or as a complete size cutoff, when merely considering masses and/or elemental composition. In fact, in the first case, the enhanced compounds with O/C > 0.4 were identified to be of aromatic character by their AI_{mod} values (i.e., $AI_{\text{mod}} \geq 0.5$, Figure S4.8), which reflect the C=C double bond density in a molecule.^{42,43} Here, additional π - π dispersion forces between electron-rich aromatic sorbate structures and the electron-poor aromatic TFN cross-linkers may have enhanced sorption. This is also reflected in a lower depletion of aromatic compounds in SRFA and SRHA samples by 6 ± 1 and 3 ± 2 percentage points, respectively, as compared to 9 ± 1 percentage points for SW samples ($\Delta\%Ar$ in Table S4.11). As for the second case, we refer to low extraction efficiencies of γ -CDP due to high SPE backpressures caused by polymer swelling that particularly entailed low signal intensities in the high m/z range (Figure S4.6a) and possibly biased FTICR MS analysis. Overall, the ΔRI patterns are in general consistent between TFN-CDPs of all cavity sizes, which means that DOM size did not significantly affect the sorption within the size range covered by FTICR MS, whereas sorbate oxygenation predominantly determined the sorption process of CHO-compounds.

4.3.4 TFN-Cross-Linked Cyclodextrin Polymers Preferentially Extract Protonated Over Nonionic CHNO-Compounds

TFN-CDPs of all cavity sizes preferentially extracted CHNO-compounds from SW and SRFA samples with H/C ratios above ~ 1.0 and N/C ratios below 0.07 (dashed circles, Figure 4.6). We suggest amino groups, which are among the most important N-containing functionalities in DOM,^{208,329} to cause this extraction preference of TFN-CDPs for relatively saturated CHNO-compounds. The strong basicity of aliphatic amines (pK_a of conjugate acid ~ 10) imparts a positive charge at pH 7 used for extraction, which likely leads to high affinities for TFN-CDPs due to electrostatic attraction by the negatively charged phenolates in the cross-linker.¹⁹⁷ In addition, the protonation of amine moieties in amino acids renders

them zwitterionic at pH 7, which may also increase the affinity for this saturated compound class. This proposed electrostatic adsorption mechanism for protonated CHNO-DOM is (i) consistent with the previously reported selectivity of β -CDP for cationic¹⁹⁴ and zwitterionic MPs²⁰² and (ii) supported by our observation of highly saturated CHNO-compounds ($H/C > 1.5$) that appeared in TFN-CDP extracts but not in the corresponding PPL-extracted DOM, which is typically used to represent the original DOM composition (Figure S4.9). Owing to their positive charge, aliphatic amines are known to be excluded by reversed-phase sorbents,²¹⁴ such as in PPL-based SPE, and can be recovered by sorbents featuring anionic functionalities as it is the case for TFN-CDPs. In contrast to this preferred retention of aliphatic amines, such a preference could not be observed for structures that could be assumed to contain highly unsaturated amines, amides, or heterocyclic nitrogen moieties ($H/C < 1.0$, blue and gray symbols).³²⁹⁻³³¹ Here, the N-containing functionalities are generally nonionic at pH 7 and their strong hydrogen bond polarity amplifies the water solubility of the molecules, in addition to possible interactions between polar nonionic and/or anionic O-functionalities with water.

In contrast, the degree of oxygenation seems to have played a dominant role in the sorption of CHNO molecules from SRHA samples as α - and β -CDP revealed preference for low-oxygenated and low-nitrogenated compounds ($O/C < 0.4$, $N/C < 0.07$) across the whole H/C range (dashed circles). No trend could, however, be inferred for γ -CDP as this sorbent was highly inefficient in retaining CHNO-compounds. The high similarity of ΔRI patterns of SW and SRFA extracts as opposed to SRHA extracts is most likely related to the higher amount of fulvic acids ($\sim 40\%$ of DOC) rather than humic acids ($\sim 10\%$ of DOC) in typical riverine DOM.²⁰⁸

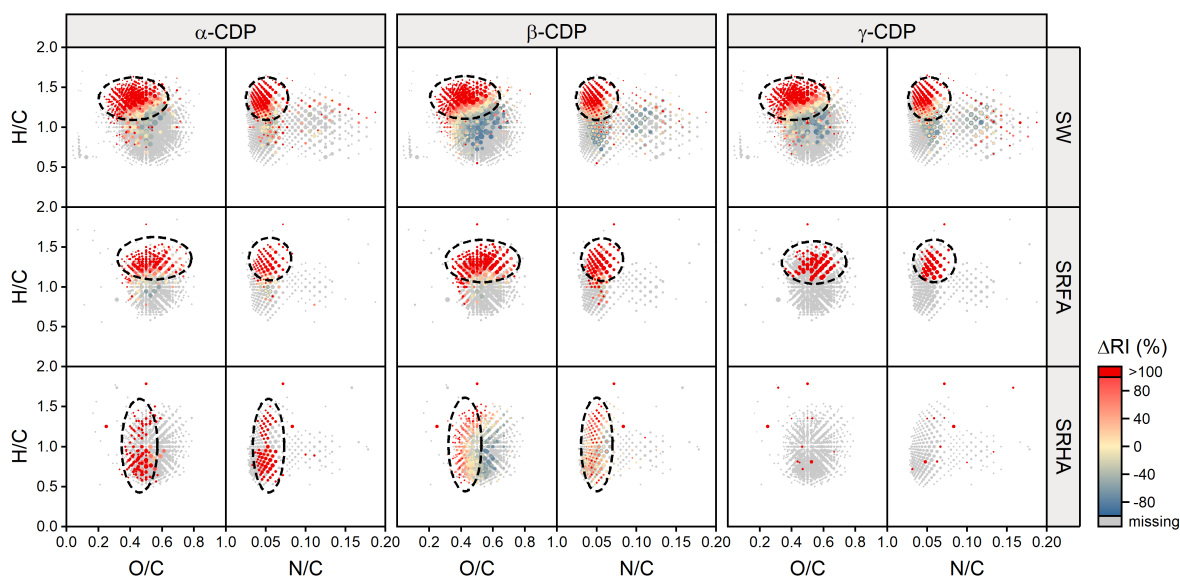


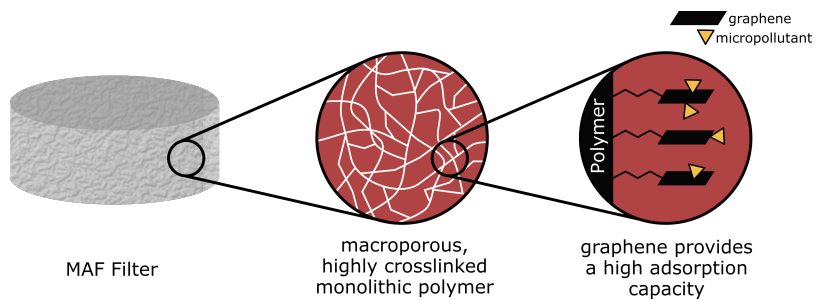
Figure 4.6. Van Krevelen diagrams (H/C versus O/C or N/C ratios) of CHNO-annotated molecular DOM compositions in α -, β -, or γ -CDP extracts of SW and SRFA and SRHA samples. Differences in relative intensities (ΔRI) were calculated relative to the original sample composition. Dashed circles denote compounds preferentially extracted by the CDPs. Symbol sizes reflect the relative signal intensities of mass peaks in the original mass spectra.

4.4 Conclusions

The present combined experimental approach provides new insights into the sorption mechanisms of TFN-cross-linked CDPs. We found no evidence of size-selectivity by (i) any of the investigated CD cavity sizes in either (ii) competition sorption experiments involving selected target analytes and the entire DOM size range (i.e., < 1 kDa to 0.45 μ m) or (iii) FTICR MS studies on extracted LMW-DOM below 1 kDa. Our findings thus challenge the hypothesized size cutoff^{196,198} and strengthen the rationale that previously observed size-dependent sorbate affinities to TFN-CDP are due to the decreasing polarity of molecules of increasing size.^{198,285} Indeed, the importance of nonpolar interactions between sorbates and polymer building blocks (i.e., van der Waals, π - π , energy changes upon host-guest inclusion) is corroborated by FTICR MS results that revealed the dominant influence of sorbate oxygenation (i.e., proxy for polarity) on DOM sorption irrespective of sorbate or CD cavity size. Furthermore, the evidence for the exclusion of anionic but preferential extraction of cationic matrix compounds points to an additional electrostatic adsorption mechanism in which ionic molecules interact with the negatively charged cross-linker. We consequently attribute the selectivity of TFN-CDP for nonionic and cationic MPs over concurrent DOM to a synergistic effect of nonpolar and electrostatic interactions. Our findings suggest that sorption on TFN-CDP, similar to decafluorobiphenyl-CDPs,²⁰⁵ occurs to a considerable extent outside the CD cavities. The exact quantitative contribution of the CD moieties and the cross-linker to sorption remains nonetheless an important question to be addressed by future research. The molecular insights in this study will help to identify polymer characteristics that can be optimized in the future development of efficient sorbent materials for specific environmental and analytical applications. For example, selectivities can be manipulated by varying the functional groups in the cross-linker to create selective phases that discriminate against or even favor certain DOM fractions.

Chapter 5

Graphene-Modified Polymer Monoliths for High-Throughput Extraction of Micropollutants: A Proof-Of-Concept Study



5.1 Introduction

The evaluation of natural degradation of organic contaminants in aquatic systems is a critical component of comprehensive environmental management strategies. Understanding the pollutants' fate by determining the rate of degradation and the mechanisms involved is essential to inform effective approaches to remediate contaminated sites or aquifers. To this end, multiple lines of evidence should be followed, since, for example, relying solely on concentration data may lead to erroneous conclusions about the rate and extent of degradation due to other nonreactive processes present (e.g., dilution, sorption).⁷⁵ The unique information provided by the isotopic signatures of individual compounds (e.g., $\delta^{13}\text{C}$, $\delta^{15}\text{N}$) is such a complementary type of evidence that bears great potential for elucidating environmental processes. Specifically, compound-specific isotope analysis (CSIA) has been proven to be a powerful tool for (i) contaminant source differentiation,⁸⁷⁻⁹¹ (ii) unequivocal identification and quantification of natural transformation processes,^{74,92-97} and (iii) characterization of these processes on a mechanistic level.^{73,76,100} Yet, due to the limited sensitivity of gas or liquid chromatography coupled to isotope-ratio mass spectrometry (GC- or LC-IRMS), transferring the CSIA approach to micropollutant (MP) applications at the catchment scale remains a challenge.^{146,147} Given the low occurrence of aquatic MPs such as pesticides in the sub- $\mu\text{g L}^{-1}$ range, enrichment of sufficient analyte mass from large volumes of water is inevitable. For instance, the sampling and extraction of 45 and 259 L of water is necessary to provide the required amount of 10 ng C and 42 ng N to GC-IRMS for accurate carbon and nitrogen isotope analysis, respectively. Thus, high-throughput concepts are warranted for large-volume extraction procedures in CSIA methodologies.

Although traditional solid-phase extraction (SPE) techniques employing particle-packed columns are available for enrichment of micropollutants, they fail in processing large volumes in feasible timescales due to limited flow rates (i.e., few mL min^{-1}).¹⁴⁹ In contrast, organic, polymer-based monoliths represent promising alternative stationary SPE phases. Their large pores in the μm range entail lower backpressures during the SPE procedure and thus allow for extraction at higher flow rates, resulting in shorter sample processing times.²³⁵ An example of such an organic monolith is the so-called *monolithic adsorption filter* (MAF), which has been successfully established for the enrichment of viruses^{332,333} and bacteria^{334,335} from aqueous matrices. MAFs are epoxy-based polymers prepared by self-polymerization of polyglycerol-3-glycidyl ether in toluene and *tert*-butyl methyl ether as porogenic solvents.³³⁶ A highly cross-linked structure with high porosity (79 %) and 22 μm pores enables the high throughput of large-volume water samples at up to 1 L min^{-1} .³³⁷ However, like most polymer-based monoliths, MAFs lack additional mesopores (i.e., 2 – 50 nm), and thus their low specific surface area of 0.68 $\text{m}^2 \text{g}^{-1}$ does not provide sufficiently large sorption capacity and kinetics toward small molecules such as organic MPs.

A strategy to extend the concept to MPs is to leverage the excellent tunability of the MAF surface chemistry by immobilizing carbonaceous graphene oxide (GO) nanosheets.

GO is a derivative of graphene, which is a single layer of sp^2 -hybridized carbon atoms arranged in a two-dimensional, honeycomb-like lattice. By incorporating this ultrahigh surface area nanomaterial (i.e., theoretically up to $2630 \text{ m}^2 \text{ g}^{-1}$), the surface area of the entire monolith can be significantly increased,²³⁸ resulting in enhanced sorption capacity and kinetics. Specifically, its large delocalized π -electron system favors the formation of strong van der Waals and π - π interactions and, consequently, offers high sorption affinities toward nonpolar aromatic compounds.²³⁹ Unlike graphene, GO is additionally rich in various oxygen-containing functionalities, such as hydroxy, carboxy, and epoxy groups, providing the material with a high degree of hydrophilicity and promoting hydrogen bonds with polar compounds.²⁴¹ Furthermore, the chemical reduction of GO to reduced GO (rGO) retains residual oxygen-containing groups on the surface imparting a *hydrophilic lipophilic balanced* (HLB) character to the sorbent, which, in turn, is favorable for the extraction of a broad range of MPs.²⁴⁷ In recent years, the applicability of graphene-modified monoliths for low-volume SPE has been demonstrated for different organic contaminants, including herbicides,²⁴² insecticides,²⁴³ benzotriazole,²⁴⁴ polychlorinated biphenyls and steroid hormones,²⁴⁵ and phenolic compounds.²⁴⁶ Nonetheless, a successful combination of rGO with the MAF platform for large-volume SPE of organic MPs has yet to be realized.

Therefore, the overall goal of this study was to exploit the synergistic effect of combining the high porosity of MAFs with the unique sorption properties of the carbon-based nanomaterial rGO for a high-throughput SPE application for organic micropollutants. The specific objectives were (i) to quantitatively evaluate the effect of chemical reduction on the sorption behavior of graphene oxide by determining the sorption parameters of GO and rGO for five model compounds through batch equilibrium experiments; (ii) to quantitatively assess the sorption kinetics of the bulk rGO material for the model compounds in comparison to the commercial HLB sorbent Oasis by batch kinetic studies, (iii) to covalently attach the graphene-based nanosheets to the MAF surface and obtain a graphene-modified monolith prototype (rGO@MAF); and (iv) to perform a proof-of-concept for the rGO@MAF concept by material characterization and a miniaturized flow-through extraction experiment to assess the applicability for future LV applications.

5.2 Experimental Section

5.2.1 Chemicals and Materials

All used reagents, solvents, and analytical standards including their CAS number, purity, and supplier are summarized in the Supporting Information (SI, Table S5.1). Target analytes in this study comprised four herbicides (i.e., chloridazon, isoproturon, *S*-metolachlor, and terbuthylazine), and the metabolite 2,6-dichlorobenzamide (BAM). Physicochemical properties and other compound-specific information are given in Table S5.2. Analytical standard stock solutions (1 g L⁻¹) were prepared in pure methanol and further processed to appropriate working solutions. All methanolic standards were stored at -20 °C in the dark. Graphene oxide powder (> 500 m² g⁻¹) was obtained from Graphitene Ltd. (Stevenage, UK) and Oasis HLB sorbent from Waters (Milford, MA, USA). Syringe filters Chromafil Xtra (GF-100/25, 1 µm pore size) and nylon membrane filters (47 mm diameter, 0.45 µm pore size) were purchased from Macherey Nagel (Düren, Germany) and GVS Filter Technology (Bologna, Italy), respectively. Ultrapure water (18.2 MΩ cm at 25 °C) was produced with a Milli-Q® Reference water purification system (Merck Millipore, USA).

5.2.2 Chemical Reduction of Graphene Oxide

The bulk graphene oxide (GO) was reduced using L-ascorbic acid as reducing agent according to an optimized literature protocol.³³⁸ Briefly, the GO was exfoliated into GO sheets at a concentration of 0.1 mg mL⁻¹ in ultrapure water by 1 h of ultrasonication. L-ascorbic acid was then added to the GO dispersion under vigorous stirring until a final concentration of 2 mmol L⁻¹ was reached. The pH of the solution was adjusted to pH 10 using a 25 % ammonia solution to prevent aggregation of the dispersed GO sheets by electrostatic repulsion. Subsequently, the dispersion was reacted at 95 °C for 15 min and cooled to room temperature. Finally, the reduced graphene oxide (rGO) was recovered on filter paper and dried at 70°C overnight.

5.2.3 Preparation and Functionalization of Monolithic Adsorption Filters

MAFs were synthesized based on the self-polymerization of an epoxy-based resin monomer (i.e., polyglycerol-3-glycidyl ether) as described by Peskoller et al.³³⁶ and according to the modified procedure reported by other authors^{332,335,339} (see reaction a in Figure 5.1). In short, the monomer and a porogen mixture of toluene and *tert*-butyl methyl ether (60:40 v/v) were first tempered at 29 °C for 1 h. Thereafter, a 1:10 dilution (v/v) of boron trifluoride diethyl etherate (BF₃·Et₂O, catalyst) and 1,4-dioxane was added to the porogenic solvents, the volume of which was equal to 1.25 % of the total volume. Once the mixture of porogens and catalyst solution was thoroughly mixed, the monomer was rapidly added in a 20:80 (v/v) monomer/porogen ratio. The solution was immediately vortex mixed for at least 1 min, subsequently transferred to custom-made PTFE molds (inner diameter: 38.6 mm, height:

10.0 mm), and incubated at 29 °C for 45 min. The polymerized MAF disks were then removed from the molds, soaked in methanol overnight to terminate the reaction and remove the porogens, and finally dried at room temperature in the fume hood.

To introduce primary amine groups to the MAF surface by coupling the highly reactive epoxy groups with polyether diamine (see reaction b in Figure 5.1), the MAF disks were fitted into MAF disk holders consisting of 50 mL dispenser tips (PD-tip, Brand GmbH, Germany), custom-made PTFE support plates (bore hole diameter: 2 mm), O-rings (nitrile butadiene rubber, 38.6 mm diameter), and a PTFE fitting for the connection to the silicone tubing. A detailed description of the set-up is provided by Wunderlich et al.³³⁵ First, the MAFs were washed by connecting the disk holders to a peristaltic pump (Vario pump system, Ismatec SA, Germany) and pumping 300 mL of ultrapure water at a flow rate of 10 mL min⁻¹ through the system. For functionalization, a 1:1 (v/v) mixture of the polyether diamine (Jeffamine ED-2003, Huntsman, USA) and carbonate bicarbonate buffer (0.015 M Na₂CO₃, 0.035 M NaHCO₃, pH 9.6) was circulated for 24 h at 60 °C through the system. After the reaction was completed, the NH₂@MAFs (Figure 5.1) were washed with ultrapure water (60 °C) for another 6 h, subsequently removed from the disk holder, and dried in a desiccator for the next functionalization step.

Prior to grafting GO onto the NH₂@MAFs, the MAFs were cut into smaller disks of 1.6 cm diameter and 0.4 cm height to suit the experimental setup used for flow-through sorption studies (see Chapter 5.2.5.2). The immobilization of GO onto NH₂@MAF (reaction c in Figure 5.1) was accomplished by coupling the carboxy groups of GO with the amine groups on the MAF surface via amide bonds using *N,N'*-dicyclohexylcarbodiimide (DCC) as a coupling agent. A detailed reaction scheme is given in Figure S5.1. To this end, the GO powder was dispersed at a concentration of 1 mg mL⁻¹ in *N,N*-dimethylformamide (DMF) by ultrasonication for 1 h and DCC was added in excess to the solution (0.2 g). Afterwards, one NH₂@MAF disk was soaked in 30 mL of the filtered (1 µm, Chromafil Xtra) GO/DMF suspension, where entrapped air was removed by applying vacuum (20 mbar) for 30 min. Once the immobilization reaction was allowed to proceed for 24 h, the GO@MAF was washed with methanol to remove the insoluble reaction product dicyclohexylisourea (DCU), the formation of which confirmed the successful reaction. Using this method, approximately 16.5 mg GO were immobilized per single MAF as determined gravimetrically.

In a final step, the reduction to rGO@MAF (reaction d in Figure 5.1) was carried out analogously to the reduction of bulk GO. For this purpose, the GO@MAFs were fitted to a comparable MAF disk holder setup as described above, but consisting of a 10 mL syringe instead of a 50 mL dispenser tip. The 2 mM aqueous L-ascorbic acid solution (pH 10) was then circulated through the system at 95 °C for 15 min at a flow rate of 10 mL min⁻¹, where the MAF disks turned darker in color. Finally, the obtained rGO@MAFs were washed with 300 mL of ultrapure water and stored in ultrapure water at 4 °C until flow-through sorption experiments were performed.

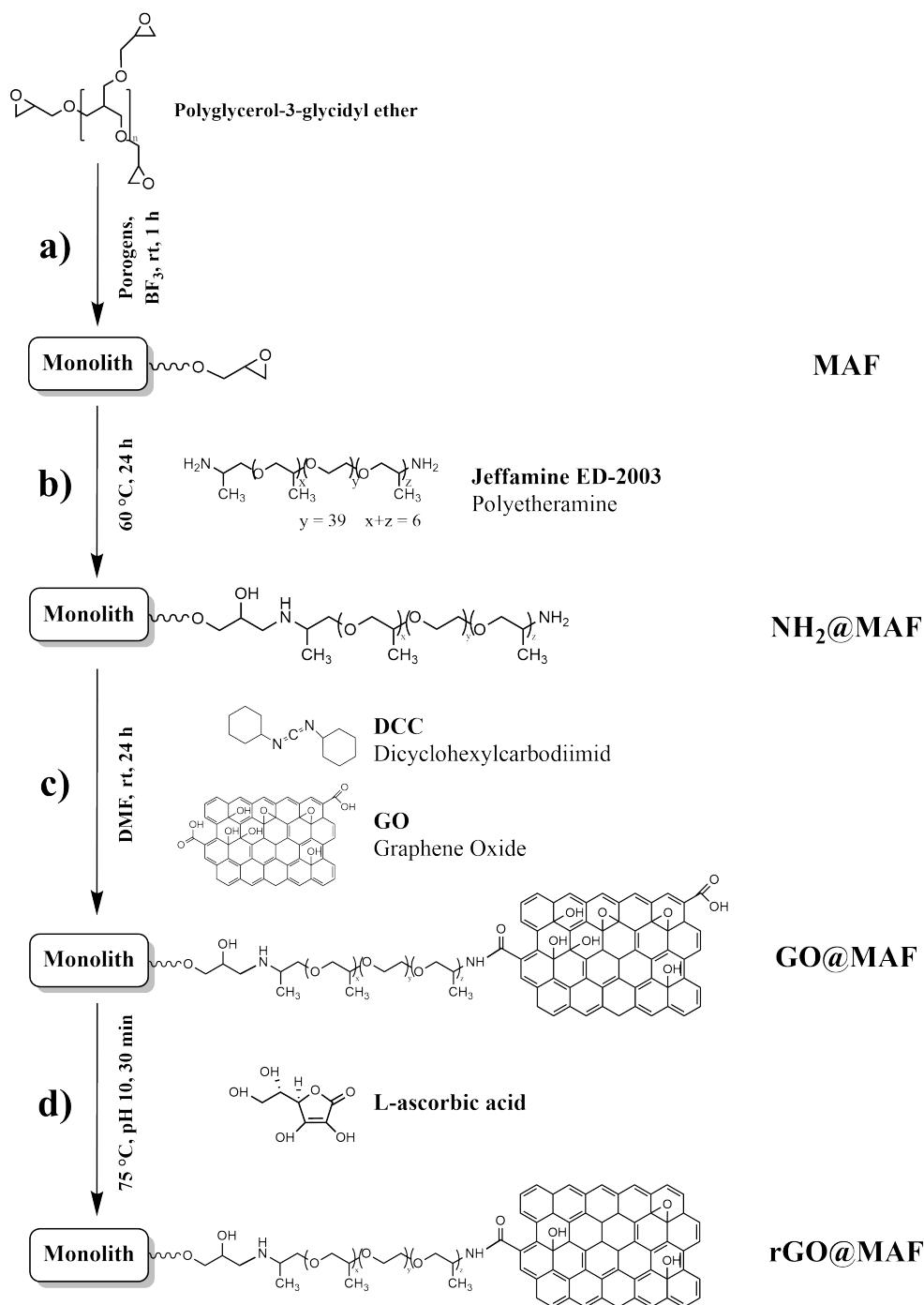


Figure 5.1. Synthesis and functionalization scheme to obtain unmodified monolithic adsorption filters (MAF), MAFs with amine functional groups ($\text{NH}_2\text{@MAF}$), and MAFs grafted with graphene oxide (GO@MAF) and reduced graphene oxide (rGO@MAF).

5.2.4 Material Characterization

5.2.4.1 FESEM imaging, FTIR and BET Measurements

Field emission scanning electron microscope (FESEM) imaging was carried out on a Sigma 300 VP instrument (Zeiss, Oberkochen, Germany) with an accelerating voltage of 10.0 kV and a sample distance of 4.4 to 9.9 mm. FESEM images were taken on the interior surface of the pristine and modified MAF polymers after cutting the disks. Fourier-transform infrared (FTIR) spectra (solid, attenuated total reflectance, ATR) were recorded using a Nicolet 6700 FTIR spectrometer (Thermo Scientific, USA) at a wavenumber range of 650 to 4000 cm^{-1} and a resolution of 4 cm^{-1} . The signal to noise ratio was improved by accumulating 32 individually recorded scans. Baseline correction was performed using the software OriginPro 2020. Brunauer–Emmett–Teller (BET) specific surface measurements were conducted with a 3Flex Adsorption Analyzer (Micromeritics Instrument Corporation, Norcross, GA, USA). The adsorption and desorption isotherms for gaseous N_2 were measured at 77 K after previous sample degassing overnight at 363.15 K under vacuum. Adsorption data was processed using the 3Flex software version 5.01.

5.2.4.2 Raman Microspectroscopy

Raman spectra were recorded using a WITec alpha 300 R confocal microscope system (WITec GmbH, Ulm, Germany), including a Cobolt DPL 532 nm excitation laser (Cobolt AB, Solna, Sweden) and a true-power module providing a constant laser power of 10 mW. The laser was focused onto the sample with a 20x microscope objective (Zeiss EC Epiplan 20x/0.4; Carl Zeiss AG, Germany). Light detection was accomplished with a fiber-coupled spectrometer (UHTS300S_VIS; WITec GmbH, Ulm, Germany) using a 600 lines/mm grating blazed at 500 nm and a Newton 970 EMCCD camera (DU970P-BVF; Andor Technology Ltd., Belfast, UK). Single spectra in the spectral range from 200 to 3800 cm^{-1} were acquired by accumulating 5 scans with an integration time of 1 s.

5.2.5 Sorption Experiments

5.2.5.1 Sorption Parameter Determination by Batch Equilibrium Studies

Sorption parameters were obtained for the 5 model compounds by means of the batch equilibrium method following OECD²⁵⁴ and US EPA guidelines.²⁵⁵ Sorption isotherms were determined on bulk GO and rGO, whereas sorption kinetics were measured on bulk rGO and Oasis HLB sorbent, according to the following procedure: Suspensions containing 5 mg sorbent in 5 mL 0.01 M CaCl_2 (pH 7) were exfoliated by ultrasonication for 2 h, pre-equilibrated by overhead shaking overnight, and subsequently spiked with analytes, where final methanol volumes did not exceed 1 % to prevent co-solvent effects. For sorption isotherm studies, spiked concentrations ranged from 2.5 to 40.0 mg L^{-1} , whereas samples were spiked at a constant concentration of 5 mg L^{-1} for sorption kinetic studies. In addition,

control samples (without sorbent) for each concentration level and blanks (without analytes) were run to account for potential instability of the analytes, adsorption to the test vials and matrix interferences, respectively. All samples were prepared in duplicates and shaken for 24 h (isotherms) and 1 to 24 h (kinetic studies) in the dark at 25 ± 1 °C. Afterwards, the suspensions were filtered (0.2 μm) and aqueous equilibrium concentrations were measured by means of HPLC as detailed below.

The sorbed amount of analyte at equilibrium (q_{eq} , isotherm studies) and the sorbed amount of analyte at a given time t (q_t , kinetic studies) were calculated via mass balance. The sorption isotherms were fitted to the Freundlich and Langmuir sorption model according to equation (5.1) and (5.2), respectively:

$$q_{eq} = K_F \times C_{aq}^{1/n} \quad (5.1)$$

$$q_{eq} = \frac{q_{max} \times K_L \times C_{aq}}{1 + K_L \times C_{aq}} \quad (5.2)$$

where q_{eq} (mg g^{-1}) is the sorbed amount of analyte at equilibrium, C_{aq} (mg L^{-1}) is the aqueous equilibrium concentration of the compound, K_F [$(\text{mg/g})/(\text{mg/L})^{1/n}$] and K_L (L mg^{-1}) are the Freundlich and Langmuir sorption coefficients, respectively, $1/n$ (-) is the degree of isotherm nonlinearity and q_{max} (mg g^{-1}) is the maximum sorption capacity. For a comparison of the sorption behavior among the different analytes on GO and rGO, individual equilibrium partition coefficients (K_d) were calculated using the Freundlich equation at a fixed aqueous concentration, C_{aq} , of 1 mg L^{-1} .

The kinetic data was fitted to the pseudo-first order (Lagergren)³⁴⁰ and pseudo-second order model (Ho and McKay)³⁴¹ for sorption processes according to equation (5.3) and (5.4), respectively:

$$q_t = q_{eq}(1 - e^{-k_1 t}) \quad (5.3)$$

$$q_t = \frac{k_2 q_{eq}^2 t}{1 + k_2 q_{eq} t} \quad (5.4)$$

where q_t (mg g^{-1}) is the amount of solute sorbed at a given time t (min), q_{eq} (mg g^{-1}) is the amount of solute sorbed at equilibrium, k_1 is the rate constant of first-order sorption (min^{-1}), and k_2 is the rate constant of second-order sorption ($\text{g mg}^{-1} \text{ min}^{-1}$). All data fitting was performed using the software OriginPro 2020 and uncertainties were propagated according to the Gaussian error propagation law.

5.2.5.2 Flow-Through Sorption Studies Utilizing Monolithic Adsorption Filters

The extraction performance of rGO@MAF was examined for the five target analytes in a miniaturized flow-through experiment (i.e., MAF disk diameter of 1.5 cm) and compared to that of the unmodified MAF and the intermediate NH₂@MAF. To this end, the MAF holder was equipped with five disks of the respective MAF type to allow for sufficient sorption capacity for the amount of target analytes in the solution (based on determined maximum sorption capacities of rGO). The MAFs were conditioned with 10 mL methanol. Then, 100 mL of 0.01 M aqueous CaCl₂ solution spiked with target analytes at 5 mg L⁻¹ were percolated at 7.8 mL min⁻¹ (i.e., 4.4 cm min⁻¹ linear velocity) through the MAFs, which corresponds to a flow rate of 51.6 mL min⁻¹ in the setup with normal sized MAF disks (i.e., 3.86 cm diameter). The permeate was collected for subsequent concentration determination by HPLC. The same procedure was performed using an empty system as a control to account for analyte sorption to the housing and tubing. The analyte removal (%) was (i) determined via a mass balance based on the initial analyte concentration in the sample solution and the remaining concentration in the permeate, and (ii) corrected for the control value.

5.2.6 Quantification by High-Performance Liquid Chromatography

The analysis of chloridazon, isoproturon, *S*-metolachlor, terbuthylazine, and BAM concentration was performed using an HPLC system (Prominence, Shimadzu, Japan) equipped with a diode array detector (SPD-M20A, Shimadzu, Japan) at a wavelength of 210 nm (terbuthylazine at 222 nm). The injection volume was 20 µL and analyte separation was achieved by a Luna C18 column (2.0 x 50 mm, 5 µm particle size, Phenomenex, USA) at 40 °C and using a gradient elution with ultrapure water (eluent A) and acetonitrile (eluent B) at a flow rate of 1.0 mL min⁻¹. After 3.0 min of 25 % B, the fraction of B was increased to 40 % within 0.5 min, followed by an increase to 90 % within 5.5 min. The fraction of 90 % B was kept constant for 3.5 min and finally the column was re-equilibrated to initial conditions for 3.5 min. An external calibration was used to quantify concentrations of the investigated analytes in aqueous solution, where limits of quantification ranged between 0.1 and 0.3 mg L⁻¹ (i.e., tenfold the background noise).

5.3 Results and Discussion

5.3.1 Effect of Chemical Reduction of Graphene Oxide on Sorption Affinity and Capacity toward Organic Micropollutants

To evaluate the influence of chemical reduction on the sorption performance of GO, the partitioning of the analytes chloridazon, isoproturon, *S*-metolachlor, terbuthylazine, and 2,6-dichlorobenzamide (BAM) between water and the unreacted and reduced solid phases (i.e., GO and rGO) was examined by means of batch equilibrium studies. The obtained sorption isotherm data was fitted to the Freundlich and Langmuir isotherm model to quantitatively describe the sorption behavior of the analytes on the two graphene derivatives (Figure S5.2). In general, the obtained data was well described by both models as indicated by coefficients of determination (R^2) ranging from 0.85 to 0.99 (Freundlich) and 0.90 to 0.99 (Langmuir). Only the BAM data resulted in poorer fits, especially for the sorption on rGO (R^2 : 0.55 to 0.92). All fitted Freundlich and Langmuir sorption parameters are summarized in Table S5.3.

The chemical reduction of GO using ascorbic acid as a reducing agent under the given conditions resulted in an increase of affinities for all tested analytes from $\log K_d$ values between 2.6 ± 0.0 (BAM) and 3.0 ± 0.0 L kg⁻¹ (terbuthylazine) for GO to 3.2 ± 0.1 (BAM) and 3.7 ± 0.0 L kg⁻¹ (chloridazon) for rGO (Figure 5.2a). This increase corresponds to improvement factors in the order 6.5 ± 0.1 (chloridazon) > 5.1 ± 0.1 (isoproturon) > 4.0 ± 0.1 (BAM) > 3.9 ± 0.1 (*S*-metolachlor) > 3.3 ± 0.0 (terbuthylazine). In parallel, an increase of maximum sorption capacities occurred in the same order and by similar improvement factors between 2.1 ± 0.1 (terbuthylazine) and 6.2 ± 0.1 (chloridazon) (Figure 5.2b). As a result, the maximum sorption capacities of rGO ranged between 2.0 ± 0.1 (BAM) and 16.2 ± 1.4 mg g⁻¹ (chloridazon).

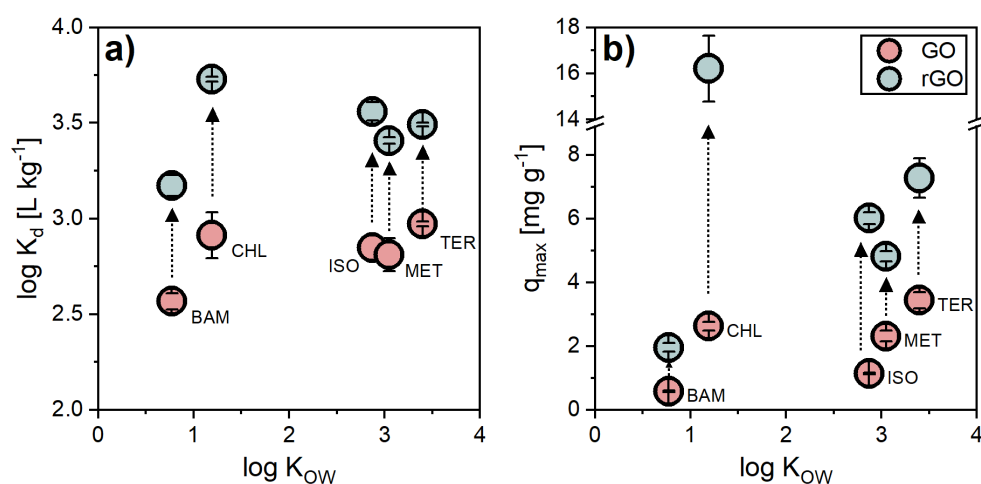


Figure 5.2. (a) Partitioning coefficients (K_d) for the analytes 2,6-dichlorobenzamide (BAM), chloridazon (CHL), isoproturon (ISO), *S*-metolachlor (MET) and terbuthylazine (TER) for the sorption on graphene oxide (GO) and reduced graphene oxide (rGO) versus the $\log K_{OW}$ value of the analytes. K_d values were calculated based on the Freundlich sorption model and a fixed equilibrium aqueous concentration of 1 mg L⁻¹. (b) Maximum sorption capacities for the analytes on GO and rGO as provided by the sorption isotherms fitted to the Langmuir sorption model.

Compared with sorption data of β -CDP and the commercial Oasis HLB sorbent presented in Chapter 2, rGO featured identical (BAM) or slightly lower K_d values (terbuthylazine, *S*-metolachlor) in the same order of magnitude (Table 5.1). In contrast, the maximum sorption capacities of rGO for all three analytes were distinctly lower than those of β -CDP and Oasis HLB (i.e., up to factor 6), despite a surface area larger than $500 \text{ m}^2 \text{ g}^{-1}$. This result was unexpected since GO and rGO are known to provide sorption capacities for structurally similar pesticides that are 1 to 3 orders of magnitude higher than those found in this study.^{342,343} It is conceivable that these discrepancies are due to the different origins of the material, since the properties of GO can vary depending on various factors such as the manufacturing process.³⁴⁴ High sorption capacities in literature are usually reported for GO and rGO that were produced using a modified Hummers' method.³⁴⁵ Due to the risks associated with this process, a commercially available high surface area GO powder was used instead in this study, which, however, was based on a proprietary production process.

Table 5.1. Partition coefficients (K_d) and maximum sorption capacities (q_{\max}) for the sorption of BAM, TER, and MET on rGO, Oasis HLB, and β -CDP sorbent.

Analyte	Sorbent	$\log K_d^\ddagger$ [L kg ⁻¹]	q_{\max} [mg g ⁻¹]
2,6-dichlorobenzamide (BAM)			
	rGO	3.2 ± 0.1	2.0 ± 0.1
	Oasis HLB*	3.1 ± 0.1	4.0 ± 0.3
	β -CDP*	3.0 ± 0.1	6.5 ± 0.3
Terbuthylazine (TER)			
	rGO	3.5 ± 0.0	7.3 ± 0.6
	Oasis HLB*	4.1 ± 0.1	21.9 ± 2.2
	β -CDP*	3.8 ± 0.1	20.9 ± 1.0
<i>S</i> -metolachlor (MET)			
	rGO	3.4 ± 0.0	4.8 ± 0.2
	Oasis HLB*	4.2 ± 0.0	27.9 ± 1.0
	β -CDP*	3.8 ± 0.1	28.3 ± 6.1

[‡]calculated based on the Freundlich model at a fixed C_{aq} of 1 mg L^{-1}

*data calculated (K_d) and adopted (q_{\max}) based on results presented in Chapter 2

5.3.2 Significance of Nonpolar Interactions for the Sorption Process

The $\log K_D$ values of BAM, isoproturon, *S*-metolachlor, and terbuthylazine showed a positive correlation with the corresponding $\log K_{\text{ow}}$ values ($R^2 = 0.93$, Figure 5.2) but no clear correlations with the corresponding LSER parameters ($R^2 < 0.5$, data not shown), which could have hinted specific intermolecular interactions (see eq. (1.7)). Although the data set is small, the observation that relatively nonpolar analytes (as proxied by higher $\log K_{\text{ow}}$ values) exhibit higher affinities for graphene-based sorbents is consistent with the notion of predominant nonpolar van der Waals and π - π interactions in the sorption process.^{239,240} Note, however, that chloridazon was an outlier exhibiting a comparatively high affinity and capacity despite its relatively low $\log K_{\text{ow}}$ value of 1.19. A likely reason

for this deviation may be the higher contribution of hydrogen bonding to the sorption of chloridazon as shown by Yan et al,³⁴⁶ which reflects the hydrophilic lipophilic balanced character of the graphene-based sorbent. However, in order to decipher the role of H-bonds and to gain more robust mechanistic insights into the sorption process, studies with larger sets of analytes are needed.

Nonetheless, the outstanding importance of nonpolar interactions is highlighted by the overall improved sorption performance of the graphene-based material upon chemical reduction. During the reduction reaction, oxygen-containing functional groups were largely removed from the surface of the GO, which enlarged the polyaromatic basal plane and, in turn, increased the affinity and capacity for all aromatic compounds through possibly enhanced π - π interactions. The removal of a majority of oxygen-containing functionalities was confirmed by FTIR spectroscopy and Raman microspectroscopy as presented in Figure 5.3. The peaks in the FTIR spectra of GO (red, Figure 5.3a) were assigned as follows: C-H bending vibrations at 865 cm^{-1} , C-O (alkoxy) stretching vibrations at 1035 cm^{-1} , C-O (epoxy) stretching vibrations at 1150 cm^{-1} , O-H (hydroxy) bending vibrations at 1325 cm^{-1} , O-H (carboxy) bending vibration at 1400 cm^{-1} , skeleton vibrations of aromatic C=C bonds at 1620 cm^{-1} , C=O (carboxy, carbonyl) stretching vibrations at 1720 cm^{-1} , and O-H (hydroxy) stretching vibrations around 3300 cm^{-1} . In the rGO spectra (green), the peaks corresponding to the oxygen-containing functionalities decreased significantly (i.e., carboxy and hydroxy O-H) or disappeared entirely (e.g., alkoxy and epoxy C-O). The structural changes associated with the chemical reduction are also reflected in the Raman spectra of GO and rGO (Figure 5.3b). Both spectra show the same prominent peaks: the D and the G band. The D band arises from disorders or defects in the graphene lattice, while the G band is attributed to the vibration of the planar configuration sp^2 bonded carbon. The D/G intensity ratio (I_D/I_G) of GO increased from 0.95 ± 0.03 to 1.30 ± 0.06 upon reduction. This increase is typical for the reduction of GO and indicates that sp^2 domains in rGO became smaller in average size due to the removal of functional groups.^{347,348} But while smaller, the sp^2 domains in rGO are more numerous than in GO and hence provide more π - π sorption sites.³⁴⁷

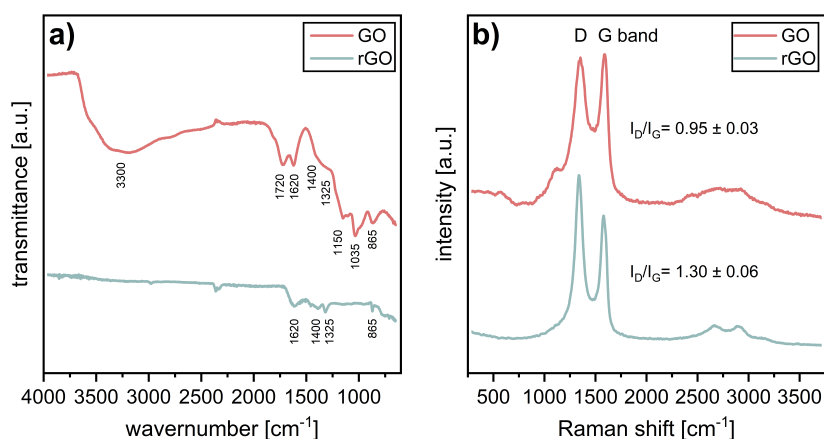


Figure 5.3. (a) Fourier transform infrared (FTIR) spectra and (b) Raman spectra of graphene oxide (GO) and reduced graphene oxide (rGO).

5.3.3 Sorption Kinetics of Reduced Graphene Oxide in Comparison to Commercial Oasis HLB

Further, the kinetics for sorption of the five model compounds on rGO were examined in comparison with the commercial sorbent Oasis HLB (Figure 5.4). The time for the sorption of all analytes to reach equilibrium was found to be approximately 840 min/14 h for rGO (Figure 5.4), with maximum analyte removal ranging from 20 % for BAM to 84 % for chloridazon (Figure S5.3). Compared with literature values for similar organic sorbates, the time for rGO to reach equilibrium was about 7 to 14 fold higher in this study.³⁴⁹⁻³⁵¹ A reason for these lower kinetics could have been the observed agglomeration of the rGO sheets during the kinetic experiment, which is known to decrease the effective surface area of the bulk material.³⁴⁷ In contrast, Oasis HLB exhibited as expected much faster kinetics and had already reached equilibrium at the first sampling time after 1 h. While Oasis HLB outperformed rGO in the fast and efficient removal of the relatively nonpolar isoproturon, *S*-metolachlor, and terbuthylazine (i.e., 95 to 98 % vs. 65 to 75 %, Figure S5.3), it showed similar low performance for the polar BAM (i.e., ~ 1 mg g⁻¹ sorbed concentration at ~ 20 % removal). Interestingly, however, Oasis HLB sorbed with 3.0 mg g⁻¹ less chloridazon at equilibrium than rGO (4.2 mg g⁻¹, Figure 5.4), although admittedly at a much faster rate. This observation is (i) consistent with the isotherm results of rGO showing highest affinity and capacity for chloridazon (Figure 5.2) and (ii) suggests superior HLB yet inferior kinetic properties of rGO compared with Oasis HLB for this specific analyte.

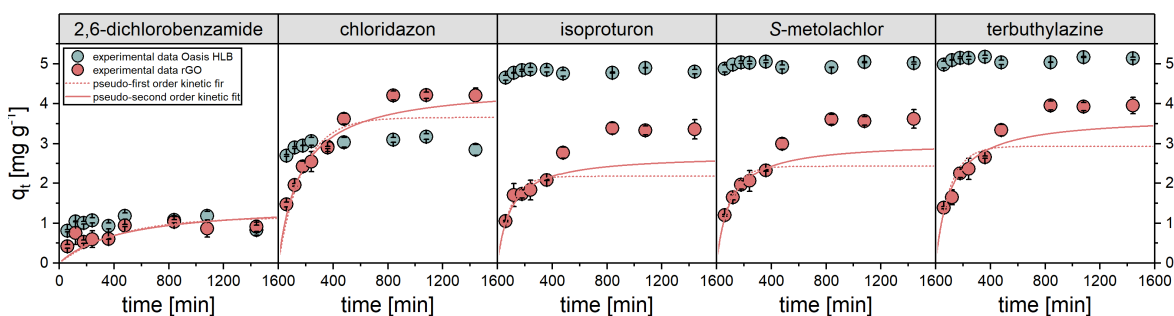


Figure 5.4. Kinetic plots for the sorption of the five model compounds on rGO (red) and Oasis HLB (green) displaying the amount of analyte sorbed (q_t) at a given time t . Red dashed and solid lines represent pseudo-first and pseudo-second order model fits of the rGO kinetic data, respectively.

For a quantitative evaluation, the experimental data was fitted to the pseudo-first order (Lagergren)³⁴⁰ and pseudo-second order kinetic sorption model (Ho and McKay)³⁴¹ as presented in Figure 5.4 and Table 5.2. As it is typical for many sorption systems,³⁴¹ the rGO data was slightly better described by the second-order rate law (R^2 : 0.93 – 0.94 vs. 0.85 – 0.90), which assumes that the sorption rate is proportional to the square of the number of unoccupied sorption sites on the sorbent surface. However, similar to the observations made for the isotherm data, only poor-quality fits could be obtained for BAM due to its weak sorption (R^2 : 0.51 for both models). Fitting of the Oasis HLB kinetic data was not possible due to the lack of data points in the dynamic kinetic range in the early sorption phase (< 1 h).

In quantitative terms, the relatively slow sorption kinetics of rGO are reflected in pseudo-second order rate constants ranging between 0.001 and 0.004 g mg min⁻¹ (Table 5.2), which are one order of magnitude lower than reported values for the sorption of organic compounds on rGO,³⁵² and even three orders of magnitude lower than those of high performance sorbents such as the cyclodextrin-based polymers introduced in the previous chapters of this thesis.^{193,253,284}

Table 5.2. Pseudo-first order and pseudo-second order kinetic model parameters for the adsorption of 2,6-dichlorobenzamide (BAM), chloridazon, isoproturon, *S*-metolachlor, and terbuthylazine on rGO.

	pseudo-first order (Lagergren)			pseudo-second order (Ho & McKay)		
	q_e [mg g ⁻¹]	k_1 [min ⁻¹]	R^2 [-]	q_e [mg g ⁻¹]	k_2 [g mg ⁻¹ min ⁻¹]	R^2 [-]
BAM	1.15 ± 0.34	0.002 ± 0.001	0.51	1.48 ± 0.57	0.001 ± 0.000	0.51
chloridazon	3.66 ± 0.28	0.006 ± 0.001	0.85	4.47 ± 0.29	0.001 ± 0.000	0.94
isoproturon	2.17 ± 0.10	0.011 ± 0.002	0.90	2.72 ± 0.17	0.004 ± 0.001	0.94
<i>S</i> -metolachlor	2.43 ± 0.11	0.011 ± 0.002	0.88	3.04 ± 0.19	0.003 ± 0.001	0.93
terbuthylazine	2.93 ± 0.19	0.010 ± 0.002	0.85	3.69 ± 0.25	0.002 ± 0.001	0.93

5.3.4 Proof-Of-Concept for Graphene-Modified MAFs in Micropollutant Extraction from Water

Scanning electron microscopy (SEM) confirmed the successful synthesis of the MAF polymers and their functionalization with GO. Figure 5.5a and b show SEM images of the pristine MAF structure featuring the typical pore sizes and shapes of the polymer globules.³³⁹ After the immobilization by coupling the carboxy groups of GO with primary amines introduced to the MAF in an intermediate step, the GO sheets were covalently attached to the surface as evident in Figure 5.5c and d as thin layers covering the polymer globules.

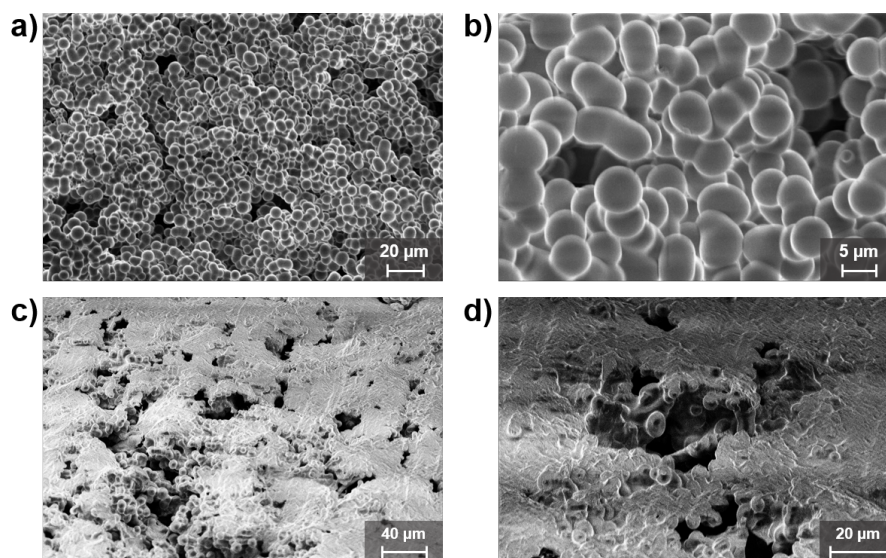


Figure 5.5. Field emission scanning electron microscope (FESEM) images of the surface of a pristine monolithic adsorption filter (MAF) (a, b), and the surface of a modified MAF exhibiting thin graphene oxide layers covalently attached to the surface (c, d).

To assess the applicability of rGO@MAF for the fast and efficient extraction of organic MPs from water, the removal of the five model compounds was quantified in a miniaturized, proof-of-concept flow-through sorption experiment. To simulate high-throughput extraction, the flow rate was set at 7.8 mL min^{-1} , which corresponds to 51.6 mL min^{-1} in the setup with normal sized MAF disks. Based on the immobilized amount and maximum sorption capacities of rGO (Table S5.3), the setups were equipped with five rGO@MAF disks to guarantee sufficiently high capacities for chloridazon, isoproturon, *S*-metolachlor, and terbuthylazine in 100 mL ultrapure water (0.01 M CaCl_2) at a concentration of 5 mg L^{-1} . However, it should be noted that not enough discs fitted into the small setup to provide enough capacity for BAM (i.e., only 33 %). The contribution of the incorporated rGO to the overall sorption performance was evaluated in comparison with the results obtained by the same setup but equipped with the same number of pristine MAFs and intermediate NH_2 @MAFs, respectively.

rGO@MAF removed with 7 (BAM) to 55 % (terbuthylazine) relatively low amounts of the analytes from the sample solution (Figure 5.6). In addition, the only 15 to 30 % lower values of MAF and NH_2 @MAF reveal that a considerable part of the observed removal can be ascribed to unspecific binding to the polymer matrix. The dependence of the removal data on the analyte polarity (as proxied by the log K_{ow} value) in the order $\text{BAM} < \text{CHL} < \text{ISO} < \text{MET} < \text{TER}$ suggests that this unspecific binding was governed by nonpolar interactions (e.g., van der Waals forces). The twelvefold increase of the MAF specific surface area from 0.68^{334} to $8.1 \pm 0.1 \text{ m}^2 \text{ g}^{-1}$ (Figure S5.4), accomplished through the incorporation of GO, was thus not sufficient to significantly increase the sorption capacity and kinetics of the MAF stationary phase for small organic compounds such as pesticides. These preliminary sorption results of the proof-of-concept experiment did not advise upscaling for a large-volume test at this stage of method development, but called for revisiting the rGO@MAF design in terms of capacity and kinetics.

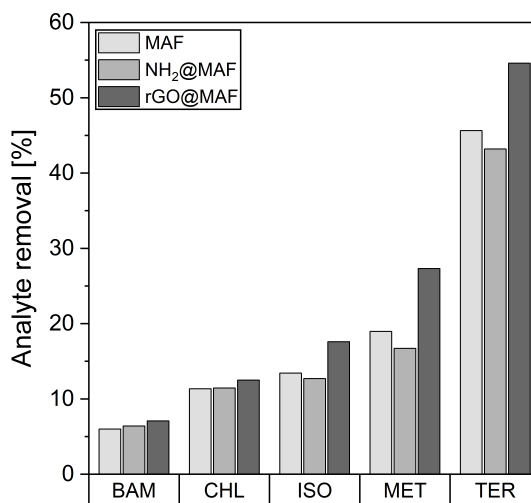


Figure 5.6. Removal (in %) of the analytes 2,6-dichlorobenzamide (BAM), chloridazon (CHL), isoproturon (ISO), *S*-metolachlor (MET), and terbuthylazine (TER) after percolating 100 mL aqueous sample (i.e., ultrapure water, 0.01 M CaCl_2 , spiked at 5 mg L^{-1}) through pristine MAF, or MAF modified with primary amines (NH_2 @MAF) or reduced graphene oxide (rGO@MAF).

5.4 Conclusions

This proof-of-concept study on the combination of monolithic polymer-based stationary phases and carbonaceous, graphene-based nanomaterials for fast and effective extraction of organic MPs from water provides valuable findings for future method development and optimization. The present results demonstrate the potential of chemical reduction of GO to significantly increase the sorption affinity and capacity toward a broad range of MPs by enhancing π - π interactions between their aromatic moieties and the more numerous sp^2 bonded carbon domains in the reduced form of GO. However, the sorption performance of GO and rGO observed and quantified in this study was well below typical literature values in terms of capacity and kinetics, and could not compete with that of high-performance sorbents (e.g., Oasis HLB, β -CDP). This finding indicates a high variability in quality of commercial GO products and implies to use the state-of-the-art Hummers' procedure³⁴⁵ in the development of future methods for obtaining a high performance sorptive GO material.

Furthermore, the reported functionalization scheme of coupling the carboxy groups of GO with previously immobilized primary amine groups (i) represents a straightforward method to graft carboxy-containing nanomaterials onto the epoxy-based MAF polymers and thus (ii) highlights the versatility of the MAF surface chemistry to be tailored for different analytical needs. Although the low specific surface area of the MAF could be increased by one order of magnitude in this way, the extraction of MPs in the proof-of-concept sorption experiment was only insufficiently improved. Hence, the outcome of this study strongly suggests to overall revise the rGO@MAF design for the efficient extraction of small organic molecules from water. Future method development may consider, for example, (i) the optimization of porogen type and composition to finetune the MAF porosity for the needs of small molecule extraction (e.g., to obtain dual porosity including mesopores), (ii) the use of different functional and cross-linking monomers such as styrene, divinylbenzene, or methacrylate, to obtain an organic polymer monolith tailored for the retention of MPs,²³⁵ (iii) the embedding of the graphene-based nanomaterials already during the monolith synthesis in order to achieve a higher degree of incorporation,²³⁶ or (iv) the use of alternative nanoparticles, such as metal-organic frameworks (MOFs)³⁵³ or molecularly imprinted polymers (MIPs)¹⁸¹ to increase selectivity and target specific classes of MPs.

Chapter 6

General Conclusion and Outlook

The overarching goal of this dissertation was to broaden the scope of compound-specific isotope analysis (CSIA) to polar organic micropollutants present in natural waters in the low ng L⁻¹ concentration range, thereby paving the path for a better understanding of their behavior and fate in the environment. Specifically, the research aimed at tackling the major analytical bottlenecks of micropollutant CSIA associated with the limited sensitivity and chromatographic resolution of chromatography-IRMS by advancing sample preparation methodologies. In this context, the novelty of this research is the focus on improving the first sample preparation step, namely the solid-phase extraction of the target analytes. As such, the work is intended to complement previous work on the same analytical problem, in which extensive efforts have been made to advance preparative cleanup procedures in the second sample preparation step. Overall, this dissertation emphasizes that the meticulous choice of a selective SPE sorbent material, a comprehensive sorbent selectivity assessment toward the target analyte and interfering matrix, and a careful method evaluation and validation are key for accurate micropollutant CSIA. In particular, the presented selective SPE method based on cyclodextrin polymers generates new opportunities for environmental CSIA studies on the catchment scale at low contaminant concentrations.

6.1 Efficacy and Limitations of Cyclodextrin Polymers for Selective Sample Preparation in CSIA Applications

In the major part of the thesis, which addressed the detrimental matrix effects caused by coextracted organic matter, it was hypothesized that micropollutant CSIA can greatly benefit from innovative sorbent technologies beyond the commercial market, which efficiently retain the target analytes but strongly discriminate against concurrent organic matrix constituents. The present work thus systematically investigated the selectivity of novel, porous cyclodextrin polymers (i.e., α -, β -, γ -CDP) toward both target analytes (i.e., a selection of pesticides) and interfering dissolved organic matter (DOM). To address this, a comprehensive approach was employed, utilizing various independent and complementary experimental designs (e.g., SPE experiments, batch and column sorption studies) and analytical techniques (e.g., GC-IRMS, ultrahigh resolution MS, LC-MS/MS, DOC analysis).

The results of Chapter 2 consistently revealed the superior selective sorption behavior of the CDPs compared to a suite of commercial benchmark sorbents (i.e., Oasis HLB, LiChrolut EN, Supel-Select HLB). The exhibited selectivity enhancement of β -CDP, reaching up to sixfold, leads to cleaner and less complex extracts, resulting in a substantial reduction of an interfering *unresolved complex mixture* (UCM) in GC-IRMS chromatograms. This effect was demonstrated for the extraction of the model compounds atrazine, *S*-metolachlor, boscalid, and azoxystrobin from a typical surface water matrix. As a result, limits for accurate $\delta^{13}\text{C}$ analysis could be successfully lowered by over half an order of magnitude when compared to conventional SPE phases. In parallel, the procedure proved to be highly versatile for various applications due to its robustness in terms of recovery and

isotope integrity over a wide range of analyte concentrations, flow velocity, and sorbent regeneration cycles. The work thus emphasizes that the developed CDP-based SPE method can be successfully integrated into sample preparation workflows to obtain environmental SPE extracts that fulfill the rigorous requirements of GC-IRMS. These outcomes further illustrate (i) that commonly used, optimized commercial sorbents are not necessarily a suitable choice for targeted CSIA studies at low environmental contaminant concentrations, and (ii) that the employment of emerging alternative SPE phases, such as the herein presented selective model sorbent β -CDP, can avoid high matrix amounts in sample extracts, which would be difficult to be completely separated off in subsequent purification steps.

Besides, the isotope data in Chapter 2 found consistent matrix-dependent limits on GC-IRMS above which accurate $\delta^{13}\text{C}$ analysis was compromised, namely concentration levels at which approximately ten times more carbon in the extract was present from the matrix than the analyte (i.e., $C_{\text{DOM}}/C_{\text{analyte}} = 10 \text{ molC molC}^{-1}$). This finding (i) agrees with previous work on the impact of surface water-derived DOM on the carbon isotope analysis of atrazine¹⁵³ and (ii) underscores the necessity for micropollutant CSIA workflows to assess the selectivity of the SPE sorbent not only toward the target contaminant but also toward the concurrent organic matrix. A systematic investigation is still warranted, however, to conclusively evaluate whether such a DOM-to-analyte threshold concentration ratio is a robust *a priori* indicator for the universal feasibility assessment of SPE-CSIA procedures targeting different sample matrices (e.g., groundwater, wastewater).

The reduction of matrix complexity in extracts of β -CDP is further corroborated by the molecular-level investigations presented in Chapter 3. The FTICR MS data elucidated the molecular chemodiversity of DOM extracted by the cyclodextrin-based and commercial SPE phases, which remained unresolved when DOM was quantified by bulk DOC analysis to obtain $C_{\text{DOM}}/C_{\text{analyte}}$ ratios in Chapter 2. This approach enabled compound classes of surface and groundwater-derived DOM to be pinpointed that were preferentially retained or excluded by the different sorbents. The results of this chapter suggest that β -CDP's superior selectivity is largely controlled by the strongest discrimination among the tested sorbents against some of the most abundant freshwater-derived DOM constituents, namely oxygenated and unsaturated compounds associated with the classes of lignin-like, tannin-like, and carboxylic-rich alicyclic molecules (CRAMs). Moreover, the data (i) support the observation in Chapter 2 that the highest sorbent selectivity can be achieved at a circumneutral sample pH, and thus (ii) reinforce the notion that ionizable interfering matrix, such as deprotonated carboxylic acids, can readily be separated when SPE is performed with reversed-phase sorbents under neutral conditions – provided that extraction pH is uncritical for the retention of the target analytes. Chapter 3 demonstrates the outstanding suitability of nontargeted ultrahigh-resolution MS for an in-depth sorbent selectivity assessment toward the interfering matrix. The detailed molecular-level information on the selective nature of β -CDP gained by this approach may contribute to further optimization of sample preparation

in future efforts, for example, by tailoring cleanup strategies for abundant interfering DOM compound classes (e.g., saturated lipid-like compounds).

The new insights into the prevalent sorption mechanisms presented in Chapter 4 provide a molecular underpinning of the selectivity of TFN-cross-linked CDPs (i.e., α -, β -, γ -CDP) as observed and described in Chapter 2 and 3. The results (i) challenge the notion of a size cut-off above 0.6 kDa induced by the uniform CD cavities, which was hypothesized in previous literature, and (ii) suggest a synergistic effect of nonpolar and additional electrostatic interactions with the negatively charged cross-linker to be governing the selective sorption behavior of TFN-CDPs. The conclusion provided in this chapter offers a rational explanation for both the observed affinity of the cyclodextrin-based sorbent toward moderately polar nonionic and cationic compounds, and the discrimination against highly polar nonionic and anionic compounds. These insights can be used, for example, in combination with a recently introduced versatile β -CDP platform based on radical polymerization that allows for straightforward tuning of the comonomers/cross-linkers,³⁵⁴ in order to further optimize efficient and selective sorbent designs for specific compound classes, including those of varying charge and polarity.

Altogether, the findings of Chapter 2, 3, and 4 emphasize the excellent suitability of TFN-cross-linked β -CDP as a selective SPE sorbent to discriminate against environmental DOM in matrix-susceptible analytical applications such as CSIA. The application of the presented selective CDP-based SPE-CSIA procedure can be extended in the future to numerous other nonionic and cationic polar organic compounds for which β -CDP exhibits excellent sorption performance.^{194,195} In the case that recovery data is not yet available, the information on the chemical space extracted by β -CDP (Chapter 3) may serve to roughly predict the sorbent selectivity toward molecular compositions of potential target compounds. Table 6.1 presents some examples of pesticides and consumer care products for which CSIA methods already exist and for which β -CDP appears to be ideally suited as a selective SPE sorbent (i.e., recovery > 90 %). However, the advantageous discrimination against highly polar nonionic and anionic compounds at circumneutral pH is inevitably associated with limitations for the applicability of the procedure to target analytes with similar molecular properties. For instance, the anionic pesticides bentazone, MCPA, mecoprop, and 2,4-D, and the anionic pharmaceuticals diclofenac and sulfamethoxazole are not or only poorly recovered by β -CDP (Table 6.1) due to electrostatic repulsion by the negatively charged TFN-cross-linker. Based on their pK_a values, a compromise between optimal sample pH for either lowest matrix co-enrichment or highest target analyte recovery might be a practical solution for some of these ionizable compounds. The recovery of bentazone ($pK_a = 3.3$), for example, can already be increased to over 60 % when the sample pH is lowered to pH 5.¹⁹⁵ However, this inevitably leads to higher amounts of matrix in the extracts, and must be thoroughly scrutinized for analytical interferences and resulting matrix-dependent limits of accurate CSIA. Identical drawbacks of the CDP-based SPE apply to highly polar, nonionic substances such as 2,6-dichlorobenzamide (BAM), as shown in Chapter 2 (Table 6.1).

For substances beyond the scope of the currently available selective CDPs, for example the phenoxy acid herbicides listed in Table 6.1, other emerging sorbent technologies should be exploited for their use as selective sorbent phases in future research. Such alternative promising SPE materials include, for instance, covalent organic frameworks (COFs)³⁵⁵ and metal-organic frameworks (MOFs),³⁵³ both of which offer uniform porosity, high surface area, and a molecular recognition capability that can be tailored for specific target analytes by manipulating their cavity size and surface chemistry.¹⁷¹ Furthermore, to enable efficient method development and integrated in-depth assessment of selectivities among different sorbent candidates (e.g., advanced CDPs, MOFs, COFs, MIPs), the establishment of a standardized, high-throughput experimental scheme would be immensely beneficial.

Table 6.1. Examples of pesticides, pesticide metabolites, pharmaceuticals, and other organic micropollutants for which CSIA methods are available, including their log K_{OW} (neutral) and log D at pH 7 (ionic) values, respectively, their recovery on β -CDP, and applicability to the CDP-based SPE-CSIA procedure presented in Chapter 2 of this dissertation.

Substance (<i>class</i>)	log K_{OW} / log D (pH 7)*	Charge (pH 7) [†]	Reference CSIA method	Recovery β -CDP (pH 7) [‡]	CDP-based SPE-CSIA applicable?
	[-]			[%]	
<i>N</i> -triazine herbicide					
Simazine	2.30	neutral	356	91 ± 7	yes
<i>Chloroacetanilide herbicides</i>					
Acetochlor	3.03	neutral	133	98 ± 3	yes
Alachlor	3.52	neutral	133,142,164	98 ± 3	yes
<i>Phenyl urea herbicide</i>					
Isoproturon	2.87	neutral	357	100 ± 0	yes
<i>Benzothiazinone herbicide</i>					
Bentazone	0.04	negative	129,358	46 ± 15	no
<i>Phenoxy acid herbicides</i>					
MCPA	-1.09	negative	359	4 ± 5	no
Mecoprop	-0.65	negative	360	0 ± 1	no
2,4-D	-0.83	negative	359	7 ± 8	no
<i>Pesticide Metabolites</i>					
Desethylatrazine	1.78	neutral	137,165,361	97 ± 5	yes
BAM	0.77	neutral	129,137,362	31 ± 3 [§]	no
<i>Pharmaceuticals</i>					
Diclofenac	1.17	negative	129,249,363	10 ± 18	no
Sulfamethoxazole	-0.56	negative	364-366	39 ± 35	no
<i>Corrosion inhibitor</i>					
Benzotriazole	1.44	neutral	166,367	94 ± 9	yes
<i>Plasticizer</i>					
Diethyl phthalate	2.71	neutral	368	90 ± 1	yes

* obtained from the ChemSpider database of the Royal Society of Chemistry³⁶⁹

[†] dominant species based on pK_a value

[‡] obtained from Li et al.,¹⁹⁵ except [§]data for BAM that was determined in Chapter 2

6.2 Implications for Large-Volume Extraction Concepts

In the second, minor part of the thesis (Chapter 5), addressing the laborious processing of large sample volumes required for micropollutant CSIA, the applicability of graphene-modified polymer monoliths (i.e., *monolithic adsorption filters* (MAFs)) for a high-throughput SPE application to organic MPs was investigated. Although the study proves the versatility of the MAF platform to be tailored for different analytical needs through straightforward surface chemistry modification, it also illustrates the challenge of increasing its low specific surface area (i.e., $< 1 \text{ m}^2 \text{ g}^{-1}$) to such an extent that it ensures sufficient sorption performance in terms of kinetics and capacity for small molecules. The presented results imply that further method development should focus either on finetuning the MAF porosity to obtain additional mesopores that suit the extraction of small molecules (e.g., by optimizing the porogen type and composition), or on using different functional and cross-linking monomers (e.g., styrene, divinylbenzene, methacrylate) to obtain an organic polymer monolith tailored for the retention of MPs. In order to also increase selectivity in this LV extraction procedure and to target specific MP classes, the rather universal graphene-based sorbent incorporated into the polymer network could be exchanged with more selective nanoparticles, such as MOFs³⁵³ or MIPs.¹⁸¹ Besides, a fundamentally alternative approach to the active sampling and processing of hundreds of liters of water in micropollutant CSIA workflows may be the use of passive integrative sampling techniques (e.g., Polar Organic Compound Integrative Sampler (POCIS))^{141,370} in combination with selective sorbent materials such as the β -CDP presented in this thesis.

6.3 Perspectives for Micropollutant CSIA in Field Studies

Overall, this dissertation emphasizes that the diligent choice of SPE sorbent material, the exhaustive sorbent selectivity assessment, and careful method evaluation and validation are key for accurate CSIA targeting aquatic organic contaminants that occur at low environmental concentrations. The presented SPE-CSIA procedure employing the selective β -CDP offers new prospects for CSIA applications at field-relevant concentrations of tens to hundreds of nanograms per liter. Figure 6.1 exemplarily illustrates the significance of the sixfold gain in sensitivity achieved by this work for an environmental CSIA workflow for the herbicide atrazine in natural water containing a typical DOC level of 2.5 mg L^{-1} . While the extraction with the commonly used Oasis HLB sorbent can ensure accurate $\delta^{13}\text{C}$ determination only to a minimum atrazine concentration of 545 ng L^{-1} , the SPE-CSIA procedure employing β -CDP allows reliable isotope analysis down to 90 ng L^{-1} under the given conditions. This highlights that micropollutant CSIA studies on the catchment scale for typical field concentrations below 100 ng/L (see Figure 1.1) are now within the realm of feasibility when selective extraction methods are combined with established cleanup strategies, such as molecularly imprinted SPE (MISPE)¹⁶⁶ and preparative HPLC.¹⁶⁵

These methodological advancements in sample preparation together with further instrumental optimization of sensitivity and peak separation in chromatography-IRMS (e.g., by comprehensive two-dimensional GC and optimized reactor designs)^{162,163} are expected to boost the implementation of CSIA in environmental monitoring strategies for MPs. By gaining comprehensive insights into the fate of these pollutants, it will be possible to develop more effective mitigation strategies, to enhance regulatory measures, and to implement targeted remediation efforts to safeguard aquatic ecosystems and ensure the sustainable management of water resources. This knowledge is crucial for identifying potential contaminant sources, understanding transformation pathways, and assessing the overall environmental impact, ultimately contributing to the preservation of the natural environment for present and future generations.

Beyond CSIA based on high-precision IRMS, recent developments in electrospray-ionization Orbitrap-MS bear great potential to further stimulate environmental isotope research on organic MPs, as the technique is now in principle able to accurately determine isotopic variations in intact molecules at natural abundance.³⁷¹ This may allow limitations inherent to gas-source IRMS instruments (e.g., the loss of molecular information) to be overcome by enabling (i) simultaneous multi-element isotopic fingerprinting, (ii) position-specific isotope analysis for the sensitive detection of isotope fractionation in large molecules, in which average isotope effects typically become diluted, and (iii) the straightforward separation of interferences by selecting the mass trace of interest.

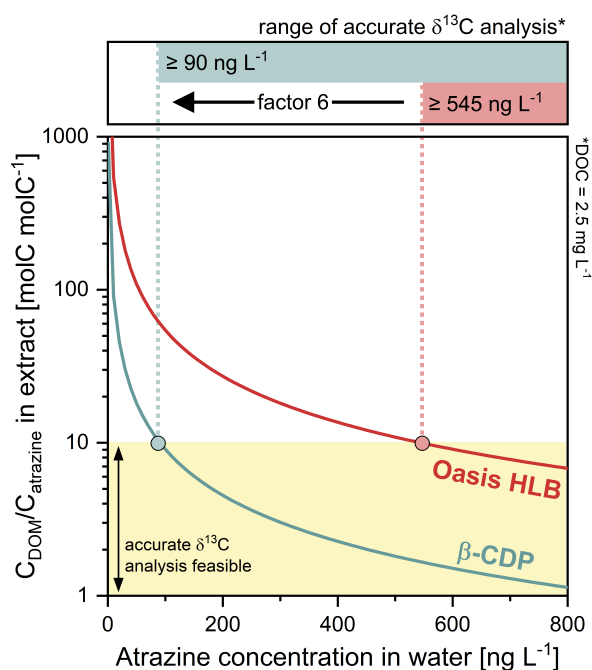


Figure 6.1. Carbon-normalized DOM-to-atrazine concentration ratio ($C_{\text{DOM}}/C_{\text{atrazine}}$) in the SPE extract as a function of atrazine concentration in a water sample containing 2.5 mg L^{-1} DOC using either Oasis HLB (red) or β -CDP (green) as a SPE sorbent. The data is based on atrazine and DOC recovery data obtained in Chapter 2 and considers two sample cleanup steps (e.g., MISPE, preparative HPLC) that improve the $C_{\text{DOM}}/C_{\text{atrazine}}$ ratio by factor 10 each. The yellow area represents the $C_{\text{DOM}}/C_{\text{atrazine}}$ range in which accurate $\delta^{13}\text{C}$ analysis is generally feasible. The upper panel indicates the environmental atrazine concentration range for which the different SPE procedures enable accurate carbon isotope analysis.

Abbreviations

AHA	Aldrich humic acid
AI_{mod}	Modified aromaticity index
ANOVA	Analysis of variance
Ar	Aromaticity
ATR	Atrazine
AZO	Azoxystrobin
BAM	2,6-dichlorobenzamide
BET	Brunauer–Emmett–Teller
BOS	Boscalid
CD	Cyclodextrin
CDP	Cyclodextrin polymer
CF	Continuous-flow
CHL	Chloridazon
COFs	Covalent organic frameworks
CRAMs	Carboxylic-rich alicyclic molecules
CSIA	Compound-specific isotope analysis
DBE	Double bond equivalent
DBE/C	Carbon-normalized double bond equivalent
DBE-O	Double bond equivalent minus count of oxygen
DCC	<i>N,N'</i> -dicyclohexylcarbodiimide
DCU	Dicyclohexylisourea
DFG	Deutsche Forschungsgemeinschaft
DIM	Dimethomorph
DMF	<i>N,N</i> -dimethylformamide
DMRM	Dynamic multi reaction monitoring
DOC	Dissolved organic carbon
DOM	Dissolved organic matter
ESI	Electrospray ionization
EtOH	Ethanol
FESEM	Field emission scanning electron microscopy
FID	Free induction decay
FTICR MS	Fourier transform ion cyclotron resonance mass spectrometry
FTIR	Fourier-transform infrared
GC	Gas chromatography
GC-IRMS	Gas chromatography – isotope ratio mass spectrometry
GO	Graphene oxide

GW	Groundwater
HCA	Hierarchical cluster analysis
HLB	Hydrophilic lipophilic balanced
HMW	High-molecular-weight
HPLC	High-performance liquid chromatography
IHSS	International Humic Substances Society
ILIS	Isotopically labeled internal standard
IRMS	Isotope ratio mass spectrometry
ISO	Isoproturon
IUPAC	International Union of Pure and Applied Chemistry
k	Capacity factor
K_d	Partition coefficient
KIE	Kinetic isotope effect
K_{ow}	Octanol-water partition coefficient
LC	Liquid chromatography
LC-IRMS	Liquid chromatography – isotope ratio mass spectrometry
LC-MS	Liquid chromatography – mass spectrometry
LC-MS/MS	Liquid chromatography – tandem mass spectrometry
LMW	Low-molecular-weight
LOD	Limit of detection
LOQ	Limit of quantification
LSERs	Linear solvation energy relationships
LV	Large volume
MAF	Monolithic adsorption filtration
MeOH	Methanol
MET	Methiocarb
MIPs	Molecularly imprinted polymers
MISPE	Molecularly imprinted solid-phase extraction
MOFs	Metal-organic frameworks
MP	Micropollutant
MQL	Method quantification limit
MS	Mass spectrometry
MTM	Metamitron
MV	McGowan volume
MW	Molecular weight
MWCO	Molecular weight cut-off

NDIR	Nondispersive infrared
NH₂@MAF	Monolithic adsorption filter modified with primary amines
NMR	Nuclear magnetic resonance
NOM	Natural organic matter
NPOC	Nonpurgeable organic carbon
PCA	Principle component analysis
PES	Polyethersulfone
pK_a	Acid dissociation constant
POCIS	Polar organic compound integrative sampler
ppb	Parts-per-billion
pp-LFERs	Polyparameter linear free energy relationships
PRO	Propiconazole
PS-DVB	Polystyrene-divinylbenzene
QSARs	Quantitative structure-activity relationships
rGO	Reduced graphene oxide
rGO@MAF	Monolithic adsorption filter modified with reduced graphene oxide
RI	Relative intensity
SEM	Scanning electron microscopy
SI	Supporting Information
SiC	Silicon carbide
SME	S-metolachlor
SPE	Solid-phase extraction
SRFA	Suwannee River fulvic acid
SRHA	Suwannee River humic acid
SW	Surface water
TDS	Total dissolved solids
TER	Terbutylazine
TFN	Tetrafluoroterephthalonitrile
TIA	Thiacloprid
TOC	Total organic carbon
UCM	Unresolved complex mixture
VPDB	Vienna PeeDee Belemnite
ΔG⁰	Standard Gibbs free energy

References

1. United Nations, *Freshwater Strategic Priorities 2022–2025*. United Nations Environment Programme (UNEP): Nairobi, Kenya, 2022.
2. Millennium Ecosystem Assessment, *Ecosystems and Human Well-being: Synthesis*. Island Press: Washington, DC, 2005.
3. Schwarzenbach, R. P.; Escher, B. I.; Fenner, K.; Hofstetter, T. B.; Johnson, C. A.; von Gunten, U.; Wehrli, B. The Challenge of Micropollutants in Aquatic Systems. *Science* **2006**, *313* (5790), 1072-1077.
4. Schwarzenbach, R. P.; Egli, T.; Hofstetter, T. B.; Gunten, U. v.; Wehrli, B. Global Water Pollution and Human Health. *Annu. Rev. Environ. Resour.* **2010**, *35* (1), 109-136.
5. Vörösmarty, C. J.; McIntyre, P. B.; Gessner, M. O.; Dudgeon, D.; Prusevich, A.; Green, P.; Glidden, S.; Bunn, S. E.; Sullivan, C. A.; Liermann, C. R.; Davies, P. M. Global threats to human water security and river biodiversity. *Nature* **2010**, *467* (7315), 555-561.
6. United Nations, *The United Nations World Water Development Report 2022: Groundwater: Making the invisible visible*. United Nations Educational, Scientific and Cultural Organization (UNESCO): Paris, France, 2022.
7. Food and Agriculture Organization of the United Nations (FAO), *AQUASTAT database*. <http://www.fao.org/aquastat/statistics/> (accessed January 15, 2023).
8. Food and Agriculture Organization of the United Nations (FAO), *FAOSTAT database*. <http://www.fao.org/faostat> (accessed January 15, 2023).
9. United States Environmental Protection Agency (US EPA), *Toxic Substances Control Act (TSCA) Chemical Substance Inventory Database*. <https://www.epa.gov/tsca-inventory> (accessed February 15, 2023).
10. European Chemicals Agency (ECHA), *Registration, Evaluation, Authorisation and Restriction of Chemicals Regulation (REACH) database*. <https://echa.europa.eu/de/information-on-chemicals/registered-substances> (accessed February 15, 2023).
11. Lapworth, D.; Baran, N.; Stuart, M.; Ward, R. Emerging organic contaminants in groundwater: a review of sources, fate and occurrence. *Environ. Pollut.* **2012**, *163*, 287-303.
12. Stuart, M.; Manamsa, K.; Talbot, J.; Crane, E., *Emerging contaminants in groundwater. British Geological Survey Open Report*. OR/11/013. 123pp. NERC: 2011.
13. Heberer, T. Occurrence, fate, and removal of pharmaceutical residues in the aquatic environment: a review of recent research data. *Toxicol. Lett.* **2002**, *131* (1), 5-17.
14. Reemtsma, T.; Weiss, S.; Mueller, J.; Petrovic, M.; González, S.; Barcelo, D.; Ventura, F.; Knepper, T. P. Polar pollutants entry into the water cycle by municipal wastewater: a European perspective. *Environ. Sci. Technol.* **2006**, *40* (17), 5451-5458.
15. Halling-Sørensen, B.; Nielsen, S. N.; Lanzky, P.; Ingerslev, F.; Lützhøft, H. H.; Jørgensen, S. Occurrence, fate and effects of pharmaceutical substances in the environment-A review. *Chemosphere* **1998**, *36* (2), 357-393.
16. Schwarzenbach, R. P.; Gschwend, P. M.; Imboden, D. M., *Environmental Organic Chemistry*. John Wiley & Sons: Hoboken, New Jersey, USA, 2016.
17. Leu, C.; Singer, H.; Stamm, C.; Müller, S. R.; Schwarzenbach, R. P. Variability of herbicide losses from 13 fields to surface water within a small catchment after a controlled herbicide application. *Environ. Sci. Technol.* **2004**, *38* (14), 3835-3841.
18. Worrall, F.; Kolpin, D. W. Aquifer vulnerability to pesticide pollution—combining soil, land-use and aquifer properties with molecular descriptors. *J. Hydrol.* **2004**, *293* (1-4), 191-204.
19. Casey, F. X.; Hakk, H.; Šimůnek, J.; Larsen, G. L. Fate and transport of testosterone in agricultural soils. *Environ. Sci. Technol.* **2004**, *38* (3), 790-798.

20. Olshansky, Y.; Polubesova, T.; Vetter, W.; Chefetz, B. Sorption–desorption behavior of polybrominated diphenyl ethers in soils. *Environ. Pollut.* **2011**, *159* (10), 2375-2379.
21. Vidon, P.; Allan, C.; Burns, D.; Duval, T. P.; Gurwick, N.; Inamdar, S.; Lowrance, R.; Okay, J.; Scott, D.; Sebestyen, S. Hot spots and hot moments in riparian zones: potential for improved water quality management. *J. Am. Water Resour. Assoc.* **2010**, *46* (2), 278-298.
22. Schaffer, M.; Börnick, H.; Nödler, K.; Licha, T.; Worch, E. Role of cation exchange processes on the sorption influenced transport of cationic β -blockers in aquifer sediments. *Water Res.* **2012**, *46* (17), 5472-5482.
23. Burke, V.; Greskowiak, J.; Asmuß, T.; Bremermann, R.; Taute, T.; Massmann, G. Temperature dependent redox zonation and attenuation of wastewater-derived organic micropollutants in the hyporheic zone. *Sci. Total Environ.* **2014**, *482-483*, 53-61.
24. Carrara, C.; Ptacek, C. J.; Robertson, W. D.; Blowes, D. W.; Moncur, M. C.; Sverko, E.; Backus, S. Fate of pharmaceutical and trace organic compounds in three septic system plumes, Ontario, Canada. *Environ. Sci. Technol.* **2008**, *42* (8), 2805-2811.
25. Johnson, A. C.; Hughes, C. D.; Williams, R. J.; Chilton, P. J. Potential for aerobic isoproturon biodegradation and sorption in the unsaturated and saturated zones of a chalk aquifer. *J. Contam. Hydrol.* **1998**, *30* (3-4), 281-297.
26. Watanabe, N.; Bergamaschi, B. A.; Loftin, K. A.; Meyer, M. T.; Harter, T. Use and environmental occurrence of antibiotics in freestall dairy farms with manured forage fields. *Environ. Sci. Technol.* **2010**, *44* (17), 6591-6600.
27. Semple, K. T.; Doick, K. J.; Wick, L. Y.; Harms, H. Microbial interactions with organic contaminants in soil: definitions, processes and measurement. *Environ. Pollut.* **2007**, *150* (1), 166-176.
28. Wick, L. Y.; Remer, R.; Würz, B.; Reichenbach, J.; Braun, S.; Schäfer, F.; Harms, H. Effect of fungal hyphae on the access of bacteria to phenanthrene in soil. *Environ. Sci. Technol.* **2007**, *41* (2), 500-505.
29. Kurt-Karakus, P. B.; Teixeira, C.; Small, J.; Muir, D.; Bidleman, T. F. Current-use pesticides in inland lake waters, precipitation, and air from Ontario, Canada. *Environ. Toxicol. Chem.* **2011**, *30* (7), 1539-1548.
30. Oppel, J.; Broll, G.; Löffler, D.; Meller, M.; Römbke, J.; Ternes, T. Leaching behaviour of pharmaceuticals in soil-testing-systems: a part of an environmental risk assessment for groundwater protection. *Sci. Total Environ.* **2004**, *328* (1-3), 265-273.
31. Reichenberger, S.; Bach, M.; Skitschak, A.; Frede, H.-G. Mitigation strategies to reduce pesticide inputs into ground- and surface water and their effectiveness; A review. *Sci. Total Environ.* **2007**, *384* (1-3), 1-35.
32. Scheytt, T.; Mersmann, P.; Leidig, M.; Pekdeger, A.; Heberer, T. Transport of pharmaceutically active compounds in saturated laboratory columns. *Groundwater* **2004**, *42* (5), 767-773.
33. Zuehlke, S.; Duennbier, U.; Heberer, T.; Fritz, B. Analysis of endocrine disrupting steroids: Investigation of their release into the environment and their behavior during bank filtration. *Ground Water Monitoring & Remediation* **2004**, *24* (2), 78-85.
34. Bertelkamp, C.; Reungoat, J.; Cornelissen, E.; Singhal, N.; Reynisson, J.; Cabo, A. J.; van der Hoek, J. P.; Verliefde, A. Sorption and biodegradation of organic micropollutants during river bank filtration: A laboratory column study. *Water Res.* **2014**, *52*, 231-241.
35. Ren, X.; Zeng, G.; Tang, L.; Wang, J.; Wan, J.; Liu, Y.; Yu, J.; Yi, H.; Ye, S.; Deng, R. Sorption, transport and biodegradation – An insight into bioavailability of persistent organic pollutants in soil. *Sci. Total Environ.* **2018**, *610-611*, 1154-1163.

36. Kelly, B. C.; Ikonou, M. G.; Blair, J. D.; Morin, A. E.; Gobas, F. A. Food web specific biomagnification of persistent organic pollutants. *Science* **2007**, *317* (5835), 236-239.
37. Kelly, B. C.; Ikonou, M. G.; Blair, J. D.; SurrIDGE, B.; Hoover, D.; Grace, R.; Gobas, F. A. Perfluoroalkyl contaminants in an Arctic marine food web: trophic magnification and wildlife exposure. *Environ. Sci. Technol.* **2009**, *43* (11), 4037-4043.
38. Boxall, A. B.; Sinclair, C. J.; Fenner, K.; Kolpin, D.; Maund, S. J. When synthetic chemicals degrade in the environment. *Environ. Sci. Technol.* **2004**, *38* (19), 368A-375A.
39. Fenner, K.; Canonica, S.; Wackett, L. P.; Elsner, M. Evaluating Pesticide Degradation in the Environment: Blind Spots and Emerging Opportunities. *Science* **2013**, *341* (6147), 752-758.
40. Reemtsma, T.; Berger, U.; Arp, H. P. H.; Gallard, H.; Knepper, T. P.; Neumann, M.; Quintana, J. B.; Voogt, P. d. Mind the Gap: Persistent and Mobile Organic Compounds—Water Contaminants That Slip Through. *Environ. Sci. Technol.* **2016**, *50* (19), 10308-10315.
41. Daughton, C. G.; Ternes, T. A. Pharmaceuticals and personal care products in the environment: agents of subtle change? *Environ. Health Perspect.* **1999**, *107* (6), 907.
42. Kolpin, D. W.; Furlong, E. T.; Meyer, M. T.; Thurman, E. M.; Zaugg, S. D.; Barber, L. B.; Buxton, H. T. Pharmaceuticals, Hormones, and Other Organic Wastewater Contaminants in U.S. Streams, 1999–2000: A National Reconnaissance. *Environ. Sci. Technol.* **2002**, *36* (6), 1202-1211.
43. Kümmerer, K. Antibiotics in the aquatic environment – A review – Part I. *Chemosphere* **2009**, *75* (4), 417-434.
44. Loos, R.; Gawlik, B. M.; Locoro, G.; Rimaviciute, E.; Contini, S.; Bidoglio, G. EU-wide survey of polar organic persistent pollutants in European river waters. *Environ. Pollut.* **2009**, *157* (2), 561-568.
45. Richardson, S. D.; Kimura, S. Y. Water Analysis: Emerging Contaminants and Current Issues. *Anal. Chem.* **2020**, *92* (1), 473-505.
46. Tixier, C.; Singer, H. P.; Oellers, S.; Müller, S. R. Occurrence and Fate of Carbamazepine, Clofibric Acid, Diclofenac, Ibuprofen, Ketoprofen, and Naproxen in Surface Waters. *Environ. Sci. Technol.* **2003**, *37* (6), 1061-1068.
47. Stan, H.-J.; Heberer, T.; Linkerhägner, M. Occurrence of clofibric acid in the aquatic system - is the use in human medical care the source of the contamination of surface, ground and drinking water? *Vom Wasser* **1994**, *83*, 57-68.
48. Ternes, T. A. Occurrence of drugs in German sewage treatment plants and rivers. *Water Res.* **1998**, *32* (11), 3245-3260.
49. Farré, M. I.; Pérez, S.; Kantiani, L.; Barceló, D. Fate and toxicity of emerging pollutants, their metabolites and transformation products in the aquatic environment. *TrAC, Trends Anal. Chem.* **2008**, *27* (11), 991-1007.
50. Barceló, D.; Petrovic, M. Challenges and achievements of LC-MS in environmental analysis: 25 years on. *TrAC, Trends Anal. Chem.* **2007**, *26* (1), 2-11.
51. Loos, R.; Locoro, G.; Comero, S.; Contini, S.; Schwesig, D.; Werres, F.; Balsaa, P.; Gans, O.; Weiss, S.; Blaha, L.; Bolchi, M.; Gawlik, B. M. Pan-European survey on the occurrence of selected polar organic persistent pollutants in ground water. *Water Res.* **2010**, *44* (14), 4115-4126.
52. Luo, Y.; Guo, W.; Ngo, H. H.; Nghiem, L. D.; Hai, F. I.; Zhang, J.; Liang, S.; Wang, X. C. A review on the occurrence of micropollutants in the aquatic environment and their fate and removal during wastewater treatment. *Sci. Total Environ.* **2014**, *473-474*, 619-641.
53. Busch, W.; Schmidt, S.; Kühne, R.; Schulze, T.; Krauss, M.; Altenburger, R. Micropollutants in European rivers: A mode of action survey to support the development of effect-based tools for water monitoring. *Environ. Toxicol. Chem.* **2016**, *35* (8), 1887-1899.

54. Attina, T. M.; Hauser, R.; Sathyanarayana, S.; Hunt, P. A.; Bourguignon, J.-P.; Myers, J. P.; DiGangi, J.; Zoeller, R. T.; Trasande, L. Exposure to endocrine-disrupting chemicals in the USA: a population-based disease burden and cost analysis. *Lancet Diabetes Endocrinol.* **2016**, *4* (12), 996-1003.
55. Kim, K.-H.; Kabir, E.; Jahan, S. A. Exposure to pesticides and the associated human health effects. *Sci. Total Environ.* **2017**, *575*, 525-535.
56. Mrema, E. J.; Rubino, F. M.; Brambilla, G.; Moretto, A.; Tsatsakis, A. M.; Colosio, C. Persistent organochlorinated pesticides and mechanisms of their toxicity. *Toxicology* **2013**, *307*, 74-88.
57. Emmanuel, E.; Pierre, M. G.; Perrodin, Y. Groundwater contamination by microbiological and chemical substances released from hospital wastewater: Health risk assessment for drinking water consumers. *Environ. Int.* **2009**, *35* (4), 718-726.
58. Alharbi, O. M. L.; Basheer, A. A.; Khattab, R. A.; Ali, I. Health and environmental effects of persistent organic pollutants. *J. Mol. Liq.* **2018**, *263*, 442-453.
59. Qing Li, Q.; Loganath, A.; Seng Chong, Y.; Tan, J.; Philip Obbard, J. Persistent Organic Pollutants and Adverse Health Effects in Humans. *J. Toxicol. Environ. Health Part A* **2006**, *69* (21), 1987-2005.
60. Baquero, F.; Martínez, J.-L.; Cantón, R. Antibiotics and antibiotic resistance in water environments. *Curr. Opin. Biotechnol.* **2008**, *19* (3), 260-265.
61. Beketov, M. A.; Kefford, B. J.; Schäfer, R. B.; Liess, M. Pesticides reduce regional biodiversity of stream invertebrates. *Proc. Natl. Acad. Sci. U.S.A.* **2013**, *110* (27), 11039-11043.
62. DeLorenzo, M. E.; Scott, G. I.; Ross, P. E. Toxicity of pesticides to aquatic microorganisms: a review. *Environ. Toxicol. Chem.* **2001**, *20* (1), 84-98.
63. Fent, K.; Weston, A. A.; Caminada, D. Ecotoxicology of human pharmaceuticals. *Aquat. Toxicol.* **2006**, *76* (2), 122-159.
64. Huerta, B.; Marti, E.; Gros, M.; López, P.; Pompêo, M.; Armengol, J.; Barceló, D.; Balcázar, J. L.; Rodríguez-Mozaz, S.; Marcé, R. Exploring the links between antibiotic occurrence, antibiotic resistance, and bacterial communities in water supply reservoirs. *Sci. Total Environ.* **2013**, *456*, 161-170.
65. Tetreault, G. R.; Bennett, C. J.; Shires, K.; Knight, B.; Servos, M. R.; McMaster, M. E. Intersex and reproductive impairment of wild fish exposed to multiple municipal wastewater discharges. *Aquat. Toxicol.* **2011**, *104* (3-4), 278-290.
66. Escher, B. I.; Stapleton, H. M.; Schymanski, E. L. Tracking complex mixtures of chemicals in our changing environment. *Science* **2020**, *367* (6476), 388-392.
67. Kortenkamp, A.; Faust, M. Regulate to reduce chemical mixture risk. *Science* **2018**, *361* (6399), 224-226.
68. Lau, S. S.; Wei, X.; Bokenkamp, K.; Wagner, E. D.; Plewa, M. J.; Mitch, W. A. Assessing additivity of cytotoxicity associated with disinfection byproducts in potable reuse and conventional drinking waters. *Environ. Sci. Technol.* **2020**, *54* (9), 5729-5736.
69. Pesce, S.; Lissalde, S.; Lavieille, D.; Margoum, C.; Mazzella, N.; Roubéix, V.; Montuelle, B. Evaluation of single and joint toxic effects of diuron and its main metabolites on natural phototrophic biofilms using a pollution-induced community tolerance (PICT) approach. *Aquat. Toxicol.* **2010**, *99* (4), 492-499.
70. Escher, B. I.; Fenner, K. Recent Advances in Environmental Risk Assessment of Transformation Products. *Environ. Sci. Technol.* **2011**, *45* (9), 3835-3847.
71. The European Parliament and the Council of the European Union, Directive (EU) 2020/2184 of the European Parliament and of the Council of 16 December 2020 on the quality of water

- intended for human consumption. *Official Journal of the European Union*, 2020, L435, pp 1 - 62.
72. Hofstetter, T. B.; Schwarzenbach, R. P.; Bernasconi, S. M. Assessing Transformation Processes of Organic Compounds Using Stable Isotope Fractionation. *Environ. Sci. Technol.* **2008**, *42* (21), 7737-7743.
 73. Elsner, M. Stable isotope fractionation to investigate natural transformation mechanisms of organic contaminants: principles, prospects and limitations. *J. Environ. Monit.* **2010**, *12* (11), 2005-2031.
 74. Meckenstock, R. U.; Morasch, B.; Griebler, C.; Richnow, H. H. Stable isotope fractionation analysis as a tool to monitor biodegradation in contaminated aquifers. *J. Contam. Hydrol.* **2004**, *75* (3), 215-255.
 75. Schmidt, T. C.; Zwank, L.; Elsner, M.; Berg, M.; Meckenstock, R. U.; Haderlein, S. B. Compound-specific stable isotope analysis of organic contaminants in natural environments: a critical review of the state of the art, prospects, and future challenges. *Anal. Bioanal. Chem.* **2004**, *378* (2), 283-300.
 76. Elsner, M.; Zwank, L.; Hunkeler, D.; Schwarzenbach, R. P. A New Concept Linking Observable Stable Isotope Fractionation to Transformation Pathways of Organic Pollutants. *Environ. Sci. Technol.* **2005**, *39* (18), 6896-6916.
 77. Hunkeler, D.; Meckenstock, R. U.; Sherwood Lollar, B.; Schmidt, T. C.; Wilson, J.; Schmidt, T.; Wilson, J., *A Guide for Assessing Biodegradation and Source Identification of Organic Ground Water Contaminants using Compound Specific Isotope Analysis (CSIA)*. Office of Research and Development, National Risk Management Research Laboratory, US Environmental Protection Agency: Ada, 2008.
 78. Aelion, C. M.; Höhener, P.; Hunkeler, D.; Aravena, R., *Environmental isotopes in biodegradation and bioremediation*. CRC Press: Boca Raton, USA, 2009.
 79. Thullner, M.; Richnow, H.-H.; Fischer, A., Characterization and quantification of in situ biodegradation of groundwater contaminants using stable isotope fractionation analysis: advantages and limitations. In *Environmental and regional air pollution*, Gallo, D.; Mancini, R., Eds. Nova Science Publishers: Hauppauge NY, 2009; pp 41-81.
 80. Elsner, M.; Jochmann, M. A.; Hofstetter, T. B.; Hunkeler, D.; Bernstein, A.; Schmidt, T. C.; Schimmelpfennig, A. Current challenges in compound-specific stable isotope analysis of environmental organic contaminants. *Anal. Bioanal. Chem.* **2012**, *403* (9), 2471-2491.
 81. McKinney, C. R.; McCrea, J. M.; Epstein, S.; Allen, H.; Urey, H. C. Improvements in mass spectrometers for the measurement of small differences in isotope abundance ratios. *Rev. Sci. Instrum.* **1950**, *21* (8), 724-730.
 82. Coplen, T. B. Guidelines and recommended terms for expression of stable-isotope-ratio and gas-ratio measurement results. *Rapid Commun. Mass Spectrom.* **2011**, *25* (17), 2538-2560.
 83. Meier-Augenstein, W., *Stable isotope forensics: an introduction to the forensic application of stable isotope analysis*. John Wiley & Sons: 2011; Vol. 3.
 84. Piper, T.; Mareck, U.; Geyer, H.; Flenker, U.; Thevis, M.; Platen, P.; Schänzer, W. Determination of $^{13}\text{C}/^{12}\text{C}$ ratios of endogenous urinary steroids: method validation, reference population and application to doping control purposes. *Rapid Commun. Mass Spectrom.* **2008**, *22* (14), 2161-2175.
 85. Kelly, S.; Heaton, K.; Hoogewerff, J. Tracing the geographical origin of food: The application of multi-element and multi-isotope analysis. *Trends Food Sci. Technol.* **2005**, *16* (12), 555-567.
 86. Liu, H.; Nie, J.; Liu, Y.; Wadood, S. A.; Rogers, K. M.; Yuan, Y.; Gan, R.-Y. A review of recent compound-specific isotope analysis studies applied to food authentication. *Food Chem.* **2023**, 135791.

87. Hunkeler, D.; Aravena, R.; Shouakar-Stash, O.; Weisbrod, N.; Nasser, A.; Netzer, L.; Ronen, D. Carbon and Chlorine Isotope Ratios of Chlorinated Ethenes Migrating through a Thick Unsaturated Zone of a Sandy Aquifer. *Environ. Sci. Technol.* **2011**, *45* (19), 8247-8253.
88. Jautzy, J.; Ahad, J. M. E.; Gobeil, C.; Savard, M. M. Century-Long Source Apportionment of PAHs in Athabasca Oil Sands Region Lakes Using Diagnostic Ratios and Compound-Specific Carbon Isotope Signatures. *Environ. Sci. Technol.* **2013**, *47* (12), 6155-6163.
89. Nijenhuis, I.; Schmidt, M.; Pellegatti, E.; Paramatti, E.; Richnow, H. H.; Gargini, A. A stable isotope approach for source apportionment of chlorinated ethene plumes at a complex multi-contamination events urban site. *J. Contam. Hydrol.* **2013**, *153*, 92-105.
90. Kaown, D.; Shouakar-Stash, O.; Yang, J.; Hyun, Y.; Lee, K.-K. Identification of Multiple Sources of Groundwater Contamination by Dual Isotopes. *Groundwater* **2014**, *52* (6), 875-885.
91. Alberti, L.; Marchesi, M.; Trefiletti, P.; Aravena, R. Compound-Specific Isotope Analysis (CSIA) Application for Source Apportionment and Natural Attenuation Assessment of Chlorinated Benzenes. *Water* **2017**, *9* (11), 872.
92. Sherwood Lollar, B.; Slater, G. F.; Sleep, B.; Witt, M.; Klecka, G. M.; Harkness, M.; Spivack, J. Stable Carbon Isotope Evidence for Intrinsic Bioremediation of Tetrachloroethene and Trichloroethene at Area 6, Dover Air Force Base. *Environ. Sci. Technol.* **2001**, *35* (2), 261-269.
93. Griebler, C.; Safinowski, M.; Vieth, A.; Richnow, H. H.; Meckenstock, R. U. Combined Application of Stable Carbon Isotope Analysis and Specific Metabolites Determination for Assessing In Situ Degradation of Aromatic Hydrocarbons in a Tar Oil-Contaminated Aquifer. *Environ. Sci. Technol.* **2004**, *38* (2), 617-631.
94. Hunkeler, D.; Aravena, R.; Berry-Spark, K.; Cox, E. Assessment of Degradation Pathways in an Aquifer with Mixed Chlorinated Hydrocarbon Contamination Using Stable Isotope Analysis. *Environ. Sci. Technol.* **2005**, *39* (16), 5975-5981.
95. Gilevska, T.; Passeport, E.; Shayan, M.; Seger, E.; Lutz, E. J.; West, K. A.; Morgan, S. A.; Mack, E. E.; Sherwood Lollar, B. Determination of in situ biodegradation rates via a novel high resolution isotopic approach in contaminated sediments. *Water Res.* **2019**, *149*, 632-639.
96. Bouchard, D.; Hunkeler, D.; Gaganis, P.; Aravena, R.; Höhener, P.; Broholm, M. M.; Kjeldsen, P. Carbon Isotope Fractionation during Diffusion and Biodegradation of Petroleum Hydrocarbons in the Unsaturated Zone: Field Experiment at Værløse Airbase, Denmark, and Modeling. *Environ. Sci. Technol.* **2008**, *42* (2), 596-601.
97. Alvarez-Zaldívar, P.; Payraudeau, S.; Meite, F.; Masbou, J.; Imfeld, G. Pesticide degradation and export losses at the catchment scale: Insights from compound-specific isotope analysis (CSIA). *Water Res.* **2018**, *139*, 198-207.
98. Rayleigh, L. L. Theoretical considerations respecting the separation of gases by diffusion and similar processes. *Lond. Edinb. Dublin philos. mag.* **1896**, *42* (259), 493-498.
99. Meyer, A. H.; Penning, H.; Elsner, M. C and N Isotope Fractionation Suggests Similar Mechanisms of Microbial Atrazine Transformation Despite Involvement of Different Enzymes (AtzA and TrzN). *Environ. Sci. Technol.* **2009**, *43* (21), 8079-8085.
100. Hofstetter, T. B.; Berg, M. Assessing transformation processes of organic contaminants by compound-specific stable isotope analysis. *TrAC, Trends Anal. Chem.* **2011**, *30* (4), 618-627.
101. Hartenbach, A. E.; Hofstetter, T. B.; Tentscher, P. R.; Canonica, S.; Berg, M.; Schwarzenbach, R. P. Carbon, hydrogen, and nitrogen isotope fractionation during light-induced transformations of atrazine. *Environ. Sci. Technol.* **2008**, *42* (21), 7751-7756.
102. Meyer, A. H.; Penning, H.; Lowag, H.; Elsner, M. Precise and Accurate Compound Specific Carbon and Nitrogen Isotope Analysis of Atrazine: Critical Role of Combustion Oven Conditions. *Environ. Sci. Technol.* **2008**, *42* (21), 7757-7763.

103. Elsner, M.; McKelvie, J.; Lacrampe Couloume, G.; Sherwood Lollar, B. Insight into methyl tert-butyl ether (MTBE) stable isotope fractionation from abiotic reference experiments. *Environ. Sci. Technol.* **2007**, *41* (16), 5693-5700.
104. Höhener, P.; Imfeld, G. Quantification of Lambda (λ) in multi-elemental compound-specific isotope analysis. *Chemosphere* **2021**, *267*, 129232.
105. Nier, A. O.; Gulbransen, E. A. Variations in the relative abundance of the carbon isotopes. *Journal of the American Chemical Society* **1939**, *61* (3), 697-698.
106. Hoefs, J., *Stable Isotope Geochemistry*. 9th ed.; Springer Nature: Switzerland, 2021.
107. Farquhar, G. D.; Ehleringer, J. R.; Hubick, K. T. Carbon isotope discrimination and photosynthesis. *Annu. Rev. Plant Biol.* **1989**, *40* (1), 503-537.
108. Urey, H. C. Oxygen isotopes in nature and in the laboratory. *Science* **1948**, *108* (2810), 489-496.
109. Wefer, G.; Berger, W. H. Isotope paleontology: growth and composition of extant calcareous species. *Mar. Geol.* **1991**, *100* (1-4), 207-248.
110. Makarewicz, C. A.; Sealy, J. Dietary reconstruction, mobility, and the analysis of ancient skeletal tissues: expanding the prospects of stable isotope research in archaeology. *J. Archaeol. Sci.* **2015**, *56*, 146-158.
111. Dawson, T. E.; Mambelli, S.; Plamboeck, A. H.; Templer, P. H.; Tu, K. P. Stable isotopes in plant ecology. *Annu. Rev. Ecol. Syst.* **2002**, *33* (1), 507-559.
112. Gannes, L. Z.; Del Rio, C. M.; Koch, P. Natural abundance variations in stable isotopes and their potential uses in animal physiological ecology. *Comp. Biochem. Physiol. A Mol. Integr. Physiol.* **1998**, *119* (3), 725-737.
113. Clark, I. D.; Fritz, P., *Environmental Isotopes in Hydrogeology*. CRC Press: Boca Raton, FL, USA, 1997.
114. Nier, A. O. A mass spectrometer for routine isotope abundance measurements. *Rev. Sci. Instrum.* **1940**, *11* (7), 212-216.
115. Nier, A. O. A mass spectrometer for isotope and gas analysis. *Rev. Sci. Instrum.* **1947**, *18* (6), 398-411.
116. Jochmann, M. A.; Schmidt, T. C., *Compound-specific Stable Isotope Analysis*. Royal Society of Chemistry: Cambridge, United Kingdom, 2012.
117. Brand, W. A. High precision isotope ratio monitoring techniques in mass spectrometry. *J. Mass Spectrom.* **1996**, *31* (3), 225-235.
118. Brenna, J. T.; Corso, T. N.; Tobias, H. J.; Caimi, R. J. High-precision continuous-flow isotope ratio mass spectrometry. *Mass Spectrom. Rev.* **1997**, *16* (5), 227-258.
119. Werner, R. A.; Brand, W. A. Referencing strategies and techniques in stable isotope ratio analysis. *Rapid Commun. Mass Spectrom.* **2001**, *15* (7), 501-519.
120. Matthews, D. E.; Hayes, J. M. Isotope-ratio-monitoring gas chromatography-mass spectrometry. *Anal. Chem.* **1978**, *50* (11), 1465-1473.
121. Sessions, A. L. Isotope-ratio detection for gas chromatography. *J. Sep. Sci.* **2006**, *29* (12), 1946-1961.
122. Merritt, D. A.; Hayes, J. Nitrogen isotopic analyses by isotope-ratio-monitoring gas chromatography/mass spectrometry. *J. Am. Soc. Mass. Spectrom.* **1994**, *5* (5), 387-397.
123. Preston, T.; Slater, C. Mass spectrometric analysis of stable-isotope-labelled amino acid tracers. *Proc. Nutr. Soc.* **1994**, *53* (2), 363-372.
124. Brand, W.; Tegtmeier, A. R.; Hilker, A. Compound-specific isotope analysis: extending toward $^{15}\text{N}/^{14}\text{N}$ and $^{18}\text{O}/^{16}\text{O}$. *Org. Geochem.* **1994**, *21* (6-7), 585-594.

125. Burgoyne, T. W.; Hayes, J. M. Quantitative production of H₂ by pyrolysis of gas chromatographic effluents. *Anal. Chem.* **1998**, *70* (24), 5136-5141.
126. Hilker, A.; Douthitt, C.; Schlüter, H.; Brand, W. Isotope ratio monitoring gas chromatography/mass spectrometry of D/H by high temperature conversion isotope ratio mass spectrometry. *Rapid Commun. Mass Spectrom.* **1999**, *13* (13), 1226-1230.
127. Krummen, M.; Hilker, A. W.; Juchelka, D.; Duhr, A.; Schlüter, H. J.; Pesch, R. A new concept for isotope ratio monitoring liquid chromatography/mass spectrometry. *Rapid Commun. Mass Spectrom.* **2004**, *18* (19), 2260-2266.
128. Qiu, S.; Eckert, D.; Cirpka, O. A.; Huenniger, M.; Knappett, P.; Maloszewski, P.; Meckenstock, R. U.; Griebler, C.; Elsner, M. Direct Experimental Evidence of Non-first Order Degradation Kinetics and Sorption-Induced Isotopic Fractionation in a Mesoscale Aquifer: ¹³C/¹²C Analysis of a Transient Toluene Pulse. *Environ. Sci. Technol.* **2013**, *47* (13), 6892-6899.
129. Schürner, H. K. V.; Maier, M. P.; Eckert, D.; Brejcha, R.; Neumann, C.-C.; Stumpp, C.; Cirpka, O. A.; Elsner, M. Compound-Specific Stable Isotope Fractionation of Pesticides and Pharmaceuticals in a Mesoscale Aquifer Model. *Environ. Sci. Technol.* **2016**, *50* (11), 5729-5739.
130. Sun, F.; Mellage, A.; Gharasoo, M.; Melsbach, A.; Cao, X.; Zimmermann, R.; Griebler, C.; Thullner, M.; Cirpka, O. A.; Elsner, M. Mass-Transfer-Limited Biodegradation at Low Concentrations—Evidence from Reactive Transport Modeling of Isotope Profiles in a Bench-Scale Aquifer. *Environ. Sci. Technol.* **2021**, *55* (11), 7386-7397.
131. Sun, F.; Mellage, A.; Wang, Z.; Bakkour, R.; Griebler, C.; Thullner, M.; Cirpka, O. A.; Elsner, M. Toward Improved Bioremediation Strategies: Response of BAM-Degradation Activity to Concentration and Flow Changes in an Inoculated Bench-Scale Sediment Tank. *Environ. Sci. Technol.* **2022**, *56* (7), 4050-4061.
132. Prieto-Espinoza, M.; Di Chiara Roupert, R.; Belfort, B.; Weill, S.; Imfeld, G. Reactive transport of micropollutants in laboratory aquifers undergoing transient exposure periods. *Sci. Total Environ.* **2023**, *856*, 159170.
133. Elsayed, O. F.; Maillard, E.; Vuilleumier, S.; Nijenhuis, I.; Richnow, H. H.; Imfeld, G. Using compound-specific isotope analysis to assess the degradation of chloroacetanilide herbicides in lab-scale wetlands. *Chemosphere* **2014**, *99*, 89-95.
134. Tang, X.; Yang, Y.; Huang, W.; McBride, M. B.; Guo, J.; Tao, R.; Dai, Y. Transformation of chlorpyrifos in integrated recirculating constructed wetlands (IRCWs) as revealed by compound-specific stable isotope (CSIA) and microbial community structure analysis. *Bioresour. Technol.* **2017**, *233*, 264-270.
135. Droz, B.; Drouin, G.; Maurer, L.; Villette, C.; Payraudeau, S.; Imfeld, G. Phase Transfer and Biodegradation of Pesticides in Water–Sediment Systems Explored by Compound-Specific Isotope Analysis and Conceptual Modeling. *Environ. Sci. Technol.* **2021**, *55* (8), 4720-4728.
136. Pérez-Rodríguez, P.; Schmitt, A.-D.; Gangloff, S.; Masbou, J.; Imfeld, G. Plants affect the dissipation and leaching of anilide pesticides in soil mesocosms: Insights from compound-specific isotope analysis (CSIA). *Agric. Ecosyst. Environ.* **2021**, *308*, 107257.
137. Melsbach, A.; Torrentó, C.; Ponsin, V.; Bolotin, J.; Lachat, L.; Prasuhn, V.; Hofstetter, T. B.; Hunkeler, D.; Elsner, M. Dual-Element Isotope Analysis of Desphenylchloridazon to Investigate Its Environmental Fate in a Systematic Field Study: A Long-Term Lysimeter Experiment. *Environ. Sci. Technol.* **2020**, *54* (7), 3929-3939.
138. Milosevic, N.; Qiu, S.; Elsner, M.; Einsiedl, F.; Maier, M. P.; Bensch, H. K. V.; Albrechtsen, H. J.; Bjerg, P. L. Combined isotope and enantiomer analysis to assess the fate of phenoxy acids in a heterogeneous geologic setting at an old landfill. *Water Res.* **2013**, *47* (2), 637-649.

139. Bashir, S.; Hitzfeld, K. L.; Gehre, M.; Richnow, H. H.; Fischer, A. Evaluating degradation of hexachlorocyclohexane (HCH) isomers within a contaminated aquifer using compound-specific stable carbon isotope analysis (CSIA). *Water Res.* **2015**, *71*, 187-196.
140. Wu, L.; Verma, D.; Bondgaard, M.; Melvej, A.; Vogt, C.; Subudhi, S.; Richnow, H. H. Carbon and hydrogen isotope analysis of parathion for characterizing its natural attenuation by hydrolysis at a contaminated site. *Water Res.* **2018**, *143*, 146-154.
141. Gilevska, T.; Masbou, J.; Baumlin, B.; Chaumet, B.; Chaumont, C.; Payraudeau, S.; Tournebize, J.; Probst, A.; Probst, J. L.; Imfeld, G. Do pesticides degrade in surface water receiving runoff from agricultural catchments? Combining passive samplers (POCIS) and compound-specific isotope analysis. *Sci. Total Environ.* **2022**, *842*, 156735.
142. Lutz, S. R.; Velde, Y. V. D.; Elsayed, O. F.; Imfeld, G.; Lefrancq, M.; Payraudeau, S.; van Breukelen, B. M. Pesticide fate on catchment scale: conceptual modelling of stream CSIA data. *Hydrol. Earth Syst. Sci.* **2017**, *21* (10), 5243-5261.
143. Masbou, J.; Payraudeau, S.; Guyot, B.; Imfeld, G. Dimethomorph degradation in vineyards examined by isomeric and isotopic fractionation. *Chemosphere* **2023**, *313*, 137341.
144. Schmidt, T. C.; Jochmann, M. A. Origin and Fate of Organic Compounds in Water: Characterization by Compound-Specific Stable Isotope Analysis. *Annu. Rev. Anal. Chem.* **2012**, *5* (1), 133-155.
145. Meier-Augenstein, W. Applied gas chromatography coupled to isotope ratio mass spectrometry. *J. Chromatogr. A* **1999**, *842* (1), 351-371.
146. Blessing, M.; Baran, N. A review on environmental isotope analysis of aquatic micropollutants: Recent advances, pitfalls and perspectives. *TrAC, Trends Anal. Chem.* **2022**, *157*, 116730.
147. Elsner, M.; Imfeld, G. Compound-specific isotope analysis (CSIA) of micropollutants in the environment — current developments and future challenges. *Curr. Opin. Biotechnol.* **2016**, *41*, 60-72.
148. Zwank, L.; Berg, M.; Schmidt, T. C.; Haderlein, S. B. Compound-Specific Carbon Isotope Analysis of Volatile Organic Compounds in the Low-Microgram per Liter Range. *Anal. Chem.* **2003**, *75* (20), 5575-5583.
149. Buszewski, B.; Szultka, M. Past, Present, and Future of Solid Phase Extraction: A Review. *Crit. Rev. Anal. Chem.* **2012**, *42* (3), 198-213.
150. Andrade-Eiroa, A.; Canle, M.; Leroy-Cancellieri, V.; Cerdà, V. Solid-phase extraction of organic compounds: A critical review (Part I). *TrAC, Trends Anal. Chem.* **2016**, *80*, 641-654.
151. Blessing, M.; Jochmann, M. A.; Schmidt, T. C. Pitfalls in compound-specific isotope analysis of environmental samples. *Anal. Bioanal. Chem.* **2008**, *390* (2), 591-603.
152. O'Malley, V. P.; Abrajano, T. A.; Hellou, J. Determination of the $^{13}\text{C}/^{12}\text{C}$ ratios of individual PAH from environmental samples: can PAH sources be apportioned? *Org. Geochem.* **1994**, *21* (6), 809-822.
153. Bakkour, R. Molecularly-imprinted polymers for compound-specific isotope analysis of polar organic micropollutants in aquatic environments. Doctoral Thesis (No. 24753), ETH Zurich, Zurich, Switzerland, 2018.
154. Westerhoff, P.; Mash, H. Dissolved organic nitrogen in drinking water supplies: a review. *J. Water Supply: Res. Technol. - AQUA* **2002**, *51* (8), 415-448.
155. Gilevska, T.; Wiegert, C.; Droz, B.; Junginger, T.; Prieto-Espinoza, M.; Borreca, A.; Imfeld, G. Simple extraction methods for pesticide compound-specific isotope analysis from environmental samples. *MethodsX* **2022**, *9*, 101880.

156. Kronimus, A.; Schwarzbauer, J.; Dsikowitzky, L.; Littke, R. Compound-specific stable carbon isotope analyses of riverine water organic contaminants. *Environ. Chem. Lett.* **2006**, *4* (1), 23-28.
157. Melsbach, A.; Pittois, D.; Bayerle, M.; Daubmeier, M.; Meyer, A. H.; Hölzer, K.; Gallé, T.; Elsner, M. Isotope fractionation of micropollutants during large-volume extraction: heads-up from a critical method evaluation for atrazine, desethylatrazine and 2,6-dichlorobenzamide at low ng/L concentrations in groundwater. *Isot. Environ. Health Stud.* **2020**, 1-18.
158. Höhener, P.; Guers, D.; Malleret, L.; Boukaroum, O.; Martin-Laurent, F.; Masbou, J.; Payraudeau, S.; Imfeld, G. Multi-elemental compound-specific isotope analysis of pesticides for source identification and monitoring of degradation in soil: a review. *Environ. Chem. Lett.* **2022**, *20* (6), 3927-3942.
159. Fenner, K.; Elsner, M.; Lueders, T.; McLachlan, M. S.; Wackett, L. P.; Zimmermann, M.; Drewes, J. E. Methodological Advances to Study Contaminant Biotransformation: New Prospects for Understanding and Reducing Environmental Persistence? *ACS ES&T Water* **2021**, *1* (7), 1541-1554.
160. Flenker, U.; Hebestreit, M.; Piper, T.; Hülsemann, F.; Schänzer, W. Improved performance and maintenance in gas chromatography/isotope ratio mass spectrometry by precolumn solvent removal. *Anal. Chem.* **2007**, *79* (11), 4162-4168.
161. Baczynski, A. A.; Polissar, P. J.; Juchelka, D.; Schwieters, J.; Hilkert, A.; Summons, R. E.; Freeman, K. H. Picomolar-scale compound-specific isotope analyses. *Rapid Commun. Mass Spectrom.* **2018**, *32* (9), 730-738.
162. Tobias, H. J.; Brenna, J. T. Microfabrication of high temperature micro-reactors for continuous flow isotope ratio mass spectrometry. *Microfluid. Nanofluidics* **2010**, *9*, 461-470.
163. Tobias, H. J.; Sacks, G. L.; Zhang, Y.; Brenna, J. T. Comprehensive two-dimensional gas chromatography combustion isotope ratio mass spectrometry. *Anal. Chem.* **2008**, *80* (22), 8613-8621.
164. Torrentó, C.; Bakkour, R.; Glauser, G.; Melsbach, A.; Ponsin, V.; Hofstetter, T. B.; Elsner, M.; Hunkeler, D. Solid-phase extraction method for stable isotope analysis of pesticides from large volume environmental water samples. *Analyst* **2019**, *144* (9), 2898-2908.
165. Schreglmann, K.; Hoeche, M.; Steinbeiss, S.; Reinnicke, S.; Elsner, M. Carbon and nitrogen isotope analysis of atrazine and desethylatrazine at sub-microgram per liter concentrations in groundwater. *Anal. Bioanal. Chem.* **2013**, *405* (9), 2857-2867.
166. Bakkour, R.; Bolotin, J.; Sellergren, B.; Hofstetter, T. B. Molecularly Imprinted Polymers for Compound-Specific Isotope Analysis of Polar Organic Micropollutants in Aquatic Environments. *Anal. Chem.* **2018**, *90* (12), 7292-7301.
167. Fontanals, N.; Marcé, R. M.; Borrull, F. New materials in sorptive extraction techniques for polar compounds. *J. Chromatogr. A* **2007**, *1152* (1), 14-31.
168. Fontanals, N.; Marcé, R. M.; Borrull, F. New hydrophilic materials for solid-phase extraction. *TrAC, Trends Anal. Chem.* **2005**, *24* (5), 394-406.
169. Fontanals, N.; Marcé, R. M.; Borrull, F. Materials for Solid-Phase Extraction of Organic Compounds. *Separations* **2019**, *6* (4), 56.
170. Poole, C. F. New trends in solid-phase extraction. *TrAC, Trends Anal. Chem.* **2003**, *22* (6), 362-373.
171. Poole, C. F., *Solid-Phase Extraction*. Elsevier: Amsterdam, Netherlands, 2020.
172. Gilart, N.; Borrull, F.; Fontanals, N.; Marcé, R. M. Selective materials for solid-phase extraction in environmental analysis. *Trends Environ. Anal. Chem.* **2014**, *1*, e8-e18.

173. Fontanals, N.; Marcé, R. M.; Borrull, F.; Cormack, P. A. Mixed-mode ion-exchange polymeric sorbents: dual-phase materials that improve selectivity and capacity. *TrAC, Trends Anal. Chem.* **2010**, *29* (7), 765-779.
174. Endo, S.; Goss, K.-U. Applications of Polyparameter Linear Free Energy Relationships in Environmental Chemistry. *Environ. Sci. Technol.* **2014**, *48* (21), 12477-12491.
175. Abraham, M. H. Scales of solute hydrogen-bonding: their construction and application to physicochemical and biochemical processes. *Chem. Soc. Rev.* **1993**, *22* (2), 73-83.
176. Abraham, M. H.; Ibrahim, A.; Zissimos, A. M. Determination of sets of solute descriptors from chromatographic measurements. *J. Chromatogr. A* **2004**, *1037* (1), 29-47.
177. Masqué, N.; Marcé, R. M.; Borrull, F. New polymeric and other types of sorbents for solid-phase extraction of polar organic micropollutants from environmental water. *TrAC, Trends Anal. Chem.* **1998**, *17* (6), 384-394.
178. Junker-Buchheit, A.; Witzemberger, M. Pesticide monitoring of drinking water with the help of solid-phase extraction and high-performance liquid chromatography. *J. Chromatogr. A* **1996**, *737* (1), 67-74.
179. Pichon, V.; Coumes, C. C. D.; Chen, L.; Guenu, S.; Hennion, M.-C. Simple removal of humic and fulvic acid interferences using polymeric sorbents for the simultaneous solid-phase extraction of polar acidic, neutral and basic pesticides. *J. Chromatogr. A* **1996**, *737* (1), 25-33.
180. Pichon, V.; Combes, A.; Delaunay, N. Immunosorbents in microextraction. *TrAC, Trends Anal. Chem.* **2019**, *113*, 246-255.
181. Martín-Esteban, A. Recent molecularly imprinted polymer-based sample preparation techniques in environmental analysis. *Trends Environ. Anal. Chem.* **2016**, *9*, 8-14.
182. Bolliet, D.; Poole, C. F. Influence of solvent effects on retention for a porous polymer sorbent in reversed phase liquid chromatography. *Chromatographia* **1997**, *46* (7), 381-398.
183. Dias, N.; Poole, C. Mechanistic study of the sorption properties of OASIS® HLB and its use in solid-phase extraction. *Chromatographia* **2002**, *56* (5), 269-275.
184. Klemes, M. J.; Skala, L. P.; Ateia, M.; Trang, B.; Helbling, D. E.; Dichtel, W. R. Polymerized Molecular Receptors as Adsorbents to Remove Micropollutants from Water. *Acc. Chem. Res.* **2020**, *53* (10), 2314-2324.
185. Crini, G. Review: A History of Cyclodextrins. *Chem. Rev.* **2014**, *114* (21), 10940-10975.
186. Szejtli, J. Introduction and General Overview of Cyclodextrin Chemistry. *Chem. Rev.* **1998**, *98* (5), 1743-1754.
187. Connors, K. A. The Stability of Cyclodextrin Complexes in Solution. *Chem. Rev.* **1997**, *97* (5), 1325-1358.
188. Rekharsky, M. V.; Inoue, Y. Complexation Thermodynamics of Cyclodextrins. *Chem. Rev.* **1998**, *98* (5), 1875-1918.
189. Morin-Crini, N.; Fourmentin, S.; Fenyvesi, É.; Lichtfouse, E.; Torri, G.; Fourmentin, M.; Crini, G. 130 years of cyclodextrin discovery for health, food, agriculture, and the industry: A review. *Environ. Chem. Lett.* **2021**, *19* (3), 2581-2617.
190. Gaidamauskas, E.; Norkus, E.; Butkus, E.; Crans, D. C.; Grincienė, G. Deprotonation of β -cyclodextrin in alkaline solutions. *Carbohydr. Res.* **2009**, *344* (2), 250-254.
191. Gentili, A. Cyclodextrin-based sorbents for solid phase extraction. *J. Chromatogr. A* **2020**, *1609*, 460654.
192. Morin-Crini, N.; Crini, G. Environmental applications of water-insoluble β -cyclodextrin-epichlorohydrin polymers. *Prog. Polym. Sci.* **2013**, *38* (2), 344-368.

193. Alsbaiee, A.; Smith, B. J.; Xiao, L.; Ling, Y.; Helbling, D. E.; Dichtel, W. R. Rapid removal of organic micropollutants from water by a porous beta-cyclodextrin polymer. *Nature* **2016**, 529 (7585), 190-4.
194. Ling, Y.; Klemes, M. J.; Xiao, L.; Alsbaiee, A.; Dichtel, W. R.; Helbling, D. E. Benchmarking Micropollutant Removal by Activated Carbon and Porous β -Cyclodextrin Polymers under Environmentally Relevant Scenarios. *Environ. Sci. Technol.* **2017**, 51 (13), 7590-7598.
195. Li, C.; Klemes, M. J.; Dichtel, W. R.; Helbling, D. E. Tetrafluoroterephthalonitrile-crosslinked β -cyclodextrin polymers for efficient extraction and recovery of organic micropollutants from water. *J. Chromatogr. A* **2018**, 1541, 52-56.
196. Ling, Y.; Alzate-Sánchez, D. M.; Klemes, M. J.; Dichtel, W. R.; Helbling, D. E. Evaluating the effects of water matrix constituents on micropollutant removal by activated carbon and β -cyclodextrin polymer adsorbents. *Water Res.* **2020**, 173, 115551.
197. Klemes, M. J.; Ling, Y.; Chiapasco, M.; Alsbaiee, A.; Helbling, D. E.; Dichtel, W. R. Phenolation of cyclodextrin polymers controls their lead and organic micropollutant adsorption. *Chem. Sci.* **2018**, 9 (47), 8883-8889.
198. Ling, Y.; Klemes, M. J.; Steinschneider, S.; Dichtel, W. R.; Helbling, D. E. QSARs to predict adsorption affinity of organic micropollutants for activated carbon and β -cyclodextrin polymer adsorbents. *Water Res.* **2019**, 154, 217-226.
199. Crini, G. Cyclodextrin-epichlorohydrin polymers synthesis, characterization and applications to wastewater treatment: a review. *Environ. Chem. Lett.* **2021**, 19 (3), 2383-2403.
200. Morin-Crini, N.; Winterton, P.; Fourmentin, S.; Wilson, L. D.; Fenyvesi, É.; Crini, G. Water-insoluble β -cyclodextrin-epichlorohydrin polymers for removal of pollutants from aqueous solutions by sorption processes using batch studies: A review of inclusion mechanisms. *Prog. Polym. Sci.* **2018**, 78, 1-23.
201. Klemes, M. J.; Ling, Y.; Ching, C.; Wu, C.; Xiao, L.; Helbling, D. E.; Dichtel, W. R. Reduction of a Tetrafluoroterephthalonitrile- β -Cyclodextrin Polymer to Remove Anionic Micropollutants and Perfluorinated Alkyl Substances from Water. *Angew. Chem. Int. Ed.* **2019**, 58 (35), 12049-12053.
202. Ching, C.; Klemes, M. J.; Trang, B.; Dichtel, W. R.; Helbling, D. E. β -Cyclodextrin Polymers with Different Cross-Linkers and Ion-Exchange Resins Exhibit Variable Adsorption of Anionic, Zwitterionic, and Nonionic PFASs. *Environ. Sci. Technol.* **2020**, 54 (19), 12693-12702.
203. Wu, C.; Klemes, M. J.; Trang, B.; Dichtel, W. R.; Helbling, D. E. Exploring the factors that influence the adsorption of anionic PFAS on conventional and emerging adsorbents in aquatic matrices. *Water Res.* **2020**, 182, 115950.
204. Ching, C.; Ling, Y.; Trang, B.; Klemes, M.; Xiao, L.; Yang, A.; Barin, G.; Dichtel, W. R.; Helbling, D. E. Identifying the physicochemical properties of β -cyclodextrin polymers that determine the adsorption of perfluoroalkyl acids. *Water Res.* **2022**, 209, 117938.
205. Choudhary, A.; Dong, D.; Tsianou, M.; Alexandridis, P.; Bedrov, D. Adsorption Mechanism of Perfluorooctanoate on Cyclodextrin-Based Polymers: Probing the Synergy of Electrostatic and Hydrophobic Interactions with Molecular Dynamics Simulations. *ACS Mater. Lett.* **2022**, 4 (5), 853-859.
206. Potter, B.; Wimsatt, J., *Method 415.3. Measurement of total organic carbon, dissolved organic carbon and specific UV absorbance at 254 nm in source water and drinking water*. US Environmental Protection Agency: Washington, DC, 2005.
207. Sandron, S.; Rojas, A.; Wilson, R.; Davies, N. W.; Haddad, P. R.; Shellie, R. A.; Nesterenko, P. N.; Kelleher, B. P.; Paull, B. Chromatographic methods for the isolation, separation and characterisation of dissolved organic matter. *Environ. Sci.: Process. Impacts* **2015**, 17 (9), 1531-1567.

208. Thurman, E., *Organic geochemistry of natural waters*. Martinus Nijhoff/Dr W. Junk Publishers: Dordrecht, The Netherlands, 1985; Vol. 2.
209. Thurman, E. M.; Malcolm, R. L. Preparative isolation of aquatic humic substances. *Environ. Sci. Technol.* **1981**, *15* (4), 463-466.
210. Cooper, W. T.; Chanton, J. C.; D'Andrilli, J.; Hodgkins, S. B.; Podgorski, D. C.; Stenson, A. C.; Tfaily, M. M.; Wilson, R. M. A History of Molecular Level Analysis of Natural Organic Matter by FTICR Mass Spectrometry and The Paradigm Shift in Organic Geochemistry. *Mass Spectrom. Rev.* **2022**, *41* (2), 215-239.
211. Qi, Y.; Xie, Q.; Wang, J.-J.; He, D.; Bao, H.; Fu, Q.-L.; Su, S.; Sheng, M.; Li, S.-L.; Volmer, D. A.; Wu, F.; Jiang, G.; Liu, C.-Q.; Fu, P. Deciphering dissolved organic matter by Fourier transform ion cyclotron resonance mass spectrometry (FT-ICR MS): from bulk to fractions and individuals. *Carbon Research* **2022**, *1* (1), 3.
212. Hertkorn, N.; Ruecker, C.; Meringer, M.; Gugisch, R.; Frommberger, M.; Perdue, E. M.; Witt, M.; Schmitt-Kopplin, P. High-precision frequency measurements: indispensable tools at the core of the molecular-level analysis of complex systems. *Anal. Bioanal. Chem.* **2007**, *389* (5), 1311-27.
213. Hertkorn, N.; Benner, R.; Frommberger, M.; Schmitt-Kopplin, P.; Witt, M.; Kaiser, K.; Kettrup, A.; Hedges, J. I. Characterization of a major refractory component of marine dissolved organic matter. *Geochim. Cosmochim. Acta* **2006**, *70* (12), 2990-3010.
214. Sleighter, R. L.; Hatcher, P. G. Molecular characterization of dissolved organic matter (DOM) along a river to ocean transect of the lower Chesapeake Bay by ultrahigh resolution electrospray ionization Fourier transform ion cyclotron resonance mass spectrometry. *Mar. Chem.* **2008**, *110* (3), 140-152.
215. Hockaday, W. C.; Purcell, J. M.; Marshall, A. G.; Baldock, J. A.; Hatcher, P. G. Electrospray and photoionization mass spectrometry for the characterization of organic matter in natural waters: a qualitative assessment. *Limnol. Oceanogr.: Methods* **2009**, *7* (1), 81-95.
216. Stubbins, A.; Spencer, R. G. M.; Chen, H.; Hatcher, P. G.; Mopper, K.; Hernes, P. J.; Mwamba, V. L.; Mangangu, A. M.; Wabakanghanzi, J. N.; Six, J. Illuminated darkness: Molecular signatures of Congo River dissolved organic matter and its photochemical alteration as revealed by ultrahigh precision mass spectrometry. *Limnol. Oceanogr.* **2010**, *55* (4), 1467-1477.
217. Arakawa, N.; Aluwihare, L. Direct Identification of Diverse Alicyclic Terpenoids in Suwannee River Fulvic Acid. *Environ. Sci. Technol.* **2015**, *49* (7), 4097-4105.
218. Lam, B.; Baer, A.; Alae, M.; Lefebvre, B.; Moser, A.; Williams, A.; Simpson, A. J. Major structural components in freshwater dissolved organic matter. *Environ. Sci. Technol.* **2007**, *41* (24), 8240-8247.
219. Leenheer, J. A.; Nanny, M. A.; McIntyre, C. Terpenoids as major precursors of dissolved organic matter in landfill leachates, surface water, and groundwater. *Environ. Sci. Technol.* **2003**, *37* (11), 2323-2331.
220. Zigah, P. K.; Minor, E. C.; Abdulla, H. A.; Werne, J. P.; Hatcher, P. G. An investigation of size-fractionated organic matter from Lake Superior and a tributary stream using radiocarbon, stable isotopes and NMR. *Geochim. Cosmochim. Acta* **2014**, *127*, 264-284.
221. Hatcher, P. G.; Maciel, G. E.; Dennis, L. W. Aliphatic structure of humic acids; a clue to their origin. *Org. Geochem.* **1981**, *3* (1-2), 43-48.
222. Stevenson, F. J., *Humus chemistry: genesis, composition, reactions*. John Wiley & Sons: 1994.
223. Hertkorn, N.; Harir, M.; Cawley, K. M.; Schmitt-Kopplin, P.; Jaffé, R. Molecular characterization of dissolved organic matter from subtropical wetlands: a comparative study through the analysis of optical properties, NMR and FTICR/MS. *Biogeosciences* **2016**, *13* (8), 2257-2277.

224. Hertkorn, N.; Harir, M.; Koch, B.; Michalke, B.; Schmitt-Kopplin, P. High-field NMR spectroscopy and FTICR mass spectrometry: powerful discovery tools for the molecular level characterization of marine dissolved organic matter. *Biogeosciences* **2013**, *10*, 1583-1624.
225. Minor, E. C.; Swenson, M. M.; Mattson, B. M.; Oyler, A. R. Structural characterization of dissolved organic matter: a review of current techniques for isolation and analysis. *Environ. Sci.: Process. Impacts* **2014**, *16* (9), 2064-2079.
226. Kim, S.; Kim, D.; Jung, M. J.; Kim, S. Analysis of environmental organic matters by Ultrahigh-Resolution mass spectrometry—A review on the development of analytical methods. *Mass Spectrom. Rev.* **2021**.
227. Bahureksa, W.; Tfaily, M. M.; Boiteau, R. M.; Young, R. B.; Logan, M. N.; McKenna, A. M.; Borch, T. Soil Organic Matter Characterization by Fourier Transform Ion Cyclotron Resonance Mass Spectrometry (FTICR MS): A Critical Review of Sample Preparation, Analysis, and Data Interpretation. *Environ. Sci. Technol.* **2021**, *55* (14), 9637-9656.
228. Sleighter, R. L.; Hatcher, P. G., Fourier Transform Mass Spectrometry for the Molecular Level Characterization of Natural Organic Matter: Instrument Capabilities, Applications, and Limitations. In *Fourier Transforms - Approach to Scientific Principles*, Nikolic, G. S., Ed. InTech: Rijeka, Croatia, 2011.
229. Kim, S.; Kramer, R. W.; Hatcher, P. G. Graphical Method for Analysis of Ultrahigh-Resolution Broadband Mass Spectra of Natural Organic Matter, the Van Krevelen Diagram. *Anal. Chem.* **2003**, *75* (20), 5336-5344.
230. Koch, B. P.; Dittmar, T. From mass to structure: an aromaticity index for high-resolution mass data of natural organic matter. *Rapid Commun. Mass Spectrom.* **2006**, *20* (5), 926-932.
231. Koch, B. P.; Dittmar, T. From mass to structure: an aromaticity index for high-resolution mass data of natural organic matter. *Rapid Commun. Mass Spectrom.* **2016**, *30* (1), 250-250.
232. Hawkes, J. A.; Kew, W., 4 - High-resolution mass spectrometry strategies for the investigation of dissolved organic matter. In *Multidimensional Analytical Techniques in Environmental Research*, Duarte, R. M. B. O.; Duarte, A. C., Eds. Elsevier: 2020; pp 71-104.
233. Svec, F.; Huber, C. G., Monolithic materials: promises, challenges, achievements. In ACS Publications: 2006.
234. Svec, F.; Lv, Y. Advances and recent trends in the field of monolithic columns for chromatography. *Anal. Chem.* **2015**, *87* (1), 250-273.
235. Masini, J. C.; Svec, F. Porous monoliths for on-line sample preparation: A review. *Anal. Chim. Acta* **2017**, *964*, 24-44.
236. Masini, J. C.; do Nascimento, F. H.; Vitek, R. Porous monolithic materials for extraction and preconcentration of pollutants from environmental waters. *Trends Environ. Anal. Chem.* **2021**, *29*, e00112.
237. Hjelmsø, M. H.; Hellmér, M.; Fernandez-Cassi, X.; Timoneda, N.; Lukjancenka, O.; Seidel, M.; Elsässer, D.; Aarestrup, F. M.; Löfström, C.; Bofill-Mas, S.; Abril, J. F.; Girones, R.; Schultz, A. C. Evaluation of Methods for the Concentration and Extraction of Viruses from Sewage in the Context of Metagenomic Sequencing. *PLOS ONE* **2017**, *12* (1), e0170199.
238. Fresco-Cala, B.; Cárdenas, S. Potential of nanoparticle-based hybrid monoliths as sorbents in microextraction techniques. *Anal. Chim. Acta* **2018**, *1031*, 15-27.
239. Sitko, R.; Zawisza, B.; Malicka, E. Graphene as a new sorbent in analytical chemistry. *TrAC, Trends Anal. Chem.* **2013**, *51*, 33-43.
240. Ibrahim, W. A. W.; Nodeh, H. R.; Sanagi, M. M. Graphene-Based Materials as Solid Phase Extraction Sorbent for Trace Metal Ions, Organic Compounds, and Biological Sample Preparation. *Crit. Rev. Anal. Chem.* **2016**, *46* (4), 267-283.

241. He, H.; Klinowski, J.; Forster, M.; Lerf, A. A new structural model for graphite oxide. *Chem. Phys. Lett.* **1998**, *287* (1), 53-56.
242. Pei, M.; Shi, X.; Wu, J.; Huang, X. Graphene reinforced multiple monolithic fiber solid-phase microextraction of phenoxyacetic acid herbicides in complex samples. *Talanta* **2019**, *191*, 257-264.
243. Jin, T.; Li, F.; Cheng, J.; Wu, S.; Zhou, H.; Cheng, M. Polymer monolithic column containing embedded graphene oxide sheets for sensitive determination of carbamate insecticides by HPLC. *Microchimica Acta* **2016**, *183* (2), 543-551.
244. Wang, X.; Wang, J.; Du, T.; Kou, H.; Du, X.; Lu, X. Determination of six benzotriazole ultraviolet filters in water and cosmetic samples by graphene sponge-based solid-phase extraction followed by high-performance liquid chromatography. *Anal. Bioanal. Chem.* **2018**, *410* (26), 6955-6962.
245. Han, Q.; Liang, Q.; Zhang, X.; Yang, L.; Ding, M. Graphene aerogel based monolith for effective solid-phase extraction of trace environmental pollutants from water samples. *J. Chromatogr. A* **2016**, *1447*, 39-46.
246. Sun, M.; Bu, Y.; Feng, J.; Luo, C. Graphene oxide reinforced polymeric ionic liquid monolith solid-phase microextraction sorbent for high-performance liquid chromatography analysis of phenolic compounds in aqueous environmental samples. *J. Sep. Sci.* **2016**, *39* (2), 375-382.
247. Liu, Q.; Shi, J.; Sun, J.; Wang, T.; Zeng, L.; Jiang, G. Graphene and Graphene Oxide Sheets Supported on Silica as Versatile and High-Performance Adsorbents for Solid-Phase Extraction. *Angew. Chem. Int. Ed.* **2011**, *50* (26), 5913-5917.
248. Lihl, C.; Douglas, L. M.; Franke, S.; Pérez-de-Mora, A.; Meyer, A. H.; Daubmeier, M.; Edwards, E. A.; Nijenhuis, I.; Sherwood Lollar, B.; Elsner, M. Mechanistic Dichotomy in Bacterial Trichloroethene Dechlorination Revealed by Carbon and Chlorine Isotope Effects. *Environ. Sci. Technol.* **2019**, *53* (8), 4245-4254.
249. Maier, M. P.; Prasse, C.; Pati, S. G.; Nitsche, S.; Li, Z.; Radke, M.; Meyer, A.; Hofstetter, T. B.; Ternes, T. A.; Elsner, M. Exploring Trends of C and N Isotope Fractionation to Trace Transformation Reactions of Diclofenac in Natural and Engineered Systems. *Environ. Sci. Technol.* **2016**, *50* (20), 10933-10942.
250. Palau, J.; Shouakar-Stash, O.; Hatijah Mortan, S.; Yu, R.; Rosell, M.; Marco-Urrea, E.; Freedman, D. L.; Aravena, R.; Soler, A.; Hunkeler, D. Hydrogen Isotope Fractionation during the Biodegradation of 1,2-Dichloroethane: Potential for Pathway Identification Using a Multi-element (C, Cl, and H) Isotope Approach. *Environ. Sci. Technol.* **2017**, *51* (18), 10526-10535.
251. Masbou, J.; Drouin, G.; Payraudeau, S.; Imfeld, G. Carbon and nitrogen stable isotope fractionation during abiotic hydrolysis of pesticides. *Chemosphere* **2018**, *213*, 368-376.
252. Andrade-Eiroa, A.; Canle, M.; Leroy-Cancellieri, V.; Cerdà, V. Solid-phase extraction of organic compounds: A critical review. part ii. *TrAC, Trends Anal. Chem.* **2016**, *80*, 655-667.
253. Xiao, L.; Ching, C.; Ling, Y.; Nasiri, M.; Klemes, M. J.; Reineke, T. M.; Helbling, D. E.; Dichtel, W. R. Cross-linker Chemistry Determines the Uptake Potential of Perfluorinated Alkyl Substances by β -Cyclodextrin Polymers. *Macromolecules* **2019**, *52* (10), 3747-3752.
254. Organisation for Economic Co-operation and Development (OECD), *Test No. 106: Adsorption -- Desorption Using a Batch Equilibrium Method*. OECD Guidelines for the Testing of Chemicals ed.; OECD Publishing: Paris, 2000.
255. U.S. Environmental Protection Agency (US EPA), *Fate, transport and transformation test guidelines. OPPTS 835.1230. Adsorption/desorption (batch equilibrium) for pesticides and toxic substances. EPA 712-C-08-009* Washington D.C., 2008.
256. Bronner, G.; Goss, K.-U. Sorption of Organic Chemicals to Soil Organic Matter: Influence of Soil Variability and pH Dependence. *Environ. Sci. Technol.* **2011**, *45* (4), 1307-1312.

257. Schenzel, J.; Goss, K.-U.; Schwarzenbach, R. P.; Bucheli, T. D.; Droge, S. T. J. Experimentally Determined Soil Organic Matter–Water Sorption Coefficients for Different Classes of Natural Toxins and Comparison with Estimated Numbers. *Environ. Sci. Technol.* **2012**, *46* (11), 6118-6126.
258. Tülp, H. C.; Fenner, K.; Schwarzenbach, R. P.; Goss, K. U. pH-Dependent sorption of acidic organic chemicals to soil organic matter. *Environ. Sci. Technol.* **2009**, *43* (24), 9189-95.
259. Bi, E.; Schmidt, T. C.; Haderlein, S. B. Practical issues relating to soil column chromatography for sorption parameter determination. *Chemosphere* **2010**, *80* (7), 787-93.
260. Bronner, G.; Goss, K.-U. Predicting Sorption of Pesticides and Other Multifunctional Organic Chemicals to Soil Organic Carbon. *Environ. Sci. Technol.* **2011**, *45* (4), 1313-1319.
261. Ulrich, N.; Endo, S.; Brown, T. N.; Watanabe, N.; Bronner, G.; Abraham, M. H.; Goss, K. U., *UFZ-LSER database v 3.2 [Internet]*. <http://www.ufz.de/lserd> (accessed October 1, 2022).
262. Abraham, M. H.; Acree, W. E. Partition coefficients and solubilities of compounds in the water–ethanol solvent system. *J. Solution Chem.* **2011**, *40* (7), 1279-1290.
263. Zhou, X.; Zhou, X. The Unit Problem in the Thermodynamic Calculation of Adsorption using the Langmuir Equation. *Chem. Eng. Commun.* **2014**, *201* (11), 1459-1467.
264. Mills, I.; Cvitas, T.; Homann, K.; Kallay, N.; Kuchitsu, K., *International Union of Pure and Applied Chemistry: Quantities, Units and Symbols in Physical Chemistry*. 2nd Edition ed.; Blackwell Science Ltd.: Oxford, 1993.
265. Jochmann, M. A.; Blessing, M.; Haderlein, S. B.; Schmidt, T. C. A new approach to determine method detection limits for compound-specific isotope analysis of volatile organic compounds. *Rapid Commun. Mass Spectrom.* **2006**, *20* (24), 3639-3648.
266. Sherwood Lollar, B.; Hirschorn, S. K.; Chartrand, M. M. G.; Lacrampe-Couloume, G. An Approach for Assessing Total Instrumental Uncertainty in Compound-Specific Carbon Isotope Analysis: Implications for Environmental Remediation Studies. *Anal. Chem.* **2007**, *79* (9), 3469-3475.
267. O'Leary, M. H. Carbon Isotopes in Photosynthesis: Fractionation techniques may reveal new aspects of carbon dynamics in plants. *BioScience* **1988**, *38* (5), 328-336.
268. Goss, K.-U.; Schwarzenbach, R. P. Rules of Thumb for Assessing Equilibrium Partitioning of Organic Compounds: Successes and Pitfalls. *J. Chem. Educ.* **2003**, *80* (4), 450.
269. Atkins, P.; De Paula, J.; Keeler, J., *Atkins' Physical Chemistry*. 11th ed.; Oxford University Press: Oxford, United Kingdom, 2018.
270. Stüber, M.; Reemtsma, T. Evaluation of three calibration methods to compensate matrix effects in environmental analysis with LC-ESI-MS. *Anal. Bioanal. Chem.* **2004**, *378* (4), 910-916.
271. Kloepfer, A.; Quintana, J. B.; Reemtsma, T. Operational options to reduce matrix effects in liquid chromatography–electrospray ionisation-mass spectrometry analysis of aqueous environmental samples. *J. Chromatogr. A* **2005**, *1067* (1-2), 153-160.
272. Powley, C. R.; George, S. W.; Ryan, T. W.; Buck, R. C. Matrix effect-free analytical methods for determination of perfluorinated carboxylic acids in environmental matrixes. *Anal. Chem.* **2005**, *77* (19), 6353-6358.
273. Matuszewski, B. K.; Constanzer, M.; Chavez-Eng, C. Strategies for the assessment of matrix effect in quantitative bioanalytical methods based on HPLC–MS/MS. *Anal. Chem.* **2003**, *75* (13), 3019-3030.
274. Antignac, J.-P.; de Wasch, K.; Monteau, F.; De Brabander, H.; Andre, F.; Le Bizec, B. The ion suppression phenomenon in liquid chromatography–mass spectrometry and its consequences in the field of residue analysis. *Anal. Chim. Acta* **2005**, *529* (1-2), 129-136.

275. Panuwet, P.; Hunter Jr, R. E.; D'Souza, P. E.; Chen, X.; Radford, S. A.; Cohen, J. R.; Marder, M. E.; Kartavenka, K.; Ryan, P. B.; Barr, D. B. Biological matrix effects in quantitative tandem mass spectrometry-based analytical methods: advancing biomonitoring. *Crit. Rev. Anal. Chem.* **2016**, *46* (2), 93-105.
276. Mei, H.; Hsieh, Y.; Nardo, C.; Xu, X.; Wang, S.; Ng, K.; Korfmacher, W. A. Investigation of matrix effects in bioanalytical high-performance liquid chromatography/tandem mass spectrometric assays: application to drug discovery. *Rapid Commun. Mass Spectrom.* **2003**, *17* (1), 97-103.
277. Hajšlová, J.; Zrostlíková, J. Matrix effects in (ultra)trace analysis of pesticide residues in food and biotic matrices. *J. Chromatogr. A* **2003**, *1000* (1), 181-197.
278. Kwon, H.; Lehotay, S. J.; Geis-Asteggiant, L. Variability of matrix effects in liquid and gas chromatography–mass spectrometry analysis of pesticide residues after QuEChERS sample preparation of different food crops. *J. Chromatogr. A* **2012**, *1270*, 235-245.
279. Taylor, P. J. Matrix effects: the Achilles heel of quantitative high-performance liquid chromatography–electrospray–tandem mass spectrometry. *Clin. Biochem.* **2005**, *38* (4), 328-334.
280. Trufelli, H.; Palma, P.; Famiglioni, G.; Cappiello, A. An overview of matrix effects in liquid chromatography–mass spectrometry. *Mass Spectrom. Rev.* **2011**, *30* (3), 491-509.
281. Erney, D. R.; Gillespie, A. M.; Gilvydis, D. M.; Poole, C. F. Explanation of the matrix-induced chromatographic response enhancement of organophosphorus pesticides during open tubular column gas chromatography with splitless or hot on-column injection and flame photometric detection. *J. Chromatogr. A* **1993**, *638* (1), 57-63.
282. Aubry, A.-F. LC–MS/MS bioanalytical challenge: ultra-high sensitivity assays. *Bioanalysis* **2011**, *3* (16), 1819-1825.
283. Yang, A.; Ching, C.; Easler, M.; Helbling, D. E.; Dichtel, W. R. Cyclodextrin Polymers with Nitrogen-Containing Tripodal Crosslinkers for Efficient PFAS Adsorption. *ACS Mater. Lett.* **2020**, *2* (9), 1240-1245.
284. Xiao, L.; Ling, Y.; Alsbauer, A.; Li, C.; Helbling, D. E.; Dichtel, W. R. β -Cyclodextrin Polymer Network Sequesters Perfluorooctanoic Acid at Environmentally Relevant Concentrations. *Journal of the American Chemical Society* **2017**, *139* (23), 7689-7692.
285. Glöckler, D.; Wabnitz, C.; Elsner, M.; Bakkour, R. Avoiding Interferences in Advance: Cyclodextrin Polymers to Enhance Selectivity in Extraction of Organic Micropollutants for Carbon Isotope Analysis *Anal. Chem.* **2023**, *95* (20), 7839-7848.
286. Tfaily, M. M.; Hodgkins, S.; Podgorski, D. C.; Chanton, J. P.; Cooper, W. T. Comparison of dialysis and solid-phase extraction for isolation and concentration of dissolved organic matter prior to Fourier transform ion cyclotron resonance mass spectrometry. *Anal. Bioanal. Chem.* **2012**, *404* (2), 447-457.
287. Perminova, I. V.; Dubinenkov, I. V.; Kononikhin, A. S.; Konstantinov, A. I.; Zhrebker, A. Y.; Andzhushev, M. A.; Lebedev, V. A.; Bulygina, E.; Holmes, R. M.; Kostyukevich, Y. I.; Popov, I. A.; Nikolaev, E. N. Molecular Mapping of Sorbent Selectivities with Respect to Isolation of Arctic Dissolved Organic Matter as Measured by Fourier Transform Mass Spectrometry. *Environ. Sci. Technol.* **2014**, *48* (13), 7461-7468.
288. Li, H.; Minor, E. C. Dissolved organic matter in Lake Superior: insights into the effects of extraction methods on chemical composition. *Environ. Sci.: Process. Impacts* **2015**, *17* (10), 1829-1840.
289. Raeke, J.; Lechtenfeld, O. J.; Wagner, M.; Herzsprung, P.; Reemtsma, T. Selectivity of solid phase extraction of freshwater dissolved organic matter and its effect on ultrahigh resolution mass spectra. *Environ. Sci.: Process. Impacts* **2016**, *18* (7), 918-927.

290. Zhrebker, A. Y.; Perminova, I. V.; Konstantinov, A. I.; Volikov, A. B.; Kostyukevich, Y. I.; Kononikhin, A. S.; Nikolaev, E. N. Extraction of humic substances from fresh waters on solid-phase cartridges and their study by Fourier transform ion cyclotron resonance mass spectrometry. *J. Anal. Chem.* **2016**, *71* (4), 372-378.
291. Li, Y.; Harir, M.; Uhl, J.; Kanawati, B.; Lucio, M.; Smirnov, K. S.; Koch, B. P.; Schmitt-Kopplin, P.; Hertkorn, N. How representative are dissolved organic matter (DOM) extracts? A comprehensive study of sorbent selectivity for DOM isolation. *Water Res.* **2017**, *116*, 316-323.
292. Li, Y.; Harir, M.; Lucio, M.; Kanawati, B.; Smirnov, K.; Flerus, R.; Koch, B. P.; Schmitt-Kopplin, P.; Hertkorn, N. Proposed guidelines for solid phase extraction of Suwannee River dissolved organic matter. *Anal. Chem.* **2016**, *88* (13), 6680-6688.
293. Dittmar, T.; Koch, B.; Hertkorn, N.; Kattner, G. A simple and efficient method for the solid-phase extraction of dissolved organic matter (SPE-DOM) from seawater. *Limnol. Oceanogr.: Methods* **2008**, *6* (6), 230-235.
294. Hertkorn, N.; Frommberger, M.; Witt, M.; Koch, B. P.; Schmitt-Kopplin, P.; Perdue, E. M. Natural Organic Matter and the Event Horizon of Mass Spectrometry. *Anal. Chem.* **2008**, *80* (23), 8908-8919.
295. Tziotis, D.; Hertkorn, N.; Schmitt-Kopplin, P. Kendrick-Analogous Network Visualisation of Ion Cyclotron Resonance Fourier Transform Mass Spectra: Improved Options for the Assignment of Elemental Compositions and the Classification of Organic Molecular Complexity. *Eur. J. Mass Spectrom.* **2011**, *17* (4), 415-421.
296. Guigue, J.; Harir, M.; Mathieu, O.; Lucio, M.; Ranjard, L.; Lévêque, J.; Schmitt-Kopplin, P. Ultrahigh-resolution FT-ICR mass spectrometry for molecular characterisation of pressurised hot water-extractable organic matter in soils. *Biogeochemistry* **2016**, *128* (3), 307-326.
297. Kellerman, A. M.; Dittmar, T.; Kothawala, D. N.; Tranvik, L. J. Chemodiversity of dissolved organic matter in lakes driven by climate and hydrology. *Nat. Commun.* **2014**, *5* (1), 3804.
298. Kim, S.; Kaplan, L. A.; Hatcher, P. G. Biodegradable dissolved organic matter in a temperate and a tropical stream determined from ultra-high resolution mass spectrometry. *Limnol. Oceanogr.* **2006**, *51* (2), 1054-1063.
299. Ohno, T.; He, Z.; Sleighter, R. L.; Honeycutt, C. W.; Hatcher, P. G. Ultrahigh Resolution Mass Spectrometry and Indicator Species Analysis to Identify Marker Components of Soil- and Plant Biomass-Derived Organic Matter Fractions. *Environ. Sci. Technol.* **2010**, *44* (22), 8594-8600.
300. Perminova, I. V.; Shirshin, E. A.; Zhrebker, A.; Pipko, I. I.; Pugach, S. P.; Dudarev, O. V.; Nikolaev, E. N.; Grigoryev, A. S.; Shakhova, N.; Semiletov, I. P. Signatures of Molecular Unification and Progressive Oxidation Unfold in Dissolved Organic Matter of the Ob-Irtysh River System along Its Path to the Arctic Ocean. *Scientific Reports* **2019**, *9* (1), 19487.
301. Stenson, A. C.; Marshall, A. G.; Cooper, W. T. Exact masses and chemical formulas of individual Suwannee River fulvic acids from ultrahigh resolution electrospray ionization Fourier transform ion cyclotron resonance mass spectra. *Anal. Chem.* **2003**, *75* (6), 1275-1284.
302. Kamjunke, N.; Hertkorn, N.; Harir, M.; Schmitt-Kopplin, P.; Griebler, C.; Brauns, M.; von Tümpling, W.; Weitere, M.; Herzsprung, P. Molecular change of dissolved organic matter and patterns of bacterial activity in a stream along a land-use gradient. *Water Res.* **2019**, *164*, 114919.
303. Leenheer, J. A.; Wershaw, R. L.; Reddy, M. M. Strong-Acid, Carboxyl-Group Structures in Fulvic Acid from the Suwannee River, Georgia. 2. Major Structures. *Environ. Sci. Technol.* **1995**, *29* (2), 399-405.

304. Han, H.; Feng, Y.; Chen, J.; Xie, Q.; Chen, S.; Sheng, M.; Zhong, S.; Wei, W.; Su, S.; Fu, P. Acidification impacts on the molecular composition of dissolved organic matter revealed by FT-ICR MS. *Sci. Total Environ.* **2022**, *805*, 150284.
305. Zhrebker, A.; Shirshin, E.; Rubekina, A.; Kharybin, O.; Kononikhin, A.; Kulikova, N. A.; Zaitsev, K. V.; Roznyatovsky, V. A.; Grishin, Y. K.; Perminova, I. V.; Nikolaev, E. N. Optical Properties of Soil Dissolved Organic Matter Are Related to Acidic Functions of Its Components as Revealed by Fractionation, Selective Deuteromethylation, and Ultrahigh Resolution Mass Spectrometry. *Environ. Sci. Technol.* **2020**, *54* (5), 2667-2677.
306. Zhrebker, A.; Shirshin, E.; Kharybin, O.; Kostyukevich, Y.; Kononikhin, A.; Konstantinov, A. I.; Volkov, D.; Roznyatovsky, V. A.; Grishin, Y. K.; Perminova, I. V.; Nikolaev, E. Separation of Benzoic and Unconjugated Acidic Components of Leonardite Humic Material Using Sequential Solid-Phase Extraction at Different pH Values as Revealed by Fourier Transform Ion Cyclotron Resonance Mass Spectrometry and Correlation Nuclear Magnetic Resonance Spectroscopy. *J. Agric. Food. Chem.* **2018**, *66* (46), 12179-12187.
307. Zhrebker, A.; Kostyukevich, Y.; Kononikhin, A.; Kharybin, O.; Konstantinov, A. I.; Zaitsev, K. V.; Nikolaev, E.; Perminova, I. V. Enumeration of carboxyl groups carried on individual components of humic systems using deuteromethylation and Fourier transform mass spectrometry. *Anal. Bioanal. Chem.* **2017**, *409* (9), 2477-2488.
308. Hockaday, W. C.; Grannas, A. M.; Kim, S.; Hatcher, P. G. The transformation and mobility of charcoal in a fire-impacted watershed. *Geochim. Cosmochim. Acta* **2007**, *71* (14), 3432-3445.
309. Chen, M.; Kim, S.; Park, J.-E.; Kim, H. S.; Hur, J. Effects of dissolved organic matter (DOM) sources and nature of solid extraction sorbent on recoverable DOM composition: Implication into potential lability of different compound groups. *Anal. Bioanal. Chem.* **2016**, *408* (17), 4809-4819.
310. Masqué, N.; Galià, M.; M. Marcé, R.; Borrull, F. Solid-phase Extraction of Phenols and Pesticides in Water With a Modified Polymeric Resin. *Analyst* **1997**, *122* (5), 425-428.
311. Wagner, S.; Dittmar, T.; Jaffé, R. Molecular characterization of dissolved black nitrogen via electrospray ionization Fourier transform ion cyclotron resonance mass spectrometry. *Org. Geochem.* **2015**, *79*, 21-30.
312. Chambers, E.; Wagrowski-Diehl, D. M.; Lu, Z.; Mazzeo, J. R. Systematic and comprehensive strategy for reducing matrix effects in LC/MS/MS analyses. *J. Chromatogr. B* **2007**, *852* (1-2), 22-34.
313. Richardson, S. D.; Ternes, T. A. Water Analysis: Emerging Contaminants and Current Issues. *Anal. Chem.* **2022**, *94* (1), 382-416.
314. Liu, Q.; Zhou, Y.; Lu, J.; Zhou, Y. Novel cyclodextrin-based adsorbents for removing pollutants from wastewater: A critical review. *Chemosphere* **2020**, *241*, 125043.
315. Tian, B.; Hua, S.; Tian, Y.; Liu, J. Cyclodextrin-based adsorbents for the removal of pollutants from wastewater: a review. *Environ. Sci. Pollut. Res.* **2021**, *28* (2), 1317-1340.
316. Jimmy, C. Y.; Jiang, Z.-T.; Liu, H.-Y.; Yu, J.; Zhang, L. β -Cyclodextrin epichlorohydrin copolymer as a solid-phase extraction adsorbent for aromatic compounds in water samples. *Anal. Chim. Acta* **2003**, *477* (1), 93-101.
317. Nojavan, S.; Yazdanpanah, M. Micro-solid phase extraction of benzene, toluene, ethylbenzene and xylenes from aqueous solutions using water-insoluble β -cyclodextrin polymer as sorbent. *J. Chromatogr. A* **2017**, *1525*, 51-59.
318. Zhang, J.; Liu, D.; Shi, Y.; Sun, C.; Niu, M.; Wang, R.; Hu, F.; Xiao, D.; He, H. Determination of quinolones in wastewater by porous β -cyclodextrin polymer based solid-phase extraction coupled with HPLC. *J. Chromatogr. B* **2017**, *1068-1069*, 24-32.

319. Moon, J.-Y.; Jung, H.-J.; Moon, M. H.; Chung, B. C.; Choi, M. H. Inclusion complex-based solid-phase extraction of steroidal compounds with entrapped β -cyclodextrin polymer. *Steroids* **2008**, *73* (11), 1090-1097.
320. Glöckler, D.; Harir, M.; Schmitt-Kopplin, P.; Elsner, M.; Bakkour, R. Selectivity of β -Cyclodextrin Polymer toward Aquatic Contaminants: Insights from Ultrahigh-Resolution Mass Spectrometry of Dissolved Organic Matter. *Anal. Chem.* **2023**, *95* (42), 15505-15513.
321. García-Zubiri, I. X.; González-Gaitano, G.; Isasi, J. R. Sorption models in cyclodextrin polymers: Langmuir, Freundlich, and a dual-mode approach. *J. Colloid Interface Sci.* **2009**, *337* (1), 11-18.
322. Romo, A.; Penas, F. J.; Isasi, J. R.; Garcia-Zubiri, I. X.; González-Gaitano, G. Extraction of phenols from aqueous solutions by β -cyclodextrin polymers. Comparison of sorptive capacities with other sorbents. *React. Funct. Polym.* **2008**, *68* (1), 406-413.
323. Xu, H.; Guo, L. Molecular size-dependent abundance and composition of dissolved organic matter in river, lake and sea waters. *Water Res.* **2017**, *117*, 115-126.
324. Assemi, S.; Newcombe, G.; Hepplewhite, C.; Beckett, R. Characterization of natural organic matter fractions separated by ultrafiltration using flow field-flow fractionation. *Water Res.* **2004**, *38* (6), 1467-1476.
325. Linden, L.; Goss, K.-U.; Endo, S. Exploring 3D structural influences of aliphatic and aromatic chemicals on α -cyclodextrin binding. *J. Colloid Interface Sci.* **2016**, *468*, 42-50.
326. Champagne, P. A.; Desroches, J.; Paquin, J.-F. Organic fluorine as a hydrogen-bond acceptor: recent examples and applications. *Synthesis* **2015**, *47* (03), 306-322.
327. Howard, J. A.; Hoy, V. J.; O'Hagan, D.; Smith, G. T. How good is fluorine as a hydrogen bond acceptor? *Tetrahedron* **1996**, *52* (38), 12613-12622.
328. Laurence, C.; Brameld, K. A.; Graton, J.; Le Questel, J.-Y.; Renault, E. The pKBHX Database: Toward a Better Understanding of Hydrogen-Bond Basicity for Medicinal Chemists. *J. Med. Chem.* **2009**, *52* (14), 4073-4086.
329. Abe, T.; Watanabe, A. X-ray photoelectron spectroscopy of nitrogen functional groups in soil humic acids. *Soil Sci.* **2004**, *169* (1), 35-43.
330. Thorn, K. A.; Cox, L. G. N-15 NMR spectra of naturally abundant nitrogen in soil and aquatic natural organic matter samples of the International Humic Substances Society. *Org. Geochem.* **2009**, *40* (4), 484-499.
331. Vairavamurthy, A.; Wang, S. Organic Nitrogen in Geomacromolecules: Insights on Speciation and Transformation with K-edge XANES Spectroscopy. *Environ. Sci. Technol.* **2002**, *36* (14), 3050-3056.
332. Kunze, A.; Pei, L.; Elsässer, D.; Niessner, R.; Seidel, M. High performance concentration method for viruses in drinking water. *J. Virol. Methods* **2015**, *222*, 132-137.
333. Pei, L.; Rieger, M.; Lengger, S.; Ott, S.; Zawadsky, C.; Hartmann, N. M.; Selinka, H.-C.; Tiehm, A.; Niessner, R.; Seidel, M. Combination of Crossflow Ultrafiltration, Monolithic Affinity Filtration, and Quantitative Reverse Transcriptase PCR for Rapid Concentration and Quantification of Model Viruses in Water. *Environ. Sci. Technol.* **2012**, *46* (18), 10073-10080.
334. Ott, S.; Niessner, R.; Seidel, M. Preparation of epoxy-based macroporous monolithic columns for the fast and efficient immunofiltration of *Staphylococcus aureus*. *J. Sep. Sci.* **2011**, *34* (16-17), 2181-92.
335. Wunderlich, A.; Torggler, C.; Elsässer, D.; Lück, C.; Niessner, R.; Seidel, M. Rapid quantification method for *Legionella pneumophila* in surface water. *Anal. Bioanal. Chem.* **2016**, *408* (9), 2203-2213.
336. Peskoller, C.; Niessner, R.; Seidel, M. Development of an epoxy-based monolith used for the affinity capturing of *Escherichia coli* bacteria. *J. Chromatogr. A* **2009**, *1216* (18), 3794-3801.

337. Elsäßer, D.; Ho, J.; Niessner, R.; Tiehm, A.; Seidel, M. Heterogeneous asymmetric recombinase polymerase amplification (haRPA) for rapid hygiene control of large-volume water samples. *Anal. Biochem.* **2018**, *546*, 58-64.
338. Fernández-Merino, M. J.; Guardia, L.; Paredes, J. I.; Villar-Rodil, S.; Solís-Fernández, P.; Martínez-Alonso, A.; Tascón, J. M. D. Vitamin C Is an Ideal Substitute for Hydrazine in the Reduction of Graphene Oxide Suspensions. *J. Phys. Chem. C*. **2010**, *114* (14), 6426-6432.
339. Göpfert, L.; Klüpfel, J.; Heinritz, C.; Elsner, M.; Seidel, M. Macroporous epoxy-based monoliths for rapid quantification of *Pseudomonas aeruginosa* by adsorption elution method optimized for qPCR. *Anal. Bioanal. Chem.* **2020**, *412* (29), 8185-8195.
340. Lagergren, S. Zur Theorie der sogenannten Adsorption gelöster Stoffe. *Kungl. Svenska Vetenskapsakad. Handl.* **1898**, *24* (4), 1-39.
341. Ho, Y.-S.; McKay, G. Pseudo-second order model for sorption processes. *Process Biochem.* **1999**, *34* (5), 451-465.
342. Shi, X.; Cheng, C.; Peng, F.; Hou, W.; Lin, X.; Wang, X. Adsorption properties of graphene materials for pesticides: Structure effect. *J. Mol. Liq.* **2022**, *364*, 119967.
343. Rahman, A. J.; Ojha, H.; Pandey, A.; Kumar, S.; Singhal, R.; Datta, A.; Singh, B. K. Kinetic, isotherm and thermodynamic adsorption studies of organophosphorus compound (phosmet) on reduced graphene oxide. *Diamond Relat. Mater.* **2022**, *127*, 109191.
344. Whitby, R. L. Chemical control of graphene architecture: tailoring shape and properties. *ACS Nano* **2014**, *8* (10), 9733-9754.
345. Marcano, D. C.; Kosynkin, D. V.; Berlin, J. M.; Sinitskii, A.; Sun, Z.; Slesarev, A.; Alemany, L. B.; Lu, W.; Tour, J. M. Improved synthesis of graphene oxide. *ACS Nano* **2010**, *4* (8), 4806-14.
346. Yan, F.; Kumar, S.; Spyrou, K.; Syari'ati, A.; De Luca, O.; Thomou, E.; Alfonsín, E. M.; Gournis, D.; Rudolf, P. Highly Efficient Remediation of Chloridazon and Its Metabolites: The Case of Graphene Oxide Nanoplatelets. *ACS ES&T Water* **2021**, *1* (1), 157-166.
347. Stankovich, S.; Dikin, D. A.; Piner, R. D.; Kohlhaas, K. A.; Kleinhammes, A.; Jia, Y.; Wu, Y.; Nguyen, S. T.; Ruoff, R. S. Synthesis of graphene-based nanosheets via chemical reduction of exfoliated graphite oxide. *Carbon* **2007**, *45* (7), 1558-1565.
348. Zhang, J.; Yang, H.; Shen, G.; Cheng, P.; Zhang, J.; Guo, S. Reduction of graphene oxide via L-ascorbic acid. *Chem. Commun.* **2010**, *46* (7), 1112-1114.
349. Rout, D. R.; Jena, H. M. Removal of phenol from aqueous solution using reduced graphene oxide as adsorbent: isotherm, kinetic, and thermodynamic studies. *Environ. Sci. Pollut. Res.* **2022**, *29* (21), 32105-32119.
350. Sharma, P.; Hussain, N.; Borah, D. J.; Das, M. R. Kinetics and adsorption behavior of the methyl blue at the graphene oxide/reduced graphene oxide nanosheet-water interface: a comparative study. *J. Chem. Eng. Data* **2013**, *58* (12), 3477-3488.
351. Zhang, Y.; Tang, Y.; Li, S.; Yu, S. Sorption and removal of tetrabromobisphenol A from solution by graphene oxide. *Chem. Eng. J.* **2013**, *222*, 94-100.
352. Li, L.; Xu, D.; Pei, Z. Kinetics and thermodynamics studies for bisphenol S adsorption on reduced graphene oxide. *RSC Adv.* **2016**, *6* (65), 60145-60151.
353. Hashemi, B.; Zohrabi, P.; Raza, N.; Kim, K.-H. Metal-organic frameworks as advanced sorbents for the extraction and determination of pollutants from environmental, biological, and food media. *TrAC, Trends Anal. Chem.* **2017**, *97*, 65-82.
354. Wang, R.; Lin, Z.-W.; Klemes, M. J.; Ateia, M.; Trang, B.; Wang, J.; Ching, C.; Helbling, D. E.; Dichtel, W. R. A Tunable Porous β -Cyclodextrin Polymer Platform to Understand and Improve Anionic PFAS Removal. *ACS Cent. Sci.* **2022**, *8* (5), 663-669.

355. Qian, H.-L.; Yang, C.-X.; Wang, W.-L.; Yang, C.; Yan, X.-P. Advances in covalent organic frameworks in separation science. *J. Chromatogr. A* **2018**, *1542*, 1-18.
356. Meyer, A. H.; Dybala-Defratyka, A.; Alaimo, P. J.; Geronimo, I.; Sanchez, A. D.; Cramer, C. J.; Elsner, M. Cytochrome P450-catalyzed dealkylation of atrazine by *Rhodococcus* sp. strain NI86/21 involves hydrogen atom transfer rather than single electron transfer. *Dalton Trans.* **2014**, *43* (32), 12175-12186.
357. Penning, H.; Sørensen, S. R.; Meyer, A. H.; Aamand, J.; Elsner, M. C, N, and H Isotope Fractionation of the Herbicide Isoproturon Reflects Different Microbial Transformation Pathways. *Environ. Sci. Technol.* **2010**, *44* (7), 2372-2378.
358. Reinnicke, S.; Bernstein, A.; Elsner, M. Small and Reproducible Isotope Effects during Methylation with Trimethylsulfonium Hydroxide (TMSH): A Convenient Derivatization Method for Isotope Analysis of Negatively Charged Molecules. *Anal. Chem.* **2010**, *82* (5), 2013-2019.
359. Qiu, S.; Gözdereliler, E.; Weyrauch, P.; Lopez, E. C. M.; Kohler, H.-P. E.; Sørensen, S. R.; Meckenstock, R. U.; Elsner, M. Small $^{13}\text{C}/^{12}\text{C}$ Fractionation Contrasts with Large Enantiomer Fractionation in Aerobic Biodegradation of Phenoxy Acids. *Environ. Sci. Technol.* **2014**, *48* (10), 5501-5511.
360. Maier, M. P.; Qiu, S.; Elsner, M. Enantioselective stable isotope analysis (ESIA) of polar herbicides. *Anal. Bioanal. Chem.* **2013**, *405* (9), 2825-2831.
361. Reinnicke, S.; Juchelka, D.; Steinbeiss, S.; Meyer, A.; Hilker, A.; Elsner, M. Gas chromatography/isotope ratio mass spectrometry of recalcitrant target compounds: performance of different combustion reactors and strategies for standardization. *Rapid Commun. Mass Spectrom.* **2012**, *26* (9), 1053-1060.
362. Reinnicke, S.; Simonsen, A.; Sørensen, S. R.; Aamand, J.; Elsner, M. C and N Isotope Fractionation during Biodegradation of the Pesticide Metabolite 2,6-Dichlorobenzamide (BAM): Potential for Environmental Assessments. *Environ. Sci. Technol.* **2012**, *46* (3), 1447-1454.
363. Maier, M. P.; De Corte, S.; Nitsche, S.; Spaett, T.; Boon, N.; Elsner, M. C & N Isotope Analysis of Diclofenac to Distinguish Oxidative and Reductive Transformation and to Track Commercial Products. *Environ. Sci. Technol.* **2014**, *48* (4), 2312-2320.
364. Birkigt, J.; Gilevska, T.; Ricken, B.; Richnow, H.-H.; Vione, D.; Corvini, P. F.-X.; Nijenhuis, I.; Cichocka, D. Carbon stable isotope fractionation of sulfamethoxazole during biodegradation by *Microbacterium* sp. strain BR1 and upon direct photolysis. *Environ. Sci. Technol.* **2015**, *49* (10), 6029-6036.
365. Willach, S.; Lutze, H. V.; Eckey, K.; Loeppenber, K.; Lüling, M.; Terhalle, J.; Wolbert, J.-B.; Jochmann, M. A.; Karst, U.; Schmidt, T. C. Degradation of sulfamethoxazole using ozone and chlorine dioxide-Compound-specific stable isotope analysis, transformation product analysis and mechanistic aspects. *Water Res.* **2017**, *122*, 280-289.
366. Willach, S.; Lutze, H. V.; Eckey, K.; Löppenber, K.; Lüling, M.; Wolbert, J.-B.; Kujawinski, D. M.; Jochmann, M. A.; Karst, U.; Schmidt, T. C. Direct Photolysis of Sulfamethoxazole Using Various Irradiation Sources and Wavelength Ranges: Insights from Degradation Product Analysis and Compound-Specific Stable Isotope Analysis. *Environ. Sci. Technol.* **2018**, *52* (3), 1225-1233.
367. Spahr, S.; Huntscha, S.; Bolotin, J.; Maier, M. P.; Elsner, M.; Hollender, J.; Hofstetter, T. B. Compound-specific isotope analysis of benzotriazole and its derivatives. *Anal. Bioanal. Chem.* **2013**, *405* (9), 2843-2856.
368. Peng, X.; Li, X. Compound-specific isotope analysis for aerobic biodegradation of phthalate acid esters. *Talanta* **2012**, *97*, 445-449.

369. Royal Society of Chemistry, *ChemSpider Chemical Structure Database*. <https://www.chemspider.com> (accessed May 1, 2023).
370. Suchana, S.; Gavazza, S.; Melo, N.; Edwards, E.; Lomheim, L.; Mack, E. E.; Passeport, E. Polar organic chemical integrative sampler (POCIS) allows compound specific isotope analysis of substituted chlorobenzenes at trace levels. **2022**.
371. Neubauer, C.; Kantnerová, K.; Lamothe, A.; Savarino, J.; Hilker, A.; Juchelka, D.; Hinrichs, K.-U.; Elvert, M.; Heuer, V.; Elsner, M.; Bakkour, R.; Julien, M.; Öztoprak, M.; Schouten, S.; Hattori, S.; Dittmar, T. Discovering Nature's Fingerprints: Isotope Ratio Analysis on Bioanalytical Mass Spectrometers. *J. Am. Soc. Mass. Spectrom.* **2023**, *34* (4), 525-537.
372. European Commission EU Pesticides Database (v2.2). https://ec.europa.eu/food/plants/pesticides/eu-pesticides-database_en (accessed Date Accessed).
373. Abraham, M. H.; McGowan, J. The use of characteristic volumes to measure cavity terms in reversed phase liquid chromatography. *Chromatographia* **1987**, *23* (4), 243-246.
374. Neale, P. A.; Escher, B. I.; Goss, K.-U.; Endo, S. Evaluating dissolved organic carbon-water partitioning using polyparameter linear free energy relationships: Implications for the fate of disinfection by-products. *Water Res.* **2012**, *46* (11), 3637-3645.
375. International Council for Harmonisation of Technical Requirements for Pharmaceuticals for Human Use (ICH), *ICH Harmonized Tripartite Guidelines. Validation of Analytical Procedures: Text and Methodology Q2 (R1)*. International Conference on Harmonization: Geneva, Switzerland, 2005.
376. Meyers, P. A. Preservation of elemental and isotopic source identification of sedimentary organic matter. *Chem. Geol.* **1994**, *114* (3), 289-302.
377. Meyers, P. A. Organic geochemical proxies of paleoceanographic, paleolimnologic, and paleoclimatic processes. *Org. Geochem.* **1997**, *27* (5), 213-250.
378. Koch, B. P.; Witt, M.; Engbrodt, R.; Dittmar, T.; Kattner, G. Molecular formulae of marine and terrigenous dissolved organic matter detected by electrospray ionization Fourier transform ion cyclotron resonance mass spectrometry. *Geochim. Cosmochim. Acta* **2005**, *69* (13), 3299-3308.
379. Kögel-Knabner, I. The macromolecular organic composition of plant and microbial residues as inputs to soil organic matter. *Soil Biol. Biochem.* **2002**, *34* (2), 139-162.

Appendices

S1 Occurrence of Organic Micropollutants in Aquatic Systems: A Case Study from Southern Germany

S1.1 Scope of the Case Study

This case study was conducted within the framework of the Collaborative Research Center CAMPOS, funded by the German Research Foundation (DFG, Grant Agreement SFB 1253/1 2017). CAMPOS focused on pollution research at the catchment scale of the River Ammer near Tübingen, Germany. Specifically, it aimed at (i) identifying landscape elements controlling storage, biogeochemical transformation, or elimination of pollutants; (ii) identifying relevant processes for pollutant transformation in different environmental compartments and their dynamics; and (iii) developing a new modeling framework to simulate and predict reactive transport and pollutant behavior on the landscape scale. The study was part of project P2 *Sub-catchments* and had the goal to measure the chemical fingerprint (i.e., the occurrence and concentration of micropollutants) at different locations along the sub-catchment of the creek Schönbrunnen (including surface and groundwater). The obtained information on the chemical inventory in water fed into the identification of target compounds for further assessment of putative reactive environmental compartments. Experimental details are described in the following sections and results of the target screening are illustrated in Figure 1.1 in the introductory Chapter 1.1 of this thesis.

S1.2 Water Sampling

Water sampling took place in May and November 2018. Surface water (SW) samples were taken at three locations in the creek Schönbrunnen, while six groundwater (GW) samples were taken using peristaltic pumps from groundwater monitoring wells located in the vicinity of the creek (Figure 1.1). The volume in the standpipe of the wells was exchanged twice before the pristine GW was collected. All samples were filled into glass bottles previously rinsed with methanol, ultrapure water, and the water sample. After refrigerated transport to the laboratory, water samples were immediately passed through pre-washed 0.45 μm nylon membrane filters (GVS Filter Technology, Bologna, Italy). Before being extracted the next day, they were stored overnight at 4 °C in the dark.

S1.3 Solid-Phase Extraction

Target analytes were enriched by means of solid phase extraction (SPE) using a 12-port vacuum SPE manifold (Supelco, Bellefonte, USA) and 500 mg Oasis HLB sorbent packed in 6 mL polypropylene cartridges (Waters, Milford, USA). Prior to loading, SPE cartridges were conditioned with 10 mL of methanol, 10 mL of ethyl acetate, and 10 mL of ultrapure water (Merck Millipore, Burlington, USA). Then, 1000 mL of filtered (0.7 μm , GF/F 47 mm, Whatman, Maidstone, UK) water were percolated through the cartridges at a volumetric flow rate of $\leq 4.0 \text{ mL min}^{-1}$, corresponding to linear flow velocity of

$\leq 3.2 \text{ cm min}^{-1}$. Once loaded, the sorbents were dried under vacuum for 45 min and subsequently eluted with 2 x 2.5 mL of methanol and 2 x 2.5 mL of ethyl acetate. The eluates were combined and filtered using a 0.2 μm polyethersulfone membranes (PES, Captiva Premium Syringe Filter, Agilent, Santa Clara, USA). Eluates were then carefully evaporated to dryness using a gentle stream of N_2 and a temperature of 40 $^\circ\text{C}$ (Vapotherm Basis Mobil II, Barkey, Leopoldshöhe, Germany). Finally, the dry residues were reconstituted in 1 mL of methanol (enrichment factor 1000) by ultra-sonication for 10 min and vortex mixing for 1 min. Exact reconstituted volumes were gravimetrically determined. All sample extracts were tightly sealed and stored at -20 $^\circ\text{C}$ until further analysis. To account for background interferences induced by the extraction process, a blank sample was prepared in the same manner by extracting 1000 mL of ultrapure water.

S1.4 Liquid Chromatography – Tandem Mass Spectrometry

The water samples were screened for 76 environmental relevant analytes using liquid chromatography (1260 Infinity LC System, Agilent, Santa Clara, USA) coupled to high resolution mass spectrometry (6490 iFunnel triple quadrupole mass spectrometer, Agilent, Santa Clara, USA). A sample volume of 2 μL was injected into the system while the flow rate was kept constant at 0.4 mL min^{-1} . Analyte separation was achieved by a reversed-phase C18 column (Poroshell 120 EC-C18, 2.7 μm particle size, 2.1 x 100 mm, Agilent, Santa Clara, USA) at 40 $^\circ\text{C}$ and using a gradient program with ultrapure water (eluent A) and acetonitrile (eluent B) both containing 0.1 % acetic acid (negative ESI) or 0.1 % formic acid (positive ESI). Fraction of B was linearly increased from 2 % to 100 % within the first 17 min and kept constant for 6 min, followed by re-equilibration to initial conditions for 7 min. Analytes were ionized by means of electrospray ionization (ESI) in both positive and negative mode (12 L min^{-1} N_2 sheath gas at 400 $^\circ\text{C}$, 16 L min^{-1} N_2 drying gas at 150 $^\circ\text{C}$, 40 psi nebulizer pressure, 4.2 kV (ESI+, ESI-) capillary potential, and 1000 V (ESI+) and 1500 V (ESI-) nozzle potential, respectively). MS/MS experiments were performed in Dynamic Multi Reaction Monitoring (DMRM), where analyte specific mass transitions were defined for respective collision energies using N_2 as collision gas. Quantification was performed based on internal calibration.

S2 Supporting Information to Chapter 2

S2.1 Chemicals

All chemicals used in this work are summarized in Table S2.1.

Table S2.1. List of reagents, solvents, and analytical standards.

Chemical	CAS number	Purity/Grade (further info.)	Supplier
<i>Reagents</i>			
calcium chloride	7440-70-2	anhydrous, Redri-Dri, ≥ 97.0 %	Sigma-Aldrich
humic acid	1415-93-6	Technical	Sigma-Aldrich
hydrochloric acid	7647-01-0	ACS reagent, 37 %	Sigma-Aldrich
potassium carbonate	584-08-7	BioXtra, ≥ 99.0 %	Sigma-Aldrich
potassium hydrogen phthalate	877-24-7	BioXtra, ≥ 99.95 %	Sigma-Aldrich
sodium hydroxide	1310-73-2	BioXtra, ≥ 98 %	Sigma-Aldrich
tetrafluoroterephthalonitrile	1835-49-0	99 %	Sigma-Aldrich
thiourea	64-65-6	ReagentPlus, ≥ 99.0 %	Sigma-Aldrich
α -cyclodextrin	10016-20-3	≥ 98.0 %	Sigma-Aldrich
β -cyclodextrin	7585-39-9	≥ 97.0 %	Sigma-Aldrich
γ -cyclodextrin	17465-86-0	≥ 98.0 %	Sigma-Aldrich
<i>Solvents</i>			
acetonitrile	75-05-8	HPLC Plus, ≥ 99.9 %	Sigma-Aldrich
dichloromethane	75-09-2	EMSURE®, for analysis	Sigma-Aldrich
ethanol	64-17-5	absolute, for HPLC, ≥ 99.8 %	Sigma-Aldrich
methanol	67-56-1	≥ 99.9 %	Sigma-Aldrich
<i>N,N</i> -dimethylformamide	68-12-2	anhydrous, 99.8 %	Sigma-Aldrich
tetrahydrofuran	109-99-9	anhydrous, ≥ 99.9 %, inhibitor-free	Sigma-Aldrich
<i>Analytical Standards</i>			
2,6-dichlorobenzamide (BAM)	2008-58-4	PESTANAL®, analytical standard	Sigma-Aldrich
atrazine	1912-24-9	PESTANAL®, analytical standard	Sigma-Aldrich
azoxystrobin	131860-33-8	PESTANAL®, analytical standard	Sigma-Aldrich
azoxystrobin-d4	n.a.	PESTANAL®, analytical standard	Sigma-Aldrich
boscalid	188425-85-6	PESTANAL®, analytical standard	Sigma-Aldrich
dimethomorph	110488-70-5	PESTANAL®, analytical standard	Sigma-Aldrich
dimethomorph-d6	n.a.	PESTANAL®, analytical standard	Sigma-Aldrich
metamitron	41394-05-2	PESTANAL®, analytical standard	Sigma-Aldrich
methiocarb	2032-65-7	PESTANAL®, analytical standard	Sigma-Aldrich
methiocarb-d3	n.a.	PESTANAL®, analytical standard	Sigma-Aldrich
propiconazole	60207-90-1	PESTANAL®, analytical standard	Sigma-Aldrich
propiconazole-d3	n.a.	PESTANAL®, analytical standard	Sigma-Aldrich
<i>S</i> -metolachlor	87392-12-9	PESTANAL®, analytical standard	Sigma-Aldrich
terbuthylazine	5915-41-3	PESTANAL®, analytical standard	Sigma-Aldrich
terbuthylazine-d5	n.a.	PESTANAL®, analytical standard	Sigma-Aldrich
thiacloprid	111988-49-9	PESTANAL®, analytical standard	Sigma-Aldrich
thiacloprid-d4	n.a.	PESTANAL®, analytical standard	Sigma-Aldrich

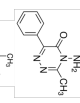
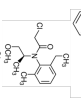
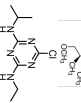
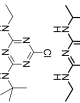
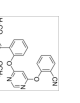
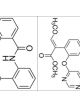
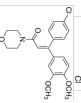
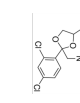
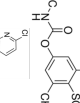
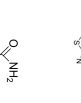
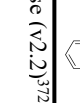
S2.2 Standard Solutions and Ultrapure Water

For sorption studies, we selected 11 model target compounds, which are covering a range of physicochemical properties, including four herbicides (i.e., atrazine, metolachlor, *S*-metolachlor and terbuthylazine), four fungicides (i.e., azoxystrobin, boscalid, dimethomorph and propiconazole), two insecticides (i.e., methiocarb and thiacloprid), as well as the metabolite 2,6-dichlorobenzamide (BAM). Detailed information about the selected compounds is given in Table S2.2. Stock solutions of analytical and isotopically labeled standards (1 g L^{-1}) were prepared in pure methanol and processed further to appropriate working solutions. Methanolic standards were stored at $-20 \text{ }^{\circ}\text{C}$ in the dark. A stock solution of Aldrich humic acid was prepared by dissolving 10 g of the dry powder in ultrapure water at pH 10 for 3 h using a magnetic stirring system. The solution was subsequently filtered ($0.45 \text{ }\mu\text{m}$), manually adjusted to pH 7, and stored at $4 \text{ }^{\circ}\text{C}$ in the dark. Ultrapure water ($18.2 \text{ M}\Omega \text{ cm}$ at $25 \text{ }^{\circ}\text{C}$) was produced with a Milli-Q® Reference water purification system (Merck Millipore, USA).

S2.3 Sorbents and Packing Materials

Oasis HLB sorbent was purchased from Waters (Milford, MA, USA), LiChrolut EN from Merck Millipore (Burlington, MA, USA) and Supel-Select HLB, as well as empty polypropylene SPE cartridges (1, 3, 6 mL) and polyethylene frits ($20 \text{ }\mu\text{m}$ pore size) from Sigma-Aldrich (Taufkirchen, Germany). Properties of the tested commercial sorbents are listed in Table S2.3. Stainless steel columns and accessories for column packing (Table S2.4) were obtained from Bischoff Chromatography (Leonberg, Germany).

Table S2.2. Physicochemical properties, CAS number, formula, structure, and classification of the selected target analytes.

Name	Formula	Structure	Classification	Molecular Weight [g mol ⁻¹]	McGowan Volume* [cm ³ mol ⁻¹ 100 ⁻¹]	log K _{ow} [-]	pK _a [-]	Charge pH 3 [-]	Percentage Neutral (pH3) [%]	Charge pH 7 [-]
<i>Herbicides</i>										
metamiton	C ₁₀ H ₁₀ N ₄ O		triazinone	202.213	1.5003	0.85	-	n	100	n
S-metolachlor	C ₁₅ H ₂₂ ClN ₂ O ₂		chloroacetanilide	283.793	2.2811	3.05	-	n	100	n
atrazine	C ₈ H ₁₄ ClN ₅		triazine	215.683	1.6196	2.70	1.70 (weak base)	n/+	95.2	n
terbutylazine	C ₉ H ₁₆ ClN ₅		triazine	229.710	1.7605	3.40	1.90 (weak base)	n/+	92.6	n
<i>Fungicides</i>										
azoxystrobin	C ₂₂ H ₁₇ N ₃ O ₅		strobilurin	403.394	2.9165	2.50	-	n	100	n
boscalid	C ₁₈ H ₁₂ Cl ₂ N ₂ O		carboxamide	343.207	2.3921	2.96	-	n	100	n
dimethomorph	C ₂₁ H ₂₂ ClN ₄ O ₄		morpholine	387.857	2.8547	2.68	-	n	100	n
propiconazole	C ₁₅ H ₁₇ Cl ₂ N ₃ O ₂		triazole	342.220	2.3429	3.72	1.09 (weak base)	n/+	98.8	n
<i>Insecticides</i>										
methiocarb	C ₁₁ H ₁₅ NO ₂ S		carbamate	225.307	1.7586	3.18	-	n	100	n
thiacloprid	C ₁₀ H ₉ ClN ₄ S		neonicotinoid	252.723	1.7275	1.26	-	n	100	n
<i>Metabolite</i>										
2,6-dichloro-benzamide (BAM)	C ₇ H ₅ Cl ₂ NO		metabolite of dichlobenil	190.027	1.2176	0.77	-	n	100	n

Data was adopted from the EU Pesticides Database (v2.2)³⁷², except for the McGowan volume which was calculated based on the analyte structure (*³⁷³)

Table S2.3. Suppliers and properties of commercial solid-phase extraction (SPE) sorbents under investigation. Data was provided by manufacturer's specifications.

sorbent	supplier	polymer type	particle size [μm]	pore size [\AA]	pore volume [mL g^{-1}]	surface area [$\text{m}^2 \text{g}^{-1}$]
Oasis HLB	Waters	N-vinylpyrrolidone-divinylbenzene	60	80	1.3	830
LiChrolut EN	Merck	ethylvinylbenzene-divinylbenzene	40 - 120	n.a.	0.75	1200
Supel-Select HLB	Supelco	hydrophilic modified styrene resin	55 - 60	87	0.88	400 - 410

Table S2.4. List of materials used for packing silicon carbide supported sorbents into empty HPLC columns.

No.*	Description	Part Number [†]
1	column nut M8	1208 0000
2	connecting nut	0208 7500
3	threaded column tube M8, stainless steel, 14x2.0 mm	0102 0000
4	fitting adapter	1216 0000
5	ZDV connector [‡]	5506 1001
6	column end plug	1205 0020
7	PTFE seal, 5.6 mm diameter	1255 0100
8	glass fiber filter	1257 0250
9	stainless steel mesh, 5 μm	1254 0100

* Numbers 1 – 9 refer to column part labels in Figure S2.10; [†] refers to order lists of the vendor Bischoff Chromatography (Leonberg, Germany); [‡] custom-drilled at the center to an inner diameter of 2.0 mm.

S2.4 Preparation and Characterization of Porous Cyclodextrin Polymers

S2.4.1 Synthesis of Porous Cyclodextrin Polymers

Table S2.5. Amounts of reagents used for synthesis of porous α -, β -, and γ -cyclodextrin polymers (CDPs).

reagent	M [g mol ⁻¹]	mol.-eq.	n [mmol]	m [g]
α -CD	972.84	1.00	3.61	3.51
β -CD	1134.98	1.00	3.61	4.10
γ -CD	1297.12	1.00	3.61	4.69
TFN*	200.09	2.85	10.28	2.06
K ₂ CO ₃	138.21	12.82	46.30	6.40

*tetrafluoroterephthalonitrile, cross-linker

S2.4.2 Field Emission Scanning Electron Microscope (FESEM) Imaging

Field emission scanning electron microscope (SEM) imaging of the cyclodextrin-based polymers was carried out on a Sigma 300 VP instrument (Zeiss, Oberkochen, Germany) with an accelerating voltage of 10.0 kV and a sample distance of 5.4 to 5.9 nm. FESEM images at magnifications between 0.5×10^3 and 3.3×10^3 are shown in Figure S2.1 and depict the porous surface morphology of α -CDP, β -CDP, and γ -CDP, respectively.

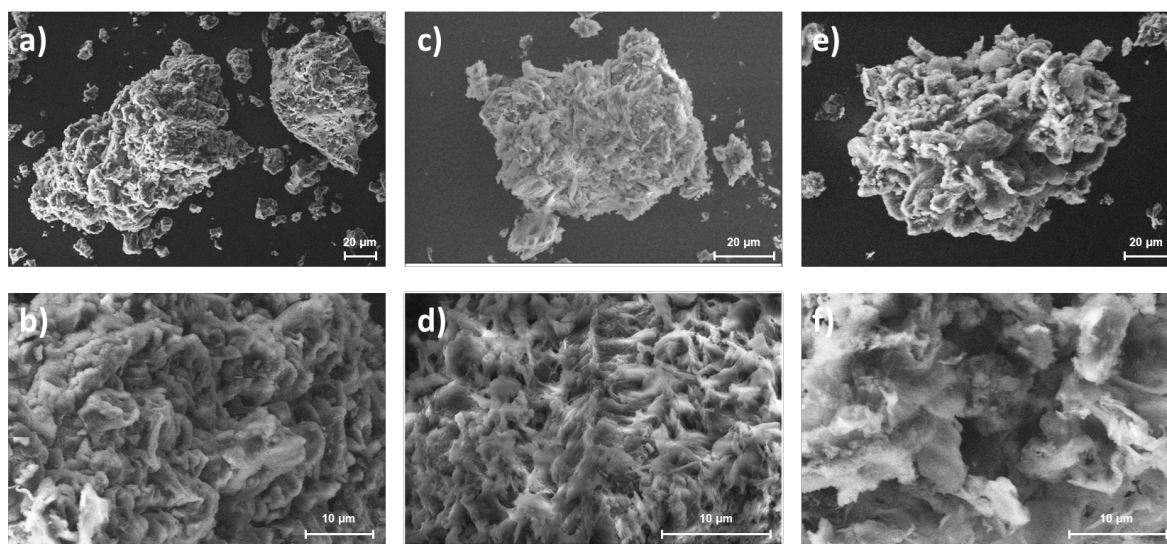


Figure S2.1. Field emission scanning electron microscope (FESEM) images of cross-linked α -CDP (a,b), β -CDP (c,d) and γ -CDP (e,f), respectively.

S2.4.3 Fourier Transform Infrared Spectroscopy

Fourier transform infrared (FTIR) spectra (solid, attenuated total reflectance, ATR) were recorded using a Nicolet 6700 FT-IR spectrometer (Thermo Scientific, USA) at a wavenumber range of 650 to 4000 cm^{-1} and a resolution of 4 cm^{-1} . The signal-to-noise ratio was improved by accumulating 32 individually recorded scans. Baseline correction was performed using the software OriginPro 2020.

According to similar structure and common functional groups, FTIR spectra of α -, β - and γ -CD showed intense absorbance at 1030 cm^{-1} , corresponding to polysaccharide C-O stretch vibrations, as well as aliphatic C-H stretch vibrations at 2930 cm^{-1} and O-H stretch vibrations around 3400 cm^{-1} (Figure S2.2). These spectral features were also found in spectra of the respective polymers (α -, β -, γ -CDP). In addition, spectra of the polymers exhibited nitrile stretches resonating at 2235 cm^{-1} and C-F stretch vibrations at 1268 cm^{-1} , which confirmed the successful incorporation of the cross-linker TFN. In comparison to the spectrum of neat TFN, C-F absorption bands in the polymer spectra were less pronounced as expected for partial substitution of fluorine during synthesis. Finally, peaks appearing at 1670 cm^{-1} and 1463 cm^{-1} are assigned to aromatic C=C stretches of both the cyclodextrins and the cross-linker TFN.

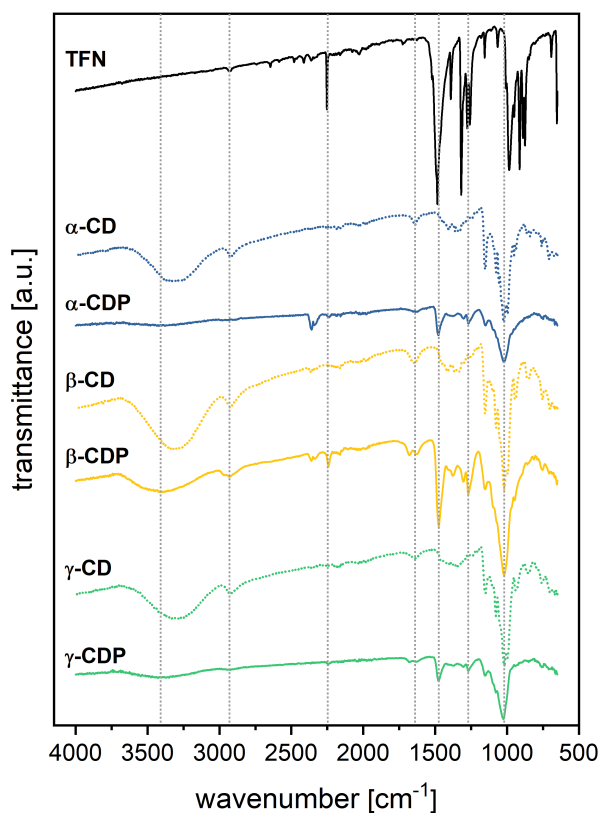


Figure S2.2. Fourier-transform infrared (FTIR) spectra of the cross-linker tetrafluoroterephthalonitrile (TFN), α -, β - and γ -cyclodextrin (α -, β -, γ -CD), as well as synthesized α -, β - and γ -cyclodextrin polymer (α -, β -, γ -CDP). Dashed vertical lines represent TFN specific absorption bands at 1268 cm^{-1} (C-F stretch vibrations) and 2235 cm^{-1} (nitrile stretch vibrations), CD specific absorption bands at 1030 cm^{-1} (C-O stretch vibrations), 2930 cm^{-1} (aliphatic C-H stretch vibrations), and 3400 cm^{-1} (O-H stretch vibrations), as well as common aromatic C=C stretch vibrations at 1464 cm^{-1} and 1670 cm^{-1} .

S2.5 Sampling and Pretreatment of Surface Water Samples

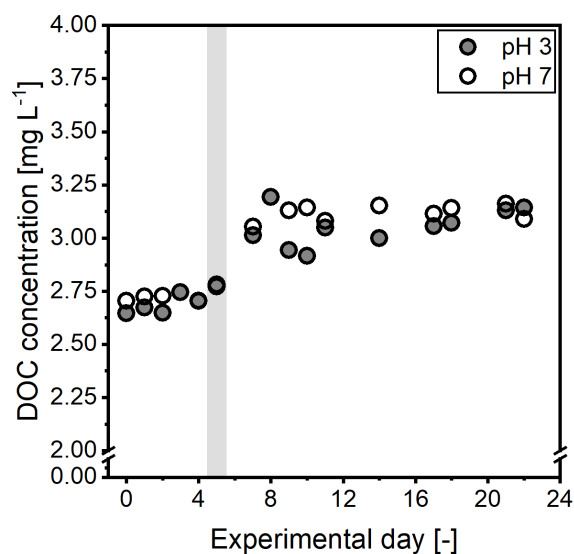


Figure S2.3. Dissolved organic carbon (DOC) concentrations in filtered (0.45 μm) surface water samples adjusted to pH 3 (gray circles) or pH 7 (white circles) and stored at 4 °C in the dark over a period of 24 days. The gray rectangular indicates maximum storage time for which DOC stability was assured.

Table S2.6. Physicochemical parameters of the surface water used for solid-phase extraction experiments in this study.

parameter	unit	value
pH	-	6.8
Conductivity	$\mu\text{S cm}^{-1}$	385
Acid capacity	mmol L^{-1}	5.03
Sodium (Na^+)	mg L^{-1}	12.50
Potassium (K^+)	mg L^{-1}	35.00
Ammonium (NH_4^+)	mg L^{-1}	< 0.04
Calcium (Ca^{2+})	mg L^{-1}	65.88
Magnesium (Mg^{2+})	mg L^{-1}	23.60
Fluoride (F^-)	mg L^{-1}	< 0.10
Chloride (Cl^-)	mg L^{-1}	15.47
Bromate (BrO_3^-)	mg L^{-1}	< 0.10
Bromide (Br^-)	mg L^{-1}	< 0.10
Iodide (I^-)	mg L^{-1}	< 0.10
Nitrite (NO_2^-)	mg L^{-1}	< 0.05
Nitrate (NO_3^-)	mg L^{-1}	1.26
Sulfate (SO_4^{2-})	mg L^{-1}	20.45
Hydrogen phosphate (HPO_4^{2-})	mg L^{-1}	< 0.10
Hydrogen carbonate (HCO_3^-)	mg L^{-1}	306.80

S2.6 Sample Preparation Procedures Using Cyclodextrin-Based and Conventional Sorbents

S2.6.1 Micropollutant and Dissolved Organic Matter Extraction

Spiking of Water Samples

To compare the extraction efficiencies of the investigated sorbents for target analytes and DOM, the latter being quantified by DOC analysis, the spiking of analytes to the water sample was carried out in a manner that avoided sample contamination by organic carbon stemming from the methanolic stock solution. Spiking of analytes at environmentally relevant concentrations of $1 \mu\text{g L}^{-1}$ was executed by transferring a 5 mL aliquot of the stock solution mix ($200 \mu\text{g L}^{-1}$) to a clean glass bottle, followed by complete evaporation under a gentle stream of N_2 . Thereafter, 1 L of water sample (2.7 mgC L^{-1}) was added, and the dry analyte residues were reconstituted overnight. This procedure removed the organic solvent, which would have compromised subsequent DOC analysis.

Solid-Phase Extraction

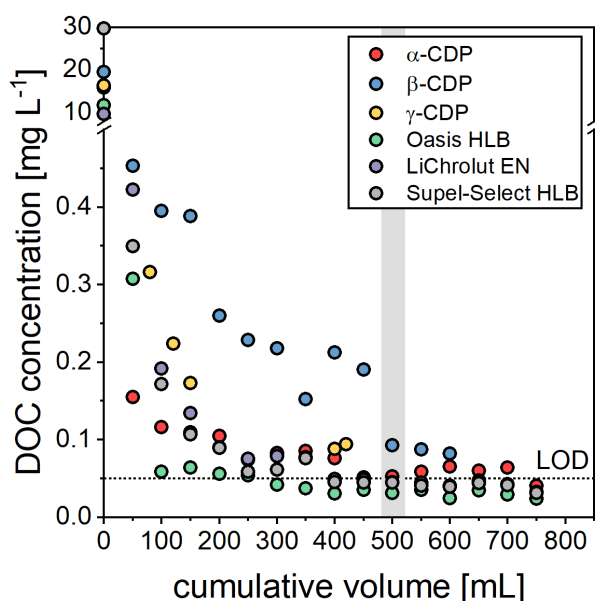


Figure S2.4. Dissolved organic carbon (DOC) concentrations in SPE breakthrough volumes of ultrapure water caused by organic carbon bleed from the sorbent material (10 mg sorbent bed weight). The horizontal dashed line represents the instrumental limit of detection and the gray rectangular indicates the volume used for sorbent conditioning, in order to reduce organic carbon bleed from the sorbent material.

S2.6.2 Validation of the SPE-CSIA Procedure Using β -Cyclodextrin Polymer

Table S2.7. Experimental parameters that were implemented for validating carbon isotope integrity of atrazine, S-metolachlor, boscalid and azoxystrobin throughout the SPE-CSIA procedure using β -CDP as SPE sorbent. SPE experiments were performed at a constant flow rate with different spiked concentrations (see “concentration dependency”) and at a constant concentration but varying flow rates/velocities (see “flow dependency”). In addition, the applicability of sorbent regeneration was examined by repetitively loading, eluting, and washing the same SPE cartridges at a constant flow rate and concentration (see “sorbent regeneration”).

experiment ID	spiked concentration [$\mu\text{g L}^{-1}$]	extracted volume [mL]	sorbent bed weight [mg]	SPE cartridge volume [mL]	volumetric flow rate [mL min ⁻¹]	linear flow velocity* [cm min ⁻¹]	elution volume (MeOH) [μL]
<i>concentration dependency</i>							
1	5	300	150	3	≤ 1.0	≤ 1.6	3000
2	25	150	75	3	≤ 1.0	≤ 1.6	2000
3	50	60	30	1	≤ 1.0	≤ 4.1	700
4	100	40	20	1	≤ 1.0	≤ 4.1	700
5	150	20	10	1	≤ 1.0	≤ 4.1	700
6	250	20	10	1	≤ 1.0	≤ 4.1	700
7	500	20	10	1	≤ 1.0	≤ 4.1	700
<i>flow dependency</i>							
1	150	20	10	1	0.50	4.9	700
2	150	20	10	1	1.25	12.3	700
3	150	20	10	1	2.00	19.6	700
4	150	20	10	1	2.50	24.6	700
5	150	20	10	1	3.00	29.5	700
6	150	20	10	1	3.50	34.4	700
7	150	20	10	1	4.00	39.3	700
<i>sorbent regeneration</i>							
1 - 7	150	20	10	1	≤ 1.0	≤ 4.1	700

*calculated on the basis of cross-sectional areas of 0.25 and 0.62 cm² for 1 and 3 mL SPE cartridges, respectively, except for flow dependency tests, where modified 1 mL cartridges with cross sectional areas of 0.10 cm² were used.

S2.7 Sorption Parameter Determination by Batch Equilibrium Sorption Studies

Batch equilibrium experiments according to guidelines provided by OECD²⁵⁴ and US EPA²⁵⁵ were performed to study the sorption behavior of the 11 model compounds on the cyclodextrin-based (i.e., α -, β -, γ -CDP) and commercial SPE sorbents (i.e., Oasis HLB, LiChrolut EN, Supel-Select HLB). Suspensions containing 10 mg sorbent in 10 mL 0.01 M CaCl₂ (pH 7) were pre-equilibrated by overhead shaking for 18 hours and, subsequently, spiked with analytes at concentrations ranging from 2.5 to 60 mg L⁻¹. After spiking, final methanol volumes did not exceed 1 % to prevent co-solvent effects. In addition, control samples (without sorbent) for each concentration level and blanks (without analytes) were

run to account for potential instability of the analytes, adsorption to the test vials and matrix interferences, respectively. All samples were prepared in triplicates and shaken for 24 hours in the dark at 25 ± 1 °C to reach sorption equilibrium. Afterwards, the suspensions were filtered (0.2 μm) and aqueous equilibrium concentrations were measured at wavelengths of maximum absorption by a high-performance liquid chromatography system (Nexera XR, Shimadzu, Japan) equipped with a diode array detector (SPD-M20A, Shimadzu, Japan). The injection volume was 20 μL and analyte separation was achieved by a XTerra RP18 column (3.0 x 150 mm, 3.5 μm particle size, Waters, USA) at 45 °C and using a gradient elution with ultrapure water (eluent A) and acetonitrile (eluent B) at a flow rate of 1.2 mL min^{-1} . After 0.75 min of 1 % B, the fraction of B was increased to 40 % within 1.5 min and was kept for 5 min, followed by a steep increase to 98 % B within 0.5 min. The fraction of 98 % B was kept for 0.5 min and, finally, the column was re-equilibrated to initial conditions for 2.5 min. Given the high surface area of LiChrolut EN (i.e., 1200 $\text{m}^2 \text{g}^{-1}$), aqueous equilibrium concentrations for all concentration levels were determined below detection limits and, hence, sorption data was not obtained for this sorbent.

The amount of analyte sorbed per mass of sorbent at equilibrium (q) was calculated via mass balance and sorption isotherms were fitted to the Freundlich and Langmuir sorption model according to equation (S2.1) and (S2.2), respectively:

$$q = K_F \times C_{aq}^{1/n} \quad (\text{S2.1})$$

$$q = \frac{q_{max} \times K_L \times C_{aq}}{1 + K_L \times C_{aq}} \quad (\text{S2.2})$$

where q (mg g^{-1}) is the amount of analyte sorbed per mass of sorbent at equilibrium, C_{aq} (mg L^{-1}) is the aqueous equilibrium concentration of the compound, K_F [$(\text{mg/g})/(\text{mg/L})^{1/n}$] and K_L (L mg^{-1}) are the Freundlich and Langmuir sorption coefficients, respectively, $1/n$ (-) is the degree of isotherm nonlinearity and q_{max} (mg g^{-1}) is the maximum sorption capacity. Isotherm fitting was performed using the software OriginPro 2020.

Figure S2.5, S2.6, S2.7, S2.8, and S2.9 depict the amount of analyte sorbed per mass of sorbent at equilibrium (q) as a function of aqueous equilibrium concentration (C_{aq}), as well as fitted Freundlich and Langmuir sorption isotherms for the 11 model compounds obtained by batch sorption experiments using α -CDP, β -CDP, γ -CDP, Oasis HLB and Supel-Select HLB, respectively. The results of data fitting, including sorption parameters and coefficients of determination (R^2), are summarized in Table S2.8. For a comparison among the sorbents, we derived partition coefficients based on the Freundlich model for a fixed aqueous equilibrium concentration, C_{aq} , of 100 $\mu\text{g L}^{-1}$, where uncertainties were propagated according to the Gaussian error propagation law (Table S2.9).

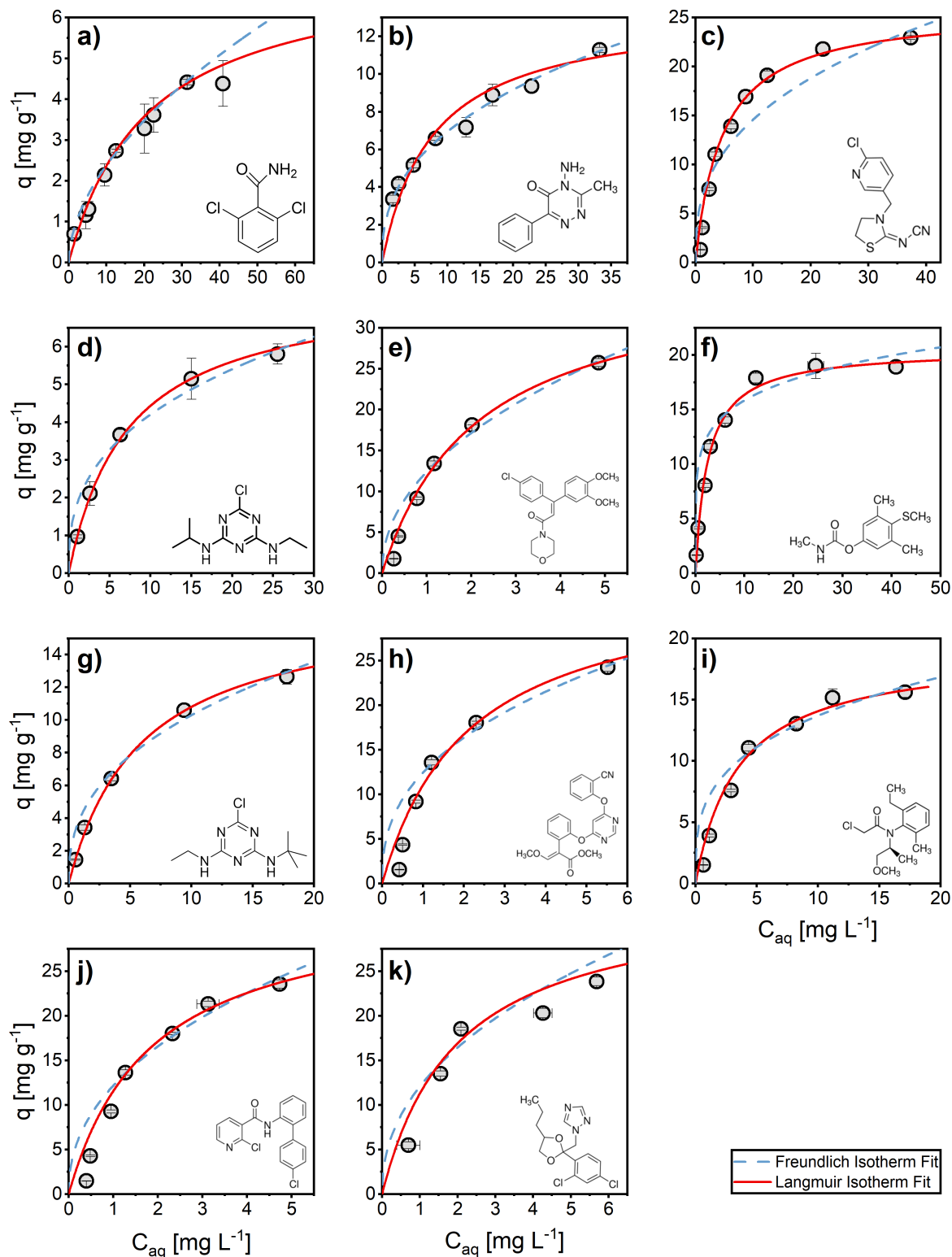


Figure S2.5. Equilibrium sorption isotherms of α -CDP at 25 ± 1 °C for 2,6-dichlorobenzamide (a), metamitron (b), thiacloprid (c), atrazine (d), dimethomorph (e), methiocarb (f), terbuthylazine (g), azoxystrobin (h), *S*-metolachlor (i), boscalid (j), and propiconazole (k). Equilibrium uptake, q (mg g^{-1}), is plotted against aqueous equilibrium concentration of compound, C_{aq} (mg L^{-1}). Error bars reflect one standard deviation ($\pm\sigma$) of triplicate experiments. Freundlich and Langmuir isotherm fits are represented by blue dashed and red lines, respectively.

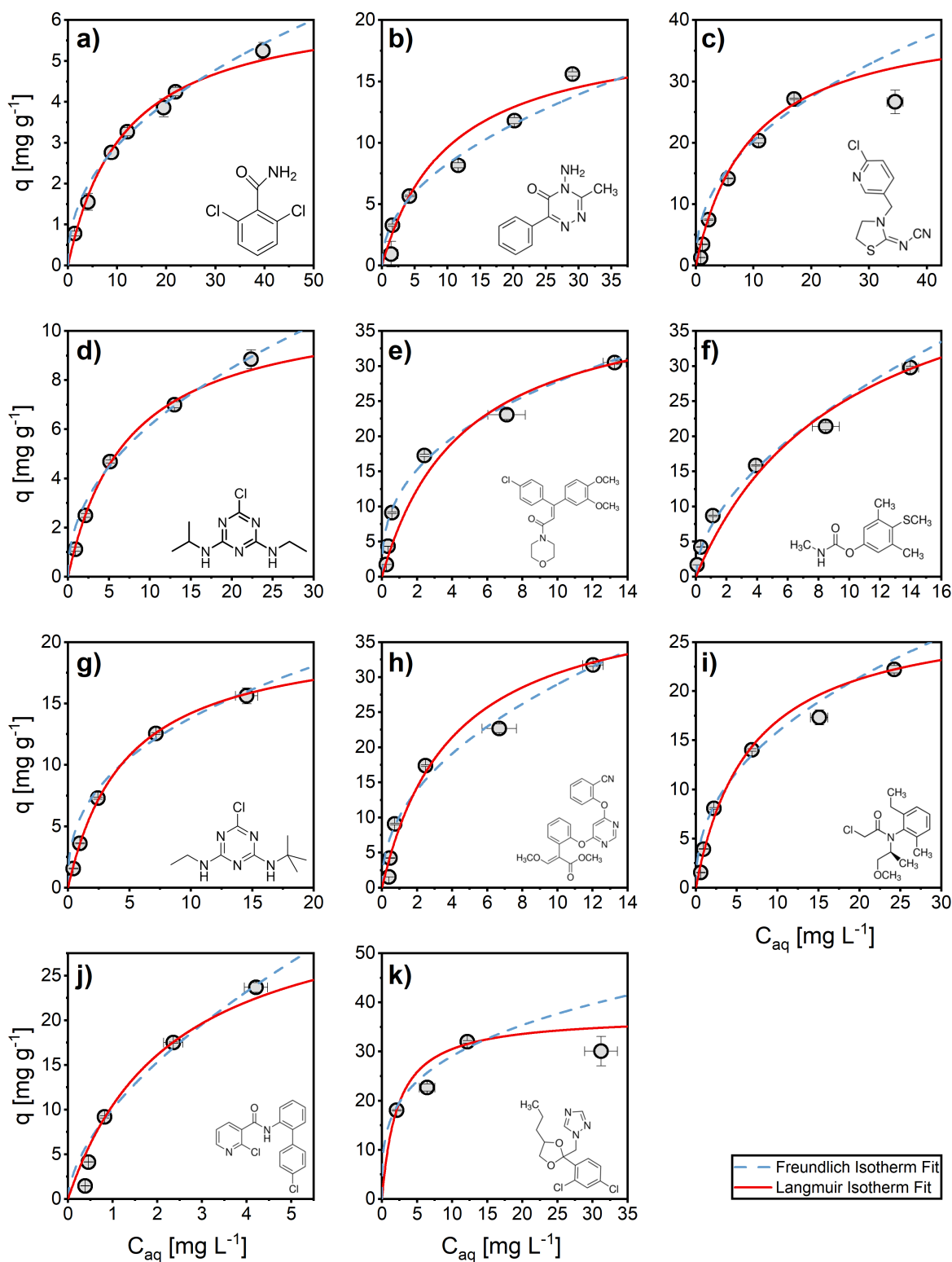


Figure S2.6. Equilibrium sorption isotherms of β -CDP at 25 ± 1 °C for 2,6-dichlorobenzamide (a), metamitron (b), thiacloprid (c), atrazine (d), dimethomorph (e), methiocarb (f), terbuthylazine (g), azoxystrobin (h), *S*-metolachlor (i), boscalid (j), and propiconazole (k). Equilibrium uptake, q (mg g^{-1}), is plotted against aqueous equilibrium concentration of compound, C_{aq} (mg L^{-1}). Error bars reflect one standard deviation ($\pm\sigma$) of triplicate experiments. Freundlich and Langmuir isotherm fits are represented by blue dashed and red lines, respectively.

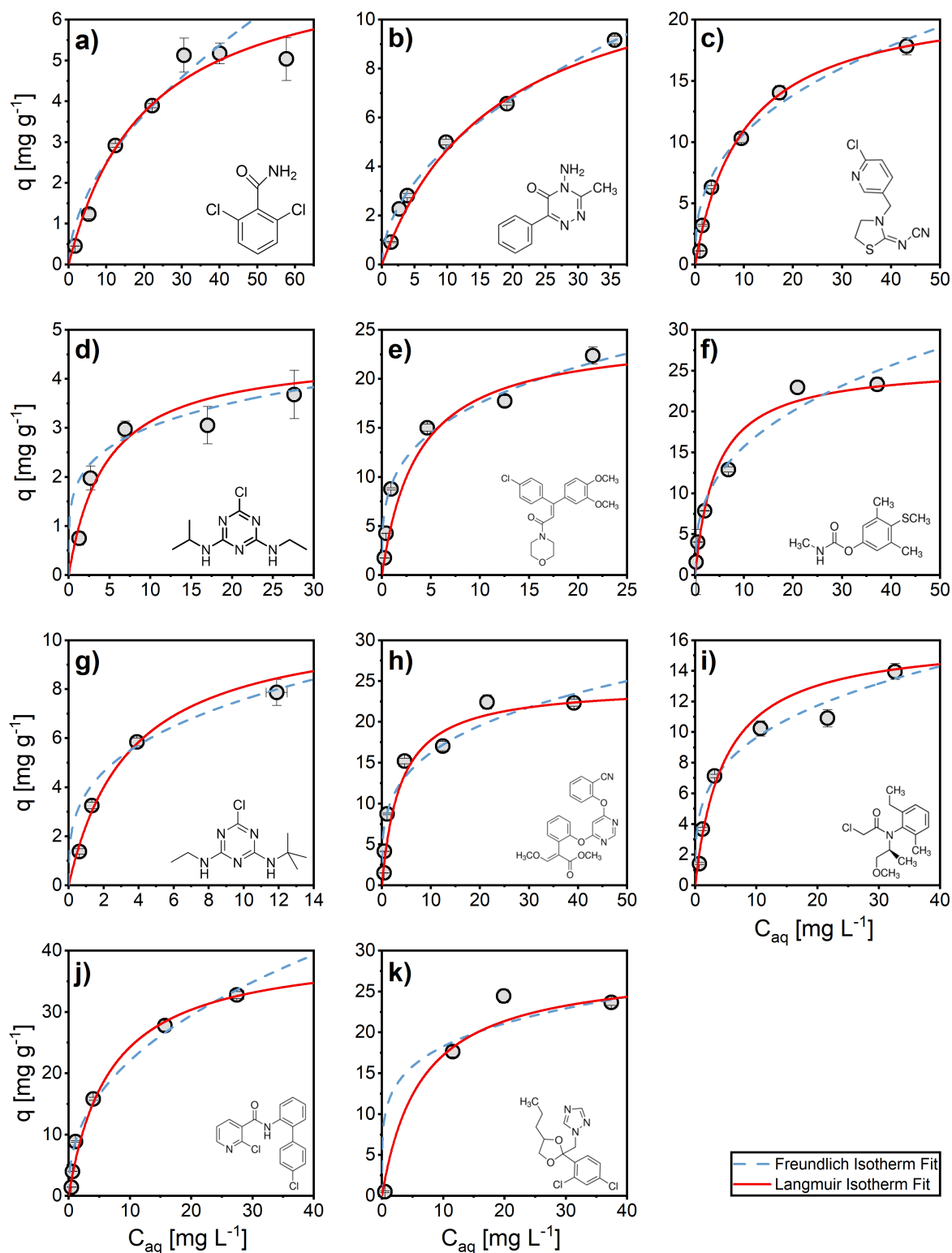


Figure S2.7. Equilibrium sorption isotherms of γ -CDP at 25 ± 1 °C for 2,6-dichlorobenzamide (a), metamitron (b), thiachlorid (c), atrazine (d), dimethomorph (e), methiocarb (f), terbuthylazine (g), azoxystrobin (h), *S*-metolachlor (i), boscalid (j), and propiconazole (k). Equilibrium uptake, q (mg g^{-1}), is plotted against aqueous equilibrium concentration of compound, C_{aq} (mg L^{-1}). Error bars reflect one standard deviation ($\pm\sigma$) of triplicate experiments. Freundlich and Langmuir isotherm fits are represented by blue dashed and red lines, respectively.

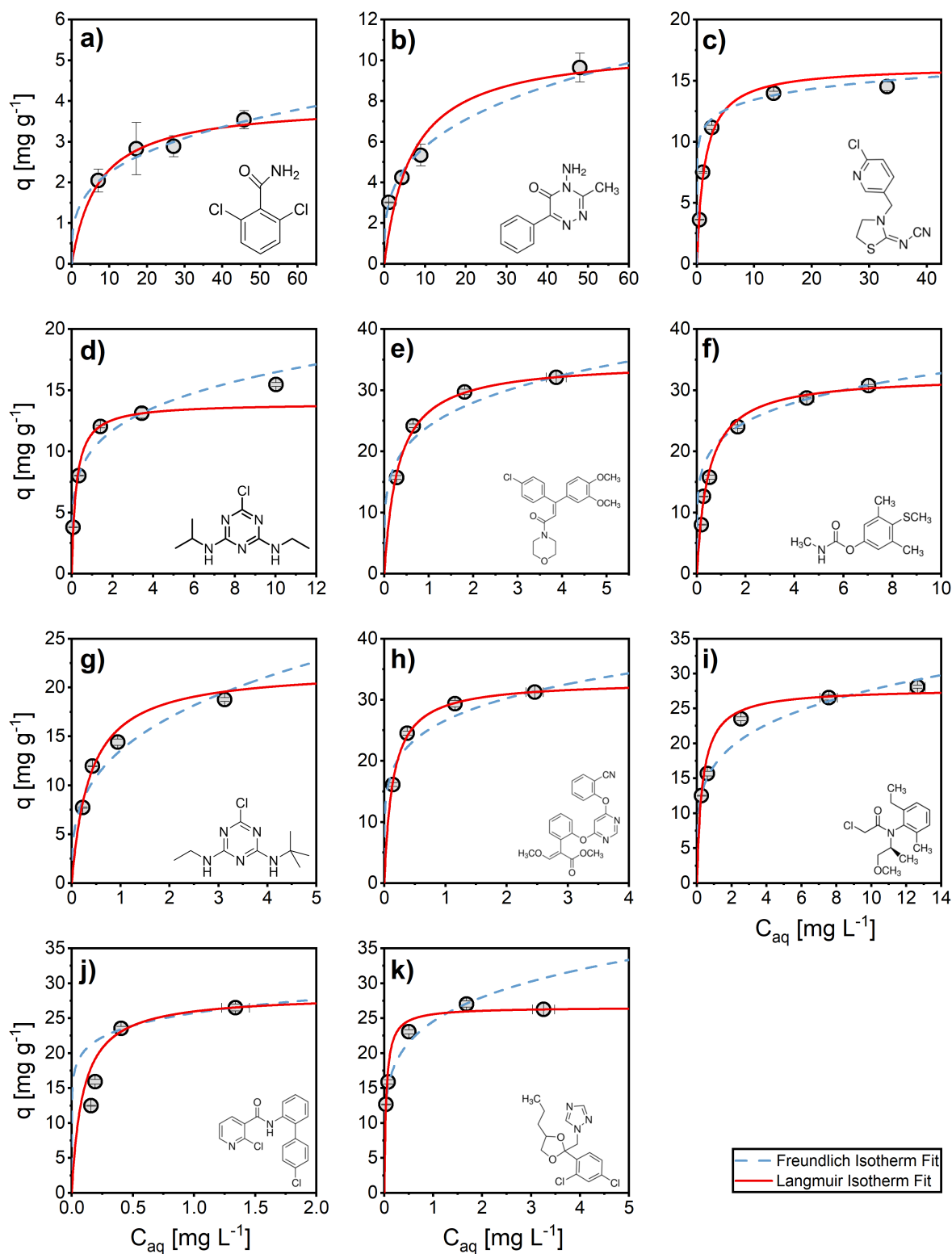


Figure S2.8. Equilibrium sorption isotherms of Oasis HLB at 25 ± 1 °C for 2,6-dichlorobenzamide (a), metatiron (b), thiacloprid (c), atrazine (d), dimethomorph (e), methiocarb (f), terbuthylazine (g), azoxystrobin (h), *S*-metolachlor (i), boscalid (j), and propiconazole (k). Equilibrium uptake, q (mg g^{-1}), is plotted against aqueous equilibrium concentration of compound, C_{aq} (mg L^{-1}). Error bars reflect one standard deviation ($\pm\sigma$) of triplicate experiments. Freundlich and Langmuir isotherm fits are represented by blue dashed and red lines, respectively.

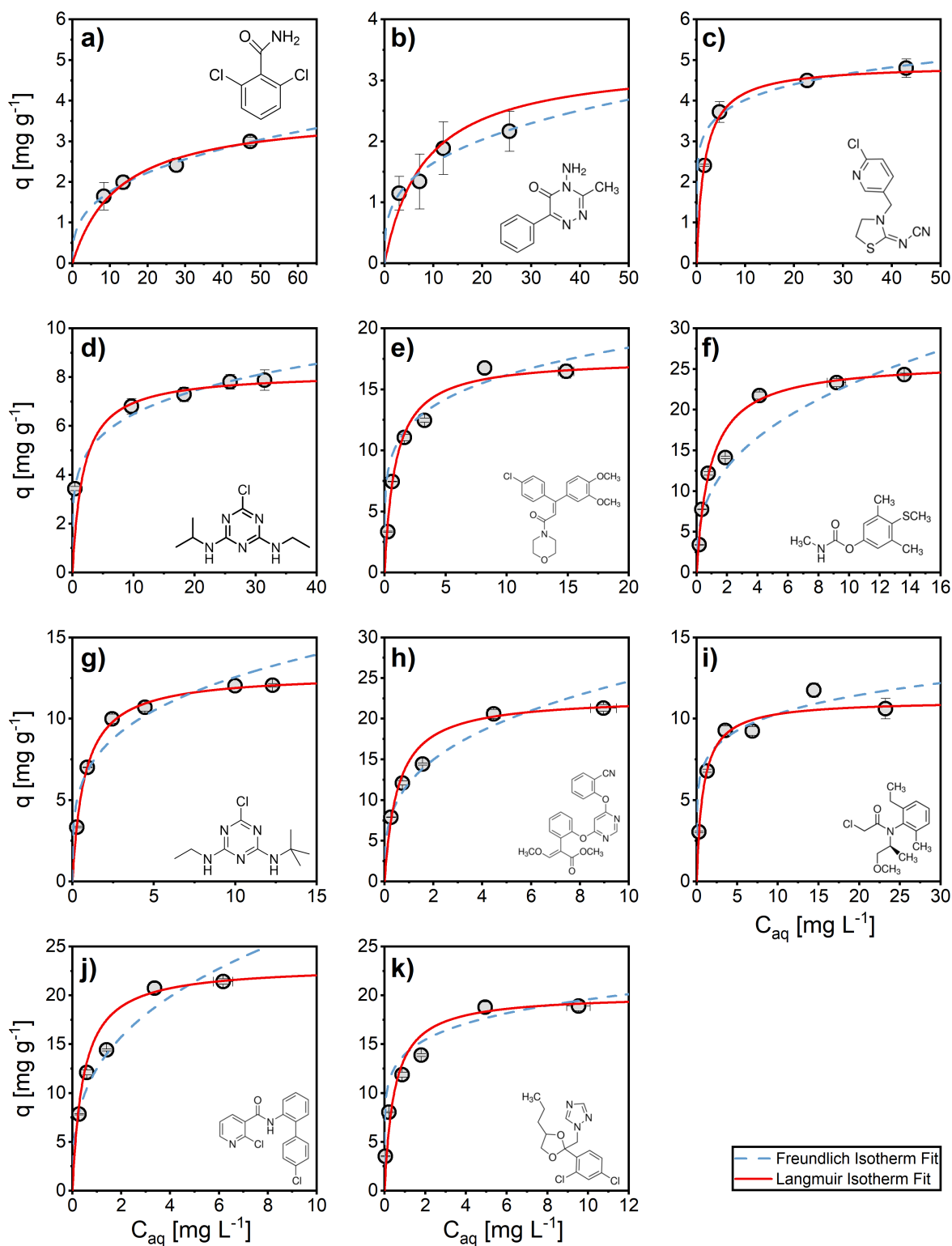


Figure S2.9. Equilibrium sorption isotherms of Supel-Select HLB at 25 ± 1 °C for 2,6-dichlorobenzamide (a), metamitron (b), thiacloprid (c), atrazine (d), dimethomorph (e), methiocarb (f), terbuthylazine (g), azoxystrobin (h), *S*-metolachlor (i), boscalid (j), and propiconazole (k). Equilibrium uptake, q (mg g^{-1}), is plotted against aqueous equilibrium concentration of compound, C_{aq} (mg L^{-1}). Error bars reflect one standard deviation ($\pm\sigma$) of triplicate experiments. Freundlich and Langmuir isotherm fits are represented by blue dashed and red lines, respectively.

Table S2.8. Sorption parameters of the 11 target analytes for cyclodextrin-based sorbents (α -, β - and γ -CDP) and the conventional SPE sorbents Oasis HLB and Supel-Select HLB. Values were obtained by fitting batch sorption data (see Figure S2.5 to Figure S2.9) to both Freundlich and Langmuir sorption isotherm models.

sorbent	isotherm model	parameter	unit	2,6-dichloro-benzamide	metamitron	thiacloprid	atrazine	dimetho-morph	methiocarb	terbutyl-azine	azoxy-strobin	S-metolachlor	boscalid	propicon-azole
α -CDP	Freundlich	K_F	$\frac{mg/g}{(mg/L)^{1/n}}$	0.67 ± 0.05	2.78 ± 0.14	6.24 ± 0.72	1.82 ± 0.24	12.39 ± 0.86	10.79 ± 1.15	4.12 ± 0.61	12.44 ± 1.09	6.87 ± 0.91	12.16 ± 1.25	12.07 ± 1.92
		n	[-]	1.83 ± 0.28	2.51 ± 0.10	2.71 ± 0.29	2.75 ± 0.35	2.14 ± 0.22	6.00 ± 1.32	2.52 ± 0.36	2.53 ± 0.37	3.34 ± 0.60	2.24 ± 0.40	2.24 ± 0.78
		R^2	[-]	0.990	0.998	0.990	0.997	1.000	0.998	0.999	1.000	1.000	0.999	1.000
α -CDP	Langmuir	K_L	[L mg ⁻¹]	0.05 ± 0.00	0.13 ± 0.02	0.21 ± 0.01	0.14 ± 0.01	0.46 ± 0.04	0.39 ± 0.04	0.17 ± 0.01	0.47 ± 0.09	0.28 ± 0.05	0.54 ± 0.10	0.50 ± 0.26
		q_m	[mg g ⁻¹]	7.33 ± 0.32	13.43 ± 0.87	25.88 ± 0.26	7.63 ± 0.29	37.20 ± 1.11	20.52 ± 0.95	17.20 ± 0.86	34.51 ± 3.32	19.01 ± 0.78	33.05 ± 2.01	33.72 ± 8.10
		R^2	[-]	0.990	0.953	1.000	0.997	1.000	0.999	0.997	0.982	1.000	1.000	0.870
β -CDP	Freundlich	K_F	$\frac{mg/g}{(mg/L)^{1/n}}$	1.05 ± 0.11	2.77 ± 0.20	7.45 ± 2.23	2.12 ± 0.21	11.78 ± 0.50	7.15 ± 0.30	5.70 ± 0.76	10.15 ± 1.28	5.86 ± 0.38	10.11 ± 1.15	15.19 ± 5.19
		n	[-]	2.24 ± 0.18	2.11 ± 0.17	2.29 ± 0.54	2.16 ± 0.17	2.68 ± 0.16	1.80 ± 0.07	2.60 ± 0.38	2.20 ± 0.26	2.31 ± 0.18	1.67 ± 0.25	3.54 ± 1.66
		R^2	[-]	0.998	0.976	1.000	0.999	0.989	0.988	1.000	0.988	1.000	0.979	1.000
β -CDP	Langmuir	K_L	[L mg ⁻¹]	0.09 ± 0.01	0.10 ± 0.03	0.10 ± 0.04	0.14 ± 0.01	0.22 ± 0.06	0.1 ± 0.03	0.21 ± 0.02	0.25 ± 0.05	0.15 ± 0.05	0.43 ± 0.06	0.45 ± 0.07
		q_m	[mg g ⁻¹]	6.47 ± 0.33	19.49 ± 2.66	41.23 ± 5.47	11.16 ± 0.53	40.90 ± 3.07	50.40 ± 7.06	20.89 ± 0.96	42.70 ± 5.12	28.34 ± 6.10	34.89 ± 2.40	37.32 ± 2.25
		R^2	[-]	0.989	0.936	1.000	0.997	1.000	1.000	0.998	0.974	0.940	0.997	0.967
γ -CDP	Freundlich	K_F	$\frac{mg/g}{(mg/L)^{1/n}}$	0.71 ± 0.16	1.47 ± 0.12	4.56 ± 0.71	1.84 ± 0.35	9.30 ± 1.05	6.96 ± 1.53	3.75 ± 0.49	8.74 ± 0.43	5.00 ± 0.69	8.43 ± 0.24	11.36 ± 5.76
		n	[-]	1.83 ± 0.26	1.95 ± 0.10	2.70 ± 0.36	4.62 ± 1.77	3.62 ± 0.58	2.83 ± 0.55	3.27 ± 0.68	3.72 ± 0.33	3.51 ± 0.57	2.40 ± 0.08	4.84 ± 3.52
		R^2	[-]	0.925	1.000	0.996	0.993	1.000	0.997	0.998	0.955	0.998	0.998	0.992
γ -CDP	Langmuir	K_L	[L mg ⁻¹]	0.05 ± 0.01	0.06 ± 0.01	0.10 ± 0.01	0.22 ± 0.09	0.27 ± 0.12	0.23 ± 0.06	0.29 ± 0.08	0.26 ± 0.07	0.21 ± 0.07	0.15 ± 0.02	0.16 ± 0.11
		q_m	[mg g ⁻¹]	7.59 ± 0.84	13.06 ± 1.16	21.94 ± 0.74	4.55 ± 0.81	24.61 ± 2.61	25.79 ± 2.91	10.89 ± 1.68	24.53 ± 1.15	16.15 ± 3.23	40.58 ± 1.27	28.24 ± 4.03
		R^2	[-]	0.971	0.993	1.000	0.911	1.000	0.992	0.975	0.999	0.916	1.000	0.995
Oasis HLB	Freundlich	K_F	$\frac{mg/g}{(mg/L)^{1/n}}$	1.14 ± 0.13	2.88 ± 0.02	10.87 ± 0.85	10.10 ± 0.83	24.12 ± 1.39	21.96 ± 0.67	13.58 ± 0.81	26.61 ± 1.01	16.79 ± 0.38	25.74 ± 0.38	24.55 ± 1.63
		n	[-]	3.40 ± 0.37	3.32 ± 0.16	10.86 ± 3.28	4.71 ± 1.12	4.68 ± 0.97	5.74 ± 0.56	3.14 ± 0.53	5.45 ± 1.18	4.61 ± 0.30	9.60 ± 3.52	5.26 ± 0.79
		R^2	[-]	0.970	0.984	0.998	0.989	0.920	1.000	0.984	0.938	0.974	1.000	0.996
Oasis HLB	Langmuir	K_L	[L mg ⁻¹]	0.14 ± 0.05	0.15 ± 0.05	0.71 ± 0.13	4.60 ± 1.19	3.20 ± 0.26	2.07 ± 0.20	2.66 ± 0.56	7.14 ± 0.38	3.05 ± 0.23	10.86 ± 3.11	25.45 ± 1.21
		q_m	[mg g ⁻¹]	3.95 ± 0.31	10.72 ± 1.47	16.17 ± 1.61	13.93 ± 1.34	34.71 ± 0.36	32.36 ± 1.36	21.92 ± 2.22	33.03 ± 0.23	27.86 ± 0.98	28.35 ± 0.55	26.56 ± 0.25
		R^2	[-]	0.930	0.996	0.957	0.942	0.994	0.982	0.951	0.997	0.984	1.000	0.997
Supel-Select HLB	Freundlich	K_F	$\frac{mg/g}{(mg/L)^{1/n}}$	0.80 ± 0.07	0.81 ± 0.10	2.97 ± 0.39	4.10 ± 0.06	10.50 ± 1.33	10.05 ± 0.81	6.93 ± 0.33	12.09 ± 0.33	7.25 ± 0.88	12.50 ± 0.38	13.96 ± 1.67
		n	[-]	2.93 ± 0.21	3.28 ± 0.48	7.62 ± 2.36	5.02 ± 0.16	5.33 ± 1.54	2.77 ± 0.33	3.87 ± 0.75	3.24 ± 0.22	6.55 ± 2.26	2.99 ± 0.25	6.80 ± 2.72
		R^2	[-]	0.980	0.999	0.931	0.995	0.990	0.897	0.841	0.971	0.994	0.968	0.990
Supel-Select HLB	Langmuir	K_L	[L mg ⁻¹]	0.08 ± 0.02	0.12 ± 0.10	0.60 ± 0.02	0.56 ± 0.20	1.13 ± 0.23	1.08 ± 0.18	1.34 ± 0.02	1.87 ± 0.59	1.20 ± 0.10	2.26 ± 0.92	2.10 ± 1.02
		q_m	[mg g ⁻¹]	3.74 ± 0.26	3.33 ± 0.97	4.89 ± 0.07	8.19 ± 0.29	17.53 ± 2.06	25.97 ± 0.31	12.77 ± 0.08	22.68 ± 0.3	11.13 ± 0.42	23.02 ± 0.72	20.10 ± 0.67
		R^2	[-]	0.940	0.685	0.998	0.998	0.955	1.000	1.000	1.000	0.991	1.000	0.999

Table S2.9. Partition coefficients between analytes in aqueous solution and sorbents (i.e., Oasis HLB, Supel-Select HLB, α -CDP, β -CDP) calculated based on the Freundlich sorption model for a fixed aqueous equilibrium concentration of 100 $\mu\text{g L}^{-1}$. Freundlich sorption parameters were obtained by fitting of the experimental batch sorption data (see Figure S2.5 to Figure S2.9, Table S2.8).

analyte	log K_{ow} [-]	McGowan Volume [$\text{cm}^3 \text{mol}^{-1}$ 100^{-1}]	K_d [L kg^{-1}]			
			Oasis HLB	Supel-Select HLB	α -CDP	β -CDP
2,6-dichlorobenzamide (BAM)	0.77	1.22	5770 \pm 773	3657 \pm 378	1909 \pm 394	3739 \pm 504
metamitron	0.85	1.50	14411 \pm 495	4027 \pm 637	11130 \pm 680	9296 \pm 1076
thiacloprid	1.26	1.73	87963 \pm 8860	21962 \pm 3512	26726 \pm 3937	27305 \pm 10434
azoxystrobin	2.50	2.92	174464 \pm 17309	59437 \pm 3334	50069 \pm 7926	35594 \pm 6313
dimethomorph	2.68	2.85	147507 \pm 17331	68139 \pm 12128	42211 \pm 5609	49918 \pm 3375
atrazine	2.70	1.62	61957 \pm 8807	25927 \pm 533	7888 \pm 1335	7323 \pm 966
boscalid	2.96	2.39	202481 \pm 18060	57904 \pm 4092	43606 \pm 9107	25410 \pm 5947
S-metolachlor	3.05	2.28	101815 \pm 4066	50986 \pm 8725	34457 \pm 6242	21678 \pm 2185
terbutylazine	3.40	1.76	65214 \pm 8997	38244 \pm 4741	16524 \pm 3268	23497 \pm 4371
propiconazole	3.72	2.34	158402 \pm 14827	99502 \pm 17994	43191 \pm 16977	79340 \pm 36255

S2.8 Column Sorption Experiments Using High-Performance Liquid Chromatography

S2.8.1 Packing of HPLC Columns

A schematic illustration of the column setup, which was used for packing silicon carbide (SiC)-supported sorbents into empty HPLC columns, is given in Figure S2.10. Table S2.4 provides further information on the individual column parts, which were purchased from Bischoff Chromatography (Leonberg, Germany). First, cyclodextrin-based (i.e., α -, β - or γ -CDP) or conventional sorbents (i.e., Oasis HLB, LiChrolut EN or Supel-Select HLB) were diluted with quasi-inert SiC in a ratio sorbent:SiC of 1:100 (w/w) by means of overhead shaking to reduce backpressure and to facilitate experiments within a reasonable time. Then, two stainless-steel columns (14 x 2.0 mm, see no. 3 in Figure S2.10) were connected by fitting adapters (no. 4), PTFE seals (no. 7) and a stainless-steel connector (no. 5) that was drilled to an inner diameter identical to the two connected columns (Figure S2.10a and b). The dry packing material was then carefully added until the entire column set was filled. During the filling procedure, a screwdriver was used to gently tap against the column wall to consolidate the material. Glass fiber filters (no. 8) and stainless steel meshes (5 μm mesh size, no. 9) on both sides ensured fixation of the packing material. After encasing, the column was connected to an HPLC system (Nexera series, Shimadzu, Japan). An initial flow rate of 0.05 mL min^{-1} allowed the column to saturate with ultrapure water, and entrapped air to leave the pore volume. Subsequently, the packing material was compressed by gradually increasing the flow rate (5-50 bar steps, hold time 30 min) until a maximum backpressure of 380 bar was reached. To finish the packing procedure, the pre-column was dismantled from

the column set, the main column was encased and closed with column end plugs (Figure S2.10c). A reference column to evaluate potential interaction between analyte and SiC support was only filled with SiC following the same procedure. Characteristics of all packed columns are listed in Table S2.10.

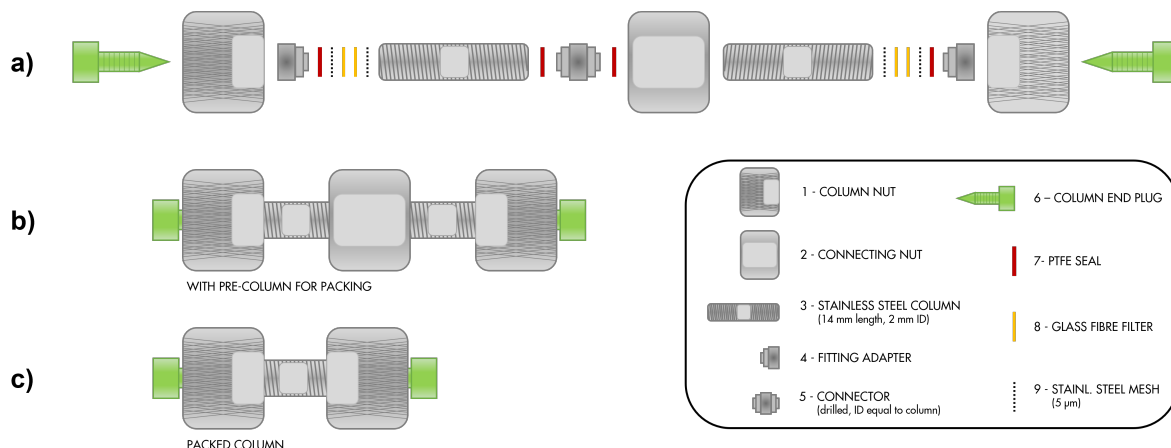


Figure S2.10. Schematic illustration of the column setup used for packing silicon carbide-supported sorbents into empty HPLC columns. The setup including a pre-column, which was used for liquid compression of the solid packing material, is depicted as exploded view in (a) and as closed setup in (b). The final setup, after completed sorbent compression and column encasing, is shown in (c). For detailed information on column packing and column parts refer to the text.

Table S2.10. Characteristics of SiC supported sorbent columns (#1-6) and SiC reference column (#7) used for HPLC-based flow-through determination of thermodynamic sorption parameters of the analyte 2,6-dichlorobenzamide (BAM).

parameter	column #:	1	2	3	4	5	6	7
	sorbent:	α -CDP	β -CDP	γ -CDP	Oasis HLB	LiChrolut EN	Supel-Select HLB	SiC
ratio sorbent:SiC	[-]	1:100	1:100	1:100	1:100	1:100	1:100	-
mass (solid phase)	[mg]	92.60	85.00	84.40	91.30	85.80	92.10	106.50
mass (sorbent)	[mg]	0.926	0.850	0.844	0.913	0.858	0.921	-
ε	[g SiC/g SiC]	0.861	0.790	0.785	0.849	0.798	0.856	1.000
ρ_b	[g cm ⁻³]	2.105	1.933	1.919	2.076	1.951	2.094	2.421
t_0	[min]	1.659	1.684	1.687	1.669	1.695	1.638	1.682
V_w	[mL]	0.029	0.031	0.032	0.030	0.032	0.027	0.031
Θ	[cm ³ cm ⁻³]	0.658	0.714	0.721	0.680	0.739	0.610	0.709

ε : mass ratio of SiC in sorbent vs. reference column #7, ρ_b : bulk density, t_0 : hold-up time for a flow rate of 0.1 mL min⁻¹, V_w : net column volume, Θ : porosity

S2.8.2 Determination of Partition Coefficient and Gibbs Free Energy of Adsorption

Table S2.11. Abraham parameters for the compound 2,6-dichlorobenzamide (BAM). Data obtained from the UFZ-LSER database.²⁶¹

V_i	E_i	S_i	A_i	B_i	L_i
1.2176	1.2	1.75	0.4	0.79	6.248

Table S2.12. pp-LFER descriptors for the water/ethanol system (9:1, v/v), and water/Aldrich humic acid system at 25 °C.

system	$v_{w,EtOH}$	$e_{w,EtOH}$	$s_{w,EtOH}$	$a_{w,EtOH}$	$b_{w,EtOH}$	c
water/EtOH*	0.45	-0.02	0	0.07	-0.37	-0.17
water/AHA†	3.94	0.29	-0.52	0.36	-3.4	-0.85

*data from Abraham and Acree²⁶² for $f_{V,EtOH} = 0.1$

†data from Neale et al.³⁷⁴

S2.8.3 Estimation of the Partitioning of 2,6-Dichlorobenzamide (BAM) between Water and Organic Carbon

The partitioning of compound i (i.e., BAM) between water (W) and the organic carbon (OC) of background Aldrich Humic Acid (AHA), $K_{i\text{ocw}}$ (L kg⁻¹), was estimated by a pp-LFER according to equation (S2.3):¹⁷⁶

$$\log K_{i\text{ocw}} = v_{\text{ocw}}V_i + e_{\text{ocw}}E_i + s_{\text{ocw}}S_i + a_{\text{ocw}}A_i + b_{\text{ocw}}B_i + c \quad (\text{S2.3})$$

Capital letters in represent compound-specific descriptors (so-called Abraham parameters) which are relevant for the partitioning process: the McGowan characteristic volume (V_i) given in cm³ mol⁻¹ 100⁻¹, the excess molar refractivity (E_i) given in cm³ mol⁻¹ 10⁻¹, dipolarity/polarizability parameter (S_i), H-donor property (A_i), and H-acceptor property (B_i). Small letters represent the complementary descriptors of the water/AHA system. Abraham parameters for BAM, obtained from the UFZ-LSER database,²⁶¹ and descriptors for the water/AHA system, derived by Neale et al.,³⁷⁴ are summarized in Table S2.11 and Table S2.12, respectively.

S2.9 Compound Quantification Using LC-MS/MS and HPLC

S2.9.1 LC-MS/MS Method

Analyte concentrations in eluates, which were obtained from water samples spiked at $1 \mu\text{g L}^{-1}$, were quantified by ultrahigh-performance liquid chromatography (UHPLC, PLATINblue, Knauer, Germany) coupled to tandem mass spectrometry (MS/MS, AB Sciex Triple-Quad 6500, Sciex, USA) using electrospray ionization (ESI) in positive mode. To this end, $100 \mu\text{L}$ aliquots of eluates were diluted with $880 \mu\text{L}$ ultrapure water and spiked with $20 \mu\text{L}$ of isotopically-labeled internal standard mixture ($100 \mu\text{g L}^{-1}$). The injection volume was $25 \mu\text{L}$. Analyte separation was achieved by a Kinetex C18 column ($3 \times 150 \text{ mm}$, $2.6 \mu\text{m}$ particle size, Phenomenex, USA) at $30 \text{ }^\circ\text{C}$ and using a gradient elution with ultrapure water containing 0.2% formic acid (eluent A) and acetonitrile (eluent B) at a flow rate of 0.5 mL min^{-1} . After 1 min of 30% B, the fraction of B was increased linearly to 45% within 15 min, followed by a steep increase to 98% B within 1 min. The fraction of 98% B was kept constant for 1.5 min and finally the column was re-equilibrated to initial conditions for 2 min. Analytes were quantified against reference standards based on extracted ion chromatograms using internal calibration with isotopically labeled internal standards. The internal standard with the closest retention time was chosen for quantitation. Analytical details used for identification and quantification, including limits of detection and quantification (LOD, LOQ) are provided in Table S2.13.

S2.9.2 HPLC Method

Concentrations of atrazine, *S*-metolachlor, boscalid and azoxystrobin in extracts, which were obtained from water samples spiked at concentrations of 5 to $500 \mu\text{g L}^{-1}$ (SPE validation experiments), were measured at analyte-specific wavelengths (i.e., 222 nm , 200 nm , 200 nm , and 200 nm , respectively) by an HPLC system (Nexera XR, Shimadzu, Japan) equipped with a diode array detector (SPD-M20A, Shimadzu, Japan). The injection volume was $20 \mu\text{L}$ and analyte separation was achieved by a Kinetex C18 column ($4.6 \times 150 \text{ mm}$, $2.6 \mu\text{m}$ particle size, Phenomenex, USA) at $40 \text{ }^\circ\text{C}$ and using a gradient elution with ultrapure water (eluent A) and acetonitrile (eluent B) at a flow rate of 1.2 mL min^{-1} . After 0.5 min of 10% B, the fraction of B was increased to 67% within 6.8 min, followed by an increase to 95% within 0.5 min. The fraction of 95% B was kept constant for 0.5 min and finally the column was re-equilibrated to initial conditions for 1.7 min. An external calibration was used to quantify concentrations of the investigated analytes in organic extracts after dilution with ultrapure water (9:1, v/v). Limits of quantification were determined with values of $25.8 \mu\text{g L}^{-1}$ (atrazine), $27.0 \mu\text{g L}^{-1}$ (*S*-metolachlor), $67.9 \mu\text{g L}^{-1}$ (boscalid) and $49.5 \mu\text{g L}^{-1}$ (azoxystrobin).

Table S2.13. Substance-specific MS/MS settings, instrumental limits of detection ($LOD_{instr.}$) and limits of quantification ($LOQ_{instr.}$).

analyte	ESI mode	retention time [min]	precursor mass [m/z]	product mass (quantifier) [m/z]	product mass (qualifier) [m/z]	collision energy [V]	collision cell exit potential [V]	declustering potential [V]	$LOD_{instr.}^*$ [$\mu\text{g L}^{-1}$]	$LOQ_{instr.}^*$ [$\mu\text{g L}^{-1}$]
2,6-dichlorobenzamide	positive	1.30	189.9	172.9	144.9	81	25	10	0.6	1.7
atrazine	positive	4.90	216.0	174.0	104.0	1	23	10	0.9	2.8
azoxystrobin	positive	13.70	404.0	372.0	329.0	46	17	26	0.3	1.0
azoxystrobin-d4	positive	13.60	408.0	376.1	333.1	1	17	24	-	-
boscalid	positive	13.71	343.0	307.0	271.0	121	25	18	0.2	0.5
dimethomorph	positive	10.00	388.1	301.0	271.0	126	27	20	0.4	1.2
dimethomorph-d6	positive	10.05	394.0	307.0	271.1	101	27	18	-	-
metamitron	positive	1.32	203.0	175.0	104.0	61	21	10	0.7	2.0
methiocarb	positive	9.95	226.0	169.0	185.0	26	11	10	0.9	2.6
methiocarb-d3	positive	9.91	229.0	169.0	121.0	56	23	14	-	-
propiconazole	positive	16.60	342.0	159.0	123.0	81	33	18	0.5	1.4
propiconazole-d3	positive	16.79	345.0	162.0	126.0	61	35	10	-	-
S-metolachlor	positive	15.10	284.0	252.1	176.2	56	19	14	0.3	0.8
terbutylazine	positive	9.33	230.0	174.0	132.0	56	21	16	1.0	3.0
terbutylazine-d5	positive	9.18	235.0	179.0	137.0	56	33	16	-	-
thiacloprid	positive	2.28	253.0	126.0	186.0	61	27	14	0.8	2.4
thiacloprid-d4	positive	2.24	257.0	126.0	166.8	76	27	14	-	-

* based on the standard deviation of the response and the slope of the calibration curve (ranging from 0.1 to 20.0 $\mu\text{g L}^{-1}$) as proposed by ICH guidelines³⁷⁵

S2.10 Compound-Specific Carbon Isotope Analysis

S2.10.1 GC-IRMS Method

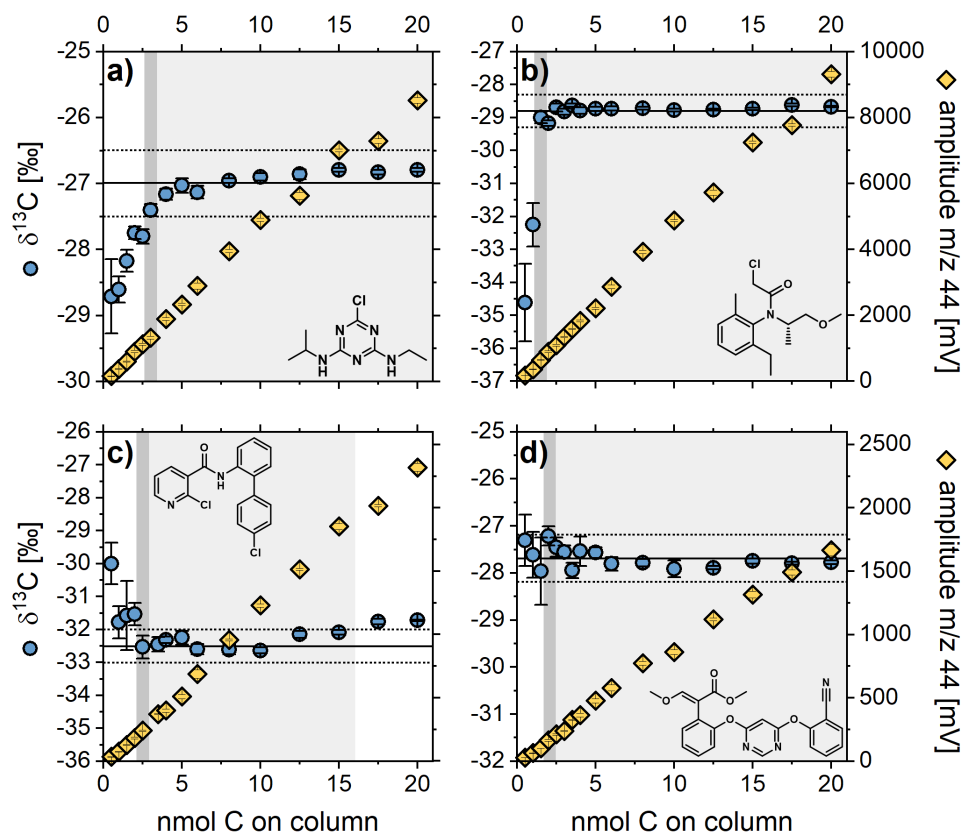


Figure S2.11. Amount-dependency of accurate carbon isotope ratio determination of the in-house standards of atrazine (a), *S*-metolachlor (b), boscalid (c), and azoxystrobin (d) by GC-IRMS. Blue circles represent mean $\delta^{13}\text{C}$ values in per mil and yellow diamonds the peak amplitudes of the main mass trace m/z 44 in mV. Error bars of both parameters reflect standard deviations ($\pm\sigma$) of quintuplicate measurements. Dark gray bars indicate method quantification limits (MQLs) determined according to the moving mean procedure reported by Jochmann et al.²⁶⁵ Calculated moving means are represented by solid lines encompassed by a ± 0.5 ‰ interval, that is, the typical uncertainty of $\delta^{13}\text{C}$ determination by GC-IRMS. Linear ranges of the GC-IRMS method are displayed by light gray rectangles.

Table S2.14. Method quantification limits (MQLs) of accurate carbon isotope analysis determined according to the moving mean procedure reported by Jochmann et al.²⁶⁵ with an uncertainty limit of ± 0.5 ‰. MQLs are expressed as injected concentration (mmol L^{-1}) and corresponding amount of carbon on column (nmol C). Mean peak amplitudes of mass m/z 44 are given in mV with standard deviations ($\pm\sigma$) of quintuplicate measurements.

analyte	MQL		amplitude m/z 44 (mV)
	mmol L^{-1}	nmol C on-column*	
atrazine	0.125	3.0	1332 ± 40
<i>S</i> -metolachlor	0.033	1.5	648 ± 9
boscalid	0.046	2.5	239 ± 6
azoxystrobin	0.030	2.0	166 ± 7

*corresponding to an injection volume of 3 μL

S2.10.2 Isotope Mass Balance

Carbon isotope ratios influenced by interfering unresolved complex mixture (UCM), $\delta^{13}\text{C}_{\text{calc}}$, were predicted using isotope mass balances according to equation (S2.4):

$$\delta^{13}\text{C}_{\text{calc}} = f_{\text{UCM}} \times \delta^{13}\text{C}_{\text{UCM}} + (1 - f_{\text{UCM}}) \times \delta^{13}\text{C}_{\text{analyte}} \quad (\text{S2.4})$$

where f_{UCM} is the fraction of UCM, and $\delta^{13}\text{C}_{\text{UCM}}$ and $\delta^{13}\text{C}_{\text{analyte}}$ are the isotope values of UCM and target analyte, respectively. To derive f_{UCM} , chromatograms (m/z 44) were first corrected for instrumental background (i.e., electronic offset determined with blank injections), and then integrated within analyte retention times specified by Isodat software. Contribution of UCM to the total peak area was distinguished using the baseline value given by the software as a threshold value. f_{UCM} was accordingly calculated as the ratio between the area contributed by UCM and the total peak area. $\delta^{13}\text{C}_{\text{UCM}}$ was estimated to reflect the mean isotopic composition of natural organic matter produced by photosynthesis of C3 plants (i.e. $\approx -27 \pm 1 \text{ ‰}$).^{267,376,377}

S2.11 Matrix-Dependent Limits of Accurate Carbon Isotope Analysis

Table S2.15. Deviations of carbon isotopic signatures ($\Delta\delta^{13}\text{C} \pm 95\% \text{ CI}$) of post-spiked atrazine, *S*-metolachlor, boscalid, and azoxystrobin from the original value for different extraction volumes on Oasis HLB and β -CDP, and corresponding carbon-normalized ratios of DOM and analyte in extracts. The data is presented in Figure 2.2 in Chapter 2.

compound	extracted volume [mL]	Oasis HLB		β -CDP	
		carbon-normalized ratio, $C_{\text{DOM}}/C_{\text{analyte}}$ [molC molC ⁻¹]	$\Delta\delta^{13}\text{C}$ [‰]	carbon-normalized ratio, $C_{\text{DOM}}/C_{\text{analyte}}$ [molC molC ⁻¹]	$\Delta\delta^{13}\text{C}$ [‰]
atrazine					
	20	7.4	0.1 ± 0.2	1.2	0.1 ± 0.2
	50	18.4	0.1 ± 0.2	3.1	0.1 ± 0.1
	100	36.8	0.0 ± 0.2	6.1	0.0 ± 0.2
	150	55.1	0.0 ± 0.2	9.2	0.2 ± 0.3
	200	73.5	0.0 ± 0.4	12.3	-0.1 ± 0.2
	300	110.3	0.1 ± 0.2	18.4	0.0 ± 0.1
<i>S</i> -metolachlor					
	20	7.4	0.1 ± 0.2	1.2	-0.1 ± 0.2
	50	18.4	0.4 ± 0.2	3.1	0.0 ± 0.1
	100	36.8	0.4 ± 0.1	6.1	0.0 ± 0.1
	150	55.1	0.3 ± 0.4	9.2	0.3 ± 0.1
	200	73.5	0.2 ± 0.1	12.3	0.3 ± 0.3
	300	110.3	0.3 ± 0.2	18.4	0.3 ± 0.2
boscalid					
	20	7.4	0.2 ± 0.3	1.2	0.0 ± 0.1
	50	18.4	0.8 ± 0.3	3.1	0.1 ± 0.3
	100	36.8	1.2 ± 0.6	6.1	0.1 ± 0.3
	150	55.1	1.4 ± 0.5	9.2	0.4 ± 0.3
	200	73.5	1.3 ± 0.3	12.3	1.0 ± 0.3
	300	110.3	1.1 ± 0.4	18.4	0.9 ± 0.3
azoxystrobin					
	20	7.4	0.1 ± 0.4	1.2	-0.1 ± 0.3
	50	18.4	0.2 ± 0.4	3.1	0.1 ± 0.3
	100	36.8	0.2 ± 0.3	6.1	-0.1 ± 0.3
	150	55.1	0.3 ± 0.3	9.2	0.0 ± 0.1
	200	73.5	0.3 ± 0.6	12.3	0.2 ± 0.3
	300	110.3	0.2 ± 0.5	18.4	0.2 ± 0.4

Table S2.16. GC-IRMS baseline response of Oasis HLB and β -CDP extracts as a function of enriched water volumes. The values reflect the slopes of the linear regressions of baseline values in Figure 2.2 in Chapter 2 including the standard error of the regression line and coefficients of determination (R^2).

analyte	baseline response (R^2) [mV L ⁻¹]	
	Oasis HLB	β -CDP
boscalid	0.25 ± 0.03 (0.94)	0.14 ± 0.02 (0.87)
atrazine	0.96 ± 0.03 (1.00)	0.32 ± 0.02 (0.97)
<i>S</i> -metolachlor	1.37 ± 0.07 (0.99)	0.44 ± 0.03 (0.97)
azoxystrobin	0.20 ± 0.03 (0.92)	0.10 ± 0.02 (0.81)

Table S2.17. Predicted deviations of carbon isotopic signatures ($\Delta\delta^{13}\text{C}_{\text{calc}}$) for samples extracted with Oasis HLB or β -CDP based on isotope mass balances (see S2.10.2), assuming a mean $\delta^{13}\text{C}$ value of matrix of -27 ± 1 ‰.^{267,376,377} Fractions of interfering matrix (f_{UCM}) at retention times of analytes were derived from GC-IRMS chromatograms. $\Delta\delta^{13}\text{C}_{\text{obs}} - \Delta\delta^{13}\text{C}_{\text{calc}}$ denote the difference between observed and predicted values. Propagated uncertainties reflect 95 % confidence intervals.

compound	sorbent	extracted volume [mL]	carbon-normalized ratio, $\text{C}_{\text{DOM}}/\text{C}_{\text{analyte}}$ [molC molC ⁻¹]	f_{UCM} [-]	$\Delta\delta^{13}\text{C}_{\text{calc}}$ [‰]	$\Delta\delta^{13}\text{C}_{\text{obs}}$ [‰]	$\Delta\delta^{13}\text{C}_{\text{obs}} - \Delta\delta^{13}\text{C}_{\text{calc}}$ [‰]
atrazine							
	Oasis HLB	20	7.4	0.02	0.0 ± 0.1	0.1 ± 0.2	0.1 ± 0.2
		50	18.4	0.06	0.0 ± 0.1	0.1 ± 0.2	0.1 ± 0.2
		100	36.8	0.12	0.0 ± 0.1	0.0 ± 0.2	0.0 ± 0.3
		150	55.1	0.22	0.0 ± 0.2	0.0 ± 0.2	0.0 ± 0.3
		200	73.5	0.25	0.0 ± 0.3	0.0 ± 0.4	0.0 ± 0.5
		300	110.3	n.a.	n.a.	0.1 ± 0.2	n.a.
	β -CDP	20	1.2	0.00	0.0 ± 0.1	0.1 ± 0.2	0.1 ± 0.3
		50	3.1	0.03	0.0 ± 0.1	0.1 ± 0.1	0.1 ± 0.2
		100	6.1	0.07	0.0 ± 0.1	0.0 ± 0.2	0.0 ± 0.2
		150	9.2	0.10	0.0 ± 0.1	0.2 ± 0.3	0.2 ± 0.3
		200	12.3	0.14	0.0 ± 0.2	-0.1 ± 0.2	-0.1 ± 0.3
		300	18.4	0.16	0.0 ± 0.2	0.0 ± 0.1	0.0 ± 0.2
<i>S</i> -metolachlor							
	Oasis HLB	20	7.4	0.04	0.1 ± 0.1	0.1 ± 0.2	0.0 ± 0.2
		50	18.4	0.09	0.2 ± 0.1	0.4 ± 0.2	0.2 ± 0.2
		100	36.8	0.19	0.3 ± 0.2	0.4 ± 0.1	0.1 ± 0.2
		150	55.1	0.33	0.6 ± 0.3	0.3 ± 0.4	-0.3 ± 0.5
		200	73.5	0.40	0.7 ± 0.4	0.2 ± 0.1	-0.5 ± 0.4
		300	110.3	n.a.	n.a.	0.3 ± 0.2	n.a.
	β -CDP	20	1.2	0.02	0.0 ± 0.1	-0.1 ± 0.2	-0.2 ± 0.2
		50	3.1	0.03	0.1 ± 0.1	0.0 ± 0.1	0.0 ± 0.1
		100	6.1	0.05	0.1 ± 0.1	0.0 ± 0.1	-0.1 ± 0.1
		150	9.2	0.12	0.2 ± 0.1	0.3 ± 0.1	0.1 ± 0.2
		200	12.3	0.14	0.3 ± 0.1	0.3 ± 0.3	0.1 ± 0.4
		300	18.4	0.23	0.4 ± 0.2	0.3 ± 0.2	-0.1 ± 0.3
boscalid							
	Oasis HLB	20	7.4	0.02	0.1 ± 0.1	0.2 ± 0.3	0.1 ± 0.4
		50	18.4	0.09	0.5 ± 0.1	0.8 ± 0.3	0.3 ± 0.3
		100	36.8	0.11	0.6 ± 0.1	1.2 ± 0.6	0.7 ± 0.6
		150	55.1	0.20	1.1 ± 0.2	1.4 ± 0.4	0.3 ± 0.4
		200	73.5	0.21	1.1 ± 0.2	1.3 ± 0.3	0.2 ± 0.4
		300	110.3	n.a.	n.a.	1.1 ± 0.4	n.a.
	β -CDP	20	1.2	0.02	0.1 ± 0.1	0.0 ± 0.1	-0.1 ± 0.2
		50	3.1	0.03	0.2 ± 0.1	0.1 ± 0.3	-0.1 ± 0.3
		100	6.1	0.03	0.2 ± 0.1	0.1 ± 0.3	-0.1 ± 0.3
		150	9.2	0.06	0.3 ± 0.1	0.4 ± 0.3	0.0 ± 0.3
		200	12.3	0.12	0.6 ± 0.1	1.0 ± 0.3	0.4 ± 0.4
		300	18.4	0.14	0.8 ± 0.2	0.9 ± 0.3	0.1 ± 0.3
azoxystrobin							
	Oasis HLB	20	7.4	0.01	0.0 ± 0.1	0.1 ± 0.4	0.1 ± 0.5
		50	18.4	0.04	0.0 ± 0.1	0.2 ± 0.4	0.2 ± 0.4
		100	36.8	0.04	0.0 ± 0.1	0.2 ± 0.3	0.2 ± 0.3
		150	55.1	0.19	0.2 ± 0.2	0.3 ± 0.3	0.1 ± 0.4
		200	73.5	0.36	0.3 ± 0.4	0.3 ± 0.6	0.0 ± 0.7
		300	110.3	n.a.	n.a.	0.2 ± 0.5	n.a.
	β -CDP	20	1.2	0.01	0.0 ± 0.1	-0.1 ± 0.3	-0.1 ± 0.3
		50	3.1	0.00	0.0 ± 0.1	0.1 ± 0.3	0.1 ± 0.3
		100	6.1	0.01	0.0 ± 0.1	-0.1 ± 0.3	-0.1 ± 0.3
		150	9.2	0.03	0.0 ± 0.1	0.0 ± 0.1	0.0 ± 0.2
		200	12.3	0.07	0.1 ± 0.1	0.2 ± 0.3	0.2 ± 0.3
		300	18.4	0.09	0.1 ± 0.1	0.2 ± 0.4	0.1 ± 0.4

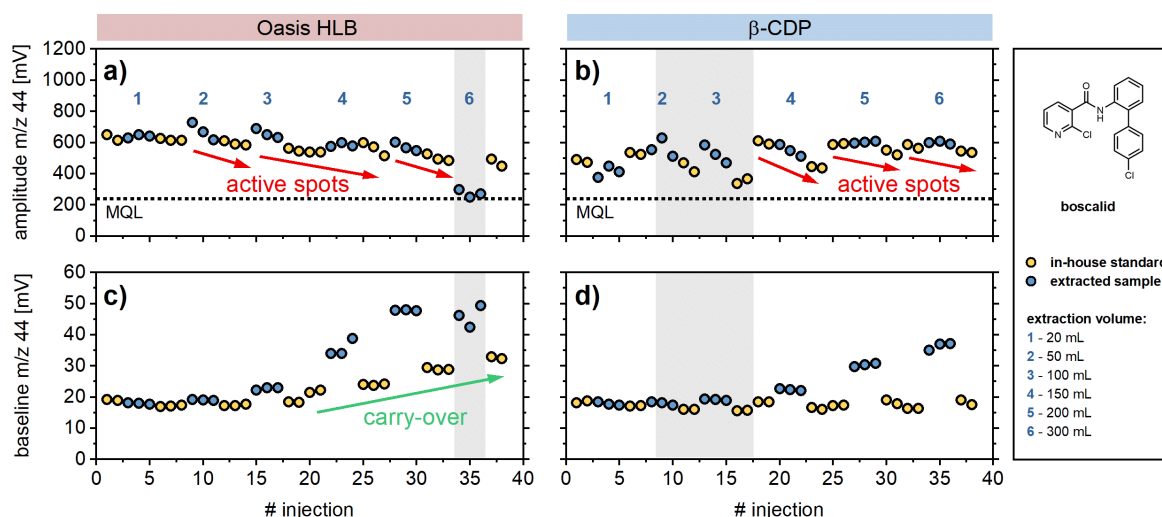


Figure S2.12. GC-IRMS intensities of the CO_2 peak (m/z 44, retention time of 15.78 min) corresponding to the analyte boscalid over the course of the measurement sequence of (a) Oasis HLB and (b) β -CDP samples, as well as associated GC-IRMS baseline values (c and d). Orange and blue circles represent in-house standards and extracted surface water samples, respectively, where the blue numbers refer to the extraction volume. Horizontal black lines in (a) and (b) represent the quantification limit of the GC-IRMS method for boscalid (refer to Table S2.14). Decreasing peak amplitudes were identified to be caused by active spots in the GC system which were removed by regular maintenance of GC liner and pre-column. Changes in amplitudes within gray areas originated from capillary leakages. Carry-over due to high matrix loads was observed for large volumes extracted with Oasis HLB.

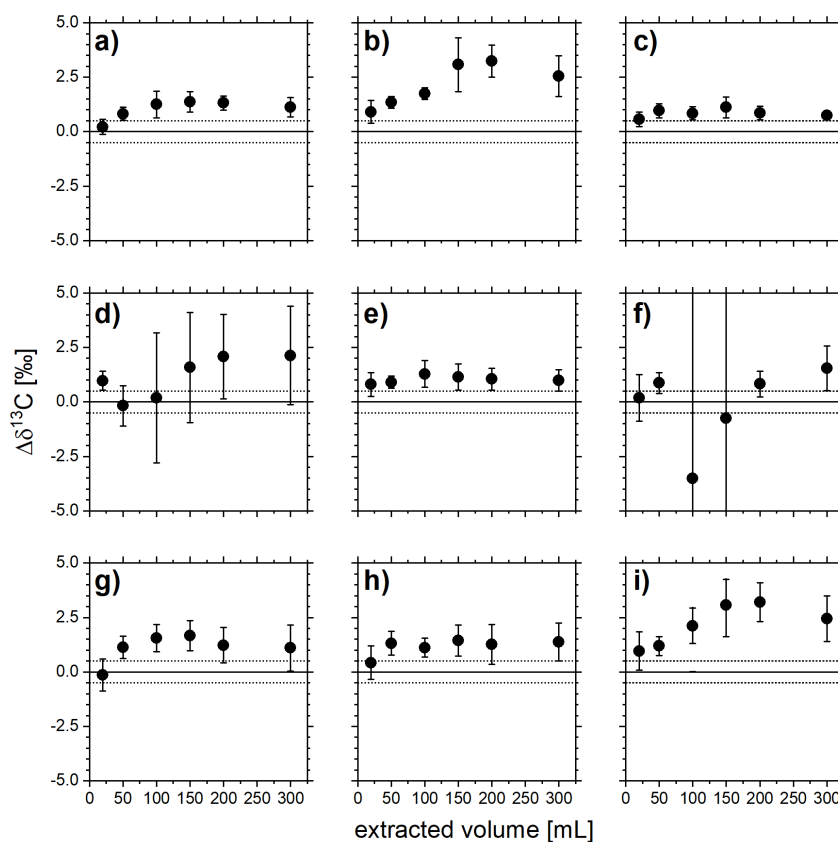


Figure S2.13. Deviations of carbon isotopic signatures ($\Delta\delta^{13}\text{C}$) of boscalid from the original value in Oasis HLB extracts obtained by SPE of different sample volumes and constant post-spiked analyte concentration in the extracts (corresponding to $1.67 \text{ mmol C L}^{-1}$). $\delta^{13}\text{C}$ values were determined applying the nine background correction algorithms offered by the Isodat software, namely a) individual, b) single, c) calc mean, d) median mean, e) low pass filtered, f) dynamic, g) base fit, h) skimmed, and i) time-based background correction. Propagated uncertainties reflect 95 % confidence intervals. For exact values refer to Table S2.18.

Table S2.18. Deviations of carbon isotopic signatures ($\Delta\delta^{13}\text{C}$) of boscalid from the original value in Oasis HLB extracts which contained a constant post-spiked analyte concentration (corresponding to $1.67 \text{ mmolC L}^{-1}$) but different amounts of extracted DOM, which are together expressed as carbon-normalized ratio of $C_{\text{DOM}}/C_{\text{analyte}}$. Comparison of $\Delta\delta^{13}\text{C}$ values obtained by applying all nine background correction algorithms offered by the Isodat software. Propagated uncertainties reflect 95 % confidence intervals.

$C_{\text{DOM}}/C_{\text{analyte}}$ in extract [molC molC ⁻¹]	$\Delta\delta^{13}\text{C}$ [%]								
	Individual	Single	Calc Mean	Median Mean	Low Pass Filtered	Dynamic	Base Fit	Skim-med	Time Based
7	0.2 ± 0.3	0.9 ± 0.5	0.6 ± 0.3	1.0 ± 0.4	0.8 ± 0.5	0.2 ± 1.1	-0.1 ± 0.7	0.4 ± 0.8	1.0 ± 0.9
18	0.8 ± 0.3	1.3 ± 0.3	1.0 ± 0.3	-0.2 ± 0.9	0.9 ± 0.3	0.9 ± 0.5	1.1 ± 0.5	1.3 ± 0.5	1.2 ± 0.4
37	1.2 ± 0.6	1.7 ± 0.3	0.8 ± 0.3	0.2 ± 3.0	1.3 ± 0.6	-3.5 ± 8.8	1.6 ± 0.6	1.1 ± 0.4	2.1 ± 0.8
55	1.4 ± 0.5	3.1 ± 1.2	1.1 ± 0.5	1.6 ± 2.5	1.1 ± 0.6	-0.7 ± 7.4	1.7 ± 0.7	1.4 ± 0.7	3.1 ± 1.4
74	1.3 ± 0.3	3.2 ± 0.7	0.8 ± 0.3	2.1 ± 1.9	1.0 ± 0.5	0.8 ± 0.6	1.2 ± 0.8	1.3 ± 0.9	3.2 ± 0.9
110	1.1 ± 0.4	2.5 ± 0.9	0.7 ± 0.2	2.1 ± 2.3	1.0 ± 0.5	1.5 ± 1.0	1.1 ± 1.1	1.4 ± 0.9	2.4 ± 1.1

S2.12 Recoveries of Target Analytes and Dissolved Organic Matter

Table S2.19. Recoveries of dissolved organic carbon (DOC) after solid-phase extraction of surface water at either pH 3 or pH 7 using conventional (i.e., Oasis HLB, LiChrolut EN, Supel-Select HLB) or cyclodextrin-based sorbents (i.e., α -, β -CDP). Uncertainties reflect one standard deviation ($\pm\sigma$) of experimental triplicates. The data is presented in Figure 2.3a in Chapter 2.

sorbent	DOC recovery [%]	
	pH 3	pH 7
Oasis HLB	43.3 \pm 3.5	9.6 \pm 1.2
LiChrolut EN	47.0 \pm 0.5	6.2 \pm 1.8
Supel-Select HLB	30.8 \pm 0.4	4.0 \pm 0.2
α -CDP	27.2 \pm 1.3	2.3 \pm 0.9
β -CDP	29.5 \pm 0.5	1.6 \pm 0.1

Table S2.20. Recoveries of target analytes after solid-phase extraction of spiked surface water at either pH 3 or pH 7 using conventional (i.e., Oasis HLB, LiChrolut EN, Supel-Select HLB) or cyclodextrin-based sorbents (i.e., α -, β -CDP). Data for methiocarb is not available for pH 7 due to instability of the analyte under neutral conditions. Uncertainties reflect one standard deviation ($\pm\sigma$) of experimental triplicates. The data is presented in Figure 2.3b and Figure 2.4 in Chapter 2.

analyte	log K_{ow} [-]	pH [-]	analyte recovery [%]				
			Oasis HLB	LiChrolut EN	Supel-Select HLB	α -CDP	β -CDP
2,6-dichloro-benzamide	0.77	3	68 \pm 5	83 \pm 7	26 \pm 1	23 \pm 3	32 \pm 2
		7	78 \pm 2	87 \pm 0	29 \pm 3	20 \pm 1	31 \pm 3
metamitron	0.85	3	87 \pm 8	89 \pm 0	54 \pm 5	51 \pm 0	67 \pm 9
		7	90 \pm 2	90 \pm 4	57 \pm 5	55 \pm 0	67 \pm 2
thiacloprid	1.26	3	91 \pm 7	80 \pm 1	73 \pm 3	88 \pm 3	84 \pm 8
		7	92 \pm 2	79 \pm 4	78 \pm 7	80 \pm 3	82 \pm 3
azoxystrobin	2.50	3	94 \pm 0	80 \pm 1	95 \pm 6	110 \pm 3	96 \pm 0
		7	107 \pm 3	89 \pm 4	104 \pm 10	108 \pm 0	108 \pm 3
dimethomorph	2.68	3	98 \pm 7	71 \pm 0	83 \pm 3	101 \pm 3	92 \pm 10
		7	103 \pm 3	73 \pm 0	93 \pm 11	102 \pm 3	99 \pm 5
atrazine	2.70	3	65 \pm 5	62 \pm 0	58 \pm 3	49 \pm 0	62 \pm 4
		7	104 \pm 0	107 \pm 5	99 \pm 8	66 \pm 3	100 \pm 0
boscalid	2.96	3	97 \pm 7	86 \pm 1	101 \pm 5	102 \pm 0	98 \pm 4
		7	94 \pm 2	90 \pm 5	101 \pm 10	97 \pm 7	97 \pm 0
S-metolachlor	3.05	3	98 \pm 6	87 \pm 7	80 \pm 4	79 \pm 3	93 \pm 3
		7	104 \pm 3	94 \pm 0	92 \pm 7	79 \pm 4	100 \pm 2
methiocarb	3.18	3	87 \pm 5	97 \pm 6	99 \pm 2	96 \pm 7	100 \pm 3
		7	n.a.	n.a.	n.a.	n.a.	n.a.
terbuthylazine	3.40	3	69 \pm 5	67 \pm 0	65 \pm 0	63 \pm 2	72 \pm 2
		7	97 \pm 0	99 \pm 6	94 \pm 10	77 \pm 0	100 \pm 3
propiconazole	3.72	3	101 \pm 7	89 \pm 0	95 \pm 3	105 \pm 3	103 \pm 3
		7	100 \pm 0	94 \pm 7	93 \pm 1	98 \pm 5	98 \pm 0

n.a. = not available

Table S2.21. Carbon-normalized ratios of C_{DOM} to C_{analyte} in extracts after solid-phase extraction of spiked surface water at either pH 3 or pH 7 using conventional (i.e., Oasis HLB, LiChrolut EN, Supel-Select HLB) or cyclodextrin-based sorbents (i.e., α -, β -CDP). Data for methiocarb is not available for pH 7 due to instability of the analyte under neutral conditions. Propagated uncertainties reflect one standard deviation ($\pm\sigma$) of experimental triplicates. The data is presented in Figure 2.3c in Chapter 2.

analyte	log K_{ow} [-]	pH [-]	$C_{\text{DOM}}/C_{\text{analyte}}$ in extract [molC molC^{-1}]				
			Oasis HLB	LiChrolut EN	Supel-Select HLB	α -CDP	β -CDP
2,6-dichloro-benzamide	0.77	3	3868 \pm 262	3453 \pm 302	7309 \pm 388	7325 \pm 843	5636 \pm 380
		7	745 \pm 18	433 \pm 1	836 \pm 74	697 \pm 41	324 \pm 29
metamitron	0.85	3	2254 \pm 209	2391 \pm 12	2608 \pm 225	2451 \pm 11	2009 \pm 275
		7	485 \pm 13	313 \pm 13	317 \pm 29	189 \pm 0	111 \pm 3
thiacloprid	1.26	3	2698 \pm 219	3355 \pm 35	2396 \pm 100	1765 \pm 58	1991 \pm 197
		7	594 \pm 14	447 \pm 21	286 \pm 26	161 \pm 6	113 \pm 4
azoxystrobin	2.50	3	1889 \pm 10	2418 \pm 18	1341 \pm 79	1017 \pm 31	1260 \pm 1
		7	369 \pm 10	288 \pm 14	157 \pm 15	87 \pm 0	62 \pm 2
dimethomorph	2.68	3	1837 \pm 134	2766 \pm 7	1530 \pm 61	1124 \pm 32	1324 \pm 141
		7	387 \pm 12	351 \pm 0	176 \pm 21	92 \pm 3	68 \pm 3
atrazine	2.70	3	4045 \pm 286	4623 \pm 5	3224 \pm 171	3364 \pm 5	2897 \pm 178
		7	557 \pm 0	352 \pm 17	241 \pm 20	210 \pm 9	99 \pm 0
boscalid	2.96	3	1904 \pm 128	2349 \pm 19	1306 \pm 61	1148 \pm 4	1285 \pm 56
		7	438 \pm 9	295 \pm 16	167 \pm 17	101 \pm 7	72 \pm 0
<i>S</i> -metolachlor	3.05	3	1886 \pm 107	2310 \pm 199	1644 \pm 73	1462 \pm 58	1348 \pm 49
		7	393 \pm 11	282 \pm 0	183 \pm 15	123 \pm 7	69 \pm 1
methiocarb	3.18	3	2303 \pm 132	2227 \pm 141	1435 \pm 25	1306 \pm 94	1361 \pm 35
		7	n.a.	n.a.	n.a.	n.a.	n.a.
terbuthylazine	3.40	3	3589 \pm 257	4041 \pm 12	2704 \pm 7	2474 \pm 70	2353 \pm 50
		7	564 \pm 0	361 \pm 22	242 \pm 25	170 \pm 1	93 \pm 3
propiconazole	3.72	3	2207 \pm 144	2701 \pm 4	1655 \pm 47	1335 \pm 40	1467 \pm 44
		7	493 \pm 2	336 \pm 26	218 \pm 2	119 \pm 6	85 \pm 0

n.a. = not available

Table S2.22. Total recovery of dissolved organic carbon (DOC) after solid-phase extraction of 20 mL surface water samples (at pH 3 and 7) using 10 mg of conventional (i.e., Oasis HLB, LiChrolut EN, Supel-Select HLB) or cyclodextrin-based sorbents (i.e., α -, β -CDP). Based on mass balances accounting for organic carbon loads in filtrates and eluates (see equation (2.3) in Chapter 2). Uncertainties reflect one standard deviation ($\pm\sigma$) of experimental triplicates.

sorbent	total DOC recovery [%]	
	pH 3	pH 7
Oasis HLB	95.9 \pm 2.6	98.8 \pm 0.6
LiChrolut EN	98.7 \pm 3.0	99.6 \pm 1.9
Supel-Select HLB	101.7 \pm 0.4	100.6 \pm 1.1
α -CDP	100.5 \pm 2.6	100.4 \pm 0.5
β -CDP	96.1 \pm 0.7	100.6 \pm 0.6

S2.13 Effect of Concurrent Dissolved Organic Matter on Gibbs Free Energy of Adsorption

Table S2.23. Recoveries, capacity factors (k) and partition coefficients (K_d) of 2,6-dichlorobenzamide (BAM) obtained from column chromatography experiments (25 ± 1 °C) using SiC supported sorbent columns (1 % sorbent, w/w) and varying background Aldrich humic acid concentrations in the mobile phase (DOC ranging from 0 to 5 mgC L⁻¹). Recoveries were obtained by comparing integrated peak areas of triplicate injections with the peak area of the same amount of analyte without passing a column. Propagated uncertainties reflect one standard deviation ($\pm\sigma$) of experimental triplicates.

sorbent	DOC [mg L ⁻¹]	recovery [%]	capacity factor, k [-]	K_d [L kg ⁻¹]	sorbent	DOC [mg L ⁻¹]	recovery [%]	capacity factor, k [-]	K_d [L kg ⁻¹]
α -CDP	0.00	96 \pm 1	0.200	44 \pm 1	Oasis HLB	0.00	n.a.	0.692	156 \pm 2
	1.25	98 \pm 1	0.183	40 \pm 1		1.25	99 \pm 1	0.559	126 \pm 1
	2.50	103 \pm 1	0.183	40 \pm 1		2.50	100 \pm 5	0.548	123 \pm 7
	3.75	101 \pm 1	0.178	39 \pm 1		3.75	91 \pm 2	0.484	109 \pm 5
	5.00	90 \pm 1	0.165	36 \pm 1		5.00*	111 \pm 2	n.d.	n.d.
β -CDP	0.00	n.a.	0.386	94 \pm 1	LiChrolut EN	0.00	105 \pm 1	2.511	610 \pm 2
	1.25	108 \pm 1	0.378	92 \pm 1		1.25	102 \pm 1	2.476	599 \pm 5
	2.50	108 \pm 1	0.375	91 \pm 1		2.50*	111 \pm 1	n.d.	n.d.
	3.75	106 \pm 2	0.371	90 \pm 2		3.75	105 \pm 1	2.418	587 \pm 5
	5.00	98 \pm 1	0.367	89 \pm 1		5.00	98 \pm 1	2.330	566 \pm 6
γ -CDP	0.00	98 \pm 1	0.803	197 \pm 2	Supel- Select HLB	0.00	98 \pm 1	0.364	80 \pm 2
	1.25	106 \pm 1	0.772	190 \pm 1		1.25	104 \pm 1	0.312	68 \pm 1
	2.50*	120 \pm 3	n.d.	n.d.		2.50	108 \pm 1	0.298	65 \pm 1
	3.75	106 \pm 2	0.761	187 \pm 2		3.75	109 \pm 3	0.293	64 \pm 1
	5.00	102 \pm 2	0.747	183 \pm 2		5.00	97 \pm 2	0.270	59 \pm 1

*data points were excluded since recovery was beyond quality limit of 90 to 110 %, n.a. = not available, n.d. = not determined

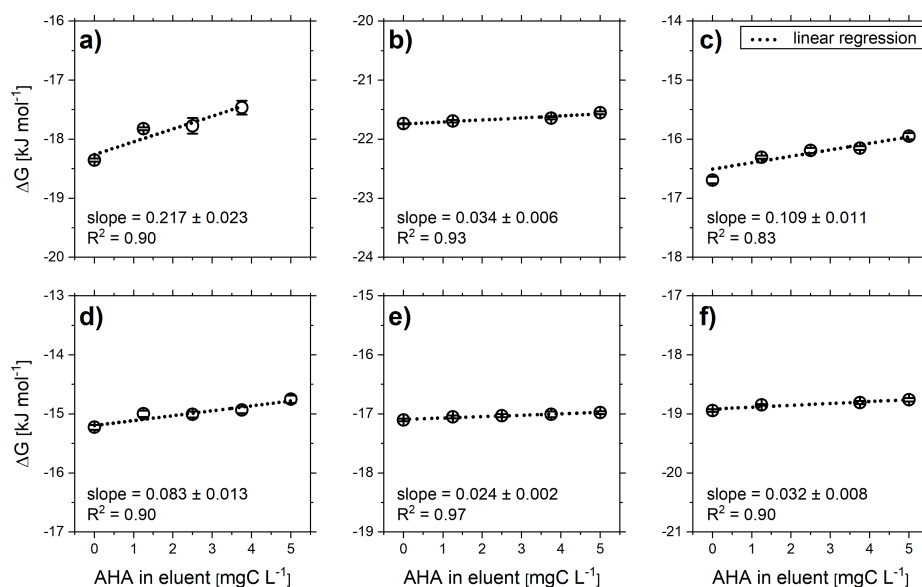


Figure S2.14. Changes of Gibbs free energy (ΔG^0) involved in the sorption process of 2,6-dichlorobenzamide (BAM) onto (a) Oasis HLB, (b) LiChrolut EN, (c) Supel-Select HLB, (d) α -CDP, (e) β -CDP, and (f) γ -CDP influenced by varying concentrations of concurrent Aldrich humic acid (0 to 5 mgC L⁻¹) in the mobile phase of the HPLC system. Experiments were performed at 25 ± 1 °C. Dotted lines represent linear regressions, the slopes of which were used to derive $\Delta\Delta G^0$ values as a function of concurrent DOC.

S2.14 Validation of Carbon Isotopic Integrity after Solid-Phase Extraction of Surface Water on β -Cyclodextrin Polymer

Table S2.24. Deviations of carbon isotopic signatures from original values ($\Delta\delta^{13}\text{C}$) and corresponding recoveries of atrazine, *S*-metolachlor, boscalid, and azoxystrobin after SPE on β -CDP performed under varying pre-spiked analyte concentrations and linear flow velocities, as well as successive extraction cycles after sorbent regeneration (see Table S2.7). Propagated uncertainties reflect 95 % confidence intervals for $\Delta\delta^{13}\text{C}$ and one standard deviation ($\pm\sigma$) of triplicate experiments for recoveries. The data is presented in Figure 2.6 in Chapter 2.

analyte	concentration dependency			flow dependency			sorbent regeneration		
	spiked conc.	$\Delta\delta^{13}\text{C}$ $\pm \text{CI}_{95\%}$	recovery $\pm \sigma$	lin. flow vel.	$\Delta\delta^{13}\text{C}$ $\pm \text{CI}_{95\%}$	recovery $\pm \sigma$	extraction cycle	$\Delta\delta^{13}\text{C}$ $\pm \text{CI}_{95\%}$	recovery $\pm \sigma$
	[$\mu\text{g L}^{-1}$]	[‰]	[%]	[cm min^{-1}]	[‰]	[%]	[-]	[‰]	[%]
atrazine									
	5	-0.1 \pm 0.3	99 \pm 1	4.9	0.0 \pm 0.1	97 \pm 3	1	0.0 \pm 0.1	97 \pm 3
	25	0.0 \pm 0.2	93 \pm 0	12.3	0.0 \pm 0.1	93 \pm 1	2	0.0 \pm 0.1	89 \pm 1
	50	-0.1 \pm 0.2	99 \pm 3	19.6	0.0 \pm 0.1	86 \pm 2	3	0.0 \pm 0.1	92 \pm 2
	100	0.0 \pm 0.3	93 \pm 0	24.6	-0.1 \pm 0.2	94 \pm 1	4	-0.1 \pm 0.3	86 \pm 2
	150	0.0 \pm 0.1	97 \pm 3	29.5	0.1 \pm 0.1	95 \pm 3	5	-0.2 \pm 0.1	89 \pm 1
	250	0.0 \pm 0.0	94 \pm 5	34.4	0.0 \pm 0.2	101 \pm 2	6	-0.3 \pm 0.2	88 \pm 2
	500	-0.1 \pm 0.1	93 \pm 2	39.3	0.0 \pm 0.1	99 \pm 6	7	-0.1 \pm 0.1	92 \pm 2
<i>S</i> -metolachlor									
	5	0.1 \pm 0.1	105 \pm 1	4.9	0.2 \pm 0.1	100 \pm 1	1	0.2 \pm 0.1	100 \pm 1
	25	0.1 \pm 0.1	101 \pm 0	12.3	-0.1 \pm 0.1	100 \pm 2	2	0.1 \pm 0.1	96 \pm 3
	50	-0.1 \pm 0.2	102 \pm 1	19.6	0.1 \pm 0.2	98 \pm 1	3	0.2 \pm 0.1	96 \pm 2
	100	0.0 \pm 0.1	100 \pm 5	24.6	0.1 \pm 0.2	101 \pm 0	4	0.1 \pm 0.2	101 \pm 1
	150	0.2 \pm 0.1	100 \pm 1	29.5	0.0 \pm 0.2	101 \pm 3	5	0.2 \pm 0.2	99 \pm 2
	250	0.1 \pm 0.3	103 \pm 3	34.4	0.0 \pm 0.2	101 \pm 2	6	0.2 \pm 0.1	98 \pm 2
	500	0.1 \pm 0.1	104 \pm 4	39.3	-0.1 \pm 0.1	103 \pm 3	7	-0.1 \pm 0.1	100 \pm 0
boscalid									
	5	0.1 \pm 0.2	102 \pm 3	4.9	0.0 \pm 0.3	100 \pm 1	1	0.0 \pm 0.3	100 \pm 1
	25	0.0 \pm 0.1	103 \pm 0	12.3	-0.2 \pm 0.2	100 \pm 2	2	0.0 \pm 0.2	100 \pm 3
	50	0.0 \pm 0.2	102 \pm 0	19.6	-0.2 \pm 0.2	101 \pm 1	3	0.1 \pm 0.3	101 \pm 2
	100	0.2 \pm 0.4	101 \pm 1	24.6	0.0 \pm 0.1	101 \pm 3	4	0.1 \pm 0.2	99 \pm 1
	150	0.0 \pm 0.3	100 \pm 1	29.5	-0.1 \pm 0.2	102 \pm 2	5	0.0 \pm 0.2	101 \pm 1
	250	0.1 \pm 0.3	103 \pm 1	34.4	0.0 \pm 0.2	103 \pm 1	6	0.0 \pm 0.1	101 \pm 2
	500	0.0 \pm 0.1	99 \pm 2	39.3	0.0 \pm 0.2	103 \pm 3	7	0.0 \pm 0.1	103 \pm 4
azoxystrobin									
	5	0.1 \pm 0.3	99 \pm 2	4.9	-0.1 \pm 0.1	98 \pm 1	1	-0.1 \pm 0.1	98 \pm 1
	25	0.2 \pm 0.2	101 \pm 1	12.3	-0.2 \pm 0.2	98 \pm 2	2	0.0 \pm 0.1	74 \pm 3
	50	0.1 \pm 0.4	101 \pm 2	19.6	-0.1 \pm 0.2	98 \pm 0	3	0.1 \pm 0.2	79 \pm 4
	100	0.0 \pm 0.1	98 \pm 1	24.6	-0.1 \pm 0.2	100 \pm 3	4	0.0 \pm 0.2	72 \pm 3
	150	-0.1 \pm 0.1	98 \pm 1	29.5	0.0 \pm 0.3	100 \pm 0	5	0.1 \pm 0.1	80 \pm 2
	250	0.1 \pm 0.3	90 \pm 1	34.4	-0.1 \pm 0.1	100 \pm 2	6	-0.2 \pm 0.0	81 \pm 2
	500	0.0 \pm 0.1	98 \pm 6	39.3	-0.1 \pm 0.2	103 \pm 1	7	0.1 \pm 0.1	74 \pm 3

Table S2.25. Linear flow velocities and corresponding volumetric flow rates for 1, 3, 6 mL SPE cartridges and 47 mm SPE disks for which carbon isotope integrity of analytes was investigated after SPE of spiked surface water samples ($V = 20$ mL, $c = 150 \mu\text{g L}^{-1}$) using β -CDP as SPE sorbent.

linear flow velocity [cm min ⁻¹]	volumetric flow rate* [mL min ⁻¹]				
	1 mL cartridge, modified [†]	1 mL cartridge [‡]	3 mL cartridge [§]	6 mL cartridge [¶]	47 mm disk [•]
4.9	0.5	1.2	3.1	6.1	85.2
12.3	1.3	3.0	7.6	15.3	213.1
19.6	2.0	4.8	12.2	24.5	340.9
24.6	2.5	6.0	15.3	30.6	426.1
29.5	3.0	7.3	18.3	36.8	511.3
34.4	3.5	8.5	21.4	42.9	596.6
39.3	4.0	9.7	24.4	49.0	681.8

*based on cross-sectional areas of SPE cartridges of [†]0.10, [‡]0.25, [§]0.62, [¶]1.25, and [•]17.35 cm²

S3 Supporting Information to Chapter 3

S3.1 Chemicals and Materials

All reagents and solvents used in this study, including their CAS number, purity, and supplier are summarized in Table S3.1. The commercial SPE sorbents Bond Elut PPL, Oasis HLB, LiChrolut EN, and Supel-Select HLB were purchased from Agilent (Santa Clara, CA, USA), Waters (Milford, MA, USA), Merck Millipore (Burlington, MA, USA), and Sigma-Aldrich (Taufkirchen, Germany), respectively. Bulk sorbents were packed into polypropylene SPE cartridges (1 mL) equipped with polyethylene frits (20 μm pore size) both obtained from Sigma-Aldrich (Taufkirchen, Germany). Nylon membrane filters (47 mm diameter, 0.45 μm pore size) were purchased from GVS Filter Technology (Bologna, Italy). Ultrapure water (18.2 M Ω cm at 25 °C) was produced with a Milli-Q® Reference water purification system (Merck Millipore, USA).

Table S3.1. List of reagents and solvents used for sorbent and sample preparation in this study.

Chemical	CAS number	Purity/Grade (further info.)	Supplier
<i>Reagents</i>			
hydrochloric acid	7647-01-0	ACS reagent, 37 %	Sigma-Aldrich
potassium carbonate	584-08-7	BioXtra, ≥ 99.0 %	Sigma-Aldrich
potassium hydrogen phthalate	877-24-7	BioXtra, ≥ 99.95 %	Sigma-Aldrich
sodium hydroxide	1310-73-2	BioXtra, ≥ 98 %	Sigma-Aldrich
tetrafluoroterephthalonitrile	1835-49-0	99 %	Sigma-Aldrich
β -cyclodextrin	7585-39-9	≥ 97.0 %	Sigma-Aldrich
<i>Solvents</i>			
dichloromethane	75-09-2	EMSURE®, for analysis	Sigma-Aldrich
methanol	67-56-1	≥ 99.9 %	Sigma-Aldrich
<i>N,N</i> -dimethylformamide	68-12-2	anhydrous, 99.8 %	Sigma-Aldrich
tetrahydrofuran	109-99-9	anhydrous, ≥ 99.9 %, inhibitor-free	Sigma-Aldrich

S3.2 Preparation and Characterization of β -Cyclodextrin Polymer

S3.2.1 Synthesis of Porous β -Cyclodextrin Polymer

Porous β -cyclodextrin polymer was prepared according to the improved synthesis procedure reported by Alsaiee et al.,¹⁹³ which is based on the nucleophilic aromatic substitution of β -cyclodextrin hydroxyl groups by the cross-linker tetrafluoroterephthalonitrile (TFN). In short, a flame-dried 500 mL round-bottom flask was charged with 4.1 g of β -cyclodextrin, 2.0 g of TFN, and 6.4 g of potassium carbonate. After adding 160 mL of anhydrous tetrahydrofuran/dimethylformamide mixture (9:1, v/v), the flask was connected to a reflux condenser, and the system was flushed with nitrogen for 10 min. After removing the nitrogen inlet, the reflux condenser was closed with a septum. The mixture was placed in an oil bath (85 °C) and stirred for 48 h. Subsequently, the suspension was slowly cooled to room temperature where the solids could settle to the bottom of the flask. The supernatant was

decanted, and the residual potassium carbonate was removed by washing with 1M hydrochloric acid until CO₂ evolution stopped. The remaining suspension was filtered and sequentially washed with 250 mL of ultrapure water (Milli-Q®, Merck Millipore, USA), 200 mL of tetrahydrofuran, 200 mL of dichloromethane and 200 mL of methanol. The yellow powder was dried under vacuum at room temperature for two days and finally sedimented in methanol to obtain particle sizes larger than 40 μm.

S3.2.2 Field Emission Scanning Electron Microscope (FESEM) Imaging

Field emission scanning electron microscope (FESEM) imaging of β-cyclodextrin polymer (β-CDP) was carried out on a Sigma 300 VP instrument (Carl Zeiss Microscopy GmbH, Jena, Germany) using an accelerating voltage of 10.0 kV and a sample distance of 6 mm. FESEM images at magnifications of 1.10×10^3 and 2.82×10^3 showing the highly porous surface morphology of β-CDP are depicted in Figure S3.1a and b, respectively.

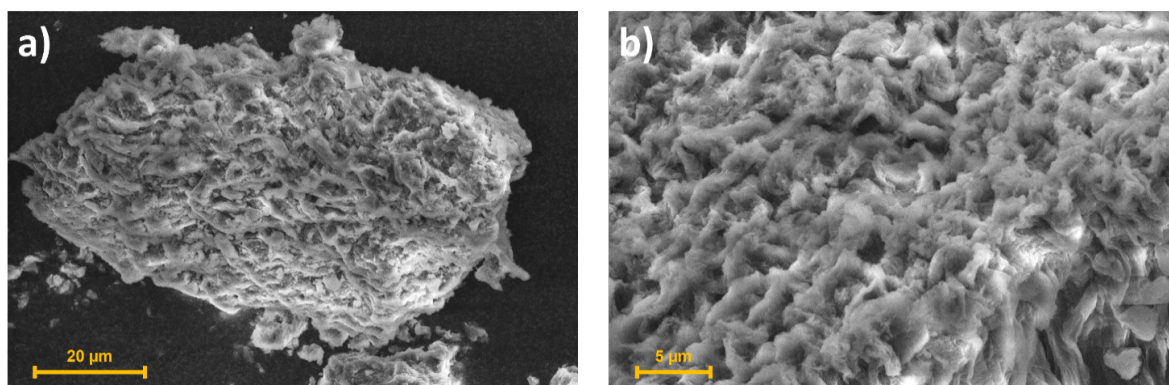


Figure S3.1. Field emission scanning electron microscope (FESEM) images of cross-linked β-cyclodextrin polymer (β-CDP) at magnifications of (a) 1.10×10^3 and (b) 2.82×10^3 .

S3.2.3 Fourier Transform Infrared Spectroscopy

Fourier transform infrared (FTIR) spectra (solid, attenuated total reflectance, ATR) were recorded using a Nicolet 6700 FT-IR spectrometer (Thermo Scientific, USA) at a wavenumber range of 4000 to 650 cm⁻¹ and a resolution of 4 cm⁻¹. The signal-to-noise ratio was improved by accumulating 32 individually recorded scans. Baseline correction was performed using the software OriginPro 2020.

FTIR spectrum of β-CD building block showed intense absorbance at 1030 cm⁻¹, corresponding to polysaccharide C-O stretch vibrations, as well as aliphatic C-H stretch vibrations at 2930 cm⁻¹ and O-H stretch vibrations around 3400 cm⁻¹ (Figure S3.2). These spectral features were also found in spectra of the cross-linked polymer (β-CDP). Furthermore, β-CDP exhibited nitrile stretches resonating at 2235 cm⁻¹ and C-F stretch vibrations at 1268 cm⁻¹, which confirmed successful incorporation of the cross-linker TFN. Compared with the spectrum of neat TFN, C-F absorption band in the β-CDP spectrum was less pronounced as expected for partial substitution of fluorine during synthesis. Finally,

peaks appearing at 1670 cm^{-1} and 1463 cm^{-1} are assigned to aromatic C=C stretches of both β -CD and TFN.

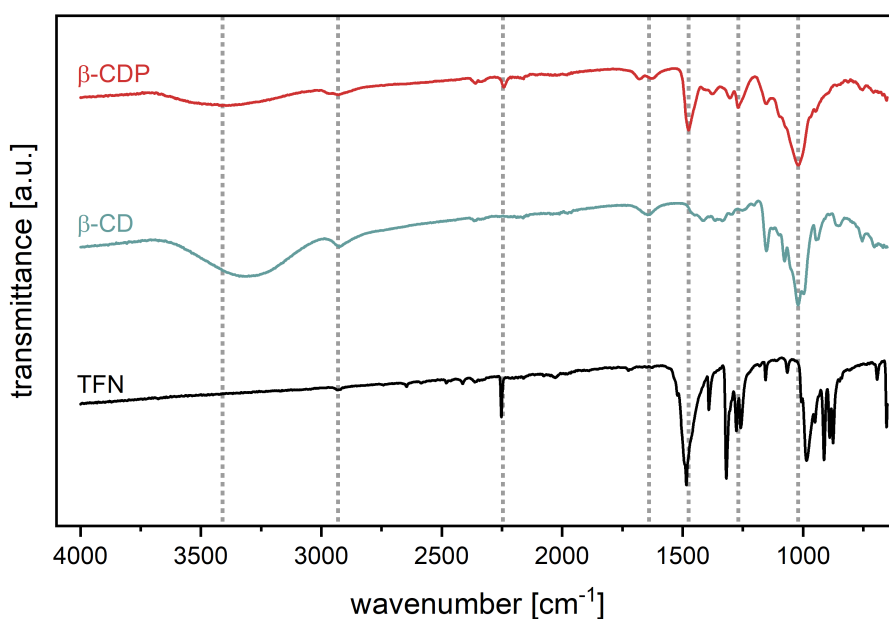


Figure S3.2. Fourier transform infrared (FTIR) spectra of β -cyclodextrin (β -CD, green), synthesized β -cyclodextrin polymer (β -CDP, red), and the cross-linker tetrafluoroterephthalonitrile (TFN, black). Dashed vertical lines represent TFN specific absorption bands at 1268 cm^{-1} (C-F stretch vibrations) and 2235 cm^{-1} (nitrile stretch vibrations), CD specific absorption bands at 1030 cm^{-1} (C-O stretch vibrations), 2930 cm^{-1} (aliphatic C-H stretch vibrations), and 3400 cm^{-1} (O-H stretch vibrations), and common aromatic C=C stretch vibrations at 1464 cm^{-1} and 1670 cm^{-1} .

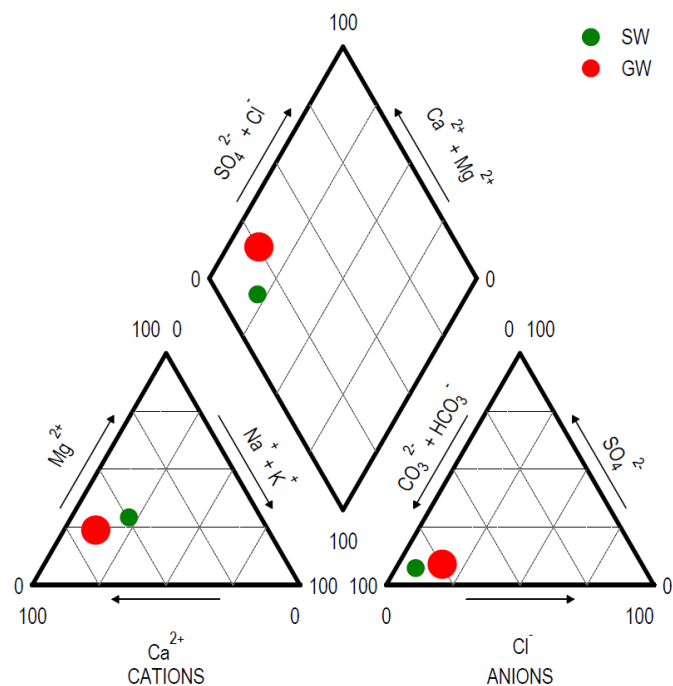
S3.3 Water Sample Collection and Treatment

Surface water (SW) was sampled in the creek Wiesäckerbach close to the Department of Chemistry of the Technical University of Munich in Garching, Germany (latitude 48.268028 , longitude 11.667509), whereas a groundwater sample (GW) was taken in a well near lake Wörthsee, Germany (latitude 48.071860 , longitude 11.187960). Samples were collected in glass bottles previously rinsed with methanol, ultrapure water, and pristine water sample. After refrigerated transport to the laboratory, water samples were immediately passed through pre-washed $0.45\text{ }\mu\text{m}$ nylon membrane filters (GVS Filter Technology, Bologna, Italy). Water samples contained 3.2 mgC L^{-1} (SW) and 7.7 mgC L^{-1} (GW), respectively. Other physicochemical parameters are given in Table S3.2. Both samples are classified as calcium bicarbonate waters, which reflect typical aquifer lithologies of the North Alpine foreland basin (Figure S3.3). Samples were separated into two aliquots, which were manually adjusted to either pH 2 or pH 7 using 1M HCl or 1M NaOH. Finally, samples were stored at $4\text{ }^{\circ}\text{C}$ in the dark until further experiments were performed as described in Chapter 3.2.

Table S3.2. Physicochemical properties of natural water samples used for experiments in this study.

parameter	unit	SW*	GW [†]
pH	-	6.8	6.6
Conductivity	$\mu\text{S cm}^{-1}$	385	1008
Acid capacity	mmol L^{-1}	5.03	7.37
DOC	mg L^{-1}	3.18	7.71
Sodium (Na^+)	mg L^{-1}	12.50	21.30
Potassium (K^+)	mg L^{-1}	35.00	9.80
Ammonium (NH_4^+)	mg L^{-1}	< 0.04	< 0.04
Calcium (Ca^{2+})	mg L^{-1}	65.88	127.80
Magnesium (Mg^{2+})	mg L^{-1}	23.60	28.50
Fluoride (F^-)	mg L^{-1}	< 0.10	< 0.10
Chloride (Cl^-)	mg L^{-1}	15.47	57.68
Bromate (BrO_3^-)	mg L^{-1}	< 0.10	< 0.10
Bromide (Br^-)	mg L^{-1}	< 0.10	< 0.10
Iodide (I^-)	mg L^{-1}	< 0.10	< 0.10
Nitrite (NO_2^-)	mg L^{-1}	< 0.05	< 0.05
Nitrate (NO_3^-)	mg L^{-1}	1.26	6.00
Sulfate (SO_4^{2-})	mg L^{-1}	20.45	42.25
Hydrogen phosphate (HPO_4^{2-})	mg L^{-1}	< 0.10	< 0.10
Hydrogen carbonate (HCO_3^-)	mg L^{-1}	306.80	449.80

* surface water from the creek Wiesäckerbach

[†] groundwater from a well near lake Wörthsee**Figure S3.3.** Piper plots for hydrochemical characterization of the surface (SW) and groundwater (GW) samples used for experiments in this study. Both water samples are classified as calcium bicarbonate waters, which reflect typical aquifer lithologies of the North Alpine foreland basin. Symbol sizes reflect amount of total dissolved solids (TDS), which amounted to 250 mg L^{-1} for SW and 655 mg L^{-1} for GW.

S3.4 Solid-Phase Extraction of Dissolved Organic Matter

S3.4.1 DOM Extraction Using β -CDP and Conventional Sorbents

Table S3.3. Parameters of solid-phase extraction (SPE) of surface water (SW) and groundwater samples (GW), including sample volume (V_{sample}), sorbent bed weight of self-packed SPE cartridges (m_{sorbent}), dissolved organic carbon (DOC) concentration of water samples, and quality control parameters (i.e., DOC and sample volume per mass sorbent).

sample	V_{sample} [mL]	m_{sorbent} [mg]	DOC			DOC/ m_{sorbent} * [mmol g ⁻¹]	$V_{\text{sample}}/m_{\text{sorbent}}$ † [L g ⁻¹]
			[mg L ⁻¹]	[mmol L ⁻¹]	[mmol]		
SW	50.0	25.0	3.2	0.26	0.013	0.53	2.0
GW	50.0	25.0	7.7	0.64	0.032	1.28	2.0

* maximum threshold: 2 mmol g⁻¹, proposed by Dittmar et al.²⁹³

† maximum threshold: 10 L g⁻¹, proposed by Dittmar et al.²⁹³

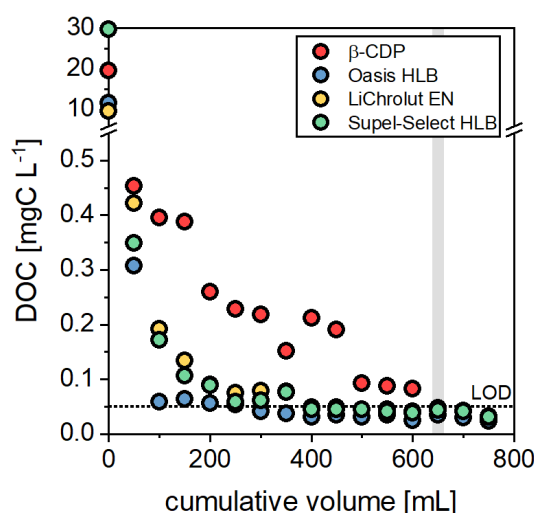


Figure S3.4. Dissolved organic carbon (DOC) concentrations in SPE breakthrough volumes of ultrapure water caused by organic carbon leaching from sorbent material. The horizontal dashed line represents the instrumental limit of detection (LOD) and the gray rectangular indicates the volume used for sorbent conditioning, in order to reduce organic carbon bleed from the sorbent material.

S3.4.2 Extraction of Representative DOM Spectra

To characterize molecular DOM compositions of both the original water samples and SPE permeates, we extracted these samples using the functionalized styrene divinylbenzene sorbent Bond Elut PPL (Agilent, CA, USA) as proposed by Li and co-workers.²⁹² Since the proprietary PPL phase offers selectivity toward a vast range of bulk environmental DOM compounds (including highly polar species),¹⁷⁷ it is most effective in extracting a representative spectrum of DOM constituents,^{289,292,293} and in turn recommended for DOM isolation from natural water.²⁸⁷ Prior to loading of 50 mL sample, SPE cartridges (25 mg sorbent, Table S3.3) were conditioned with 1 mL of methanol followed by 1 mL of ultrapure water (pH 2). The acidified samples (pH 2) were then percolated through the cartridges at a volumetric flow rate of ≤ 1.0 mL min⁻¹ corresponding to a linear flow velocity of ≤ 4.1 cm min⁻¹. Subsequently, the cartridges were washed with 1 mL of ultrapure water (pH 2), dried under vacuum overnight, and eluted with 1 mL of methanol.

S3.5 Determination of Dissolved Organic Matter

Dissolved organic carbon (DOC) concentrations were determined as nonpurgeable organic carbon (NPOC) using a total organic carbon analyzer (TOC-L, Shimadzu, Japan) equipped with a combustion catalytic oxidation reactor (680 °C) and a nondispersive infrared (NDIR) detector. The instrument was calibrated immediately prior to sample analysis by measuring standard solutions of potassium hydrogen phthalate. Quality control measurements of bracketed blanks ensured background DOC values below the detection limit of the instrument (i.e., 0.05 mg L⁻¹). DOC concentrations in methanolic extracts were measured and validated after complete evaporation of the organic solvent under a gentle stream of nitrogen at 65 °C using an automated solvent evaporation system (TurboVap LV, Biotage, Sweden), followed by reconstitution of the dry residues in ultrapure water by ultrasonication for 15 min and vortex mixing for 1 min.

S3.6 Compound Class Assignment in the Van Krevelen Diagram

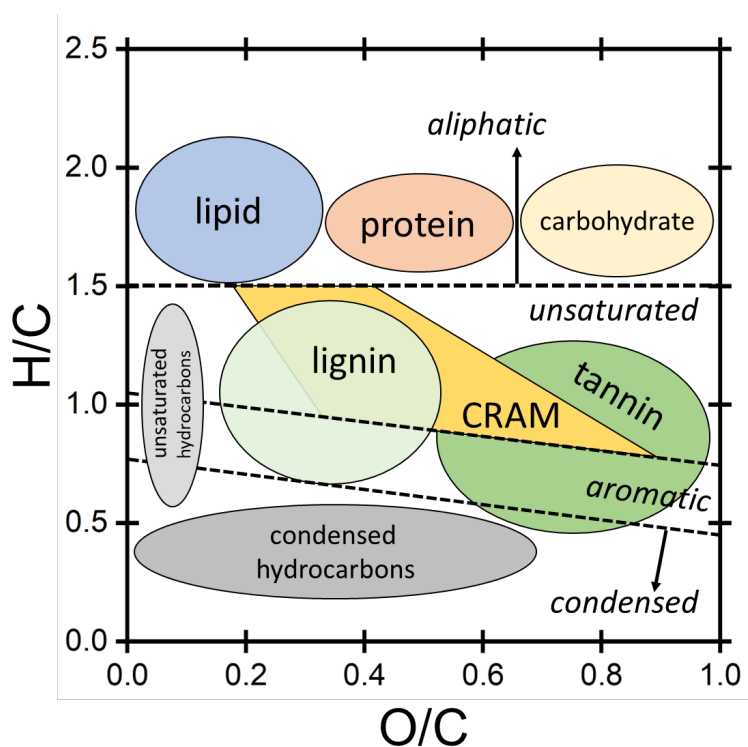


Figure S3.5. Approximate areas of different compound classes in the van Krevelen diagram based on the characteristic H/C versus O/C ratios of the biogeochemical precursor materials as derived from previous studies.^{213-216,294,296-299} The assignment of the aromatic and condensed regions in the van Krevelen diagram was based on the modified aromaticity index (AI_{mod}) proposed by Koch and Dittmar,^{230,231} where AI_{mod} values ≥ 0.5 indicate the aromatic character of molecules.

S3.7 Molecular-Level Characterization of SPE Permeates by FTICR MS

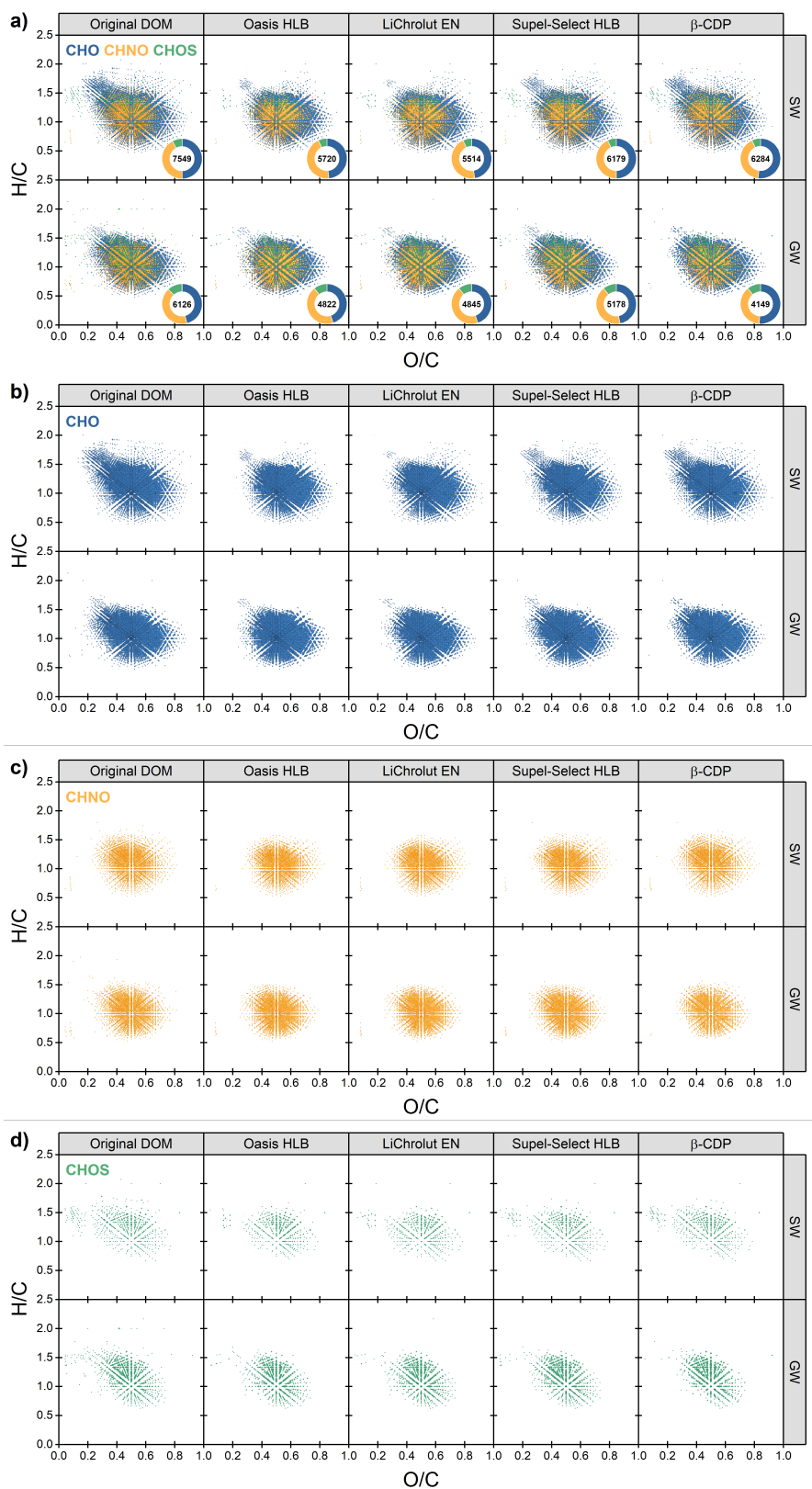


Figure S3.6. (a) Molecular composition of original surface water (SW) and groundwater (GW) DOM compared with DOM in permeates after SPE with conventional (i.e., Oasis HLB, LiChrolut EN, Supel-Select HLB) and β -CDP sorbent projected onto van Krevelen diagrams. Symbols are color-coded according to CHO (blue), CHNO (orange), and CHOS (green) molecular series. Symbol sizes reflect relative signal intensities of each mass peak. Insert pie charts indicate relative proportions of molecular series, with total number of assigned formulas provided. Panels (b) – (d): van Krevelen diagrams for individual molecular series.

Table S3.4. Counts and relative proportions (in brackets) of m/z ions for original and sorbent permeate DOM sorted according to CHO, CHNO, and CHOS molecular composition; intensity-weighted averages of elemental compositions, elemental and mass-to-charge ratios, and chemical indices; and percentages of aromatic compounds as computed from negative ESI 12 T FTICR mass spectra for singly charged ions reported in neutral form.

sample	compounds							intensity-weighted average										%Ar*
	total	CHO	CHNO	CHOS	H (%)	C (%)	O (%)	N (%)	S (%)	H/C	O/C	C/N	C/S	m/z	DBE	DBE/C	AI _{mod}	
<i>Surface Water (SW)</i>																		
Original DOM	7549	3768 (50%)	3157 (42%)	624 (8%)	43.9	37.4	18.0	0.6	0.1	1.18	0.48	62	578	491	11	0.46	0.28	12.2
Oasis HLB [†]	5720	2766 (48%)	2530 (44%)	424 (7%)	42.1	37.4	19.9	0.6	0.1	1.13	0.53	60	732	481	11	0.47	0.29	13.2
LiChrolut-EN [†]	5514	2597 (47%)	2507 (45%)	410 (7%)	41.8	37.5	20.0	0.6	0.0	1.11	0.53	58	752	491	11	0.50	0.30	13.9
Supel-Select HLB [†]	6179	3082(50%)	2644 (43%)	453 (7%)	42.7	37.4	19.2	0.6	0.1	1.14	0.51	61	723	492	11	0.48	0.29	12.7
β -CDP [†]	6284	3256(52%)	2558 (41%)	470 (7%)	43.4	37.4	18.6	0.5	0.1	1.16	0.50	68	679	493	11	0.47	0.28	11.5
<i>Groundwater (GW)</i>																		
Original DOM	6126	2820 (46%)	2583 (42%)	723 (12%)	42.4	38.2	18.6	0.6	0.1	1.11	0.49	63	327	493	12	0.50	0.33	14.2
Oasis HLB [†]	4822	2163 (45%)	2147 (45%)	512 (11%)	40.9	38.5	19.9	0.7	0.1	1.06	0.52	55	378	475	11	0.52	0.34	16.1
LiChrolut-EN [†]	4845	2179 (45%)	2141 (44%)	525 (11%)	41.0	38.4	19.8	0.7	0.1	1.07	0.51	57	371	482	12	0.52	0.34	15.5
Supel-Select HLB [†]	5178	2435 (47%)	2175 (42%)	568 (11%)	41.7	38.5	19.1	0.6	0.1	1.08	0.50	61	360	484	12	0.51	0.34	15.1
β -CDP [†]	4139	2141 (52%)	1560 (38%)	438 (11%)	42.1	38.3	19.0	0.5	0.1	1.10	0.50	78	382	483	11	0.50	0.32	13.6

* Percentage of aromatic compounds with modified aromaticity index (AI_{mod}) ≥ 0.5

[†] Values for SPE permeates, which were collected, acidified and extracted with Bond Elut PPL sorbent as detailed in section S3.4.2

S3.8 Molecular-Level Characterization of SPE Extracts by FTICR MS

S3.8.1 Characteristic Features in FTICR Mass Spectra of DOM Extracts

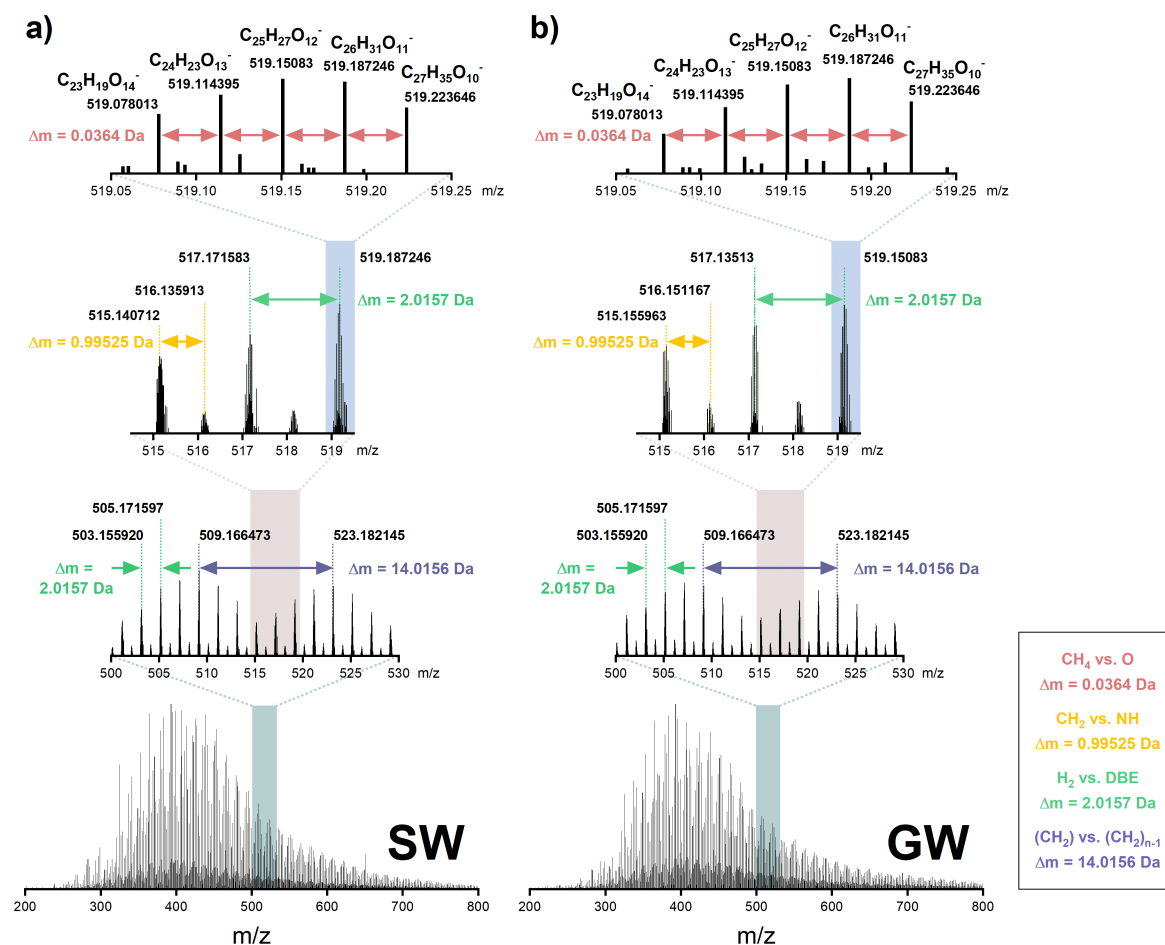


Figure S3.7. Negative ESI 12 T FTICR mass spectra from m/z 200 - 800 of the original (a) surface water (SW) and (b) groundwater (GW) DOM (bottom). Examples of the recurring mass spacing patterns attributed to the addition/subtraction of CH_2 or H_2 , or the nominal exchange of CH_2 vs. NH , or CH_4 vs. O (ref. 213,301,378) are highlighted in scale-expanded segments from m/z 500 - 530 (third row) and m/z 514.5 - 519.5 (second row), and at nominal mass 519 (top).

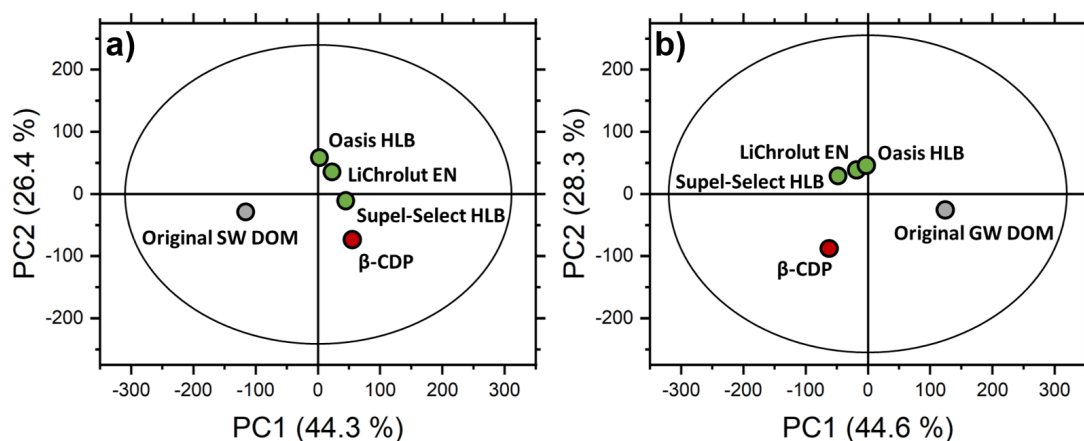


Figure S3.8. Principal component analysis (PCA) score plots derived from normalized negative ESI 12 T FTICR mass spectra of original (a) surface water (SW) and (b) groundwater (GW) DOM (gray) and the respective sorbent extracts (β -CDP: red, conventional sorbents: green). The first two principal components accounted for 70.7 % and 72.9 % of the variance in SW and GW data sets, respectively.

Table S3.5. Counts and relative proportions (in brackets) of m/z ions for original and sorbent extract DOM sorted according to CHO, CHNO, and CHOS molecular composition; intensity-weighted averages of elemental compositions; elemental and mass-to-charge ratios, and chemical indices; and percentages of aromatic compounds as computed from negative ESI 12 T FTICR mass spectra for singly charged ions reported in neutral form.

sample	compounds						intensity-weighted average										%Ar*	
	total	CHO	CHNO	CHOS	H (%)	C (%)	O (%)	N (%)	S (%)	H/C	O/C	C/N	C/S	m/z	DBE	DBE/C		A_{mod}
<i>Surface Water (SW)</i>																		
Original DOM	7549	3768 (50%)	3157 (42%)	624 (8%)	43.9	37.4	18.0	0.6	0.1	1.18	0.48	62	578	491	11	0.46	0.28	12.2
Oasis HLB	5571	2818 (51%)	2187 (39%)	566 (10%)	48.3	36.5	14.5	0.5	0.2	1.32	0.40	71	216	488	9	0.39	0.23	7.2
LiChrolut EN	4173	2185 (52%)	1511 (36%)	477 (11%)	48.4	36.0	15.0	0.5	0.2	1.35	0.42	72	215	467	9	0.38	0.20	5.2
Supel-Select HLB	2824	1857 (66%)	691 (24%)	276 (10%)	50.4	35.8	13.4	0.3	0.1	1.41	0.37	128	261	462	8	0.34	0.19	5.0
β -CDP	2031	1189 (59%)	644 (32%)	198 (10%)	52.3	35.4	11.4	0.7	0.2	1.48	0.32	50	144	443	7	0.32	0.18	4.1
<i>Groundwater (GW)</i>																		
Original DOM	6126	2820 (46%)	2583 (42%)	723 (12%)	42.4	38.2	18.6	0.6	0.1	1.11	0.49	63	327	493	12	0.50	0.33	14.2
Oasis HLB	6173	2996 (49%)	2312 (37%)	865 (14%)	47.3	38.0	14.1	0.4	0.2	1.25	0.37	87	249	493	11	0.42	0.26	9.9
LiChrolut EN	5212	2273 (44%)	2210 (42%)	729 (14%)	47.6	37.5	14.1	0.6	0.2	1.27	0.38	61	242	483	10	0.41	0.24	6.9
Supel-Select HLB	6014	3174 (53%)	1880 (31%)	960 (16%)	49.1	37.8	12.6	0.3	0.2	1.30	0.33	129	221	496	10	0.39	0.25	8.8
β -CDP	3469	1939 (56%)	1114 (32%)	416 (12%)	51.5	37.0	10.8	0.5	0.1	1.39	0.29	76	268	461	9	0.35	0.23	5.4

* Percentage of aromatic compounds with modified aromaticity index ($A_{\text{mod}} \geq 0.5$)

Table S3.6. Annotated CHO-formulas derived from ions observed in both SW and GW DOM spectra at nominal mass 471, and corresponding computed elemental ratios (i.e., H/C, O/C) and chemical indices (i.e., DBE, DBE/C, AI_{mod}).

m/z (Da)	formula (neutral form)	H/C	O/C	DBE	DBE/C	AI_{mod}
<i>formula series 1</i> (green in Figure 3.1 in Chapter 3)						
471.056889	C ₂₂ H ₁₆ O ₁₂	0.73	0.55	15	0.68	0.56
471.093283	C ₂₃ H ₂₀ O ₁₁	0.87	0.48	14	0.61	0.49
471.129686	C ₂₄ H ₂₄ O ₁₀	1.00	0.42	13	0.54	0.42
471.166087	C ₂₅ H ₂₈ O ₉	1.12	0.36	12	0.48	0.37
471.202475	C ₂₆ H ₃₂ O ₈	1.23	0.31	11	0.42	0.32
<i>formula series 2</i> (black in Figure 3.1 in Chapter 3)						
471.078001	C ₁₉ H ₂₀ O ₁₄	1.05	0.74	10	0.53	0.25
471.114390	C ₂₀ H ₂₄ O ₁₃	1.20	0.65	9	0.45	0.19
471.150805	C ₂₁ H ₂₈ O ₁₂	1.33	0.57	8	0.38	0.13
471.187214	C ₂₂ H ₃₂ O ₁₁	1.45	0.50	7	0.32	0.09

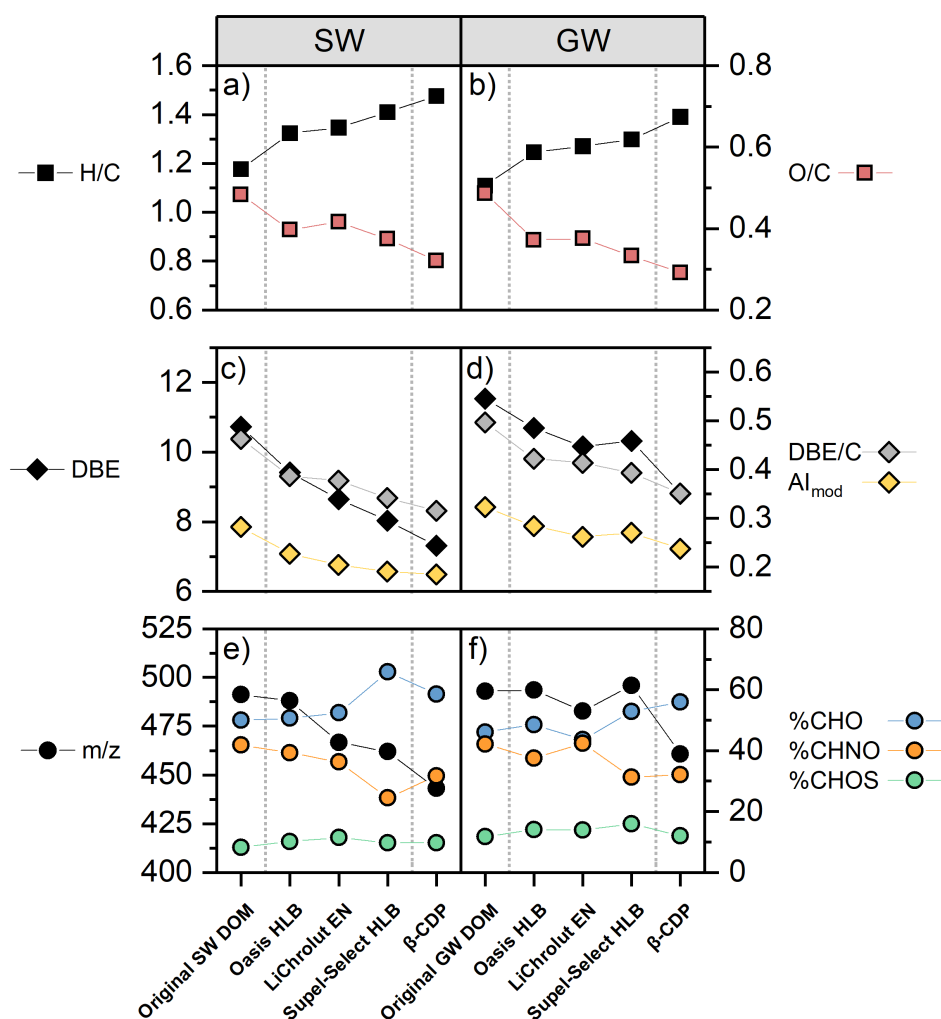


Figure S3.9. Intensity-weighted average H/C and O/C (a,b) ratios, DBE, DBE/C and AI_{mod} indices (c,d), and mass-to-charge ratios (e,f) for SW and GW samples, respectively, as computed from negative ESI 12 T FTICR mass spectra. Relative proportions of CHO, CHNO and CHOS molecular compositions are additionally shown in panel (e) and (f).

S3.8.2 Chemodiversity of DOM Extracted by β -CDP and Universal SPE Sorbents

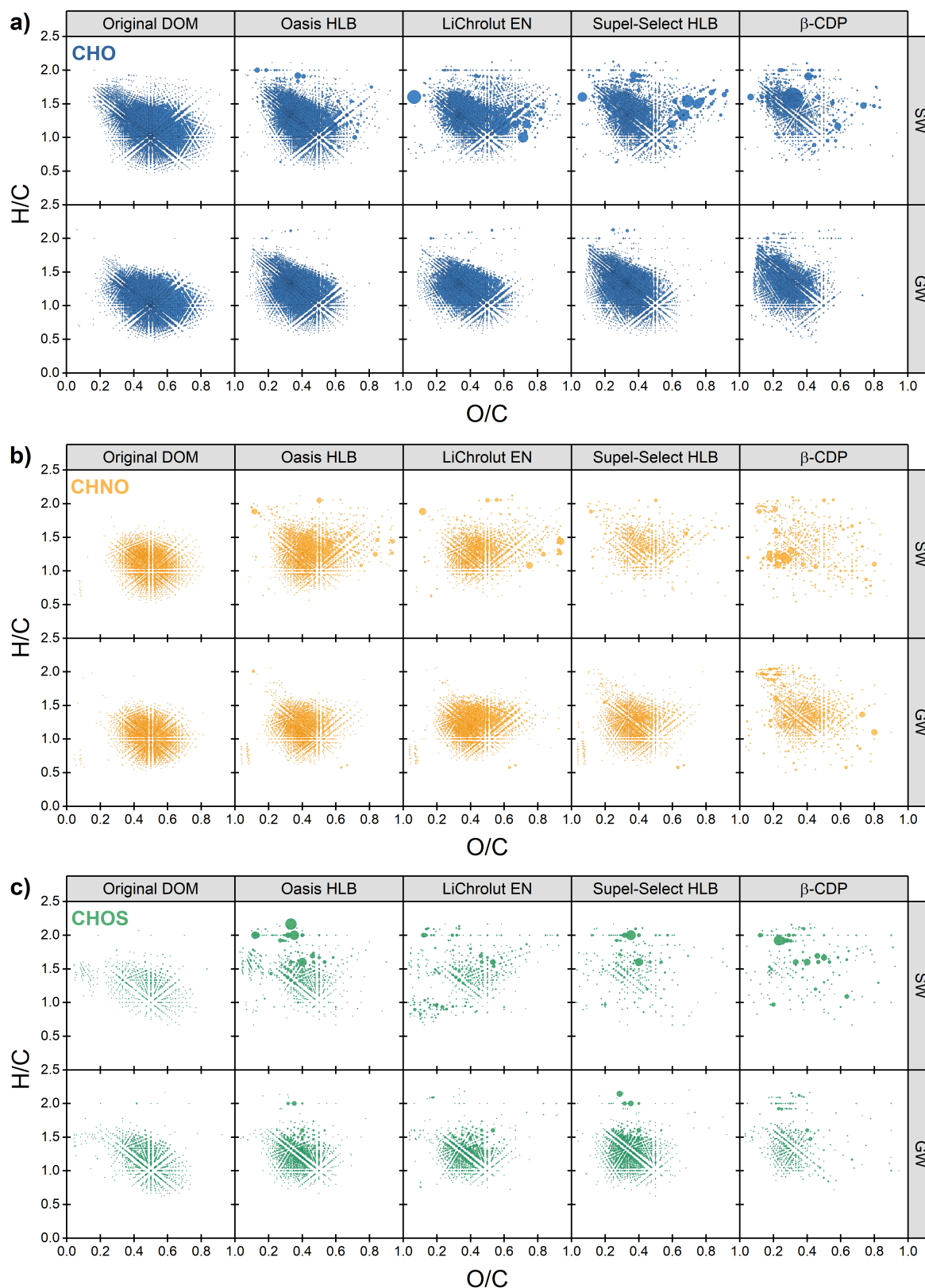


Figure S3.10. Molecular composition of original surface water (SW) and groundwater (GW) DOM, compared to DOM in conventional (i.e., Oasis HLB, LiChrolut EN, Supel-Select HLB) and β -CDP sorbent extracts projected onto van Krevelen diagrams sorted according to the assigned molecular CHO (a), CHNO (b), and CHOS (c) series. Symbol sizes reflect relative signal intensities of each mass peak.

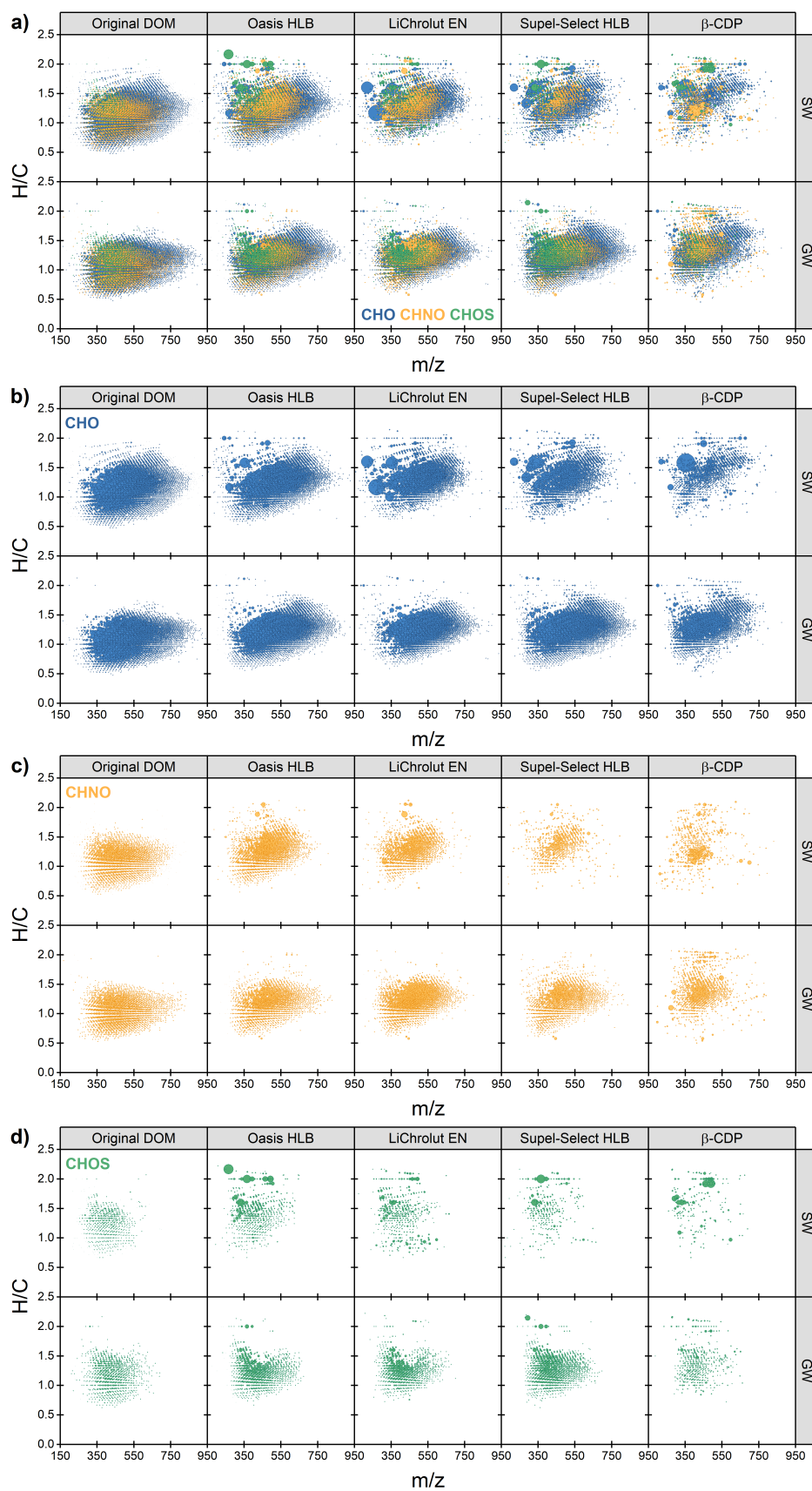


Figure S3.11. (a) Mass-edited H/C ratios of molecular compositions of original surface water (SW) and groundwater (GW) DOM, compared to DOM in conventional (i.e., Oasis HLB, LiChrolut EN, Supel-Select HLB) and β -CDP sorbent extracts. Symbols are color-coded according to CHO (blue), CHNO (orange), and CHOS (green) molecular series, and symbol sizes reflect relative signal intensities of each mass peak. In addition, panel (b), (c), and (d) depict mass-edited H/C ratios of individual molecular series, that is, CHO, CHNO, and CHOS, respectively.

Molecular Characterization of Original DOM Compositions

Original DOM compositions were characterized by high chemodiversity, as reflected in high numbers of assigned formulas (i.e., 7549 for SW, 6126 for GW) occupying a wide range in the CHO-compositional space (H/C: 0.5 – 2.0, O/C: 0.04 – 0.9) (Table S3.5, Figure S3.10). A majority of 63 % of assigned formulas were shared in both samples (Figure S3.12), and covered regions in the van Krevelen diagrams commonly ascribed to the major biogeochemical precursors of lignin-like,^{214,215,298,299} and tannin-like compounds,^{216,296} and refractory carboxylic-rich alicyclic molecules (CRAMs)²¹³. CRAMs represent highly diverse transformation products of terpenoid origin,²¹² which are prominent constituents in freshwater DOM,²¹⁷⁻²²⁰ and their co-presence with lignin- and tannin-like compounds suggests terrestrial biomass residues (e.g., vascular/higher plants) as main DOM source.³⁷⁹ Besides, 12 and 14 % of molecular compositions in SW and GW DOM, respectively, were identified to be of aromatic character ($AI_{\text{mod}} \geq 0.5$,^{230,231} Table S3.5), typical of freshwater-derived DOM.²¹² Differences between the two DOM sources were unveiled by molecular signatures uniquely detected in either water sample (Figure S3.12). SW DOM exclusively contained a range of unsaturated sulfolipids and numerous aliphatic CHO-compounds with $H/C > 1.5$,²⁹⁷ the latter resulting in higher relative abundance of CHO molecular members compared to GW DOM (50 vs. 46 %, Table S3.5). In contrast, CHOS-compounds were relatively more abundant in GW DOM (12 vs. 8 %) due to considerable unique sulfonated compounds in the CRAM region. N-bearing compounds were equally abundant at 42 % in both samples, but unique CHNO signatures tended to be more unsaturated in GW DOM.

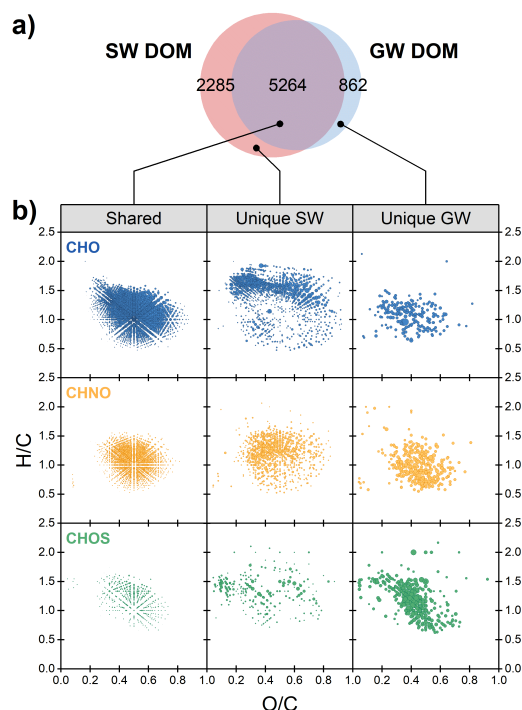


Figure S3.12. (a) Venn diagram indicating number of shared and unique molecular signatures in original SW and GW DOM compositions. (b) Shared and unique elemental compositions of original SW and GW DOM projected onto van Krevelen diagrams, separated according to CHO (blue), CHNO (orange), and CHOS (green) molecular series. Symbol sizes reflect relative signal intensities of each mass peak.

Molecular DOM Characterization in Sorbent Extracts

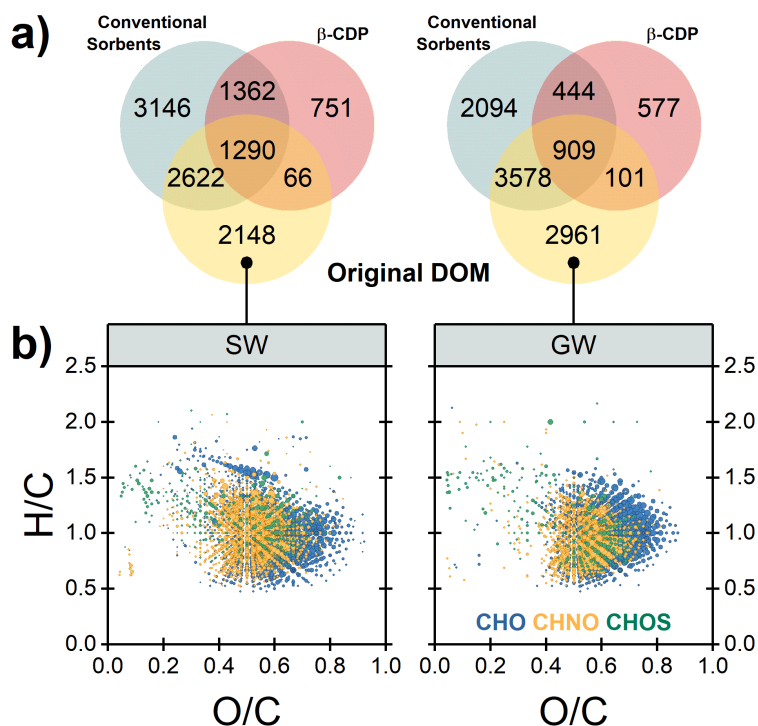


Figure S3.13. (a) Venn diagrams indicating shared and unique molecular signatures in conventional sorbent extracts (red), β-CDP extracts (green), and the original SW (left side) and GW DOM (right side), respectively. (b) Molecular composition that were not extracted with either of the tested sorbents (i.e., unique to original DOM) projected onto van Krevelen diagrams. Symbols are color-coded according to CHO (blue), CHNO (orange), and CHOS (green) molecular series, and symbol sizes reflect relative signal intensities of each mass peak.

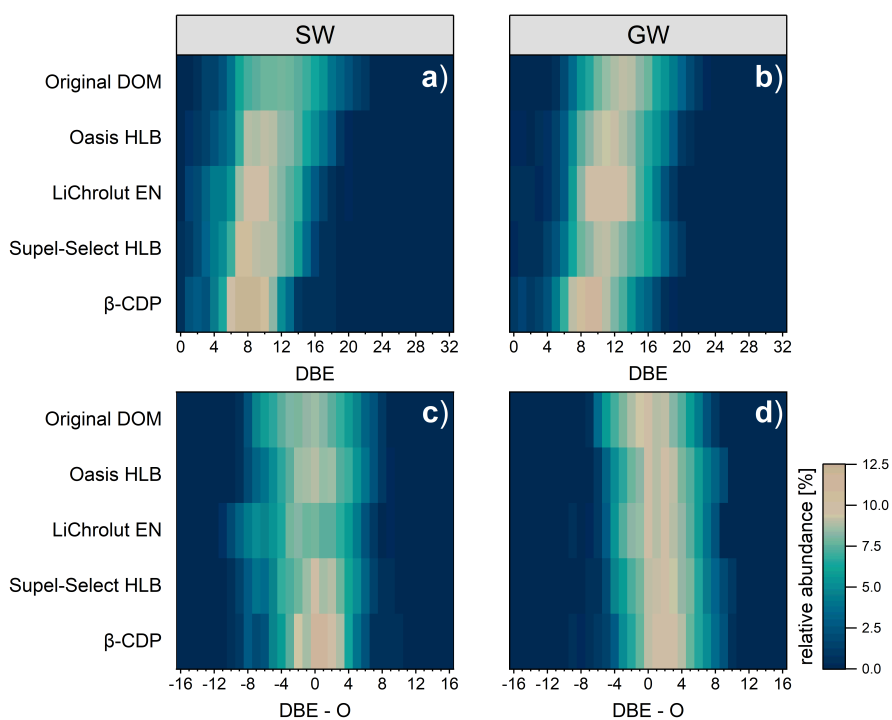


Figure S3.14. Relative abundance of CHO-annotated formulas as a function of double bond equivalent (DBE) values and DBE minus count of oxygen (DBE-O) values for surface water (a, c) and groundwater samples (b, d), respectively.

S3.8.3 High-abundance and Unique Molecular Signatures in Sorbent Extracts

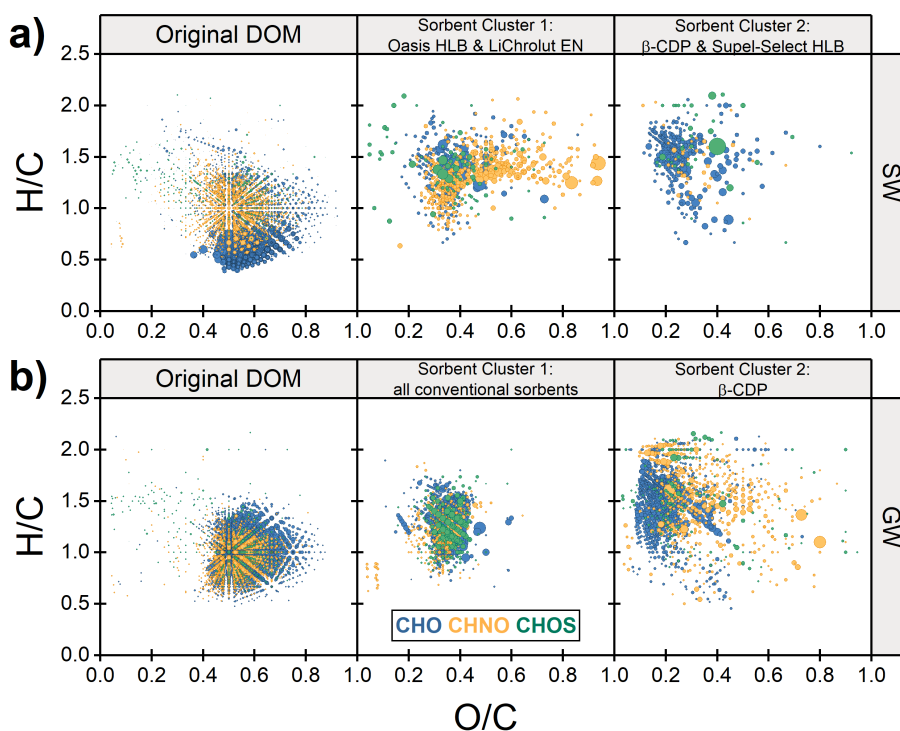


Figure S3.15. Comparative analysis of FTICR mass spectra of (a) surface (SW) and (b) groundwater (GW) samples based on similarity indices using Pearson correlation coefficient. Van Krevelen diagrams depict molecular compositions with relatively high abundance for groups of highest similarity identified by hierarchical cluster analysis (cf. Chapter 3).

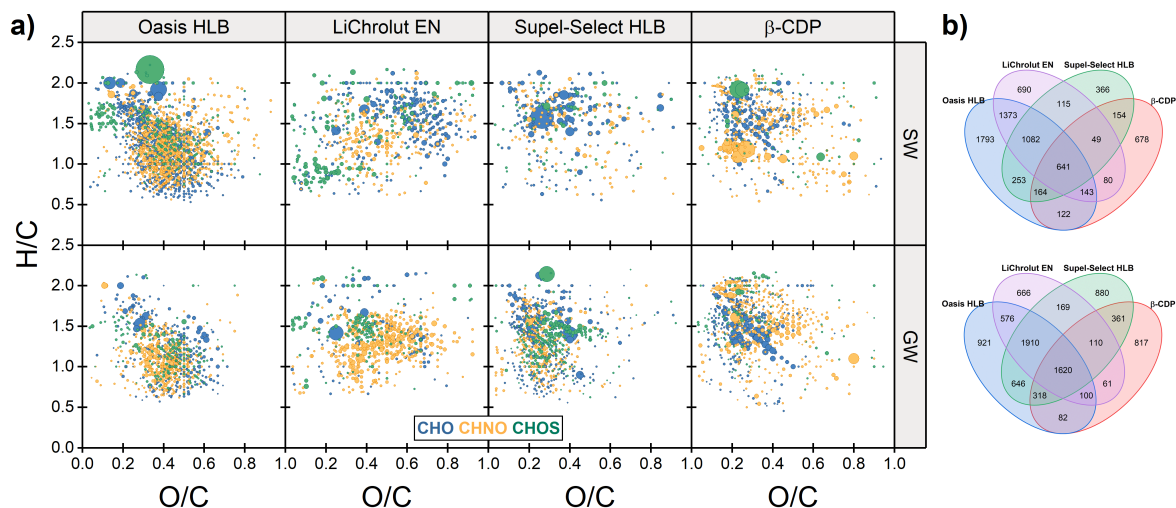


Figure S3.16. (a) Van Krevelen diagrams of unique molecular compositions present in Oasis HLB, LiChrolut EN, Supel-Select HLB, or β -CDP extracts. Symbols are color-coded according to CHO (blue), CHNO (orange), and CHOS (green) molecular series, and symbol sizes reflect relative signal intensities of each mass peak. (b) Venn diagrams indicating counts of shared and unique molecular compositions.

S3.9 Literature Data on Recovery of Nonionic Micropollutants after Solid-Phase Extraction Using β -CDP as Sorbent

Table S3.7. Recovery data for target analytes uncharged at neutral pH conditions after solid-phase extraction using β -CDP sorbent. The data was adopted from literature and used for data visualization in Figure 3.5b in Chapter 3. The table additionally lists the compound classification, CAS number, formula, molecular weight, elemental H/C and O/C ratio, log K_{OW} value, and McGowan volume (MV).

compound	comp. class*	CAS	MW [†]	formula	H/C	O/C	log K_{OW}	MV [‡]	Recovery (%)	Ref. [§]
10,11-dihydrocarbamazepine	Pharm.	3564-73-6	238.28	C ₁₅ H ₁₄ N ₂ O	0.93	0.07	2.46	1.85	84 ± 12	Li et al.
6-benzylaminopurine	Pest.	1214-39-7	225.25	C ₁₂ H ₁₁ N ₅	0.92	0.00	1.57	1.67	100 ± 0	Li et al.
Abacavir	Pharm.	136470-78-5	286.33	C ₁₄ H ₁₈ N ₆ O	1.29	0.07	1.62	2.09	100 ± 0	Li et al.
Acetamidiprid	Pest.	135410-20-7	222.67	C ₁₀ H ₁₁ ClN ₄	1.10	0.00	2.55	1.67	98 ± 4	Li et al.
Acetochlor	Pest.	34256-82-1	269.77	C ₁₄ H ₂₀ ClNO ₂	1.43	0.14	4.14	2.14	98 ± 3	Li et al.
Adrenosterone	Horm.	382-45-6	300.40	C ₁₉ H ₂₄ O ₃	1.26	0.16	1.41	2.36	99 ± 1	Li et al.
Alachlor	Pest.	15972-60-8	269.77	C ₁₄ H ₂₀ ClNO ₂	1.43	0.14	3.52	2.14	98 ± 3	Li et al.
Amcinonide	Pharm.	51022-69-6	502.60	C ₂₈ H ₃₅ FO ₇	1.25	0.25	3.56	3.62	100 ± 0	Li et al.
Atrazin-2-Hydroxy	Pest.	2163-68-0	197.24	C ₈ H ₁₃ N ₅ O	1.88	0.13	1.40	1.56	99 ± 1	Li et al.
Atrazine	Pest.	1912-24-9	215.68	C ₈ H ₁₄ ClN ₅	1.75	0.00	2.70	1.62	100 ± 0	Glöckler et al.
Azoxystrobin	Pest.	131860-33-8	403.40	C ₂₂ H ₁₇ N ₃ O ₅	0.77	0.23	2.50	2.92	108 ± 3	Glöckler et al.
Bendiocarb	Pest.	22781-23-3	223.22	C ₁₁ H ₁₃ NO ₄	1.18	0.36	1.70	1.60	84 ± 11	Li et al.
Benzisothiazolin-3-on	Pest.	2634-33-5	151.18	C ₇ H ₅ NOS	0.71	0.14	0.64	1.03	94 ± 8	Li et al.
Benzotriazole	Indust.	95-14-7	119.12	C ₆ H ₅ N ₃	0.83	0.00	1.17	0.86	86 ± 18	Li et al.
Benzotriazole-methyl-1H	Indust.	136-85-6	266.30	C ₇ H ₇ N ₃	1.00	0.00	1.71	1.01	99 ± 2	Li et al.
Boscalid	Pest.	188425-85-6	343.20	C ₁₈ H ₁₂ Cl ₂ N ₂ O	0.67	0.06	2.96	2.39	97 ± 0	Glöckler et al.
Bromacil	Pest.	314-40-9	261.12	C ₉ H ₁₃ BrN ₂ O ₂	1.44	0.22	2.11	1.63	77 ± 15	Li et al.
Carbamazepine	Pharm.	298-46-4	236.27	C ₁₅ H ₁₂ N ₂ O	0.80	0.07	2.45	1.81	90 ± 8	Li et al.
Carbaryl	Pest.	63-25-2	201.22	C ₁₂ H ₁₁ NO ₂	0.92	0.17	2.36	1.50	97 ± 2	Ling et al.
Carbendazim	Pest.	10605-21-7	191.19	C ₉ H ₉ N ₃ O ₂	1.00	0.22	1.55	1.36	100 ± 0	Li et al.
Carbofuran	Pest.	1563-66-2	221.25	C ₁₂ H ₁₅ NO ₃	1.25	0.25	2.32	1.69	87 ± 4	Ling et al.
Carisoprodol	Pharm.	78-44-4	260.33	C ₁₂ H ₂₄ N ₂ O ₄	2.00	0.33	2.36	2.15	77 ± 13	Li et al.
Chloridazon	Pest.	1698-60-8	221.64	C ₁₀ H ₈ ClN ₃ O	0.80	0.10	1.14	1.52	98 ± 3	Li et al.
Corticosterone	Pharm.	50-22-6	346.50	C ₂₁ H ₃₀ O ₄	1.43	0.19	1.94	2.74	99 ± 2	Li et al.
Coumarin	Natural	91-64-5	146.14	C ₉ H ₆ O ₂	0.67	0.22	1.51	1.06	99 ± 3	Li et al.
Cyflufenamid	Pest.	180409-60-3	412.40	C ₂₀ H ₁₇ F ₅ N ₂ O ₂	0.85	0.10	5.60	2.66	100 ± 0	Li et al.
Diethyltoluamide (DEET)	Pest.	134-62-3	191.27	C ₁₂ H ₁₇ NO	1.42	0.08	2.02	1.68	95 ± 3	Ling et al.
Dexamethasone	Pharm.	50-02-2	392.50	C ₂₂ H ₂₉ FO ₅	1.32	0.23	1.83	2.91	90 ± 9	Li et al.
Diazinon	Pest.	333-41-5	304.35	C ₁₂ H ₂₁ N ₂ O ₃ PS	1.75	0.25	3.81	2.30	100 ± 0	Ling et al.
Diethyl Phthalate	Indust.	84-66-2	222.24	C ₁₂ H ₁₄ O ₄	1.17	0.33	2.47	1.71	77 ± 11	Li et al.
Dimethachlor	Pest.	50563-36-5	255.74	C ₁₃ H ₁₈ ClNO ₂	1.38	0.15	2.17	2.00	87 ± 11	Li et al.
Dimethomorph	Pest.	110488-70-5	387.90	C ₂₁ H ₂₂ ClNO ₄	1.05	0.19	2.68	2.85	99 ± 5	Glöckler et al.
Diuron	Pest.	330-54-1	233.09	C ₉ H ₁₀ Cl ₂ N ₂ O	1.11	0.22	2.68	1.60	100 ± 0	Li et al.
Efavirenz	Pharm.	154598-52-4	315.67	C ₁₄ H ₉ ClF ₃ N ₂ O ₂	0.64	0.14	4.70	1.89	100 ± 0	Li et al.
Estrone	Horm.	53-16-7	270.40	C ₁₈ H ₂₂ O ₂	1.22	0.11	3.13	2.16	100 ± 0	Li et al.
Ethofumesate	Pest.	26225-79-6	286.35	C ₁₃ H ₁₈ O ₅ S	1.38	0.38	2.70	2.05	100 ± 1	Li et al.
Famciclovir	Pharm.	104227-87-4	321.33	C ₁₄ H ₁₉ N ₅ O ₄	1.36	0.29	0.64	2.34	99 ± 1	Li et al.
Hexazinone	Pest.	51235-04-2	252.31	C ₁₂ H ₂₀ N ₄ O ₂	1.67	0.17	1.85	1.97	92 ± 7	Li et al.
Hydrocortisone	Pharm.	50-23-7	362.50	C ₂₁ H ₃₀ O ₅	1.43	0.24	2.16	2.80	91 ± 8	Li et al.
Isophorone Diisocyanate	Indust.	4098-71-9	222.28	C ₁₂ H ₁₈ O ₂ N ₂	1.50	0.17	4.75	1.84	79 ± 17	Li et al.
Isoproturon	Pest.	34123-59-6	206.28	C ₁₂ H ₁₈ N ₂ O	1.50	0.08	2.87	1.78	100 ± 0	Li et al.
Lamotrigine	Pharm.	84057-84-1	256.09	C ₉ H ₇ Cl ₂ N ₅	0.78	0.00	2.57	1.65	100 ± 0	Li et al.
Linuron	Pest.	330-55-2	249.09	C ₉ H ₁₀ Cl ₂ N ₂ O ₂	1.11	0.22	3.20	1.66	100 ± 0	Li et al.
Malaoxon	Metab.	1634-78-2	314.29	C ₁₀ H ₁₉ O ₇ PS	1.90	0.70	0.97	2.20	99 ± 1	Ling et al.
Metaxalone	Pharm.	1665-48-1	221.26	C ₁₂ H ₁₅ NO ₃	2.60	1.69	0.25	1.25	99 ± 1	Li et al.
Methiocarb	Pest.	2032-65-7	225.31	C ₁₁ H ₁₅ NO ₂ S	1.36	0.18	3.18	1.76	96 ± 2	Glöckler et al.
Methocarbamol	Pharm.	532-03-6	241.24	C ₁₁ H ₁₅ NO ₅	1.36	0.45	0.61	1.77	87 ± 10	Li et al.

Metolachlor	Pest.	51218-45-2	283.79	C ₁₅ H ₂₂ ClNO ₂	1.47	0.13	3.05	2.28	100 ± 2	Glöckler et al.
Metribuzin	Pest.	21087-64-9	214.24	C ₈ H ₁₄ N ₄ OS	1.75	0.13	1.49	1.62	96 ± 2	Ling et al.
Molinate	Pest.	2212-67-1	187.30	C ₉ H ₁₇ NOS	1.89	0.11	3.21	1.55	99 ± 2	Li et al.
Oxazepam	Pharm.	604-75-1	286.71	C ₁₅ H ₁₁ ClN ₂ O ₂	0.73	0.13	2.24	1.99	93 ± 6	Li et al.
Oxcarbazepine	Pharm.	28721-07-5	252.27	C ₁₅ H ₁₂ N ₂ O ₂	0.80	0.13	1.11	1.87	85 ± 12	Li et al.
Oxybenzone	Lifest.	131-57-7	228.24	C ₁₄ H ₁₂ O ₃	0.86	0.21	3.79	1.74	100 ± 0	Li et al.
Pentoxifylline	Pharm.	6493-05-6	278.31	C ₁₃ H ₁₈ N ₄ O ₃	1.38	0.23	0.56	2.08	98 ± 4	Li et al.
Phenytoin (Dilantin)	Pharm.	57-41-0	252.27	C ₁₅ H ₁₂ N ₂ O ₂	0.80	0.13	2.47	1.87	93 ± 7	Li et al.
Pirimicarb	Pest.	23103-98-2	238.29	C ₁₁ H ₁₈ N ₄ O ₂	1.64	0.18	1.70	1.89	99 ± 1	Li et al.
Pirimiphos-Ethyl	Pest.	23505-41-1	333.39	C ₁₃ H ₂₄ N ₃ O ₃ PS	1.85	0.23	4.85	2.55	100 ± 0	Li et al.
Primidone	Pharm.	125-33-7	218.25	C ₁₂ H ₁₄ N ₂ O ₂	1.17	0.17	0.91	1.68	84 ± 27	Li et al.
Progesterone	Horm.	57-83-0	314.50	C ₂₁ H ₃₀ O ₂	1.43	0.10	3.87	2.62	100 ± 1	Li et al.
Prometon	Pest.	1610-18-0	225.29	C ₁₀ H ₁₉ N ₅ O	1.90	0.10	2.99	1.84	99 ± 1	Li et al.
Propachlor	Pest.	1918-16-7	211.69	C ₁₁ H ₁₄ ClNO	1.27	0.09	2.18	1.66	97 ± 3	Ling et al.
Propazine	Pest.	139-40-2	229.71	C ₉ H ₁₆ ClN ₅	1.78	0.00	2.93	1.76	100 ± 0	Li et al.
Propiconazole	Pest.	60207-90-1	342.20	C ₁₅ H ₁₇ Cl ₂ N ₃ O ₂	1.13	0.13	3.72	2.34	98 ± 0	Glöckler et al.
Propoxur	Pest.	114-26-1	209.24	C ₁₁ H ₁₅ NO ₃	1.36	0.27	1.52	1.65	84 ± 11	Li et al.
Propyzamide	Pest.	23950-58-5	256.12	C ₁₂ H ₁₁ Cl ₂ NO	0.92	0.08	3.43	1.84	100 ± 0	Li et al.
Pyrazophos	Pest.	13457-18-6	373.37	C ₁₄ H ₂₀ N ₃ O ₅ PS	1.43	0.36	3.80	2.61	100 ± 0	Li et al.
Siduron	Pest.	1982-49-6	232.32	C ₁₄ H ₂₀ N ₂ O	1.43	0.07	3.80	1.95	100 ± 0	Li et al.
Simazine	Pest.	122-34-9	201.66	C ₇ H ₁₂ ClN ₅	1.71	0.00	2.18	1.48	91 ± 7	Li et al.
Sulfadimethoxine	Pharm.	122-11-2	310.33	C ₁₂ H ₁₄ N ₄ O ₄ S	1.17	0.33	1.17	2.21	81 ± 15	Li et al.
TDCPP	Indust.	13674-87-8	430.90	C ₉ H ₁₃ Cl ₆ O ₄ P	1.67	0.44	3.65	2.55	83 ± 5	Li et al.
Temazepam	Pharm.	846-50-4	300.74	C ₁₆ H ₁₃ ClN ₂ O ₂	0.81	0.13	2.19	2.13	96 ± 6	Li et al.
Terbutylazine	Pest.	5915-41-3	229.71	C ₉ H ₁₆ ClN ₅	1.78	0.00	3.40	1.76	100 ± 3	Glöckler et al.
Testosterone	Horm.	58-22-0	288.40	C ₁₉ H ₂₈ O ₂	1.47	0.11	3.32	2.38	100 ± 0	Li et al.
Thiabendazole	Pharm.	148-79-8	201.25	C ₁₀ H ₇ N ₅ S	0.70	0.00	2.47	1.40	100 ± 0	Li et al.
Thiacloprid	Pest.	111988-49-9	252.72	C ₁₀ H ₉ ClN ₄ S	0.90	0.00	1.26	1.73	82 ± 3	Glöckler et al.
Triamterene	Pharm.	396-01-0	253.26	C ₁₂ H ₁₁ N ₇	0.92	0.00	0.98	1.83	100 ± 0	Li et al.
Tributyl phosphate (TBP)	Indust.	126-73-8	266.31	C ₁₂ H ₂₇ O ₄ P	2.25	0.33	4.00	2.24	98 ± 3	Li et al.
Triclosan	Pest.	3380-34-5	289.50	C ₁₂ H ₇ Cl ₃ O ₂	0.58	0.17	4.76	1.81	100 ± 0	Li et al.
Tris (2-chloroethyl) phosphate (TCEP)	Indust.	115-96-8	285.50	C ₆ H ₁₂ Cl ₃ O ₄ P	2.00	0.67	1.44	1.76	88 ± 11	Li et al.

*Pharm. = Pharmaceutical, Pest. = Pesticide, Metab. = Metabolite, Indust. = Industrial, Horm. = Hormone, Lifest. = Lifestyle

†Molecular weight in g mol⁻¹

‡McGowan volume in cm³ mol⁻¹ 100⁻¹

§Recovery data obtained from Ling et al. 2017,¹⁹⁴ Li et al. 2018,¹⁹⁵ or Glöckler et al. 2023²⁸⁵

S4 Supporting Information to Chapter 4

S4.1 Chemicals and Materials

All reagents, solvents, and analytical standards used in this study, including their CAS number, purity, and supplier, are summarized in Table S4.1. Natural organic matter reference standards of Suwannee River Humic (SRHA III, CN: 3S101H) and Fulvic Acid (SRFA III, CN: 3S101F) were obtained from the International Humic Substances Society (IHSS, St. Paul, MN, USA). Bond Elut PPL sorbent was purchased from Agilent (Santa Clara, CA, USA) and empty polypropylene SPE cartridges (1 mL) and polyethylene frits (20 μm pore size) were obtained from Sigma-Aldrich (Taufkirchen, Germany). Nylon membrane filters (47 mm diameter, 0.45 μm pore size) were obtained from GVS Filter Technology (Bologna, Italy), and centrifugal filter devices with molecular weight cut-offs of 1, 3, and 10 kDa (Macrosep Advance, 20 mL) were purchased from the Pall Corporation (Port Washington, NY, USA).

S4.2 Standard Solutions and Ultrapure Water

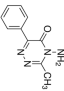
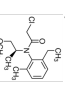
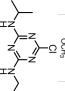
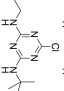
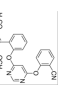
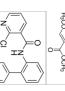
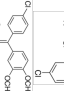
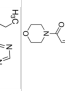
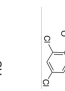
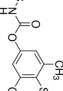
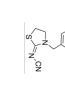
We selected 11 model target compounds, which are covering a range of physicochemical properties, including four herbicides (i.e., atrazine, metamitron, *S*-metolachlor and terbuthylazine), four fungicides (i.e., azoxystrobin, boscalid, dimethomorph and propiconazole), two insecticides (i.e., methiocarb and thiacloprid), and the metabolite 2,6-dichlorobenzamide (BAM). Their physicochemical properties along with other compound-specific information are given in Table S4.2. Stock solutions of analytical and isotopically labeled standards (1 g L⁻¹) were prepared in pure methanol and processed further to appropriate working solutions. Methanolic standards were stored at -20 °C in the dark. Ultrapure water (18.2 M Ω cm at 25 °C) was produced with a Milli-Q® Reference water purification system (Merck Millipore, USA).

Table S4.1. List of reagents, solvents, and analytical standards used in this study.

Chemical	CAS number	Purity/Grade (further info.)	Supplier
<i>Reagents</i>			
hydrochloric acid	7647-01-0	ACS reagent, 37 %	Sigma-Aldrich
potassium carbonate	584-08-7	BioXtra, ≥99.0 %	Sigma-Aldrich
potassium hydrogen phthalate	877-24-7	BioXtra, ≥99.95 %	Sigma-Aldrich
sodium hydroxide	1310-73-2	BioXtra, ≥98 %	Sigma-Aldrich
tetrafluoroterephthalonitrile	1835-49-0	99 %	Sigma-Aldrich
α-cyclodextrin	10016-20-3	≥98.0 %	Sigma-Aldrich
β-cyclodextrin	7585-39-9	≥97.0 %	Sigma-Aldrich
γ-cyclodextrin	17465-86-0	≥98.0 %	Sigma-Aldrich
<i>Solvents</i>			
acetonitrile	75-05-8	HPLC Plus, ≥99.9%	Sigma-Aldrich
dichloromethane	75-09-2	EMSURE®, for analysis	Sigma-Aldrich
methanol	67-56-1	≥99.9 %	Sigma-Aldrich
<i>N,N</i> -dimethylformamide	68-12-2	anhydrous, 99.8 %	Sigma-Aldrich
tetrahydrofuran	109-99-9	anhydrous, ≥99.9 %, inhibitor-free	Sigma-Aldrich
<i>Analytical standards</i>			
2,6-dichlorobenzamide (BAM)	2008-58-4	PESTANAL®, analytical standard	Sigma-Aldrich
atrazine	1912-24-9	PESTANAL®, analytical standard	Sigma-Aldrich
azoxystrobin	131860-33-8	PESTANAL®, analytical standard	Sigma-Aldrich
azoxystrobin-d4	n.a.	PESTANAL®, analytical standard	Sigma-Aldrich
boscalid	188425-85-6	PESTANAL®, analytical standard	Sigma-Aldrich
dimethomorph	110488-70-5	PESTANAL®, analytical standard	Sigma-Aldrich
dimethomorph-d6	n.a.	PESTANAL®, analytical standard	Sigma-Aldrich
metamitron	41394-05-2	PESTANAL®, analytical standard	Sigma-Aldrich
methiocarb	2032-65-7	PESTANAL®, analytical standard	Sigma-Aldrich
methiocarb-d3	n.a.	PESTANAL®, analytical standard	Sigma-Aldrich
propiconazole	60207-90-1	PESTANAL®, analytical standard	Sigma-Aldrich
propiconazole-d3	n.a.	PESTANAL®, analytical standard	Sigma-Aldrich
<i>S</i> -metolachlor	87392-12-9	PESTANAL®, analytical standard	Sigma-Aldrich
terbuthylazine	5915-41-3	PESTANAL®, analytical standard	Sigma-Aldrich
terbuthylazine-d5	n.a.	PESTANAL®, analytical standard	Sigma-Aldrich
thiacloprid	111988-49-9	PESTANAL®, analytical standard	Sigma-Aldrich
thiacloprid-d4	n.a.	PESTANAL®, analytical standard	Sigma-Aldrich

n.a. = not available.

Table S4.2. Physicochemical properties, CAS number, formula, structure, and classification of the selected target analytes.

Name	Formula	Structure	Classification	Molecular Weight [g mol ⁻¹]	McGowan Volume* [cm ³ mol ⁻¹ 100 ⁻¹]	log K _{ow} [-]	pK _a [-]	Charge pH 7 [-]
<i>Herbicides</i>								
metamitron	C ₁₀ H ₁₀ N ₄ O		triazinone	202.213	1.5003	0.85	-	n
S-metolachlor	C ₁₅ H ₂₂ ClNO ₂		chloroacetanilide	283.793	2.2811	3.05	-	n
atrazine	C ₈ H ₁₄ ClN ₅		triazine	215.683	1.6196	2.70	1.70 (weak base)	n
terbutylazine	C ₉ H ₁₆ ClN ₅		triazine	229.710	1.7605	3.40	1.90 (weak base)	n
<i>Fungicides</i>								
azoxystrobin	C ₂₂ H ₁₇ N ₃ O ₅		strobulurin	403.394	2.9165	2.50	-	n
boscalid	C ₁₈ H ₁₂ Cl ₂ N ₂ O		carboxamide	343.207	2.3921	2.96	-	n
dimethomorph	C ₂₁ H ₂₂ ClNO ₄		morpholine	387.857	2.8547	2.68	-	n
propiconazole	C ₁₅ H ₁₇ Cl ₂ N ₃ O ₂		triazole	342.220	2.3429	3.72	1.09 (weak base)	n
<i>Insecticides</i>								
methiocarb	C ₁₁ H ₁₅ NO ₂ S		carbamate	225.307	1.7586	3.18	-	n
thiacloprid	C ₁₀ H ₉ ClN ₄ S		neonicotinoid	252.723	1.7275	1.26	-	n
<i>Metabolite</i>								
2,6-dichloro- benzamide (BAM)	C ₇ H ₅ Cl ₂ NO		metabolite of diclobenil	190.027	1.2176	0.77	-	n

Data was adopted from the EU Pesticides Database (v2.2),³⁷² except for * the McGowan volume which was calculated based on the analyte structure³⁷³

S4.3 Preparation and Characterization of β -Cyclodextrin Polymer

S4.3.1 Synthesis of Porous Cyclodextrin Polymers

Porous cyclodextrin polymers (CDPs) were synthesized based on the nucleophilic aromatic substitution of cyclodextrin hydroxyl groups by tetrafluoroterephthalonitrile (TFN) as shown in Figure S4.1. The improved procedure reported by Alsaiee et al.¹⁹³ was utilized for the synthesis of β -CDP and adapted for the synthesis of α - and γ -CDP. A flame-dried 500 mL round-bottom flask was charged with the respective amounts of reagents (Table S4.3) at a molar ratio of 1.0:2.9:12.8 of cyclodextrin:cross-linker:potassium carbonate, respectively. After adding 160 mL of an anhydrous tetrahydrofuran/dimethylformamide mixture (9:1, v/v) the flask was connected to a reflux condenser, and the system was flushed with nitrogen for 10 min. Subsequently, the nitrogen inlet was removed, and the reflux condenser was closed with a septum. The mixture was placed in an oil bath (85 °C) and stirred for 48 h. Thereafter, the suspension was slowly cooled to room temperature while the solids could settle at the bottom of the flask. The supernatant was decanted, and the residual potassium carbonate was removed by washing with 1 M hydrochloric acid until CO₂ evolution stopped. The remaining suspension was filtered and sequentially washed with 250 mL of ultrapure water, 200 mL of tetrahydrofuran, 200 mL of dichloromethane and 200 mL of methanol. The polymers were finally dried under vacuum for 48 h. Successful synthesis was verified by scanning electron microscopy (S4.3.2) and Fourier-transform infrared spectroscopy (S4.3.3).

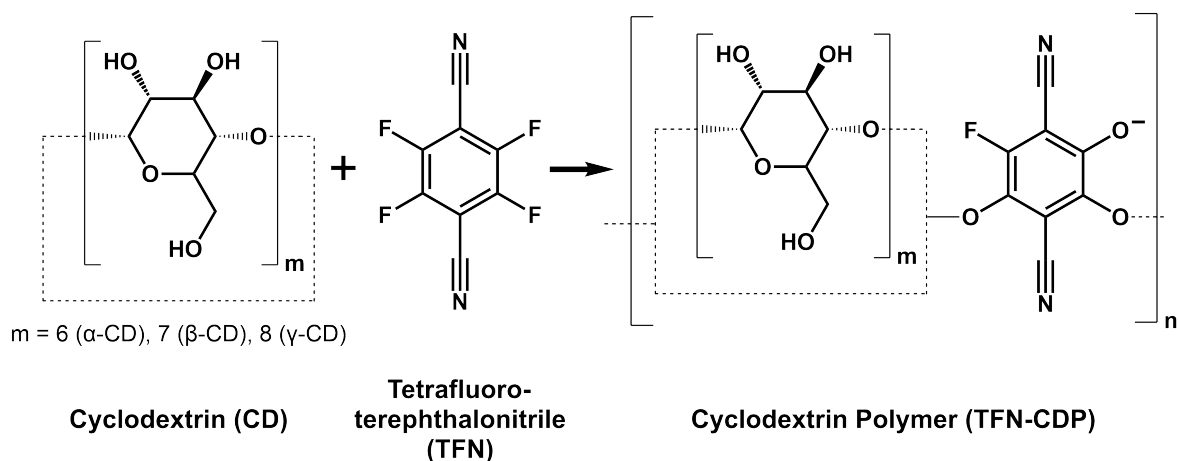


Figure S4.1. Synthesis scheme for the cross-linking of α -, β -, or γ -cyclodextrin (CD) with tetrafluoro-terephthalonitrile (TFN) to form mesoporous cyclodextrin polymers (TFN-CDPs) according to the procedure reported by Alsaiee et al.¹⁹³ The scheme depicts negatively charged phenolates in the cross-linker, which are introduced during the synthesis by a side reaction, as identified by Klemes et al.¹⁹⁷

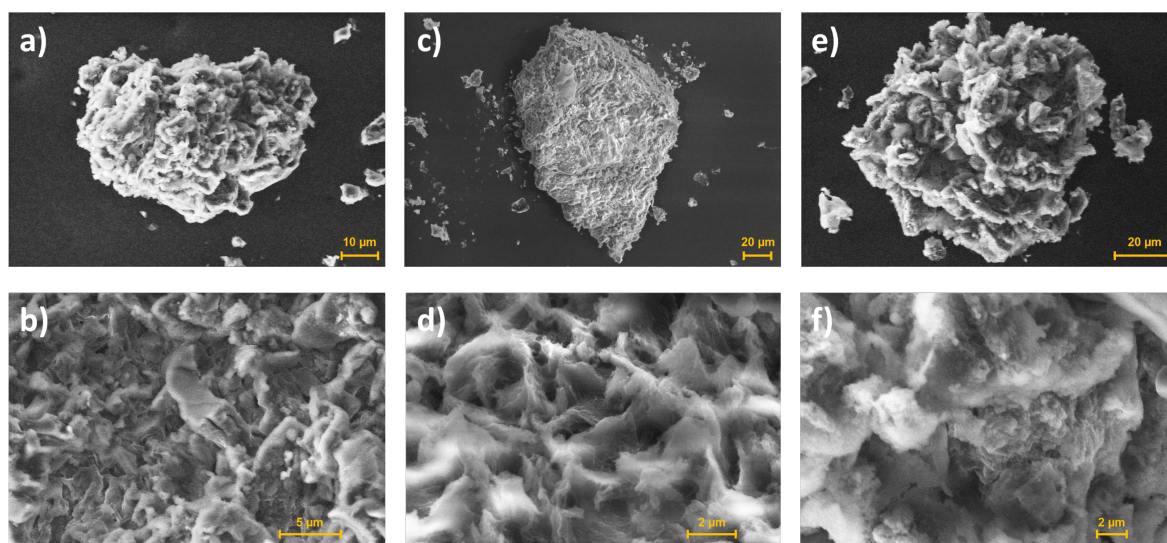
Table S4.3. Amounts of reagents used for synthesis of porous α -, β -, and γ -cyclodextrin polymers (CDPs).

reagent	M [g mol ⁻¹]	mol.-eq.	n [mmol]	m [g]
α -CD	972.84	1.00	3.61	3.51
β -CD	1134.98	1.00	3.61	4.10
γ -CD	1297.12	1.00	3.61	4.69
TFN*	200.09	2.85	10.28	2.06
K ₂ CO ₃	138.21	12.82	46.30	6.40

*tetrafluoroterephthalonitrile, cross-linker

S4.3.2 Field Emission Scanning Electron Microscope (FESEM) Imaging

Field emission scanning electron microscope (FESEM) imaging of the cyclodextrin-based sorbents was carried out on a Sigma 300 VP instrument (Carl Zeiss Microscopy GmbH, Jena, Germany) using an accelerating voltage of 10.0 kV and a sample distance of 5.4 to 5.9 mm. Figure S4.2 depicts FESEM images at magnifications between 0.4×10^3 and 7.5×10^3 showing the porous surface morphology of α -CDP (a,b), β -CDP (c,d), and γ -CDP (e,f), respectively.

**Figure S4.2.** Field emission scanning electron microscope (FESEM) images of synthesized cross-linked cyclodextrin polymers. The panels (a) and (b) depict SEM images of α -CDP, (c) and (d) of β -CDP, and (e) and (f) of γ -CDP.

S4.3.3 Fourier Transform Infrared (FTIR) Spectroscopy

Fourier transform infrared (FTIR) spectra (solid, attenuated total reflectance, ATR) were recorded using a Nicolet 6700 FT-IR spectrometer (Thermo Scientific, USA) at a wavenumber range of 650 to 4000 cm^{-1} and a resolution of 4 cm^{-1} . The signal-to-noise ratio was improved by accumulating 32 individually recorded scans. Baseline correction was performed using the software OriginPro 2020.

According to similar structure and common functional groups, the FT-IR spectra of the α -, β - and γ -CD building blocks showed intense absorbance at 1030 cm^{-1} , corresponding to polysaccharide C-O stretch vibrations, as well as aliphatic C-H stretch vibrations at 2930 cm^{-1} and O-H stretch vibrations around 3400 cm^{-1} (Figure S4.3). These spectral features were also found in spectra of the cross-linked polymer (β -CDP). In addition, all three CDPs exhibited nitrile stretches resonating at 2235 cm^{-1} and C-F stretch vibrations at 1268 cm^{-1} , which confirmed successful incorporation of the cross-linker TFN. Compared with the spectrum of neat TFN, C-F absorption band in the CDP spectra was less pronounced as expected for partial substitution of fluorine during synthesis. Finally, peaks appearing at 1670 cm^{-1} and 1463 cm^{-1} are assigned to aromatic C=C stretches of both the CD building block and the cross-linker.

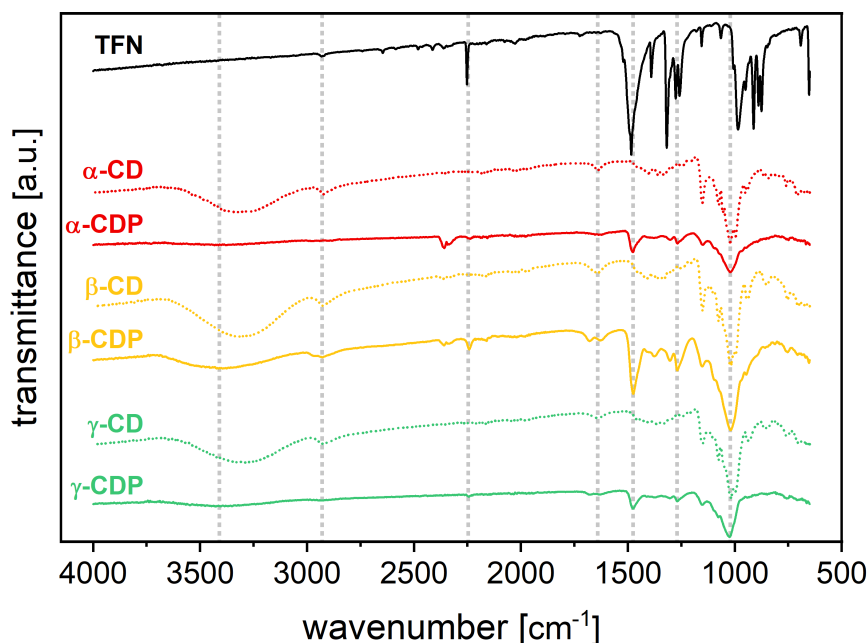


Figure S4.3. Fourier-transform infrared (FTIR) spectra of the cross-linker tetrafluoroterephthalonitrile (TFN), α -, β - and γ -cyclodextrin (α -, β -, γ -CD), and synthesized α -, β - and γ -cyclodextrin polymer (α -, β -, γ -CDP). Dashed vertical lines represent TFN specific absorption bands at 1268 cm^{-1} (C-F stretch vibrations) and 2235 cm^{-1} (nitrile stretch vibrations), CD specific absorption bands at 1030 cm^{-1} (C-O stretch vibrations), 2930 cm^{-1} (aliphatic C-H stretch vibrations), and 3400 cm^{-1} (O-H stretch vibrations), and common aromatic C=C stretch vibrations at 1464 cm^{-1} and 1670 cm^{-1} .

S4.4 Sampling of Surface Water and Preparation of Dissolved Organic Matter Reference Standards

Pristine surface water was sampled in the creek Wiesäckerbach, Garching, Germany (latitude 48.121905, longitude 11.511416) and in lake Kirchsee located in a marshland in Southern Bavaria, Germany (latitude 47.820473, longitude 11.625132). Grab samples were collected in glass bottles previously rinsed with methanol, ultrapure water, and natural water from the sampling site. After sampling, the water was immediately passed through pre-washed 0.45 μm nylon membrane filters (47 mm, GVS, USA). The dissolved organic carbon (DOC) in the samples amounted to 8.2 and 4.3 mgC L^{-1} , respectively. Other physicochemical parameters are given in Table S4.4. The sample taken in the creek Wiesäckerbach was used for investigating the competition between MPs and DOM compounds of varying molecular size. Lake Kirchsee water was used for experiments involving molecular-level investigation by Fourier transform ion cyclotron resonance MS.

Suwannee River Humic (SRHA) and Fulvic Acid (SRFA) reference standards were used as received from the International Humic Substances Society (IHSS, St. Paul, MN, USA) and dissolved in ultrapure water (50 mg L^{-1}) by stirring for 2 h followed by filtration (0.45 μm). This procedure resulted in DOC concentrations of 14.9 and 22.4 mgC L^{-1} for the aqueous SRHA and SRFA standard, respectively. All samples were separated into two aliquots, which were manually adjusted to either pH 2 or pH 7 using 1 M HCl or 1 M NaOH. Finally, samples were stored at 4 $^{\circ}\text{C}$ in the dark until further experiments were performed as described in Chapter 4.2.

Table S4.4. Physicochemical properties of the surface water sampled in lake Kirchsee and the creek Wiesäckerbach.

parameter	unit	Wiesäckerbach	Kirchsee
pH	-	6.8	6.1
Conductivity	$\mu\text{S cm}^{-1}$	385	205
Acid capacity	mmol L^{-1}	5.03	3.04
DOC	mg L^{-1}	4.34	8.17
Sodium (Na^+)	mg L^{-1}	12.50	8.60
Potassium (K^+)	mg L^{-1}	35.00	2.00
Ammonium (NH_4^+)	mg L^{-1}	< 0.04	< 0.04
Calcium (Ca^{2+})	mg L^{-1}	65.88	35.39
Magnesium (Mg^{2+})	mg L^{-1}	23.60	10.40
Fluoride (F^-)	mg L^{-1}	< 0.10	< 0.10
Chloride (Cl^-)	mg L^{-1}	15.47	0.71
Bromate (BrO_3^-)	mg L^{-1}	< 0.10	< 0.10
Bromide (Br^-)	mg L^{-1}	< 0.10	< 0.10
Iodide (I^-)	mg L^{-1}	< 0.10	< 0.10
Nitrite (NO_2^-)	mg L^{-1}	< 0.05	< 0.05
Nitrate (NO_3^-)	mg L^{-1}	1.26	0.70
Sulfate (SO_4^{2-})	mg L^{-1}	20.45	1.21
Hydrogen phosphate (HPO_4^{2-})	mg L^{-1}	< 0.10	< 0.10
Hydrogen carbonate (HCO_3^-)	mg L^{-1}	306.80	185.58

S4.5 Sample Preparation Procedures

S4.5.1 Centrifugal Ultrafiltration and Analyte Spiking of Surface Water

The dissolved organic matter (DOM) in the SW sample (Wiesäckerbach) was fractionated according to molecular size by ultrafiltration following the procedure reported by Xu and Guo.³²³ To this end, we used centrifugal devices equipped with modified polyethersulfone (PES) filters of different molecular weight cut-offs (1, 3, 10 kDa MWCO, Macrosep® Advance 20 mL, Pall Corporation, USA). The centrifugal devices were successively rinsed with 20 mL of 0.05 M NaOH, 20 mL of 0.02 M HCl, 6 x 20 mL of ultrapure water, and 20 mL of SW sample to reduce organic carbon leaching from filter membranes and polypropylene housings (Figure S4.4a). The surface water was then sequentially centrifuged at a relative centrifugal force of 4000 g using membranes of decreasing cut-off. After every centrifugation cycle both supernatant (approx. 0.5 mL) and filtrate were collected. While filtrates were used for the next fractionation step, supernatants were combined and analyzed for dissolved organic carbon (DOC) concentration. DOC recoveries ranging between 99 and 105 % after every ultrafiltration step (Table S4.5) confirmed successful DOM fractionation without significant DOC loss or contamination. Partitioning of DOM among the size ranges was determined based on DOC concentration and exact volume of the different molecular size fractions. The DOC in the MW fractions of <1 kDa, 1 – 3 kDa, 3 – 10 kDa, and >10 kDa accounted for 38.2, 26.2, 20.8, and 14.7 % of the total SW DOC (Figure S4.5).

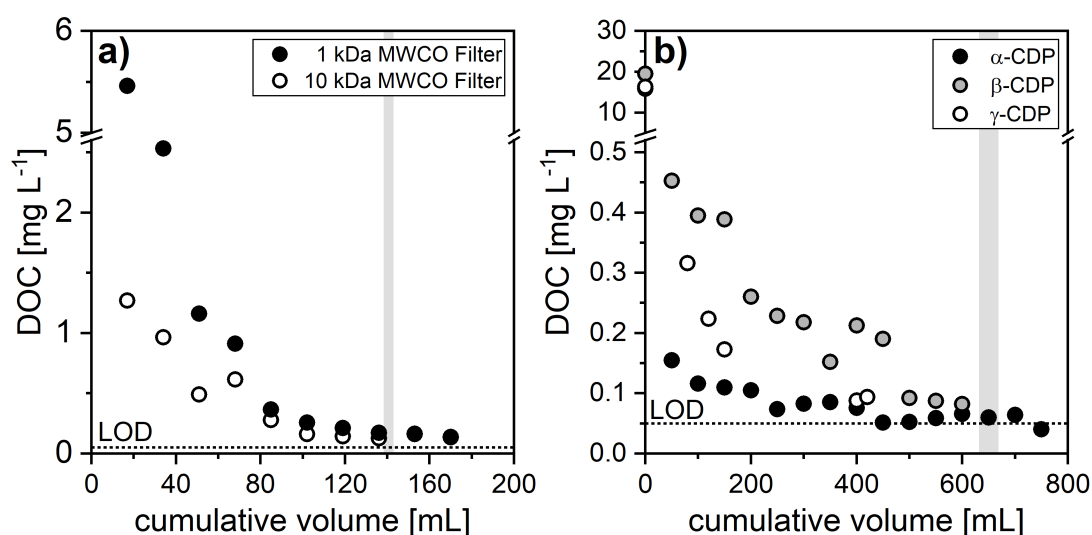


Figure S4.4. (a) DOC concentration in ultrapure water after ultrafiltration using centrifugal devices with molecular weight cut-offs of 1 and 10 kDa (Macrosep Advance 20 mL, Pall Corporation, USA), which had previously been rinsed with 20 mL of 0.05M NaOH and 20 mL of 0.02M HCl. (b) DOC concentrations in SPE breakthrough volumes of ultrapure water caused by organic carbon bleed from sorbent material. The horizontal dashed lines represent the instrumental limit of detection (LOD) and the gray rectangles indicate the volumes used for centrifugal device and sorbent washing.

Table S4.5. Dissolved organic carbon (DOC) recoveries after every ultrafiltration cycle of surface water sample SW using centrifugal devices with molecular weight cut-offs (MWCO) of 10, 3, and 1 kDa.

Ultrafiltration cycle	MWCO [kDa]	DOC recovery [%]
1	10	103.2
2	3	105.0
3	1	98.6

Table S4.6. DOC and spiked target analyte concentrations in the different molecular weight fractions, and resulting ratios of DOC to analyte prior to SPE experiments.

MW fraction [kDa]	DOC concentration [$\mu\text{g L}^{-1}$]	target analyte concentration [$\mu\text{g L}^{-1}$]	DOC:analyte ratio [-]
> 10	5281	1.15	4592
3 - 10	2275	0.50	4550
1 - 3	2088	0.45	4640
< 1	3030	0.65	4662

S4.5.2 Extraction of Dissolved Organic Matter for Molecular-Level Analysis

Table S4.7. Parameters of solid-phase extraction (SPE) of surface water (SW) and DOM reference standards (SRFA, SRHA) including sample volume (V_{sample}), sorbent bed weight of self-packed SPE cartridges (m_{sorbent}), dissolved organic carbon (DOC) concentration of water samples, and quality control parameters (i.e., DOC and sample volume per mass sorbent).

sample	V_{sample} [mL]	m_{sorbent} [mg]	DOC			DOC/ m_{sorbent} * [mmol g ⁻¹]	$V_{\text{sample}}/m_{\text{sorbent}}$ † [L g ⁻¹]
			[mg L ⁻¹]	[mmol L ⁻¹]	[mmol]		
SW	50.0	25.0	8.2	0.68	0.034	1.36	2.0
SRFA	50.0	50.0	22.4	1.86	0.093	1.86	1.0
SRHA	50.0	50.0	14.9	1.24	0.062	1.24	1.0

* maximum threshold: 2 mmol g⁻¹, proposed by Dittmar et al.²⁹³

† maximum threshold: 10 L g⁻¹, proposed by Dittmar et al.²⁹³

S4.6 Chemical Analyses

S4.6.1 Liquid Chromatography – Tandem Mass Spectrometry (LC-MS/MS) Analysis

Quantification of target analytes was performed using an ultrahigh-performance liquid chromatography system (PLATINblue, Knauer, Germany) coupled to tandem mass spectrometry (AB Sciex Triple-Quad 6500, Sciex, USA) using electrospray ionization (ESI) in positive mode. Prior analysis, sample aliquots (100 μL) were diluted with 880 μL ultrapure water and spiked with 20 μL of isotopically labeled internal standard (ILIS) mixture to a final ILIS concentration of 2 $\mu\text{g L}^{-1}$. 25 μL of samples were injected and separated on a reversed-phased analytical column (Kinetex C18, 3 x 150 mm, 2.6 μm particle size, Phenomenex, USA) at 30 $^{\circ}\text{C}$ at a constant flow rate of 0.5 mL min^{-1} . We used an elution gradient with ultrapure water amended with 0.2 vol% formic acid as eluent A and acetonitrile as eluent B. First, the fraction of B was kept constant at 30 % for one minute. Within the next 15 min the fraction of B was increased linearly to 45 %, followed by a steep increase to 98 % within 1 min, which was kept constant for another 1.5 min. Finally, the column was re-equilibrated to initial conditions for 2 min. Analytes were quantified against reference standards based on extracted ion chromatograms using internal calibration with ILIS. The internal standard with the closest retention time was chosen for quantitation. Analytical details used for identification and quantification, including LODs and LOQs, are provided in Table S4.8.

S4.6.2 High-field Fourier Transform Ion Cyclotron Resonance Mass Spectrometry (FTICR MS) Analysis

FTICR MS Measurement

Ultrahigh-resolution Fourier transform ion cyclotron resonance (FTICR) MS analyses were acquired in negative ionization mode using a Solarix mass spectrometer equipped with a 12 T superconducting magnet and coupled to an Apollo II electrospray ionization (ESI) source (Bruker Daltonics, Bremen, Germany). Prior to continuous infusion of methanolic extracts at a constant flow rate of 2 $\mu\text{L min}^{-1}$, SW and SRFA samples were diluted with methanol to a concentration of 5 $\mu\text{gC mL}^{-1}$, whereas SRHA samples were diluted to 20 $\mu\text{gC mL}^{-1}$. These DOC concentrations in extracts were optimized to ensure appropriately high peak intensities, while still preventing significant ionization suppression, adduct formation, and overloading of the ICR cell. The ESI source was operated with a nebulizer gas pressure of 138 kPa and a drying gas pressure of 103 kPa, while a source heater temperature of 200 $^{\circ}\text{C}$ guaranteed rapid desolvation of ionized droplets. 400 scans with a time domain of 4 megawords and within a m/z range of 174.4 to 1400 were averaged and post-calibrated based on clusters of arginine and reference mass lists of known internal DOM calibrants. A mass accuracy below 100 ppb was achieved. Post-processing was executed using the software Compass DataAnalysis 4.1 (Bruker Daltonics, Bremen, Germany).

Data Analysis

Intensity-weighted averages of bulk parameters (X_{wa}), such as elemental ratios or chemical indices, were calculated based on peak intensities (Int) of each assigned formula (i) according to equation (S4.1):

$$X_{wa} = \frac{\sum_{i=1}^n X_i \times Int_i}{\sum_{i=1}^n Int_i} \quad (S4.1)$$

Relative peak intensities (RI), were calculated based on summarized total peak intensity according to equation (S4.2):

$$RI = \frac{Int_i}{\sum_{i=1}^n Int_i} \times 1000 \quad (S4.2)$$

Chemical indices to study the degree of unsaturation and aromaticity of compounds, including double bond equivalent (DBE), carbon-normalized DBE (DBE/C), and the modified aromaticity index (AI_{mod}), were derived according to equation (S4.3) and (S4.4) as described by Koch and Dittmar:^{230,231}

$$DBE = 1 + \frac{1}{2}(2C - H + N) \quad (S4.3)$$

$$AI_{mod} = \frac{1 + C - \frac{1}{2}O - S - \frac{1}{2}(H + N)}{C - \frac{1}{2}O - N - S} \quad (S4.4)$$

where C, H, N, O, and S are the numbers of carbon, hydrogen, nitrogen, oxygen, and sulfur atoms, respectively, in the molecular structure.

Table S4.8. Substance specific MS/MS settings and instrumental limits of detection ($LOD_{instr.}$) and limits of quantification ($LOQ_{instr.}$).

analyte	ESI mode	retention time [min]	precursor mass [m/z]	product mass (quantifier) [m/z]	product mass (qualifier) [m/z]	collision energy [V]	collision cell exit potential [V]	declustering potential [V]	$LOD_{instr.}^*$ [$\mu\text{g L}^{-1}$]	$LOQ_{instr.}^*$ [$\mu\text{g L}^{-1}$]
2,6-dichlorobenzamide	positive	1.30	189.9	172.9	144.9	81	25	10	0.6	1.7
atrazine	positive	4.90	216.0	174.0	104.0	1	23	10	0.9	2.8
azoxystrobin	positive	13.70	404.0	372.0	329.0	46	17	26	0.3	1.0
azoxystrobin-d4	positive	13.60	408.0	376.1	333.1	1	17	24	-	-
boscalid	positive	13.71	343.0	307.0	271.0	121	25	18	0.2	0.5
dimethomorph	positive	10.00	388.1	301.0	165.0	126	27	20	0.4	1.2
dimethomorph-d6	positive	10.05	394.0	307.0	171.1	101	27	18	-	-
metamitron	positive	1.32	203.0	175.0	104.0	61	21	10	0.7	2.0
methiocarb	positive	9.95	226.0	169.0	185.0	26	11	10	0.9	2.6
methiocarb-d3	positive	9.91	229.0	169.0	121.0	56	23	14	-	-
propiconazole	positive	16.60	342.0	159.0	123.0	81	33	18	0.5	1.4
propiconazole-d3	positive	16.79	345.0	162.0	126.0	61	35	10	-	-
S-metolachlor	positive	15.10	284.0	252.1	176.2	56	19	14	0.3	0.8
terbutylazine	positive	9.33	230.0	174.0	132.0	56	21	16	1.0	3.0
terbutylazine-d5	positive	9.18	235.0	179.0	137.0	56	33	16	-	-
thiacloprid	positive	2.28	253.0	126.0	186.0	61	27	14	0.8	2.4
thiacloprid-d4	positive	2.24	257.0	126.0	166.8	76	27	14	-	-

* based on the standard deviation of the response and the slope of the calibration curve (ranging from 0.1 to 20.0 $\mu\text{g L}^{-1}$) as proposed by ICH guidelines^{37/5}

S4.7 Results

S4.7.1 Micropollutant Extraction in Presence of Dissolved Organic Matter of Varying Molecular Size

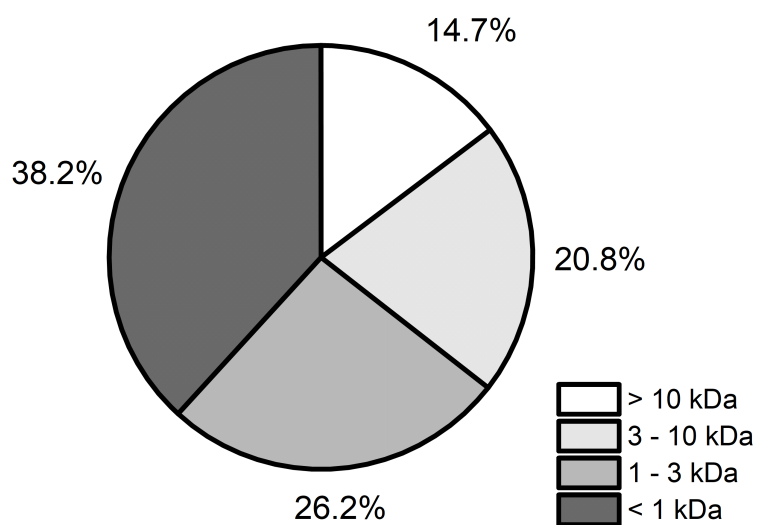


Figure S4.5. Partitioning of dissolved organic carbon (DOC) among different molecular weight fractions (i.e., < 1 kDa, 1-3 kDa, 3-10 kDa, > 10 kDa) in the surface water (SW) sample.

Table S4.9. Recoveries (in %) of target analytes and dissolved organic carbon (DOC) after solid-phase extraction of spiked molecular weight (MW) fractions (i.e., > 10, 3 – 10, 1 – 3, < 1 kDa) of the surface water sample using α -CDP, β -CDP, or γ -CDP. Uncertainties reflect one standard deviation ($\pm\sigma$) of experimental triplicates.

DOM MW fraction [kDa]	[†] BAM	MTM	TIA	AZO	DIM	ATR	BOS	SME	MET	TER	PRO	DOC
α -CDP	> 10	43 ± 9	83 ± 6	86 ± 2	84 ± 2	69 ± 13	86 ± 3	100 ± 11	94 ± 1	87 ± 3	87 ± 2	4.7 ± 0.7
	3 - 10	47 ± 4	80 ± 4	86 ± 4	81 ± 2	65 ± 3	94 ± 4	88 ± 2	100 ± 2	75 ± 1	94 ± 2	2.9 ± 0.8
	1 - 3	50 ± 2	71 ± 3	88 ± 2	n.a.	74 ± 4	88 ± 0	97 ± 16	80 ± 6	67 ± 4	92 ± 5	3.0 ± 0.9
	< 1	40 ± 3	80 ± 3	85 ± 4	73 ± 3	78 ± 1	85 ± 1	98 ± 1	96 ± 12	69 ± 12	88 ± 8	4.3 ± 0.1
p-value*	0.631	0.746	0.214	0.839	0.010	0.896	0.105	0.869	0.204	0.104	0.480	0.115
β -CDP	> 10	29 ± 4	75 ± 11	83 ± 10	98 ± 6	89 ± 8	91 ± 11	108 ± 2	96 ± 8	100 ± 12	102 ± 8	2.5 ± 0.3
	3 - 10	25 ± 2	72 ± 4	84 ± 3	80 ± 6	82 ± 4	99 ± 6	105 ± 6	99 ± 3	93 ± 5	97 ± 6	2.2 ± 0.1
	1 - 3	24 ± 1	68 ± 1	80 ± 4	98 ± 4	n.a.	95 ± 1	100 ± 4	95 ± 1	89 ± 2	102 ± 4	2.0 ± 0.3
	< 1	25 ± 3	80 ± 3	86 ± 3	96 ± 5	84 ± 2	95 ± 3	103 ± 6	95 ± 1	97 ± 4	105 ± 2	2.0 ± 0.0
p-value*	0.363	0.419	0.849	0.007	0.401	0.749	0.895	0.235	0.355	0.570	0.656	0.100
γ -CDP	> 10	11 ± 4	27 ± 13	46 ± 26	64 ± 22	63 ± 26	39 ± 14	65 ± 23	61 ± 24	57 ± 27	66 ± 23	3.3 ± 0.4
	3 - 10	10 ± 1	16 ± 1	23 ± 1	34 ± 2	33 ± 1	41 ± 3	42 ± 2	49 ± 2	42 ± 3	44 ± 2	4.2 ± 0.7
	1 - 3	11 ± 5	34 ± 20	46 ± 30	66 ± 38	n.a.	56 ± 19	65 ± 35	64 ± 38	56 ± 26	67 ± 36	3.9 ± 1.0
	< 1	8 ± 1	15 ± 2	26 ± 4	50 ± 9	40 ± 8	34 ± 8	53 ± 10	65 ± 7	44 ± 7	55 ± 9	4.3 ± 0.1
p-value*	0.783	0.404	0.531	0.498	0.207	0.502	0.658	0.755	0.877	0.816	0.709	0.426

*tests of statistical significance were performed by means of one-way ANOVA, where group mean values are statistically different at $p \leq 0.05$.

[†]BAM: 2,6-dichlorobenzamide, MTM: metatitron, TIA: thiacloprid, AZO: azoxystrobin, DIM: dimethomorph, ATR: atrazine, BOS: boscalid, SME: S-metolachlor, MET: methiocarb, TER: terbuthylazine, PRO: propiconazole, DOC: dissolved organic carbon

S4.7.2 Literature data on Recovery of Uncharged Micropollutants after Solid-Phase Extraction using β -CDP as Sorbent

Table S4.10. Recovery data for 88 target analytes uncharged at neutral pH conditions after solid-phase extraction using β -CDP sorbent. The data was adopted from literature and used for data visualization in Figure 4.3 in Chapter 4. The table additionally lists the compound classification, CAS number, formula, molecular weight, elemental H/C and O/C ratio, log K_{OW} value, and McGowan volume (MV).

compound	comp. class*	CAS	MW [†]	formula	H/C	O/C	log K_{OW}	MV [‡]	Recovery (%)	Ref. [§]
10,11-dihydrocarbamazepine	Pharm.	3564-73-6	238.28	C ₁₅ H ₁₄ N ₂ O	0.93	0.07	2.46	1.85	84 ± 12	Li et al.
6-benzylaminopurine	Pest.	1214-39-7	225.25	C ₁₂ H ₁₁ N ₅	0.92	0.00	1.57	1.67	100 ± 0	Li et al.
Abacavir	Pharm.	136470-78-5	286.33	C ₁₄ H ₁₈ N ₆ O	1.29	0.07	1.62	2.09	100 ± 0	Li et al.
Acetaminophen	Pharm.	103-90-2	151.16	C ₈ H ₉ NO ₂	1.13	0.25	0.46	1.17	50 ± 6	Ling et al.
Acetamidiprid	Pest.	135410-20-7	222.67	C ₁₀ H ₁₁ CIN ₄	1.10	0.00	2.55	1.67	98 ± 4	Li et al.
Acetochlor	Pest.	34256-82-1	269.77	C ₁₄ H ₂₀ ClNO ₂	1.43	0.14	4.14	2.14	98 ± 3	Li et al.
Adrenosterone	Horm.	382-45-6	300.40	C ₁₉ H ₂₄ O ₃	1.26	0.16	1.41	2.36	99 ± 1	Li et al.
Alachlor	Pest.	15972-60-8	269.77	C ₁₄ H ₂₀ ClNO ₂	1.43	0.14	3.52	2.14	98 ± 3	Li et al.
Allopurinol	Pharm.	315-30-0	136.11	C ₅ H ₄ N ₄ O	0.80	0.20	-0.55	0.90	25 ± 9	Ling et al.
Amcinonide	Pharm.	51022-69-6	502.60	C ₂₈ H ₃₅ FO ₇	1.25	0.25	3.56	3.62	100 ± 0	Li et al.
Atrazine-2-Hydroxy	Pest.	2163-68-0	197.24	C ₈ H ₁₃ N ₅ O	1.88	0.13	1.40	1.56	99 ± 1	Li et al.
Atrazine-desethyl	Pest.	6190-65-4	203.63	C ₆ H ₁₀ CIN ₅	1.67	0.00	1.51	1.34	54 ± 46	Li et al.
Bendiocarb	Pest.	22781-23-3	223.22	C ₁₁ H ₁₃ NO ₄	1.18	0.36	1.70	1.60	84 ± 11	Li et al.
Benzisothiazolin-3-on (BIT)	Pest.	2634-33-5	151.18	C ₇ H ₅ NOS	0.71	0.14	0.64	1.03	94 ± 8	Li et al.
Benzotriazole	Indust.	95-14-7	119.12	C ₆ H ₅ N ₃	0.83	0.00	1.17	0.86	86 ± 18	Li et al.
Benzotriazole-methyl-1H	Indust.	136-85-6	266.30	C ₇ H ₇ N ₃	1.00	0.00	1.71	1.01	99 ± 2	Li et al.
Bromacil	Pest.	314-40-9	261.12	C ₉ H ₁₃ BrN ₂ O ₂	1.44	0.22	2.11	1.63	77 ± 15	Li et al.
Caffeine	Lifest.	58-08-2	194.19	C ₈ H ₁₀ N ₄ O ₂	1.25	0.25	0.16	1.36	11 ± 20	Li et al.
Carbamazepine	Pharm.	298-46-4	236.27	C ₁₅ H ₁₂ N ₂ O	0.80	0.07	2.45	1.81	90 ± 8	Li et al.
Carbaryl	Pest.	63-25-2	201.22	C ₁₂ H ₁₁ NO ₂	0.92	0.17	2.36	1.50	97 ± 2	Ling et al.
Carbendazim	Pest.	10605-21-7	191.19	C ₉ H ₉ N ₃ O ₂	1.00	0.22	1.55	1.36	100 ± 0	Li et al.
Carbofuran	Pest.	1563-66-2	221.25	C ₁₂ H ₁₅ NO ₃	1.25	0.25	2.32	1.69	87 ± 4	Ling et al.
Carisoprodol	Pharm.	78-44-4	260.33	C ₁₂ H ₂₄ N ₂ O ₄	2.00	0.33	2.36	2.15	77 ± 13	Li et al.
Chloridazon	Pest.	1698-60-8	221.64	C ₁₀ H ₈ CIN ₃ O	0.80	0.10	1.14	1.52	98 ± 3	Li et al.
Chloroxylonol	Pharm.	88-04-0	156.61	C ₈ H ₉ ClO	1.13	0.13	3.27	1.20	56 ± 13	Ling et al.
Corticosterone	Pharm.	50-22-6	346.50	C ₂₁ H ₃₀ O ₄	1.43	0.19	1.94	2.74	99 ± 2	Li et al.
Coumarin	Natural	91-64-5	146.14	C ₉ H ₆ O ₂	0.67	0.22	1.51	1.06	99 ± 3	Li et al.
Cyanazine	Pest.	21725-46-2	240.69	C ₉ H ₁₃ CIN ₆	1.44	0.00	2.22	1.77	68 ± 30	Li et al.
Cyflufenamid	Pest.	180409-60-3	412.40	C ₂₀ H ₁₇ F ₃ N ₂ O ₂	0.85	0.10	5.60	2.66	100 ± 0	Li et al.
Diethyltoluamide (DEET)	Pest.	134-62-3	191.27	C ₁₂ H ₁₇ NO	1.42	0.08	2.02	1.68	95 ± 3	Ling et al.
Dehydroacetic	Pest.	520-45-6	168.15	C ₈ H ₈ O ₄	1.00	0.50	0.78	1.19	16 ± 15	Li et al.
Dexamethasone	Pharm.	50-02-2	392.50	C ₂₂ H ₂₉ FO ₅	1.32	0.23	1.83	2.91	90 ± 9	Li et al.
Diazinon	Pest.	333-41-5	304.35	C ₁₂ H ₂₁ N ₂ O ₃ PS	1.75	0.25	3.81	2.30	100 ± 0	Ling et al.
Diethyl Phthalate	Indust.	84-66-2	222.24	C ₁₂ H ₁₄ O ₄	1.17	0.33	2.47	1.71	77 ± 11	Li et al.
Dimethachlor	Pest.	50563-36-5	255.74	C ₁₃ H ₁₈ ClNO ₂	1.38	0.15	2.17	2.00	87 ± 11	Li et al.
Dimethoate	Pest.	60-51-5	229.30	C ₅ H ₁₂ NO ₃ PS ₂	2.40	0.60	0.78	1.58	75 ± 33	Li et al.
Diuron	Pest.	330-54-1	233.09	C ₉ H ₁₀ Cl ₂ N ₂ O	1.11	0.22	2.68	1.60	100 ± 0	Li et al.
Efavirenz	Pharm.	154598-52-4	315.67	C ₁₄ H ₉ ClF ₃ N ₂ O ₂	0.64	0.14	4.70	1.89	100 ± 0	Li et al.
Estrone	Horm.	53-16-7	270.40	C ₁₈ H ₂₂ O ₂	1.22	0.11	3.13	2.16	100 ± 0	Li et al.
Ethofumesate	Pest.	26225-79-6	286.35	C ₁₃ H ₁₈ O ₅ S	1.38	0.38	2.70	2.05	100 ± 1	Li et al.
Famciclovir	Pharm.	104227-87-4	321.33	C ₁₄ H ₁₉ N ₅ O ₄	1.36	0.29	0.64	2.34	99 ± 1	Li et al.
Fluconazole	Pharm.	86386-73-4	306.27	C ₁₃ H ₁₂ F ₂ N ₆ O	0.92	0.08	0.25	2.01	22 ± 16	Li et al.
Hexametapol	Indust.	680-31-9	179.20	C ₆ H ₁₈ N ₃ OP	3.00	0.17	-0.22	1.52	13 ± 3	Li et al.
Hexazinone	Pest.	51235-04-2	252.31	C ₁₂ H ₂₀ N ₄ O ₂	1.67	0.17	1.85	1.97	92 ± 7	Li et al.
Hydrocortisone	Pharm.	50-23-7	362.50	C ₂₁ H ₃₀ O ₅	1.43	0.24	2.16	2.80	91 ± 8	Li et al.
Isophorone Diisocyanate	Indust.	4098-71-9	222.28	C ₁₂ H ₁₈ O ₂ N ₂	1.50	0.17	4.75	1.84	79 ± 17	Li et al.
Isoproturon	Pest.	34123-59-6	206.28	C ₁₂ H ₁₈ N ₂ O	1.50	0.08	2.87	1.78	100 ± 0	Li et al.

Lamotrigine	Pharm.	84057-84-1	256.09	C ₉ H ₇ Cl ₂ N ₅	0.78	0.00	2.57	1.65	100 ± 0	Li et al.
Linuron	Pest.	330-55-2	249.09	C ₉ H ₁₀ Cl ₂ N ₂ O ₂	1.11	0.22	3.20	1.66	100 ± 0	Li et al.
Malaoxon	Metab.	1634-78-2	314.29	C ₁₁ H ₁₉ O ₇ PS	1.90	0.70	0.97	2.20	99 ± 1	Ling et al.
Meprobamate	Pharm.	57-53-4	218.25	C ₉ H ₁₈ N ₂ O ₄	2.00	0.44	0.70	1.73	38 ± 22	Li et al.
Metalaxyl	Pest.	57837-19-1	279.33	C ₁₃ H ₂₁ NO ₄	1.40	0.27	1.65	2.23	75 ± 13	Li et al.
Methocarbamol	Pharm.	532-03-6	241.24	C ₁₁ H ₁₅ NO ₅	1.36	0.45	0.61	1.77	87 ± 10	Li et al.
Methomyl	Pest.	16752-77-5	162.21	C ₅ H ₁₀ N ₂ O ₂ S	2.00	0.40	0.60	1.20	36 ± 14	Ling et al.
Metribuzin	Pest.	21087-64-9	214.24	C ₈ H ₁₄ N ₄ OS	1.75	0.13	1.49	1.62	96 ± 2	Ling et al.
Molinate	Pest.	2212-67-1	187.30	C ₉ H ₁₇ NOS	1.89	0.11	3.21	1.55	99 ± 2	Li et al.
Oxazepam	Pharm.	604-75-1	286.71	C ₁₃ H ₁₁ ClN ₂ O ₂	0.73	0.13	2.24	1.99	93 ± 6	Li et al.
Oxcarbazepine	Pharm.	28721-07-5	252.27	C ₁₃ H ₁₂ N ₂ O ₂	0.80	0.13	1.11	1.87	85 ± 12	Li et al.
Oxybenzone	Lifest.	131-57-7	228.24	C ₁₄ H ₁₂ O ₃	0.86	0.21	3.79	1.74	100 ± 0	Li et al.
Paraxanthine	Lifest.	611-59-6	180.16	C ₇ H ₈ N ₄ O ₂	1.14	0.29	-0.39	1.22	17 ± 19	Li et al.
Penciclovir	Pharm.	39809-25-1	253.26	C ₁₀ H ₁₅ N ₅ O ₃	1.50	0.30	-1.14	1.80	22 ± 8	Ling et al.
Pentoxifylline	Pharm.	6493-05-6	278.31	C ₁₃ H ₁₈ N ₄ O ₃	1.38	0.23	0.56	2.08	98 ± 4	Li et al.
Phenytoin (Dilantin)	Pharm.	57-41-0	252.27	C ₁₃ H ₁₂ N ₂ O ₂	0.80	0.13	2.47	1.87	93 ± 7	Li et al.
Pirimicarb	Pest.	23103-98-2	238.29	C ₁₁ H ₁₈ N ₄ O ₂	1.64	0.18	1.70	1.89	99 ± 1	Li et al.
Pirimiphos-Ethyl	Pest.	23505-41-1	333.39	C ₁₃ H ₂₄ N ₃ O ₃ PS	1.85	0.23	4.85	2.55	100 ± 0	Li et al.
Primidone	Pharm.	125-33-7	218.25	C ₁₂ H ₁₄ N ₂ O ₂	1.17	0.17	0.91	1.68	84 ± 27	Li et al.
Progesterone	Horm.	57-83-0	314.50	C ₂₁ H ₃₀ O ₂	1.43	0.10	3.87	2.62	100 ± 1	Li et al.
Prometon	Pest.	1610-18-0	225.29	C ₁₁ H ₁₉ N ₃ O	1.90	0.10	2.99	1.84	99 ± 1	Li et al.
Propachlor	Pest.	1918-16-7	211.69	C ₁₁ H ₁₄ ClNO	1.27	0.09	2.18	1.66	97 ± 3	Ling et al.
Propazine	Pest.	139-40-2	229.71	C ₉ H ₁₆ ClN ₅	1.78	0.00	2.93	1.76	100 ± 0	Li et al.
Propoxur	Pest.	114-26-1	209.24	C ₁₁ H ₁₅ NO ₃	1.36	0.27	1.52	1.65	84 ± 11	Li et al.
Propyzamide	Pest.	23950-58-5	256.12	C ₁₂ H ₁₁ Cl ₂ NO	0.92	0.08	3.43	1.84	100 ± 0	Li et al.
Pyrazophos	Pest.	13457-18-6	373.37	C ₁₄ H ₂₀ N ₃ O ₅ PS	1.43	0.36	3.80	2.61	100 ± 0	Li et al.
Siduron	Pest.	1982-49-6	232.32	C ₁₄ H ₂₀ N ₂ O	1.43	0.07	3.80	1.95	100 ± 0	Li et al.
Simazine	Pest.	122-34-9	201.66	C ₇ H ₁₂ ClN ₅	1.71	0.00	2.18	1.48	91 ± 7	Li et al.
Sucralose	Lifest.	56038-13-2	397.60	C ₁₂ H ₁₉ Cl ₃ O ₈	1.58	0.67	-1.00	2.42	8 ± 14	Li et al.
Sulfadimethoxine	Pharm.	122-11-2	310.33	C ₁₂ H ₁₄ N ₄ O ₄ S	1.17	0.33	1.17	2.21	81 ± 15	Li et al.
Sulfamethazine	Pharm.	57-68-1	278.33	C ₁₂ H ₁₄ N ₄ O ₂ S	1.17	0.17	0.14	2.00	38 ± 37	Li et al.
Sulfamethoxazole	Pharm.	723-46-6	253.28	C ₁₀ H ₁₁ N ₃ O ₃ S	1.10	0.30	0.48	1.72	39 ± 35	Li et al.
TDCPP	Indust.	13674-87-8	430.90	C ₉ H ₁₃ Cl ₆ O ₄ P	1.67	0.44	3.65	2.55	83 ± 5	Li et al.
Temazepam	Pharm.	846-50-4	300.74	C ₁₆ H ₁₃ ClN ₂ O ₂	0.81	0.13	2.19	2.13	96 ± 6	Li et al.
Testosterone	Horm.	58-22-0	288.40	C ₁₉ H ₂₈ O ₂	1.47	0.11	3.32	2.38	100 ± 0	Li et al.
Theophylline	Pharm.	58-55-9	180.16	C ₇ H ₈ N ₄ O ₂	1.14	0.29	-0.39	1.22	17 ± 19	Li et al.
Thiabendazole	Pharm.	148-79-8	201.25	C ₁₀ H ₇ N ₃ S	0.70	0.00	2.47	1.40	100 ± 0	Li et al.
Triamterene	Pharm.	396-01-0	253.26	C ₁₂ H ₁₁ N ₇	0.92	0.00	0.98	1.83	100 ± 0	Li et al.
Tributyl phosphate (TBP)	Indust.	126-73-8	266.31	C ₁₂ H ₂₇ O ₄ P	2.25	0.33	4.00	2.24	98 ± 3	Li et al.
Triclosan	Pest.	3380-34-5	289.50	C ₁₂ H ₇ Cl ₃ O ₂	0.58	0.17	4.76	1.81	100 ± 0	Li et al.
Tris (2-chloroethyl) phosphate (TCEP)	Indust.	115-96-8	285.50	C ₆ H ₁₂ Cl ₃ O ₄ P	2.00	0.67	1.44	1.76	88 ± 11	Li et al.

*Pharm. = Pharmaceutical, Pest. = Pesticide, Metab. = Metabolite, Indust. = Industrial, Horm. = Hormone, Lifest. = Lifestyle

[†]Molecular weight in g mol⁻¹

[‡]McGowan volume in cm³ mol⁻¹ 100⁻¹

[§]Recovery data obtained from Ling et al.¹⁹⁴ or Li et al.¹⁹⁵

S4.7.3 Molecular-Level Characterization of Dissolved Organic Matter by FTICR MS

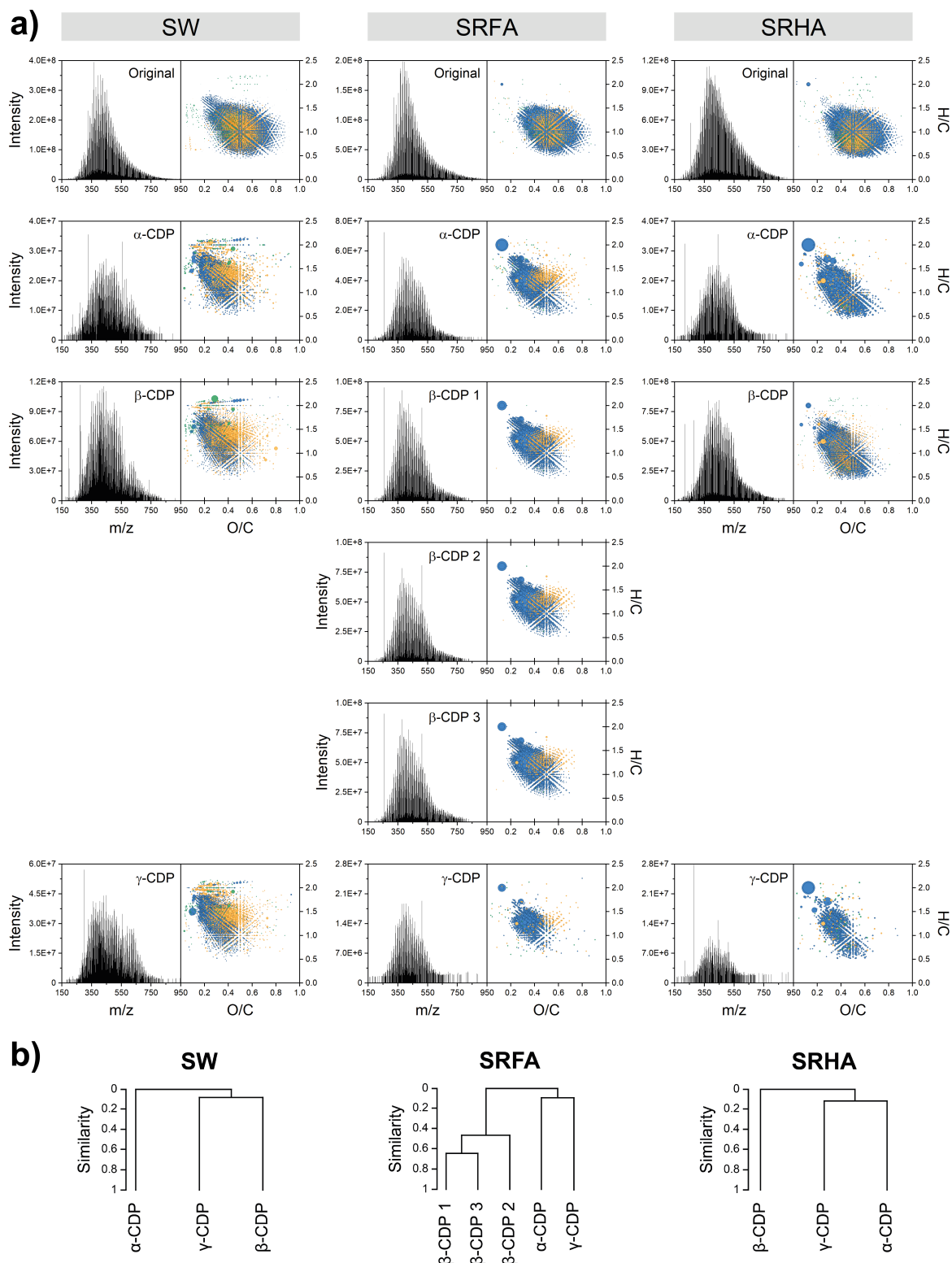


Figure S4.6. (a) Negative ESI 12 T FTICR mass spectra (left panels) and corresponding Van Krevelen diagrams (right panels) of the original surface water (SW) and Suwannee River Fulvic and Humic (SRFA, SRHA) samples and respective extracts of α -, β -, and γ -CDP. (b) Hierarchical cluster analysis (HCA) of all m/z ions based on normalized peak intensities and Pearson similarity indices.

Table S4.11. Counts and relative proportions (in brackets) of m/z ions for original and sorbent extract DOM sorted according to CHO, CHNO, and CHOS molecular composition, intensity-weighted averages of elemental compositions, elemental and mass-to-charge ratios, and chemical indices, and percentages of aromatic compounds as computed from negative ESI 12 T FTICR mass spectra for singly charged ions reported in neutral form.

sample	compounds										intensity-weighted average										%Ar _*
	total	CHO	CHNO	CHOS	H (%)	C (%)	O (%)	N (%)	S (%)	H/C	O/C	C/N	C/S	m/z	DBE	DBE/C	AI _{mod}				
<i>Surface Water (SW)</i>																					
Original	7010	3955 (56%)	2559 (37%)	496 (7%)	43.0	38.3	18.3	0.3	0.0	1.12	0.48	112	827	497	12	0.49	0.33	17.2			
α -CDP	2963	1901 (64%)	938 (32%)	124 (4%)	51.8	36.6	11.1	0.4	0.1	1.41	0.30	92	570	476	9	0.34	0.23	8.5			
β -CDP	4721	2713 (57%)	1773 (38%)	235 (5%)	51.1	36.8	11.5	0.4	0.1	1.39	0.31	83	491	472	9	0.35	0.23	9.3			
γ -CDP	3780	2294 (61%)	1308 (35%)	178 (5%)	52.5	36.1	10.9	0.4	0.1	1.45	0.30	88	659	474	8	0.32	0.20	7.4			
<i>Savannee River Fulvic Acid (SRFA)</i>																					
Original	3696	2670 (72%)	810 (22%)	216 (6%)	42.0	38.3	19.6	0.1	0.0	1.10	0.51	336	1918	493	11	0.50	0.33	16.1			
α -CDP	2209	1760 (80%)	397 (18%)	52 (2%)	48.3	37.9	13.6	0.1	0.0	1.27	0.36	255	1919	464	10	0.41	0.28	11.7			
β -CDP #1	2280	1926 (84%)	350 (15%)	4 (0%)	47.8	38.1	14.1	0.1	0.0	1.25	0.37	388	39845	465	10	0.42	0.29	11.1			
β -CDP #2	2114	1800 (85%)	309 (15%)	5 (0%)	47.8	38.1	14.0	0.1	0.0	1.26	0.37	401	36325	465	10	0.41	0.29	11.1			
β -CDP #3	2219	1899 (86%)	316 (14%)	4 (0%)	47.7	38.1	14.1	0.1	0.0	1.25	0.37	451	41982	469	10	0.42	0.29	11.1			
γ -CDP	963	802 (83%)	131 (14%)	30 (3%)	48.4	37.9	13.5	0.2	0.1	1.28	0.36	210	722	436	9	0.41	0.28	8.0			
<i>Savannee River Humic Acid (SRHA)</i>																					
Original	4227	2981 (71%)	1002 (24%)	244 (6%)	39.2	40.0	20.6	0.1	0.0	0.98	0.52	282	1189	499	13	0.55	0.40	28.0			
α -CDP	1947	1705 (88%)	218 (11%)	24 (1%)	45.4	39.7	14.8	0.1	0.0	1.14	0.37	323	3188	457	11	0.47	0.37	27.0			
β -CDP	4026	2936 (73%)	987 (25%)	103 (3%)	44.3	40.0	15.5	0.2	0.0	1.11	0.39	216	2034	483	12	0.49	0.37	26.0			
γ -CDP	936	829 (89%)	67 (7%)	40 (4%)	48.3	38.4	13.1	0.2	0.1	1.26	0.34	252	504	429	9	0.42	0.31	21.4			

* Percentage of compounds with modified aromaticity index (AI_{mod}) ≥ 0.5

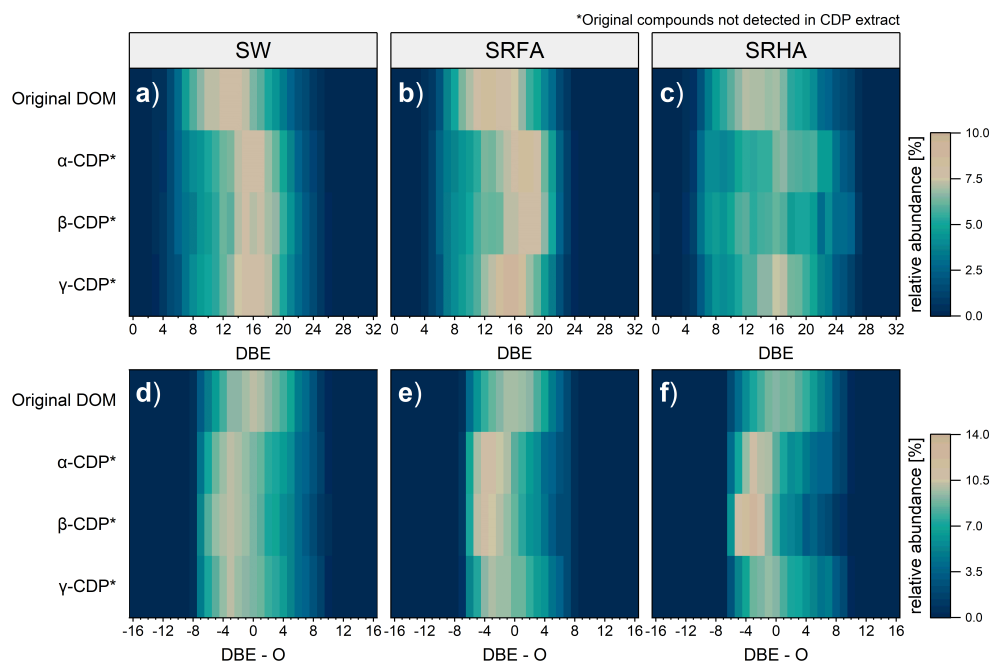


Figure S4.7. Relative abundance of CHO-annotated formulas as a function of double bond equivalent (DBE) and DBE minus count of oxygen (DBE-O) values for surface water (a, d), Suwannee River fulvic acid (b, e) and Suwannee River humic Acid (c, f) samples, respectively. Original DOM sample compositions are compared with compositions of compounds that were not detected in extracts obtained after solid-phase extraction using α -, β -, and γ -CDP as sorbent.

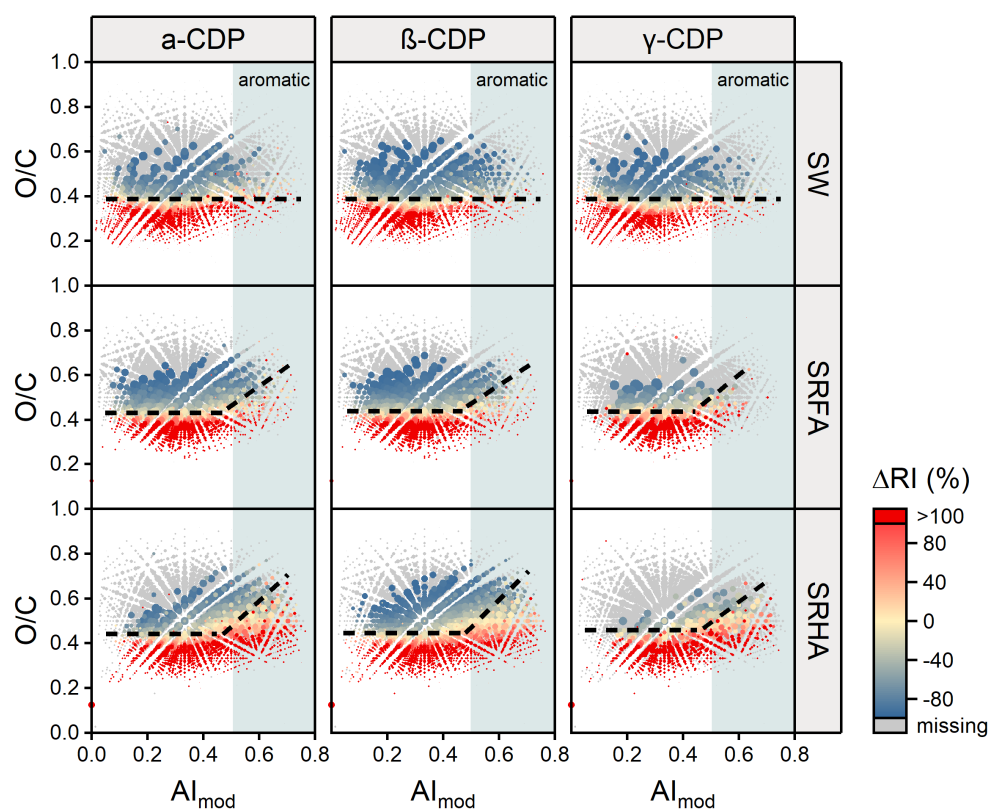


Figure S4.8. O/C versus modified aromaticity index (AI_{mod}) diagrams of CHO-annotated molecular DOM compositions in α -, β -, and γ -CDP extracts of surface water (SW) and Suwannee River Fulvic and Humic Acid (SRFA, SRHA) samples. Differences in relative intensities (ΔRI) were calculated relative to the original sample composition. Dashed lines denote approximate boundaries between relative enhancement (red) and depletion (blue, gray) of compounds in CDP extracts whereas the green area indicate molecules with aromatic moieties (i.e., $AI_{mod} \geq 0.5$). Symbol sizes reflect the relative signal intensities of mass peaks in the original mass spectra.

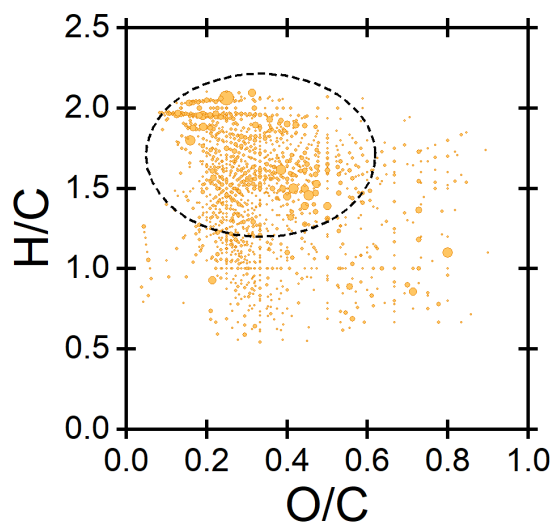


Figure S4.9. Van Krevelen diagram of uniquely detected CHNO-annotated molecular formulas in cyclodextrin polymer (CDP) extracts of the surface water samples. The dashed circle signifies highly saturated CHNO-compounds, possibly cationic aliphatic amines, which were selectively extracted by CDPs due to their negative surface charge.

S5 Supporting Information to Chapter 5



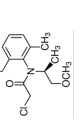

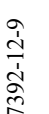
S5.1 Chemicals

Table S5.1. List of chemicals used in Chapter 5.

chemical	CAS number	purity/grade	supplier
<i>Reagents</i>			
ammonia	7664-41-7	puriss., anhydrous, $\geq 99.9\%$	Sigma-Aldrich
boron trifluoride diethyl etherate	109-63-7	for synthesis	Sigma-Aldrich
calcium chloride	10043-52-4	free-flowing, Redi-Dri, $\geq 97\%$	Sigma-Aldrich
graphene oxide	1034343-98-0	n.a.	Graphitene Ltd.
hydrochloric acid	7647-01-0	ACS reagent, 37 %	Sigma-Aldrich
L-ascorbic acid	50-81-7	BioXtra, $\geq 99.0\%$, crystalline	Sigma-Aldrich
<i>N,N'</i> -dicyclohexylcarbodiimide	538-75-0	for synthesis	Sigma-Aldrich
polyether diamine	65605-36-9	Jeffamine ED-2003	Huntsman, USA
polyglycerol-3-glycidyl ether	118549-88-5	Polypox R9	UPPC, Mietingen
sodium bicarbonate	144-55-8	ACS reagent, $\geq 99.7\%$	Sigma-Aldrich
sodium carbonate	497-19-8	ACS reagent, $\geq 99.5\%$	Sigma-Aldrich
sodium hydroxide	1310-73-2	BioXtra, $\geq 98\%$	Sigma-Aldrich
<i>Solvents</i>			
1,4-dioxane	123-91-1	ACS reagent, $\geq 99.0\%$	Sigma-Aldrich
acetonitrile	75-05-8	HPLC Plus, $\geq 99.9\%$	Sigma-Aldrich
methanol	67-56-1	$\geq 99.9\%$	Sigma-Aldrich
<i>N,N</i> -dimethylformamide	68-12-2	ACS reagent, $\geq 99.8\%$	Sigma-Aldrich
<i>tert</i> -butyl methyl ether	1634-04-4	ACS reagent, $\geq 99.0\%$	Sigma-Aldrich
toluol	108-88-3	puriss. p.a., ACS reagent, $\geq 99.7\%$	Sigma-Aldrich
<i>Analytical standards</i>			
2,6-dichlorobenzamide (BAM)	2008-58-4	PESTANAL®, anal. standard	Sigma-Aldrich
chloridazon	1698-60-8	PESTANAL®, anal. standard	Sigma-Aldrich
isoproturon	34123-59-6	PESTANAL®, anal. standard	Sigma-Aldrich
<i>S</i> -metolachlor	87392-12-9	PESTANAL®, anal. standard	Sigma-Aldrich
terbuthylazine	5915-41-3	PESTANAL®, anal. standard	Sigma-Aldrich

n.a. = not available

Table S5.2. Physicochemical properties, CAS number, formula, structure, and classification of the selected target analytes in chapter 5.

name	CAS number	formula	structure	classification	molecular weight [g mol ⁻¹]	McGowan volume [cm ³ mol ⁻¹ 100 ⁻¹]	log K _{ow} [-]	pK _a [-]	charge pH 7 [-]
herbicides									
chloridazon	1698-60-8	C ₁₀ H ₈ ClN ₃ O		pyridazinone	221.643	1.5229	1.19	3.38	n
isoproturon	34123-59-6	C ₁₂ H ₁₈ N ₂ O		phenylurea	206.284	1.7771	2.87	-	n
S-metolachlor	87392-12-9	C ₁₅ H ₂₂ ClNO ₂		chloroacetanilide	283.793	2.2811	3.05	-	n
terbuthylazine	5915-41-3	C ₉ H ₁₆ ClN ₅		triazine	229.710	1.7605	3.40	1.9	n
metabolite									
2,6-dichloro-benzamide (BAM)	2008-58-4	C ₇ H ₅ Cl ₂ NO		metabolite of diclobenil	190.027	1.2176	0.77	-	n

Data was adopted from the EU Pesticides Database (v2.2),³⁷² except for the McGowan volume which was calculated based on the analyte structure (*).³⁷³

S5.2 MAF Functionalization

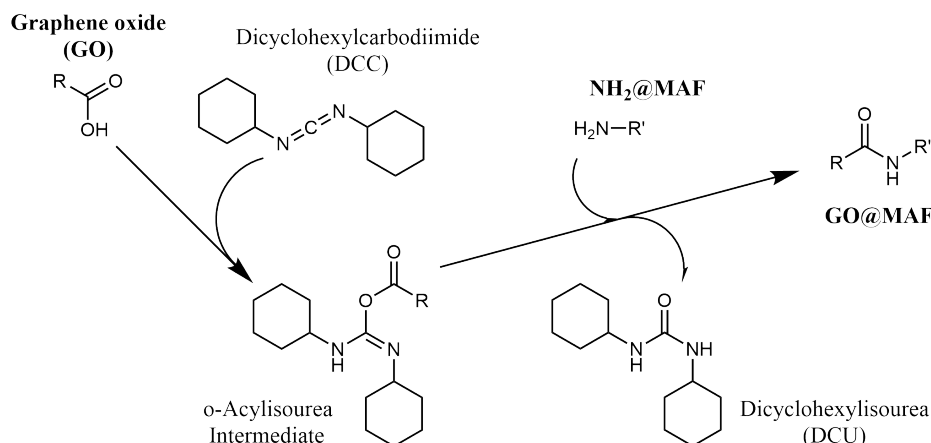


Figure S5.1. Reaction scheme of the coupling of graphene oxide (GO) with primary amines on the surface of monolithic adsorption filters (NH₂@MAF) using dicyclohexylcarbodiimide (DCC) as activation agent.

S5.3 Results and Discussion

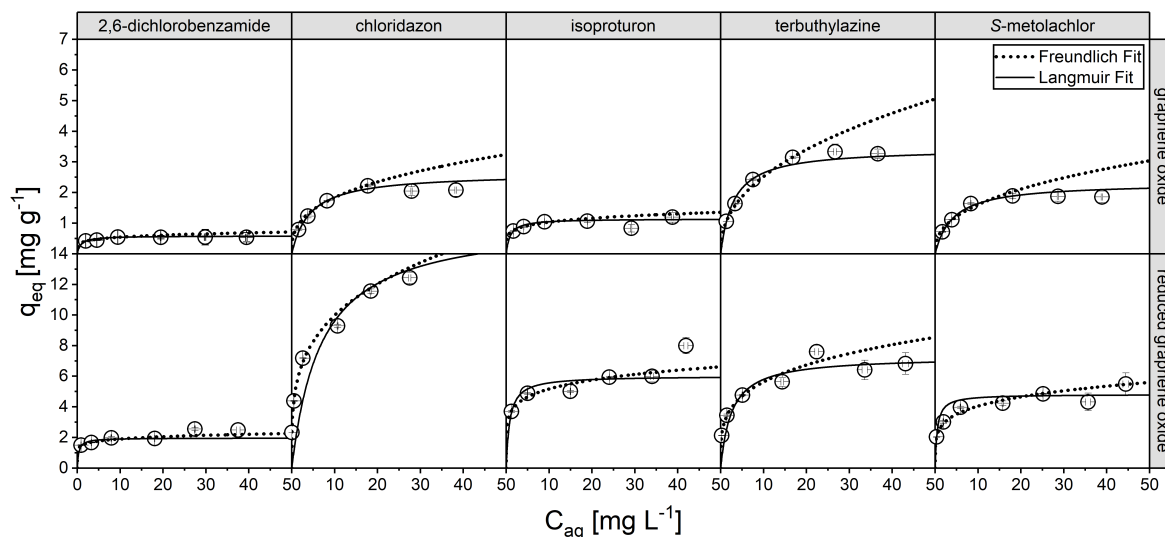


Figure S5.2. Equilibrium sorption isotherms of graphene oxide (GO) and reduced graphene oxide (rGO) at 25 ± 1 °C for 2,6-dichlorobenzamide, chloridazon, isotreturon, terbuthylazine, and S-metolachlor. The sorbed analyte concentration at equilibrium, q_{eq} (mg g⁻¹), is plotted against the aqueous equilibrium concentration of the compound, C_{aq} (mg L⁻¹). Freundlich and Langmuir isotherm fits are represented by dashed and solid lines, respectively.

Table S5.3. Sorption parameters of the 5 target analytes for graphene oxide (GO) and reduced graphene oxide (rGO). Values were obtained by fitting batch sorption data (Figure S5.2) to both Freundlich and Langmuir sorption isotherm models.

Sorbent	Isotherm	Parameter	Unit	BAM	CHL	ISO	TER	MET
Graphene Oxide (GO)	Freundlich	K_F	$\frac{mg/g}{(mg/L)^{1/n}}$	0.37 ± 0.02	0.82 ± 0.10	0.71 ± 0.05	0.94 ± 0.01	0.65 ± 0.06
		n	[-]	5.94 ± 0.79	2.84 ± 0.45	6.00 ± 1.2	2.32 ± 0.11	2.53 ± 0.37
		R^2	[-]	0.92	0.91	0.85	0.98	0.89
	Langmuir	K_L	[L mg ⁻¹]	1.21 ± 0.28	0.24 ± 0.04	1.11 ± 0.16	0.33 ± 0.04	0.24 ± 0.03
		q_m	[mg g ⁻¹]	0.58 ± 0.02	2.63 ± 0.14	1.14 ± 0.03	3.44 ± 0.26	2.31 ± 0.17
		R^2	[-]	0.86	0.98	0.95	0.97	0.97
Reduced Graphene Oxide (rGO)	Freundlich	K_F	$\frac{mg/g}{(mg/L)^{1/n}}$	1.49 ± 0.08	5.35 ± 0.07	3.63 ± 0.18	3.10 ± 0.03	2.55 ± 0.04
		n	[-]	9.27 ± 2.39	3.69 ± 0.06	6.53 ± 0.73	3.87 ± 0.10	4.98 ± 0.15
		R^2	[-]	0.79	0.99	0.95	0.99	0.99
	Langmuir	K_L	[L mg ⁻¹]	2.94 ± 1.61	0.15 ± 0.05	1.23 ± 0.27	0.39 ± 0.17	2.09 ± 0.24
		q_m	[mg g ⁻¹]	1.96 ± 0.13	16.22 ± 1.43	6.01 ± 0.18	7.27 ± 0.62	4.81 ± 0.16
		R^2	[-]	0.55	0.99	0.90	0.99	0.97

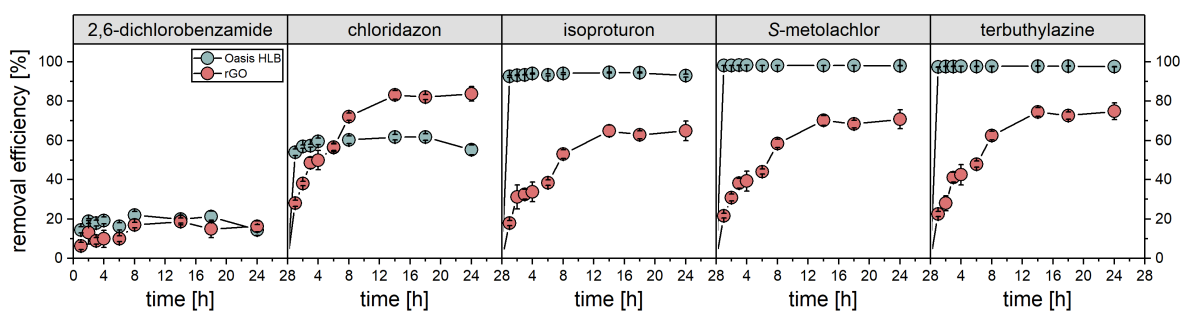


Figure S5.3. Kinetic plots for the sorption of the five model compounds on rGO (red) and Oasis HLB (green) displaying the percentage of removal versus the time.

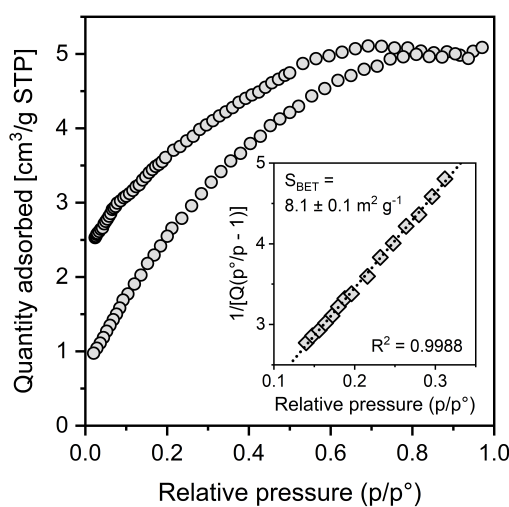


Figure S5.4. Nitrogen adsorption-desorption isotherm of rGO@MAF. Insert: BET isotherm linear plot of the section $p/p_0 = 0.05 - 0.35$, which was used for determining the specific surface area.

S6 Reprint Permissions

S6.1 Reprinted Figures in Chapter 1

Reprint permission for Figure 1.2b in Chapter 1.2.1 *Principle of the CSIA Technique*:

Reprinted from Trends in Analytical Chemistry, Vol. 30, No. 4, Hofstetter, T.B.; Berg, M., Assessing transformation processes of organic contaminants by compound-specific stable isotope analysis, 618-627, Copyright © 2010, with permission from Elsevier.



Assessing transformation processes of organic contaminants by compound-specific stable isotope analysis

Author: Thomas B. Hofstetter, Michael Berg
 Publication: TrAC Trends in Analytical Chemistry
 Publisher: Elsevier
 Date: April 2011

Copyright © 2010 Elsevier Ltd. All rights reserved.

Order Completed

Thank you for your order.

This Agreement between Mr. David Glöckler ("You") and Elsevier ("Elsevier") consists of your license details and the terms and conditions provided by Elsevier and Copyright Clearance Center.

Your confirmation email will contain your order number for future reference.

License Number 5647031025203

License date Oct 13, 2023

Licensed Content

Licensed Content Elsevier
 Publisher Elsevier
 Licensed Content TrAC Trends in Analytical Chemistry
 Publication TrAC Trends in Analytical Chemistry
 Assessing transformation processes of organic contaminants by compound-specific stable isotope analysis
 Licensed Content Title
 Licensed Content Thomas B. Hofstetter, Michael Berg
 Author Thomas B. Hofstetter, Michael Berg
 Licensed Content Apr 1, 2011
 Date Apr 1, 2011
 Licensed Content 30
 Volume 30
 Licensed Content 4
 Issue 4
 Licensed Content 10
 Pages 10

Order Details

Type of Use reuse in a thesis/dissertation
 Portion figures/tables/illustrations
 Number of figures/tables/illustrations 1
 Format both print and electronic
 Are you the author of this Elsevier article? No
 Will you be translating? No

About Your Work

Title Tailor-made Sorbents to Enhance Sensitivity in Stable Isotope Analysis of Aquatic Micropollutants: Comprehensive Investigations on the Selectivity of Cyclodextrin Polymers
 Institution name Technical University of Munich
 Expected presentation date Nov 2023

Additional Data

Order reference number 231013
 Portions Figure 4

Reprint permission for Figure 1.3 in Chapter 1.2.2 *Measurement of Compound-Specific Isotope Ratios*:

Reprinted from Analytical and Bioanalytical Chemistry, Vol. 403, No. 9, Elsner, M.; Jochmann, M.A.; Hofstetter, T.B.; Hunkeler, D.; Bernstein, A.; Schmidt, T.C.; Schimmelmann, A., Current challenges in compound-specific stable isotope analysis of environmental organic contaminants, 2471-2491, Copyright © 2012, with permission from Springer Nature.



SPRINGER NATURE

Current challenges in compound-specific stable isotope analysis of environmental organic contaminants

Author: Martin Elsner et al
 Publication: Analytical and Bioanalytical Chemistry
 Publisher: Springer Nature
 Date: Feb 3, 2012

Copyright © 2012, Springer-Verlag

Order Completed

Thank you for your order.

This Agreement between Mr. David Glöckler ("You") and Springer Nature ("Springer Nature") consists of your license details and the terms and conditions provided by Springer Nature and Copyright Clearance Center.

Your confirmation email will contain your order number for future reference.

License Number 5647050731692

License date Oct 13, 2023

Licensed Content

Licensed Content Publisher Springer Nature
 Licensed Content Publication Analytical and Bioanalytical Chemistry
 Licensed Content Title Current challenges in compound-specific stable isotope analysis of environmental organic contaminants
 Licensed Content Author Martin Elsner et al
 Licensed Content Date Feb 3, 2012

Order Details

Type of Use Thesis/Dissertation
 Requestor type academic/university or research institute
 Format print and electronic
 Portion figures/tables/illustrations
 Number of figures/tables /illustrations 1
 Will you be translating? no
 Circulation/distribution 1 - 29
 Author of this Springer Nature content no

About Your Work

Title Tailor-made Sorbents to Enhance Sensitivity in Stable Isotope Analysis of Aquatic Micropollutants: Comprehensive Investigations on the Selectivity of Cyclodextrin Polymers
 Institution name Technical University of Munich
 Expected presentation date Nov 2023

Additional Data

Order reference number 231013
 Portions Figure 1

S6.2 Reprinted Publication in Chapter 2



Avoiding Interferences in Advance: Cyclodextrin Polymers to Enhance Selectivity in Extraction of Organic Micropollutants for Carbon Isotope Analysis

Author: David Glöckler, Christopher Wabnitz, Martin Elsner, et al
Publication: Analytical Chemistry
Publisher: American Chemical Society
Date: May 1, 2023

Copyright © 2023, American Chemical Society

PERMISSION/LICENSE IS GRANTED FOR YOUR ORDER AT NO CHARGE

This type of permission/license, instead of the standard Terms and Conditions, is sent to you because no fee is being charged for your order. Please note the following:

- Permission is granted for your request in both print and electronic formats, and translations.
- If figures and/or tables were requested, they may be adapted or used in part.
- Please print this page for your records and send a copy of it to your publisher/graduate school.
- Appropriate credit for the requested material should be given as follows: "Reprinted (adapted) with permission from {COMPLETE REFERENCE CITATION}. Copyright {YEAR} American Chemical Society." Insert appropriate information in place of the capitalized words.
- One-time permission is granted only for the use specified in your RightsLink request. No additional uses are granted (such as derivative works or other editions). For any uses, please submit a new request.

If credit is given to another source for the material you requested from RightsLink, permission must be obtained from that source.

[BACK](#) [CLOSE WINDOW](#)

S6.3 Reprinted Publication in Chapter 3



Selectivity of β -Cyclodextrin Polymer toward Aquatic Contaminants: Insights from Ultrahigh-Resolution Mass Spectrometry of Dissolved Organic Matter

Author: David Glöckler, Mourad Harir, Philippe Schmitt-Kopplin, et al
Publication: Analytical Chemistry
Publisher: American Chemical Society
Date: Oct 1, 2023

Copyright © 2023, American Chemical Society

PERMISSION/LICENSE IS GRANTED FOR YOUR ORDER AT NO CHARGE

This type of permission/license, instead of the standard Terms and Conditions, is sent to you because no fee is being charged for your order. Please note the following:

- Permission is granted for your request in both print and electronic formats, and translations.
- If figures and/or tables were requested, they may be adapted or used in part.
- Please print this page for your records and send a copy of it to your publisher/graduate school.
- Appropriate credit for the requested material should be given as follows: "Reprinted (adapted) with permission from {COMPLETE REFERENCE CITATION}. Copyright {YEAR} American Chemical Society." Insert appropriate information in place of the capitalized words.
- One-time permission is granted only for the use specified in your RightsLink request. No additional uses are granted (such as derivative works or other editions). For any uses, please submit a new request.

If credit is given to another source for the material you requested from RightsLink, permission must be obtained from that source.

[BACK](#) [CLOSE WINDOW](#)

S6.4 Reprinted Publication in Chapter 4



Discriminative Behavior of Cyclodextrin Polymers against Dissolved Organic Matter: Role of Cavity Size and Sorbate Properties

Author: David Glöckler, Mourad Harir, Philippe Schmitt-Kopplin, et al

Publication: Analytical Chemistry

Publisher: American Chemical Society

Date: Oct 1, 2023

Copyright © 2023, American Chemical Society

PERMISSION/LICENSE IS GRANTED FOR YOUR ORDER AT NO CHARGE

This type of permission/license, instead of the standard Terms and Conditions, is sent to you because no fee is being charged for your order. Please note the following:

- Permission is granted for your request in both print and electronic formats, and translations.
- If figures and/or tables were requested, they may be adapted or used in part.
- Please print this page for your records and send a copy of it to your publisher/graduate school.
- Appropriate credit for the requested material should be given as follows: "Reprinted (adapted) with permission from {COMPLETE REFERENCE CITATION}. Copyright {YEAR} American Chemical Society." Insert appropriate information in place of the capitalized words.
- One-time permission is granted only for the use specified in your RightsLink request. No additional uses are granted (such as derivative works or other editions). For any uses, please submit a new request.

If credit is given to another source for the material you requested from RightsLink, permission must be obtained from that source.

[BACK](#)

[CLOSE WINDOW](#)